Vol. 170 No. 2, April 15, 1985 ISSN 0003-2670
(Including Cumulative Author, Subject and Technique Indexes for Volumes 161–170)

ANALYTICA CHIMICA ACTA

International journal devoted to all branches of analytical chemistry

ELSEVIER

ANALYTICA CHIMICA ACTA

International journal devoted to all branches of analytical chemistry
Revue internationale consacrée à tous les domaines de la chimie analytique
Internationale Zeitschrift für alle Gebiete der analytischen Chemie

PUBLICATION SCHEDULE FOR 1985

	J	F	M	A	M	J	J	A	S	O	N	D
Analytica Chimica Acta	167	168	169	170/1 170/2	171	172	173	174	175	176	177	178

Scope. *Analytica Chimica Acta* publishes original papers, short communications, and reviews dealing with even aspect of modern chemical analysis, both fundamental and applied.

Submission of Papers. Manuscripts (three copies) should be submitted as designated below for rapid and efficien handling:

Papers from the Americas to: Professor Harry L. Pardue, Department of Chemistry, Purdue University, West Lafayette IN 47907, U.S.A.

Papers from all other countries to: Dr. A. M. G. Macdonald, Department of Chemistry, The University, P.O. Box 363 Birmingham B15 2TT, England. Papers dealing particularly with computer techniques to: Professor J. T. Clerc Universität Bern, Pharmazeutisches Institut, Baltzerstrasse 5, CH-3012 Bern, Switzerland.

Submission of an article is understood to imply that the article is original and unpublished and is not being considere for publication elsewhere. Upon acceptance of an article by the journal, authors will be asked to transfer the copyrigh of the article to the publisher. This transfer will ensure the widest possible dissemination of information.

Information for Authors. Papers in English, French and German are published. There are no page charges Manuscripts should conform in layout and style to the papers published in this Volume. Authors should consul Vol. 170 for detailed information. Reprints of this information are available from the Editors or from: Elsevier Editoria Services Ltd., Mayfield House, 256 Banbury Road, Oxford OX2 7DH (Great Britain).

Reprints. Fifty reprints will be supplied free of charge. Additional reprints (minimum 100) can be ordered. An orde form containing price quotations will be sent to the authors together with the proofs of their article.

Advertisements. Advertisement rates are available from the publisher.

Subscriptions. Subscriptions should be sent to: Elsevier Science Publishers B.V., Journals Department, P.O. Bo 211, 1000 AE Amsterdam, The Netherlands. Tel: 5803 911, Telex: 18582.

Publication. *Analytica Chimica Acta* appears in 12 volumes in 1985. The subscription for 1985 (Vols. 167–178) i Dfl. 2400.00 plus Dfl. 264.00 (p.p.h.) (total approx. US $986.70). All earlier volumes (Vols. 1–166) except Vols. 2 and 28 are available at Dfl. 215.00 (US $79.60), plus Dfl. 15.00 (US $5.60) p.p.h., per volume.

Our p.p.h. (postage, packing and handling) charge includes surface delivery of all issues, except to subscribers in th U.S.A., Canada, Japan, Australia, New Zealand, China, India, Israel, South Africa, Malaysia, Singapore, South Korea Taiwan, Pakistan, Hong Kong and Brazil who receive all issues by air delivery (S.A.L. — Surface Air Lifted) at no extr cost. For the rest of the world, airmail and S.A.L. charges are available upon request.

Claims for issues not received should be made within three months of publication of the issues. If not they cannot b honoured free of charge.

For further information, or a free sample copy of this or any other Elsevier Science Publishers journal, readers in th U.S.A. and Canada can contact the following address: Elsevier Science Publishing Co. Inc., Journal Informatio Center, 52 Vanderbilt Avenue, New York, NY 10017, U.S.A., Tel: (212) 916-1250.

Analytica Chimica Acta, 170 (1985) 159—175
Elsevier Science Publishers B.V., Amsterdam — Printed in The Netherlands

Review

THE DETERMINATION OF MOISTURE IN SOLIDS
A Selected Review

J. W. PYPER
Lawrence Livermore National Laboratory, Livermore, CA 94550 (U.S.A.)
(Received 23rd July 1984)

SUMMARY

The scientific literature published since Pande's comprehensive monograph *Handbook of Moisture Determination and Control* (1974) was surveyed (to mid-1984) for new or improved techniques of determining moisture in solids. Particular attention is given to methods that might distinguish between bound and free moisture in organic solids. The classification of moisture is discussed, as well as pitfalls in sampling, in sample handling, and in the comparison of different methods. Six methods that show promise of being able to distinguish between bound and free moisture were identified: dynamic dielectric thermal analysis, coherent microwave measurements, infrared spectrometry, near-infrared reflectance spectrometry, thermal methods and nuclear magnetic resonance spectrometry.

Water is truly the ubiquitous substance. Bodies of water cover three-fourths of the earth's surface. Animal and plant life are composed largely of water. Even the atmosphere contains a few percent of water as vapor. Although water is essential for life, paradoxically, "life would be simpler, many times, if water did not hide in every crack and crevice, spread itself out over every surface it contacts, and permeate many solids whether they are porous or not" [1].

In addition to its ubiquity, water is unusually reactive because of its high polarity. It not only bonds strongly to itself and other polar molecules, but also bonds by physical forces to many other substances. These two factors, abundance and chemical reactivity, cause moisture and the determination of moisture to be of great concern to many industries such as food, paper, and plastics, in which acceptable levels of moisture content vary from material to material, but in some cases even trace amounts can adversely affect product quality [1]. Hundreds of methods have been developed for determining moisture in concentrations from parts per million (ppm; mg l^{-1}) to percent. Indeed, the easiest way to obtain a patent may well be to invent a new moisture analyzer or humidity meter, because water interacts with so many substances [2].

A search of the chemical literature of the last 10 years revealed two comprehensive monographs plus a number of collections of papers from past

0003-2670/85/$05.95

years and some recent specialized reviews from Europe, none in English. The monograph by Pande [3], entitled *Handbook of Moisture Determination and Control*, covers the literature up to 1974 and is a very lucid description of the properties of water and the various methods of quantifying moisture in liquid and solid materials. I made the assumption that the literature up to and including 1973 was thoroughly assessed in Pande's monograph. This review will consider only advances made in the last decade and is intended to be an update of Pande's monograph. The second monograph (in three parts), entitled *Aquametry*, by Mitchell and Smith [4] is even more comprehensive. Part I discusses the structure and physical properties of water and the chemical, thermal, spectroscopic and physical methods of moisture determination and includes references to 1976. Part II includes an update of the methods in the first part with references to 1978, plus 800 pages on the Karl Fischer titration. Volume III has 1300 pages on various electrical methods including dielometry, conductometry and coulometry with references to 1979. Of particular use to this reviewer was the index on methods to distinguish between bound and free moisture. Even though the present review also covers the 1970s, there does not seem to be much overlap, apparently because of the differences in abstract sources used. Therefore, both reviews supplement each other in this time period. There have been several collections of papers from symposia that have been used as general references. Perhaps the best known is the four-volume compendium *Humidity and Moisture—Measurement and Control in Science and Industry* [5], which is based on the 1963 International Symposium on Humidity and Moisture (Washington, DC). A later collection is based on the 1971 Imeko Symposium on Moisture Measurement [6]. These compilations are useful in indicating the state of the art in a particular year, but they are obviously less useful than the cited monographs.

Reviews since Pande are more specialized. They focus primarily on methods for rapid, continuous measurement of moisture in solids on processing lines in industry [7—10]. Lueck [10] critically examines these continuous methods; his review is particularly useful for the processing industries. Another specialized review [11] covers determinations of moisture measurement in the glass and ceramic industry. Although important subjects, they are of specialized interest. The Russian journal *Izmeritel'naya Tekhnika* (*Measurement Techniques*) had a series of papers on moisture gauges in 1980. Individual papers from this collection will be cited at appropriate places in this review; two papers, however, were general descriptions of moisture measurement gauges developed by the "Proektpribor" Special Design Office and methods of checking the calibration of these instruments [12, 13]. A recent review [14] covers the available instrumentation for measuring moisture content of building materials.

The references that were obtained for this literature review were obtained from a computer search of five separate data bases: Chemical Abstracts (1967—mid 1984), INSPEC (1969—mid 1984), Energy (1974—mid 1984),

NTIS (U.S. Government reports, 1966—mid 1984), and DROLS (classified literature, 1954—mid 1984).

The organization of this review will generally parallel that of Pande [3] except for those sections of his monograph that are not directly applicable to solids. First, the nature of bound and free water will be explored. Then gravimetric methods (including thermal techniques), the Karl Fischer titration, electrical methods (including microwave techniques), infrared and mass spectrometric methods, and nuclear methods (including n.m.r. and neutron-scattering techniques) will be assessed. Detailed descriptions of the techniques can be found in the previously cited monographs.

CLASSIFICATION OF MOISTURE IN SOLIDS

Classifying the moisture in solid materials is not easy. There are many pitfalls that can occur in the construction of simple models or classifications [15, 16]. This review will consider three ways of classifying the states of moisture in solids: (1) operational, (2) energetic, and (3) structural. Each has its advantages and disadvantages. Most workers choose the operational definition as the easiest way out of the morass; and in many cases, it is sufficient. If one is seeking scientific understanding, however, either of the latter two classification methods is more satisfying and useful.

Operational definition. The simple classification of moisture as "bound" or "free" is an example of an operational definition. In using such a simple definition, it is necessary to specify the conditions. For example, an operational definition of free moisture might be "that moisture which can be driven off by heating the substance at 110° C for one hour in air at atmospheric pressure". Any water that is not driven off is considered bound, if a method is available for determining the total amount of water in the substance. A more complex example is cited by Riley [17], who classifies four kinds of moisture in coal (inherent moisture, surface moisture, decomposition moisture, and water of hydration) by the temperature ranges in which water is evolved. Despite the oversimplification of this type of classification, it might be sufficient in many cases for which detailed information is not needed.

Energetic definition. In examining the states of moisture in energetic terms, Catalano [15] calls his approach "pseudothermodynamic"; it has the virtue of being able to describe the binding of moisture in quantitative terms. He begins by defining an interaction energy, which is the energy necessary to overcome the interaction of the water with the material (or some part of the material) and to remove the water to a specified standard state (gaseous non-associated water vapor at ambient temperature). The lowest value on this scale would be water interacting with itself (agglomerates of water molecules in the liquid state), having an energy of interaction of about 5 kcal mol^{-1}. The maximum value on this scale is equivalent to energies that cause disproportionation of simple molecules (approximately 100 kcal mol^{-1}). The scale

is continuous. Strictly speaking, the term "free" moisture should be used for only the lowest interaction energy, although workers have commonly used "free" to describe water that has been bound by energies of 5—20 kcal mol^{-1}. In this classification scheme, then, the various states of moisture in solids would be described as "water bound with X kcal mol^{-1}". The obvious disadvantage of this method is that for it to be useful, a method must be available to measure the binding energy of the various states of water.

Structural definition. Sugitani [16] and Rasmussen [18] have proposed structural classifications, which are combined here. The Sugitani scheme is the more detailed one, particularly in the area of chemical bonding.

Water taken up by solid materials is generally classified as water bound by physical forces or water bound by chemical bonds. Physically bound water includes adsorbed water, trapped or liquid-inclusion water and absorbed water. The physical adsorption of water occurs when water condenses or is held on the surface; the surface includes, of course, the cracks, crevices, etc. of real materials. Liquid inclusion occurs during the crystallization process when bubbles of water are trapped. Water absorption is the process of taking up and retaining water uniformly throughout the structure of the host. Examples of materials that can absorb large amounts of water are silica gel, cellulose, starch and agar.

The chemically bound water, or water of crystallization, is divided into two main categories, namely, bound water and zeolite water. They are distinguished by the fact that when the water is removed, the crystal structure is altered if it is bound water but the original skeletal structure remains if it is zeolite water.

The bound water can be subdivided into several categories, i.e., coordinated water, lattice water, hydronium-ion water, hydrogen-bonded water and decomposition water. Coordinated water occurs when the water molecule is directly coordinated with the metal ion in a crystal, as in $MgCl_2 \cdot 6H_2O$. Lattice water occurs when the water is not directly coordinated with the central ion but forms hydrogen bonds with the other water species. For example, in $CuSO_4 \cdot 5H_2O$, four water molecules are directly coordinated with the central metal ion. One (lattice) water molecule, however, is hydrogen-bonded to the coordinated water, thus stabilizing the crystal. Hydronium-ion water means that the water is present in the crystal as H_3O^+ ions, such as in uranophene $[Ca(H_3O)_2(UO_2)_2(SiO_4)_2 \cdot 3H_2O]$, a uranium-containing mineral. In the case of hydrogen-bonded water, the water molecules themselves form a three-dimensional skeletal structure by hydrogen bonding; other ions and rare gases are assumed to be enclosed in the cavities formed by the bonded waters. Glauber's salt ($Na_2SO_4 \cdot 10H_2O$) and gas hydrates such as $Cl_2 \cdot 10H_2O$ are examples of this type. Decomposition water is contained as hydroxide ions, as in $Ca(OH)_2$. When hydroxides are dehydrated, they are converted to the oxides, giving off the decomposition water.

Zeolite water can be further subclassified according to the shape of the gaps into which the water is taken. An example is beryl [$Be_3Al_2(SiO_3)_6 \cdot nH_2O$], in which the water molecules are enclosed in a tunnel structure formed by the piling up of hexagonal rings of Si_6O_{18}.

This classification scheme is summarized in Fig. 1. Again, the obvious disadvantage of this method of classification is that much detailed data must be gathered to classify the water in a particular substance such as a chemical explosive. Sugitani [16] discusses in detail how n.m.r., i.r., thermal methods, dielectric dispersion, and photoacoustic spectroscopy can be used to provide this structural information.

SAMPLING, SAMPLE HANDLING AND COMPARISON OF METHODS

The determination of moisture is not a trivial task. Great care must be taken in sampling, sample handling, and in the measurement itself. In any quantitative procedure, the importance of obtaining a representative sample cannot be overemphasized. Pande's monograph [3] has a detailed section on this important topic (Vol. 1, pp. 26—42). Once a representative sample has been obtained, the next problem is to make sure that the moisture content does not change before it is quantified. Because many solid materials are hygroscopic, they must be protected from any humidity condition except the original condition under which the processing and sampling were done. The importance of this point is aptly illustrated by the following anecdote [19]. A large manufacturer of an organic product hired a chemist for the summer to evaluate several commercial instruments for quantifying moisture. The chemist and his assistants sampled the product on the production line, placed the many samples in glass sample vials, and processed them using several commercial instruments. After three months of work, the conclusion

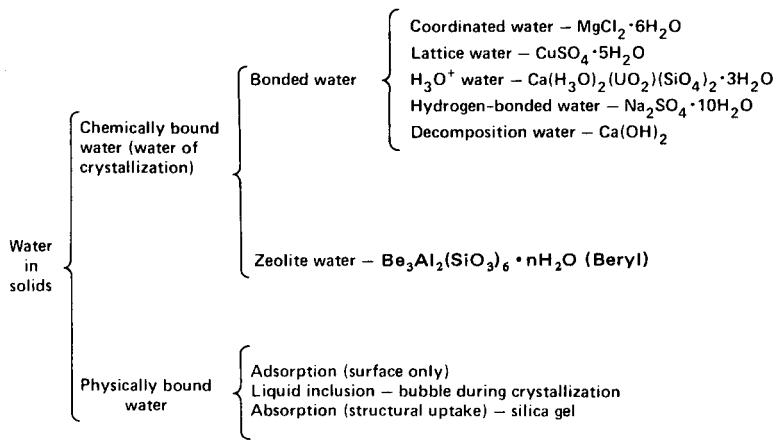

Fig. 1. Structural classification of water in solids.

of the study was that none of the instruments was suitable. No correlations were found between what was expected and what was found. Later evaluation by others discovered that the cap liner of the sample vials was hygroscopic. The moisture from this source equilibrated with the product samples, thus invalidating the study. Sample containers should not incorporate hygroscopic materials and should enclose a minimal dead volume, which then is dominated by the moisture content of the sample.

There are also pitfalls in comparing various methods. For example, in a recent study [20] of moisture in a high explosive, four different techniques (oven drying, Karl Fischer titration, flowing afterglow spectroscopy, and an electrolytic moisture device) were compared. The authors obtained four significantly different values of the moisture content, for reasons that were not apparent; they preferred the Karl Fischer method because it is direct and relatively unambiguous. Differences in sample handling, the possibility that the methods are really measuring different quantities and the influence of adsorbed moisture in the sample chamber could be causes of the discrepancies.

GRAVIMETRIC METHODS, AZEOTROPIC DISTILLATION AND CHROMATOGRAPHIC METHODS

Under this category, Pande [3] included much detailed information on the theory of drying; it has not been supplanted. In addition to oven drying, he discussed thermal, azeotropic distillation and chromatographic methods.

Oven-drying and weighing is the commonest method of determining moisture in solids. Although it is simple in concept, there are implicit assumptions and many pitfalls. First among these is the assumption that water is the only volatile species that will evaporate under the specified drying conditions. Unless this assumption is reasonably assured by analysis of the gases produced, the results will be meaningless. Secondly, the conditions of drying (i.e., time, temperature, pressure and atmosphere) must be carefully specified. Thirdly, the relationship of the moisture evolved from the substance under the specified conditions to the total moisture content cannot be known without a detailed experimental program. This program must involve absolute and specific methods such as the Karl Fischer titration. Nevertheless, the convenience of this method makes it the one of choice in many circumstances. It has been made even more convenient in recent years by the advent of automated oven-and-balance combinations. No recent papers on oven drying were found in the present survey.

Two papers [21, 22] were published on thermo-vacuum aquametry. This method is based on measurement of the temperature change of the sample as the moisture in the sample is evaporated in a vacuum. It is said to be particularly useful for artificial fertilizers and salts of mineral acids. Moisture contents up to 3—4% with an overall accuracy of 0.08—0.15% in a measuring time of 10—12 min were reported.

Mitchell and Smith [4] reviewed the use of differential thermal analysis (d.t.a.) and thermogravimetric analysis (t.g.a.) for studying bound moisture in solids. Chaladze and Melkumyan [23] described a standard thermogravimetric instrument designed for calibrating and certifying moisture meters used to determine moisture in industrial and agricultural products, thus providing a national standard for quantifying moisture in solids.

In an earlier paper on the explosive triaminotrinitrobenzene (TATB), Colmenares and McDavid [24] described a novel method of determining the moisture content and the equilibrium water vapor pressure. This method is based on measuring the diffusion of water vapor through a membrane that has a low moisture permeability, such as Mylar. Water on the low-partial-pressure side was quantified with an electrolytic hygrometer. Moisture contents of several plastic-bonded explosives were found to be in the range 0.0021—0.0165%. Moisture has also been determined by using kinetic mass transfer [25], manometry [26], volumetric measurements [27], thermal heat conduction [28, 29], and by heating in an argon stream with a hygrometer as the detector [30].

Moisture in solid and liquid substances has been determined by using the distillation properties of azeotropic mixtures. After the distillation, the amount of water collected is determined volumetrically. Slaczka [31] suggested that moistening the condenser and receiver walls with hydrophobic chloromethylsilane prevents the adherence of water, thus increasing the accuracy of the determination.

Three references were found that utilized gas chromatographic (g.c.) methods for the determination of moisture in solids. Shvetsova and Mamaeva [32] used a g.c. method with a thermal conductivity detector to determine free water, hygroscopic water, and crystallization water at 80—90°C, 100—175°C, and 500°C, respectively. Kolb et al. [33] used multiple head-space extraction to determine moisture in poly(vinyl chloride). A device was patented [34] that utilizes a reactor to convert water present in a solid sample to acetylene which is measured by a thermal conductivity detector.

THE KARL FISCHER METHOD AND ITS APPLICATION

The Karl Fischer [35] titration has become a standard method for the determination of moisture in liquids and solids. Where applicable (various substances can interfere), it is the method of choice for the absolute determination of water because of its selectivity, high precision, and speed [36, 37]. The titration is readily automated.

The theory of determining the moisture in free-flowing solids by measuring the heat of reaction between moisture and the Karl Fischer reagent was developed and tested by using dextrin as the free-flowing material. The control method was vacuum-drying and the accuracy was ±0.05% [38]. The heat of reaction between water and Karl Fischer reagent is appreciable and

under appropriate conditions the temperature rise is proportional to the water content of substances. On this basis, a direct injection enthalpimetric method was developed for the determination of moisture in a number of organic solvents and solid samples [39].

Some samples are slow to dissolve in solvents that are compatible with the Karl Fischer titration. By analyzing the titration curve, Yap et al. [40] were able to develop an estimation of the moisture content for such samples.

The pyridine in Karl Fischer reagent is toxic. Scholz [41, 42] was able to prepare improved and less toxic reagents with other amines such as morpholine, tris(hydroxymethyl)aminomethane, and diethanolamine. Renner [43] used the Scholz reagent to determine the moisture in a double-base propellant. The new reagent is superior to the Karl Fischer reagent in storage stability, titration speed, end-point accuracy, toxicity, and convenience. The titration times with the improved reagents were shorter and visual end-point detection was possible. Other recent applications of the Karl Fischer method were for the determination of moisture in wood sawdust [44], in the explosive TATB [45], in oil sands [46], and in sand, ammonium nitrate, and foundry loam [47]. It was not appropriate for silica gel or coal [47]. Middleton [48] compared semi-automatic titrators with a fully automatic titrator. He concluded that the latter is superior because it is 67% faster and is constantly standardized electrically rather than by the usual complicated two-hour procedure.

ELECTRICAL AND ELECTRONIC METHODS

In his chapter under this heading, Pande [3] included electrical conductivity, capacitance, ultrasonic, microwave, and coulometric techniques. In the library search for this review, papers were found on only three of these techniques, namely, capacitance, microwave, and coulometric methods. These methods, as well as the others to be discussed below, are indirect (physical) methods as opposed to the direct methods that have been discussed above. In direct methods, moisture is normally removed from the solid material by drying, distillation, etc., and its quantity is found by weighing, titration, etc. In indirect methods, moisture is not removed from the material, but properties of the wet solid that depend on the amount of water or number of hydrogen atoms are measured instead. These indirect methods must be calibrated with standards that have been prepared by using one of the direct methods.

Dielectric or capacitance methods

The dielectric constant of air at 25°C is slightly greater than 1, most organic materials are in the range 2—5, and water is 78. Therefore, the presence of even a small amount of water in an organic material causes a considerable change in the dielectric constant of the combined system. A separate calibration curve of dielectric constant versus moisture content must be constructed for each substance of interest.

During the last ten years, two Japanese patents were issued to Japan Kokai Tokyo Koho for moisture determinations based on this principle. In one [49], the dielectric constant of a solid substance is measured by attaching an electrode to the substance and then using the probe to measure the dielectric constant between the electrode and ground. In the other [50], a single electrode is attached to the surface of the material and the dielectric constant between the electrode and ground is measured with a resistor-capacitor oscillation circuit. A German patent was issued [51] for a screw conveyor device for continuous monitoring of bulk materials as they are fed through the system. The screw conveyer and the housing serve as the electrodes for the dielectric measurement.

The theory for using a dielectric moisture gauge for materials that absorb a large amount of energy from an electric field was developed by Podkin [52]. Terekhov et al. [53] described the theory for a thermal-capacitive moisture meter that measures not only the change in capacitance but also the heat effects (as a function of time) that take place during measurement. From these parameters, the moisture content is determined. Boiko et al. [54] developed a two-frequency method of capacitance measurement that allowed them to quantify moisture more accurately under field conditions. The use of multiple frequencies allows the exclusion of effects caused by temperature, density, chemical composition, etc. Dynamic dielectric thermal analysis can be used to quantify the amount of moisture in electrical insulators. Hedvig [55] has reviewed the application of this technique to polymers. Free water has a relaxation time (time constant for the aligned dipoles to return to the unpolarized state) of 10^{-10} to 10^{-11} s at temperatures between 0 and 100°C, whereas sorbed water has relaxation times between 10^{-2} and 10^{-8} s. This suggests that the technique might be used to determine bound and free water in polymers. Jain et al. [56] showed how dielectric methods can be used to determine simultaneously the density and moisture content of wood.

Microwave methods

It is well known that water attenuates microwave signals. This effect has been utilized to quantify moisture content in solids for many years. This method is again based on the sizeable dielectric constant of water compared with those of organic materials.

Kraszewski [57] has recently reviewed the applications of microwave technology to moisture determinations, giving references from 1972 to 1980. He described the theory, measurement methods and instrumentation. The disadvantages of simple (one-parameter) microwave moisture meters is that they have relatively low sensitivity and limited range for moisture measurements, and they depend on the fluctuation of the material density in the volume measured. Kraszewski showed that the effect of density fluctuations can be minimized by simultaneously measuring the attenuation and phase shift of the radiation. He also indicated that microwave methods can be used

to determine the amounts of bound and free moisture in organic materials, because the relaxation frequencies are quite different (17 GHz for liquid water and 900 MHz for bound water). Meyer and Schilz [58] also obtained a density-independent calibration curve for moisture content by deriving a material-specific function at frequencies $\geqslant 8$ GHz. Their method requires only one frequency and involves measurements of the complex dielectric constant. Berliner and Spiridonov [59] criticized the two-parameter method of Kraszewski [57] and gave a detailed description of their own composite microwave moisture gauge, which includes a built-in compensator for temperature variations. This method quantifies only surface moisture. Assuming that the moisture content is uniform through the cross-section of a ceramic rod, production tests of the transducer showed that the absolute error was less than 0.2%. Ismatullaer and Granvalid [60] described their two-parameter (amplitude and phase shift) u.h.f. method, which they applied to cottonseed products. King and Styles [61] developed an open-ended coaxial microwave resonator which is able to quantify the moisture content of solid materials to 0.05% in situ. It appears that there is enough sensitivity in these techniques to extend the measurements to even lower moisture contents.

Coulometric methods

Coulometric techniques usually involve adsorption of the moisture evolved from a material during heating onto a hygroscopic material, generally phosphorus pentoxide; thus, this technique is really a direct method. The adsorbed water is subsequently electrolyzed. The current required for electrolysis is proportional to the original water content. Hassel [1] gave a lucid discussion of this technique as it is applied to polymers and described a commercial instrument. Czuha [62] discussed a method of avoiding the overloading of such a coulometric cell by alternately purging the cell with a dry gas stream. Trufanova and Glyuk [63] described a similar technique applied to minerals and rocks; the calibration curve was linear over the range 1—100 μg of water and the mean relative error was 4—6%. Finally, the use of the Barkal-3 gas moisture meter for determining the moisture content of solids has been described [64].

SPECTROMETRIC METHODS

In this section, infrared and mass spectrometric techniques are considered, followed by methods based on gamma and other nuclear rays and nuclear magnetic resonance.

Light refraction has been applied to quantify moisture in sand and coke [65]. The solids were extracted with various organic solvents and the water was determined from the n_D^{20} (refractive index at 20° C, D line of sodium) of this extract.

Infrared spectrometry

Yanasawa and Hashimoto [66] described an infrared method developed to quantify moisture in solid metal oxides in the 20—50 000 mg kg^{-1} range. This method is applicable to moisture in titanium dioxide, alumina and magnesium oxide. Svirgun [67] reviewed the use of an i.r. absorption instrument for solids, liquids, and gases. Deb [68] used an infrared technique to show that commercial Nd-YAG laser rods have entrained moisture in their crystal structure. The detailed design of a three-frequency infrared instrument for quantifying moisture in cinematographic film was described by Gross et al. [69]. The advantage of using three frequencies is that the temperature and structural dependence of the measurement is reduced, thereby increasing measurement reliability. Lin and Senturia [70] studied the aging rate of thin hydrated aluminum oxide films at 40% relative humidity. Three moisture states ("physisorbed" water, "chemisorbed" water, and "fixed" water) were observed by using a combination of i.r. spectrometry and isotope exchange.

Near-infrared reflectance spectrometry utilizes the near-infrared diffuse reflectance radiation from a solid sample at several discrete wavelengths to predict moisture and other chemical species in the material. This method was developed for foodstuffs [71] but has general applicability to organic materials. Rotolo [71] gave a detailed review of its utility in the food industry, including the instrumental components, calibration procedures, and the computer regression techniques. Hirschfeld [72] found that it can be used to determine bound and free moisture after calibration with appropriate standards.

Near-infrared photoacoustic spectrometry has also been used to determine moisture in opaque solid materials such as paper and foodstuffs [73]. This technique is considerably more flexible than reflectance in sample preparation and handling, and despite its lower signal levels it may be superior under the appropriate circumstances.

Flowing afterglow method

In this technique [74], a glow discharge in an inert gas such as argon or helium provides a source of highly energetic metastable atoms which react with a secondary gas stream from a sample pyrolysis chamber, resulting in a chemiluminescence spectrum. The reactions for water vapor are

$$He^* + H_2O \rightarrow He + H_2O^+ + e^-;\ H_2O^+ + e^- \rightarrow H_2O^* \rightarrow OH^{*\cdot} + H^{*\cdot};$$

$$OH^{*\cdot} \rightarrow OH\cdot + h\nu$$

The resulting radiation is resolved by using a low-resolution, high-speed optical monochromator and is detected with a photometer. Copeland [20] applied this method to the determination of moisture in the high explosive TATB. He was unable to correlate the results from this technique with those from the Karl Fischer titration, oven drying, and an electrolytic method. Bystroff and Stout [75] also applied this moisture technique in analyses of nitrocellulose. They found that a stainless steel reactor produced an increased

sensitivity of an order of magnitude relative to that of the standard glass reactor. Although this technique has a low detection limit (0.02 mg kg^{-1}), it is subject to the usual water-background effects in high vacuum systems: the walls of the reactor absorb water and release it in the flowing gases. This results in a virtual leak [75], thus limiting the usefulness of the technique.

Mass spectrometric methods

Because of adsorption and desorption of water on the exposed surfaces in a vacuum system and the attendant "memory effect" described above, mass spectrometry has not been extensively used to quantify moisture in solids. Carlson and Morgan [76], however, developed a method in which the evolved moisture from solids is concentrated cryogenically and treated with calcium carbide to produce acetylene, which is readily quantified by standard mass spectrometric techniques. In a calibration experiment, the authors found that their method yielded results that were 3% lower than the theoretical values for two hydrated salts. Another worker [77], using the same method, found values 5—8% higher than the theoretical values for two different hydrated substances. This method, therefore, is not very attractive.

Nuclear magnetic resonance (n.m.r.)

The low-resolution broad-banded n.m.r. spectrum of water and ice (Fig. 2) shows that the tightly bound protons in the solid and the mobile water protons in the liquid can be separately quantified. This approach can also be used to determine the amounts of free and bound moisture in solid substances; the narrow liquid-resonance peak represents the free moisture and the broad solid peak represents the bound moisture plus any other bound protons in the substance [4, 78].

In a German patent, Winterhoff and Bette [79] described a n.m.r. method that continuously monitors the tightly and loosely bound protons in solids. First, the magnetic d.c. field is modulated by a triangular field, which induces

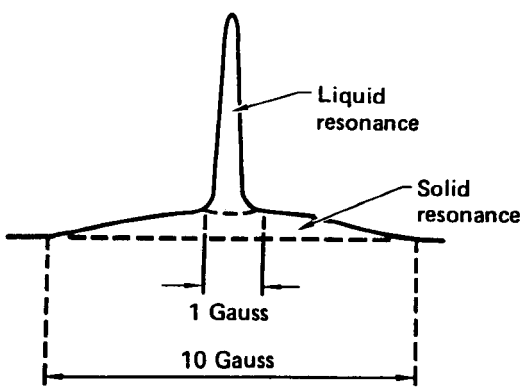

Fig. 2. N.m.r. spectrum of water and ice.

low-frequency nuclear resonance signals from loosely bound protons. Next, the magnetic d.c. field is modulated by a higher field to induce signals that represent the loosely and strongly bound protons. The signals integrated over both time intervals are evaluated by taking their ratio. Low-resolution n.m.r. methods have been used to quantify moisture in coal [80]. Use was made of the difference in width between the n.m.r. signal from liquid water and tightly bound water by using a variable-gate technique. The method showed a linear correlation with oven-drying techniques and was both rapid and accurate. Brosio et al. [81] applied pulsed n.m.r. techniques to the determination of exchangeable hydrogen atoms in solids. Hydrogen atoms that generally belong to such functional groups as hydroxyl, carboxyl and amine, plus crystal water are exchanged with D_2O, thus making such hydrogens "mobile". The data are interpreted in terms of the fraction of the hydrogen atoms made mobile by this technique. The application discussed was for the hydration of starch in durum wheat semolina. Danilyuk and Rytsar [82] developed a mathematical treatment for estimating the error inherent in the n.m.r. measurement of moisture in solids; the mathematical approaches were illustrated by graphs. Ward et al. [83] applied a broad-band n.m.r. technique to determine the mobile water protons in the explosive triaminotrinitrobenzene. This method has a detection limit of about 0.25% water.

Neutron and γ-ray scattering methods

Energetic neutrons or γ-rays are scattered by nuclei and lose their energy. This moderation process forms the basis of a determination of moisture. Because of its large cross-section for collision, hydrogen is the most effective moderator for neutrons. Experimentally, the sample is bombarded with fast neutrons and the density of slow neutrons produced is measured. This method is applicable to substances that are relatively proton-free.

Stroikovskii et al. [84] described a neutron device that was developed to measure the moisture content of blast-furnace coke in the range 0—10% water. They provided a schematic diagram of the device and discussed its measurement algorithm. The absolute error was claimed to be less than ±0.5%. Pershkin and Glushkova [85] surveyed existing neutron-based meters used to quantify moisture in the Soviet Union and discussed their characteristics. They proposed a method of calibrating these meters by using simulators. Sojka [86] described a neutron apparatus for determining the moisture content of ceramics and coal. A Japanese patent [87] described a method in which both neutrons and γ-rays are scattered by the solid sample. The signals arising from the γ-rays are converted into different rise times and are counted as pulses having different wave heights. A similar system [88] was described in which the separate counting of neutrons and γ-rays results in elimination of the bulk-density effect. Lutsik [89] described a γ-ray method used to determine moisture in cellulose filters. The decrease in intensity of the γ-radiation is exponentially related to the moisture content. Tominaga et al. [90] used the transmission of fast neutrons and γ-rays from ^{252}Cf to measure

simultaneously the density and moisture content in large heterogeneous objects. An online test of coke in an iron-making process revealed an improvement in precision over previous methods of approximately 4. Mathew et al. [91] used the moderation of neutrons to determine the level of solids or liquids. This gauge can also be used to determine moisture levels down to 0.5% water.

Conclusions

Direct methods for the determination of moisture in solids, with the exception of thermal methods, will not distinguish between bound and free moisture in organic materials. Thermal methods have traditionally been used to specify the kinds of moisture in materials. Indirect methods which show promise of distinguishing between bound and free moisture in organic materials are the dynamic dielectric thermal method and microwave, i.r., near-i.r. reflectance, and n.m.r. spectrometry.

This work was done under the auspices of the U.S. Department of Energy by the Lawrence Livermore National Laboratory under Contract W-7405-Eng-48.

REFERENCES

1 R. L. Hassel, Am. Lab., (1976) 33.
2 F. C. Quinn, Industrial Moisture Measurement and Control, Short course by The Center for Professional Advancement, East Brunswick, NJ, January, 1983.
3 A. Pande, Handbook of Moisture Determination and Control, M. Dekker, New York, 1974.
4 J. Mitchell, Jr. and D. M. Smith, Aquametry, Wiley, New York, Part I, 1977; Part II, 1980; Part III, 1984.
5 A. Wexler, Humidity and Moisture — Measurement and Control in Science and Industry, Reinhold, New York, 1965 (4 vols.).
6 International Measurement Confederation, Proc. Imeko-Symposition on Moisture Measurement, Esztergom, Hungary, October, 1971, Imeko Secretariat, Budapest, Hungary.
7 M. Hampel, Glueckauf, 109(10) (1973) 524; Chem. Abstr., 79 (1973) 48833g.
8 Continuous Measurement of Moisture in Solids, Circ. Inf. Techn., Cent. Doc. Sider, 34(1) (1977) 97.
9 E. S. Krichevskii, V. S. Roife and I. Y. Klugman, Theory and Practice of the High-Speed Monitoring of the Moisture Content of Solid and Liquid Materials, Energiya, Moscow, 1980; Chem. Abstr., 94 (1981) 185024t.
10 W. Lueck, Regelungstech. Prax. Prozess-Rechentech., 16(3) (1974) 60.
11 J. Kaplanek, Sklar Keram., 31(3) (1981) 71.
12 A. E. Bandzeladze, G. M. Tsaladze, N. G. Kanteladze, P. V. Akaraishvili and T. G. Gogisvanidze, Izmeritel'naya Tekhnika, 23(4) (1980) 62; Meas. Tech. (USSR), 23(4) (1980) 364.
13 V. G. Romanov, Izmeritel'naya Tekhnika, 23(3) (1980) 49; Meas. Tech. (USSR), 23(3) (1980) 257.
14 D. Whiting, Assessment of Potential Techniques for In-Situ, Real-Time Moisture Measurements in Building Envelope Systems: A Literature Survey. Oak Ridge National Laboratory, ORNL-23-40122, 1983.

15 E. Catalano, Comments on Some of the Physical Chemical Questions Associated with the Analysis of Water in Earth Material, Lawrence Livermore National Laboratory, Livermore, CA, UCRL-50630, 1969.
16 Y. Sugitani, Bunseki, 7 (1979) 427.
17 J. T. Riley, Am. Lab., (1983) 17.
18 K. E. Rasmussen, Nor. Apotekerforen. Tidsskr., 78(8) (1970) 142.
19 L. E. Maley, Industrial Moisture Measurement and Control, Short course by the Center for Professional Advancement, East Brunswick, NJ, January, 1983.
20 R. J. Copeland, Use of the Flowing Afterglow Technique for the Analysis of Moisture in TATB Formulations, Mason and Hanger — Silas Mason Co., Pantex Plant, Amarillo, TX, MHSMP-81-02, 1981.
21 E. S. Krichevskii, A. G. Volchenko, Y. V. Podgornyi, R. M. Proskuryakov and V. I. Roskin, Izmeritel'naya Tekhnika, (1976) 69; Meas. Tech. (USSR), 19 (1976) 1042.
22 A. G. Volchenko, E. S. Krichevskii and R. M. Proskuryakov, Izmeritel'naya Tekhnika, (1980) 63; Meas. Tech. (USSR), 23 (1980) 281.
23 A. P. Chaladze and V. E. Melkumyan, Izmeritel'naya Tekhnika, (1980) 50; Meas. Tech. (USSR), 23 (1980) 346.
24 C. Colmenares and L. C. McDavid, Equilibrium Water Vapor Pressure and Total Moisture Content Measurements on TATB, Lawrence Livermore National Laboratory, Livermore, CA, UCID-17049, 1976.
25 M. V. Venediktov and R. I. Venediktova, Metody Prib. Anal. Sostava Veshchestva, 2 (1973) 39; Chem. Abstr., 83 (1975) 90273g.
26 V. D. Man, Measuring the Degree of Humidity of Solids, French Patent 2,198,401, Sept. 12, 1972; Chem. Abstr., 81 (1974) 106648e.
27 I. Tanahashi, Measuring the Absolute Volume and the Adsorbed Water Content of a Solid, Japanese Patent 80,103,425, Feb. 3, 1979; Chem. Abstr., 94 (1981) 144413a.
28 R. K. Azimov, P. R. Ismatullaev and A. A. Zamov, Izmeritel'naya Tekhnika (1980) 57; Meas. Tech. (USSR), 23 (1980) 356.
29 K. G. Gupta, M. J. Laubitz and A. Feingold, Lett. Heat Mass Transfer, 5 (1978) 89.
30 H. Lepatit and H. Rozenblum, Analusis, 8 (1980) 381; Chem. Abstr., 94 (1981) 40864g.
31 A. Slaczka, Chem. Anal. (Warsaw), 20 (1975) 417; Chem. Abstr., 83 (1975) 118326c.
32 T. V. Shvetsova and V. P. Mamaeva, Khim. Prom-st., Ser.: Metody Anal. Kontrolya Kach. Prod. Khim. Pron-sti (1982) 6; Chem. Abstr., 96 (1982) 210124b.
33 B. Kolb, M. Auer and R. Pospisil, Angew. Chromatogr., 35E (1981); Chem. Abstr., 95 (1981) 98696r.
34 Shimodzu Seisakusho Ltd., Apparatus for High Sensitivity Water Determination, Japanese Patent 8,302,653, Jan. 8, 1983; Chem. Abstr., 99 (1983) 47255w.
35 A. S. Bobrow, Am. Lab., (1983) 92.
36 F. E. Jones, Anal. Chem., 53 (1981) 1955.
37 1981 Annual Book of ASTM Standards, Part 30, American Society for Testing and Materials, Philadelphia, PA, ASTM E 203-75, 1981, pp.803—810.
38 G. S. Uchitel, A. A. Pekarskii, A. A. Despotuli and A. A. Pustobaev, Tr. Novocherk. Piltekh. Inst., 314 (1975) 30; Chem. Abstr., 85 (1975) 96200u.
39 P. Marik-Korda, Therm. Anal. (Proc. Int. Conf. Therm. Anal.), 6(1) (1980) 529; Chem. Abstr., 94 (1981) 76241r.
40 W. T. Yap, A. L. Cummings, S. A. Margolis and R. Schaffer, Anal. Chem., 51 (1979) 1595.
41 E. Scholz, Fresenius Z. Anal. Chem., 303 (1980) 203.
42 E. Scholz, Titration Agent for Determining the Moisture Content of Solids or Liquid, German Patent 3,008,421, Sept. 10, 1981.
43 R. H. Renner, Proc. Joint Symp. Plastics/Materials with Explosives, Propellants, Pyrotechnics and Ingredients, Lake Ozark, MO, 1983.
44 L. V. Strebkova, O. G. Potekhim and V. G. Romanov, Zavod. Lab., 45 (1979) 35; Chem. Abstr., 90 (1979) 153599k.

45 J. Sadoval, Titrimetric Determination of Water in TATB Using Karl Fischer Reagent, Mason and Hanger — Silas Mason Co., Inc., Pantex Plant, Amarillo, TX, MHSMP-80-59, 1980.
46 D. L. Ball, E. D. Cook, J. M. Cooky, M. C. Hamilton and R. Schutte, Can. J. Chem., 59 (1981) 1527.
47 G. I. Gridchina and L. K. Savchuk, Metody Prib. Anal. Sostava Veshchestva, 2 (1973) 88; Chem. Abstr., 83 (1975) 107694v.
48 H. W. Middleton, Comparison of Semiautomatic and Fully Automatic Water Titrators, General Electric Co., Neutron Devices, Dept., St. Petersburg, FL, GEPP-TIS-569, May 22, 1981.
49 K. K. Seiwa Giken, Probe for Water Content Determination, Japanese Patent 80,80,048, June 16, 1980; Chem. Abstr., 94 (1981) 86207g.
50 S. Kawasaki and N. Sato, Determination of Water Content, Japanese Patent 79,95,296, July 27, 1979; Chem. Abstr., 91 (1979) 213020x.
51 E. Fischer, Device and Methods for Continuous Measurement of the Water Content of Bulk Materials, German Patent DG 3,329,135, Mar. 8, 1984; Chem. Abstr., 10 (1984) 25469b.
52 Y. G. Podkin, Izmeritel'naya Tekhnika, (1980) 65; Meas. Tech. (USSR), 23 (1980) 284.
53 V. P. Terekhov, E. S. Krichevskii and S. S. Galushkin, Izmeritel'naya Tekhnika, (1980) 55; Meas. Tech. (USSR), 23 (1980) 354.
54 V. O. Boiko, P. N. Platonov and A. A. Pikersjil, Izmeritel'naya Tekhnika, (1980) 59; Meas. Tech. (USSR), 23 (1980) 359.
55 P. Hedvig, Dielectric Spectroscopy of Polymers, Wiley, New York, 1977, pp. 293—296.
56 V. K. Jain, S. N. Sanyal and S. F. H. Rizvi, J. Inst. Eng. (India) Electr. Eng. Div., 63 (1983) 230.
57 A. Kraszewski, Proc. 10th European Microwave Conference, Warsaw, 1980, pp. 48—58; J. Microwave Power, 15 (1980) 209.
58 W. Meyer and W. Schilz, J. Phys. D., 13 (1980) 1823.
59 M. A. Berliner and V. I. Spiridonov, Izmeritel'naya Tekhnika, (1980) 60; Meas. Tech. (USSR), 23 (1980) 277.
60 P. R. Ismatullaer and A. B. Granvalid, Izmeritel'naya Tekhnika, (1980) 60; Meas. Tech. (USSR), 23 (1980) 361.
61 R. J. King and P. Styles, Proc. Prog. Quantitative Nondestructive Evaluation, 34 (1984) 1073.
62 M. Czuha, Jr., Apparatus for Moisture Determination in Solids, U.S. Patent 3,823,082, July 9, 1974.
63 L. G. Trufanova and D. S. Glyuk, Geokhimiya, (1979) 475; Chem. Abstr., 90 (1979) 197032v.
64 G. Larikova, V. N. Kotova, O. V. Gorlinova and L. M. Knyazeva, Zh. Anal. Khim., 35 (1980) 1777; Chem. Abstr., 94 (1980) 10669e.
65 J. Neiser, Sb. Pr. Pedagoq. Fak. Ostrave, Rada E, E-3 (1973) 115; Chem. Abstr., 82 (1975) 50951g.
66 H. Yanasawa and N. Hashimoto, Determination of Water Contents in Solid Metal Oxides, Japanese Patent 75,23,698, March 13, 1975.
67 S. P. Svirgun, Khim. Prom-st., Ser.: Avtom. Khim. Proizvod, (1979) 56; Chem. Abstr., 92 (1980) 121041x.
68 K. K. Deb, Spectrosc. Lett., 15 (1982) 243.
69 L. G. Gross, V. F. Kulikov, V. V. Berdnik, V. D. Kochkina and I. D. Grachev, Izmeritel'naya Tekhnika, (1980) 64; Meas. Tech. (USSR), 23 (1980) 367.
70 C. Lin and S. D. Senturia, Sensors Actuators, 4 (1983) 497.
71 P. Rotolo, Cereal Foods World, 24 (1979) 94.
72 T. Hirschfeld, Lawrence Livermore National Laboratory, Livermore, CA, private communication, June, 1983.
73 Q. Jin, G. F. Kirkbright and D. E. M. Spillane, Appl. Spectrosc., 36 (1982) 120.

74 G. W. Taylor, J. Phys. Chem., 77 (1973) 124.
75 R. I. Bystroff and N. D. Stout, The Flowing Afterglow in Argon and Helium: Difference in Two Reactor Designs in Application to the Analysis of Moisture, Lawrence Livermore National Laboratory, Livermore, CA, UCRL-87023, 1982.
76 G. L. Carlson and W. R. Morgan, Appl. Spect., 31 (1977) 48.
77 J. R. Walton, Mass Spectrometric Determination of Moisture, Oak Ridge National Laboratory, Oak Ridge, TN, ORNL/TM-7, 1981.
78 R. L. Ward, Lawrence Livermore National Laboratory, Livermore, CA, private communication, September, 1982.
79 H. Winterhoff and W. Bette, Determination of Moisture and Liquids in Solids by NMR, German Patent 2,212,047, October 18, 1973.
80 S. D. Robertson, F. Cunliffe, C. S. Fowler and I. J. Richmond, Fuel, 58 (1979) 770.
81 E. Brosio, F. Conti and M. Paci, J. Mag. Res., 34 (1979) 593.
82 I. S. Danilyuk and B. E. Rytsar, Izmeritel'naya Tekhnika, (1981) 46; Meas. Tech. (USSR), 24 (1981) 875.
83 R. L. Ward, T. Felver and J. W. Pyper, J. Hazardous Materials, 9 (1984) 69.
84 A. K. Stroikovskii, A. A. Pershkin and A. N. Sheikin, Izmeritel'naya Tekhnika (1980) 54; Meas. Tech. (USSR), 23 (1980) 351.
85 A. A. Pershkin and L. T. Glushkova, Izmeritel'naya Tekhnika, (1980) 51; Meas. Tech. (USSR), 23 (1980) 348.
86 J. Sojka, Radio meter for Determining the Moisture Content of Bulk Solids, Czech. Patent 159,506, August 15, 1974; Chem. Abstr., 82 (1975) 92694y.
87 Japan Atomic Energy Research Institute, Hitachi Limited, Moisture Determination Using Radiation Transmission, Japanese Patent 82,63,440, April 16, 1982; Chem. Abstr., 97 (1982) 103626r.
88 Hitachi Limited, Moisture Determination, Japanese Patent 81,22,941, March 4, 1981; Chem. Abstr., 95 (1981) 117642p.
89 P. P. Lutsik, Legka Prom., (1967) 17; Chem. Abstr., 68 (1968) 14381r.
90 H. Tominaga, N. Wada, N. Tachikawa, Y. Kuramochi, S. Horrachi, Y. Sase, H. Amano, N. Okabo and H. Nishikawa, Int. J. Appl. Radiat. Isot., 34 (1983) 429.
91 P. J. Mathew, C. Ceravolo, P. Huppert and J. F. Miles, Int. J. Appl. Radiat. Isot., 34 (1983) 1377.

Analytica Chimica Acta, 170 (1985) 177—185
Elsevier Science Publishers B.V., Amsterdam — Printed in The Netherlands

SOLID-SURFACE DERIVATIVE ROOM-TEMPERATURE LUMINESCENCE SPECTROMETRY OF MIXTURES

V. P. SENTHILNATHAN and R. J. HURTUBISE*
Department of Chemistry, The University of Wyoming, Laramie, WY 82071 (U.S.A.)
(Received 28th August 1984)

SUMMARY

Derivative solid-surface room-temperature fluorescence and phosphorescence were combined for the identification of components in binary and ternary mixtures of nanogram amounts of nitrogen heterocycles. Direct, and first and second derivative room-temperature phosphorescence excitation, room-temperature fluorescence and room-temperature phosphorescence spectra were used in the identification of the components in the mixtures by matching spectral wavelengths from mixtures with spectral wavelengths from standards. The criteria for matching wavelengths, subtracting background signals and obtaining derivative spectra at the 0.5-ng level are discussed.

Recently, research involving luminescence spectrometry of compounds adsorbed on solid supports has centered on the development of room-temperature phosphorescence (r.t.p.) as a useful analytical technique. The r.t.p. work has been summarized in recent reports [1—4]. For inducing r.t.p., filter paper has been the most widely used surface for aromatic compounds. Senthilnathan et al. [5] improved the sensitivity and limits of detection for various compounds by using polyacrylic acid-treated filter paper. Considerable work has been reported on room-temperature fluorescence (r.t.f.) of a variety of organic compounds adsorbed on solid surfaces [1].

There have been few reports of the combined use of room-temperature solid-surface fluorescence and phosphorescence and the combined use of derivative solid-surface fluorescence and phosphorescence. Ford and Hurtubise [6] characterized 5,6-benzoquinoline and phenanthridine in shale oil by using both solid-surface r.t.f. and r.t.p. Senthilnathan and Hurtubise [7] recently reported a simple and sensitive method for the quantitation of components in mixtures with solid-surface room-temperature luminescence. In this approach, both room-temperature solid-surface fluorescence and phosphorescence were used to determine components in mixtures at the nanogram level without prior separation. Dalterio and Hurtubise [8] reported the identification of components in hydroxyl aromatic mixtures employing zeroth and second derivative solid-surface r.t.f. and r.t.p. In later work, these workers showed that direct and second-derivative solid-surface r.t.f. and r.t.p. could be used to identify hydroxyl aromatics in fractions from

0003-2670/85/$03.30

high-performance liquid chromatography (h.p.l.c.) [9]. The method was applicable to solvents from both normal-phase and reversed-phase h.p.l.c. systems. In this work, additional aspects of r.t.f. and r.t.p. have been considered for qualitative studies of nitrogen heterocycle mixtures. In particular, direct and first and second derivative luminescence spectra are used for the identification of components in a mixture.

EXPERIMENTAL

Apparatus

Luminescence excitation and emission spectra were obtained with a Farrand MK-2 spectrofluorimeter fitted with a phosphorescence rotary chopper. Source radiation was provided by a 150-W xenon lamp (Canrad Hanovia, Newark, NJ), and the detector was a R928 photomultiplier tube (Hamamatsu). For r.t.p. measurements, metal slits giving a bandwidth of 10 nm were used at the entrance and exit positions of both the excitation and emission monochromators. For fluorescence measurements, 5-nm slits were used in the excitation monochromator and 2.5-nm slits were used in the emission monochromator. For qualitative studies, samples were adsorbed on 4 × 1-cm filter paper strips, which were held between two small aluminum blocks during the luminescence measurements.

A Bascom-Turner model 4120 data handling system with floppy disc data-storage capabilities was connected to the spectrofluorimeter for electronically calculating first and second derivative luminescence spectra.

Reagents

Absolute ethanol was purified by distillation. Gold-label 5,6-benzoquinoline (Aldrich Chemical Co.) and secondary standard polyacrylic acid (Scientific Polymer Products, Ontario, NY) were used as received. The filter paper (Whatman No. 1) was developed in ethanol to collect impurities at one end prior to use. 4-Azafluorene and phenanthridine (Aldrich Chemical Co.) were recrystallized from ethanol.

Procedures

Luminescent compounds were adsorbed onto filter paper from a 1-μl solution containing either standard components or a mixture. Ethanolic polyacrylic acid solutions were used in the r.t.f. measurements and ethanolic 0.1 M hydrobromic acid solutions of polyacrylic acid were used in the r.t.p. measurements. The polyacrylic acid solutions were prepared so that 1 μl of solution contained 20 μg of polyacrylic acid. Further details were given earlier [5]. The filter paper with sample was dried in an oven at 80°C for 10—15 min before luminescence measurements. Luminescence spectra were stored in the Bascom-Turner recorder system, and then first and second derivatives were calculated and plotted.

All the r.t.p. excitation spectra were scanned from 250 to 400 nm, r.t.f. emission spectra were scanned from 330 to 480 nm, and r.t.p. emission spectra were scanned from 400 to 600 nm, all with the same scanning speed of 100 nm min^{-1}. The sampling rate for the r.t.p. excitation and the r.t.f. emission spectra was 180 ms per point for 500 points and for the r.t.p. emission spectra 240 ms per point for 500 points. Additional experimental details have been reported elsewhere [8].

All the luminescence spectra were first compressed to 20% of the X-axis scale of the Bascom-Turner recorder. Then, a spectrum was smoothed (5-point moving average) twice as described in the Bascom-Turner manual to reduce noise in the spectrum and the first derivative was taken. The second derivative spectrum was obtained from the first derivative spectrum with the Bascom-Turner recorder.

RESULTS AND DISCUSSION

Binary mixtures

Direct and first and second derivative r.t.p. excitation, r.t.f. emission, and r.t.p. emission spectra were obtained for 5,6-benzoquinoline (10 ng) and 4-azafluorene (100 ng) mixtures adsorbed on polyacrylic acid-treated filter paper. It was found earlier that polyacrylic acid added to filter paper enhanced the r.t.p. of various compounds [5]. The r.t.f. signals were about 6—18 times stronger with the polyacrylic acid solution than those obtained with the polyacrylic acid solution in 0.1 M hydrobromic acid. Correspondingly, the r.t.p. signals were about 2 times stronger with the polyacrylic acid solution in 0.1 M hydrobromic acid than those obtained with the polyacrylic acid solution. These results are most likely due to the heavy-atom effect of bromide. The direct spectra indicated the presence of two components (5,6-benzoquinoline and 4-azafluorene). However, for many analytical situations, the information obtained from the direct spectra would be inadequate to characterize or to identify the two components because of the broad structureless characteristics of the spectra. More spectral information is obtained with the first and second derivative spectra. For example, if the component of interest gives both fluorescence and phosphorescence, then six spectra can be obtained: two excitation spectra (first and second derivatives), two r.t.f. spectra (first and second derivatives), and r.t.p. spectra (first and second derivatives). If one includes the direct spectra, then nine spectra can be obtained from the mixture. In this work, both negative bands (orientated down) and positive bands (orientated up) in the first and second derivative luminescence spectra were used for identification purposes because of the large amount of information obtained. In addition, the general spectral features of the derivative spectra were used as an aid in identification.

Figure 1 shows a typical first derivative r.t.f. spectrum and a typical r.t.p. second derivative spectrum for the binary mixture. For all the derivative spectra, the background signals were subtracted with the computerized

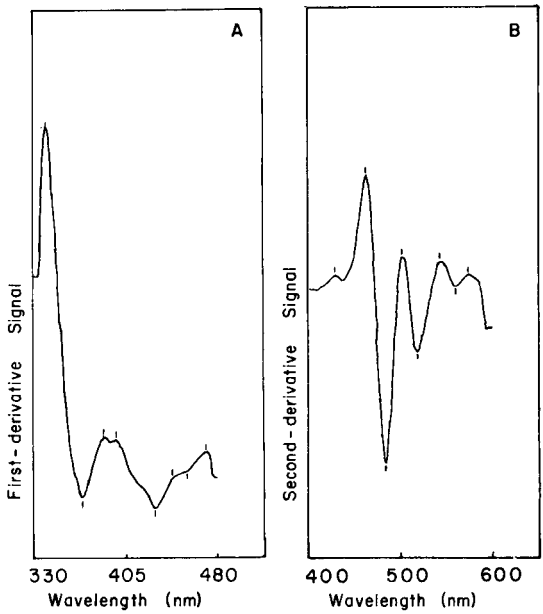

Fig. 1. First derivative r.t.f. spectrum (A) excited at 285 nm for a mixture of 5,6-benzoquinoline (10 ng) and 4-azafluorene (100 ng) adsorbed on polyacrylic acid-treated filter paper, and second derivative r.t.p. spectrum (B) excited at 370 nm for the same mixture adsorbed on 0.1 M HBr/polyacrylic acid-treated filter paper.

recorder. Recent results have indicated that for the particular computerized system used in this work, it is important to obtain the second derivative spectrum from the appropriate first derivative spectrum rather than obtaining the second derivative spectrum from the direct spectrum. If the latter approach is used, some spectral bands in a given second derivative spectrum are split into two bands. Interestingly this does not occur for all the second derivative spectra.

The primary approach for identifying the components in the mixture was to tabulate and compare the various wavelengths in the mixture with the corresponding standard compounds. Table 1 shows such a comparison with some of first derivative spectral data. An identification was made if a first-derivative wavelength was within ±4 nm of a band of an individual standard and if the band was properly orientated up or down. The criterion of ±4 nm was determined empirically by comparison of the spectral bands of standards with those of mixtures for the first and second derivative excitation spectra. The criterion was based on the reproducibility of the spectral wavelengths (±0.8 nm) and small spectral shifts that can occur with some spectra consisting of two or more components. The last factor is discussed later for second derivative r.t.p. spectra. The results in Table 1 show that both components can be easily identified even with 4-azafluorene present at 10 times the amount of 5,6-benzoquinoline. A similar table was prepared for the second

TABLE 1

Comparison of first derivative wavelengths for a mixture of 5,6-benzoquinoline (5,6-BQ; 10 ng) and 4-azafluorene (4-AZ; 100 ng)[a]

5,6-BQ	4-AZ	Mixture	Mixture
Excitation spectra (nm)			
λ_{em} = 480 nm	λ_{em} = 467 nm	λ_{em} = 480 nm	λ_{em} = 467 nm
+272	−263	−266 (4-AZ)	−264 (4-AZ)
−290	+313	+313 (4-AZ)	+314 (4-AZ)
+348	−339	−341 (4-AZ)	−339 (4-AZ)
−380	+387	−384 (5,6-BQ)	+384 (4-AZ)
R.t.f. spectra (nm)			
λ_{ex} = 285 nm	λ_{ex} = 290 nm	λ_{ex} = 285 nm	λ_{ex} = 290 nm
+345	+340	+341 (4-AZ, 5,6-BQ)	+338 (4-AZ)
−361	−373	−365 (5,6-BQ)	−369 (4-AZ)
+386	+406	+385 (5,6-BQ)	+386 (5,6-BQ)
−435	+424	+400 —	
	+449	−431 (5,6-BQ)	
	−460	+422 (4-AZ)	
	+472	+451 (4-AZ)	
		−458 (4-AZ)	
		+473 (4-AZ)	
R.t.p. spectra (nm)			
λ_{ex} = 370 nm	λ_{ex} = 330 nm	λ_{ex} = 370 nm	λ_{ex} = 330 nm
+469	+430	+468 (5,6-BQ)	+431 (4-AZ)
−492	−484	−493 (5,6-BQ)	−486 (4-AZ)
+505	−510	+503 (5,6-BQ)	−509 (4-AZ)
−530		−530 (5,6-BQ)	
+553		+550 (5,6-BQ)	
−564		−564 (5,6-BQ)	

[a]The plus sign refers to spectral bands orientated up and the negative sign refers to spectral bands orientated down.

derivative data and substantially more data were obtained. Again, each component was easily identified. A similar binary mixture but with 50 ng of each compound was investigated. Because the relative luminescence intensities for both components were roughly the same, the bands in the several derivative luminescence spectra were easily discernible. It was found that the quality of the spectra at very low levels of luminescent components was improved by subtracting the background signal.

Ternary mixtures

As with the binary mixtures, direct, first and second derivative r.t.p. excitation, r.t.f. emission and r.t.p. emission spectra were obtained. The ternary mixture, 5,6-benzoquinoline (10 ng), 4-azafluorene (50 ng), and phenanthridine (100 ng), was investigated. This was a particularly difficult

mixture to resolve because phenanthridine was present at 10 times the level of 5,6-benzoquinoline and the corresponding excitation, r.t.f. and r.t.p. spectra of these two compounds overlapped extensively. The various 4-azafluorene spectra also overlapped though less severely.

Figure 2 shows the extensive overlap of the direct derivative r.t.p. spectra of 5,6-benzoquinoline and phenanthridine. The wavelength data from the first and second derivative luminescence spectra of the standards and mixture were tabulated and compared. The wavelengths of excitation and emission were chosen to maximize the luminescence of the components in the mixture. A substantial amount of data was obtained. For example, three second-derivative r.t.f. spectra were obtained by exciting at 270, 285 and 290 nm. The first spectrum showed 12 peaks, the second 11 peaks and the third 9 peaks. Many of the bands in the three spectra were the same. However, peaks appeared at one excitation wavelength and not another or the spectral resolution of some of the peaks was enhanced by using different excitation wavelengths. Table 2 shows the data obtained from the second derivative r.t.p. spectra, and Fig. 3 shows a representative second derivative r.t.p. spectrum of the ternary mixture. The same empirical guideline of ±4 nm which was discussed above was used to match the wavelengths for mixtures with those for standards.

Table 2 indicates that one wavelength was not matched with the standards. Close inspection of the data shows that this wavelength (+533) is 1 nm beyond the empirical wavelength criterion when compared to the standard wavelength for 4-azafluorene. Griffiths et al. [10] have discussed the occurrence of shifts of even-order derivative bands caused by overlap of adjacent bands. The derivative band shift cannot generally be predicted because each

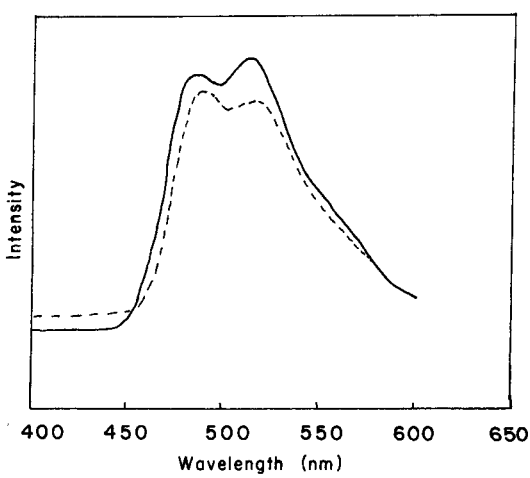

Fig. 2. R.t.p. spectra: (———) 5,6-benzoquinoline excited at 370 nm; (——) phenanthridine excited at 330 nm. Compounds were adsorbed onto 0.1 M HBr/polyacrylic acid-treated filter paper.

TABLE 2

Comparison of second derivative r.t.p. wavelengths for a mixture of 5,6-benzoquinoline (5,6-BQ; 10 ng), 4-azafluorene (4-AZ; 50 ng), and phenanthridine (PH; 100 ng)[a]

5,6-BQ	4-AZ	PH	Mixture	Mixture
λ_{ex} = 370 nm	λ_{ex} = 330 nm	λ_{ex} = 330 nm	λ_{ex} = 370 nm	λ_{ex} = 330 nm
−419	+424	−418	+428 (5,6-BQ, 4-AZ)	+426 (PH, 4-AZ)
+432	−442	+430	+466 (5,6-BQ)	−441 (4-AZ)
+465	+460	+458	−480 (5,6-BQ, PH)	+456 (PH, 4-AZ)
−484	−472	−480	+493 (PH, 4-AZ)	−477 (PH)
+504	+490	+497	−515 (PH)	+497 (PH)
−521	−506	−517	+536 (PH, 4-AZ)	−513 (PH)
+546	+515	+540	−560 (5,6-BQ)	+533 —
−564	−530	−566	+580 (5,6-BQ, PH)	−544 (4-AZ)
+579	+538	+578		+553 (4-AZ)
	−543			−568 (5,6-BQ, PH)
	+555			+578 (5,6-BQ, PH)
	−575			
	+586			

[a]See Table 1.

combination of bands and the extent of their overlap is unique [10]. The one wavelength mentioned may have been shifted because of adjacent bands. In this work, no attempt was made to break down the mixture spectral bands into their individual component bands. In further comparing the data in Table 2, several wavelengths in the mixture correspond to two components and these wavelengths could not be used for identification purposes. More importantly, four wavelengths correspond to phenanthridine, three to 4-azafluorene and two to 5,6-benzoquinoline. The latter results confirm that three components are present. However, when the results from first derivative excitation, r.t.f. and r.t.p. spectra and the second derivative excitation and r.t.f. spectra were considered, there was additional evidence that three components were present.

The same experiment was done with a mixture of the three compounds containing 50 ng of each component. With the large amount of data obtained from the derivative spectra and the relatively strong luminescence signals, the three components were easily identified. There were several second derivative wavelengths in the mixture spectra that did not match with the standards. Because of this there would be some ambiguity about the presence of only three components in a sample with no prior information about the mixture. Thus, the technique identifies and characterizes individual components in a mixture, but does not necessarily establish the exact number of components in the mixture.

The results for the ternary mixture are important because the luminescence spectra of 5,6-benzoquinoline and phenanthridine overlapped extensively, and the latter component was present at ten times the level of the former. Also, because of the variety of luminescence spectra (excitation, r.t.f. and r.t.p.), one can select certain spectra for difficult situations. For example, if

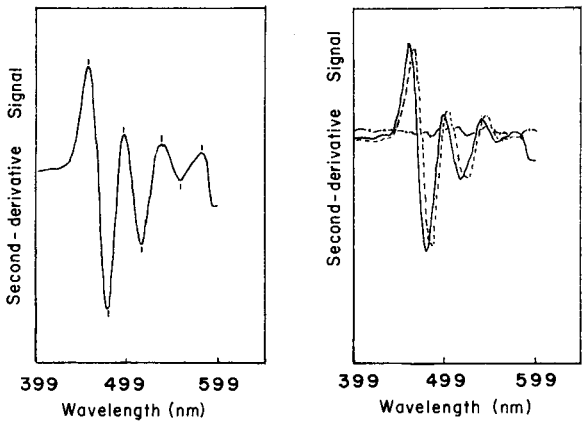

Fig. 3. Second derivative r.t.p. spectrum excited at 370 nm for a mixture of 5,6-benzoquinoline (10 ng), 4-azafluorene (50 ng), and phenanthridine (100 ng) adsorbed onto 0.1 M HBr/polyacrylic acid-treated filter paper.

Fig. 4. Second derivative r.t.p. spectra excited at 370 nm: (——) 5,6-benzoquinoline (0.5 ng); (—·—) 4-azafluorene (0.5 ng); (— — —) mixture of the compounds (0.5 ng each). All adsorbed onto 0.1 M HBr/polyacrylic acid-treated filter paper.

a sample shows considerable interference in the phosphorescence region then the r.t.f. and/or the excitation region may prove helpful.

Derivative spectra with small amounts of components

Even though the binary and ternary mixtures discussed above were at the nanogram level, it is important to consider the approximate minimum levels at which useful luminescence spectra can be obtained. It was found earlier that the r.t.p. limit of detection of 5,6-benzoquinoline on polyacrylic acid/hydrobromic acid-treated filter paper was 0.07 ng [5]. In this work, a mixture of 5,6-benzoquinoline and 4-azafluorene (0.5 ng each) was investigated which was above the limit of detection for 5,6-benzoquinoline. This amount gave a r.t.p. signal for 4-azafluorene of approximately ten times the background signal and a r.t.p. signal for 5,6-benzoquinoline of approximately six times the background signal at the corresponding maximum excitation wavelengths. The r.t.f. signals for both compounds were about the same as the background signals, and thus the r.t.f. signals were not useful at the 0.5-ng level.

Figure 4 shows the second derivative r.t.p. spectra of 4-azafluorene (0.5 ng), 5,6-benzoquinoline (0.5 ng), and a mixture of the two components (0.5 ng each) excited at a maximum excitation wavelength for 5,6-benzoquinoline (370 nm). It can be seen that the r.t.p. of 4-azafluorene contributes little to the r.t.p. of the mixture. When the maximum excitation wavelength for 4-azafluorene (330 nm) was used, 5,6-benzoquinoline contributed relatively little r.t.p. to the mixture. Thus, by selective excitation it was possible

to have spectral regions that were essentially free of interference from a given component. Figure 4 shows that the derivative spectrum of the mixture is almost superimposed onto the 5,6-benzoquinoline spectrum. The mixture spectrum does show some small shifts relative to the 5,6-benzoquinoline spectrum. The major cause of the shifts is most likely the contribution of 4-azafluorene to the mixture spectrum. By comparison of several r.t.p. spectra of mixtures with the r.t.p. spectra of the individual components, it was clear that relatively small shifts occurred for some bands in the mixture spectra when two or more bands appeared in the same spectral region. The shifts were usually within a 2—4 nm range with a 6 nm shift occasionally observed. These aspects are important considerations for the identification of components in mixtures. The small spectral shifts should be considered in determining empirical criteria for the identification of components in mixtures.

Similar r.t.p. experiments were done with the ternary mixture, 4-azafluorene, 5,6-benzoquinoline, and phenanthridine (0.5 ng each). Because three components were present and because of the extensive overlap of the r.t.p. second derivative spectra for the latter two compounds, it was more difficult to discern the second derivative bands for these compounds. Their bands were relatively weak in contrast to the second derivative r.t.p. bands for 4-azafluorene. However, r.t.p. bands were detected for the three components at the 0.5-ng level by selectively exciting with two wavelengths. The approach described is useful for the identification of compounds in two- and three-component mixtures. For more complex mixtures, the technique could be used to characterize major components.

Financial support for this project was provided by the Department of Energy, Division of Basic Energy Sciences, Contract DE-AC02-80ER10624.

REFERENCES

1 R. J. Hurtubise, Solid Surface Luminescence Analysis: Theory, Instrumentation, Applications, M. Dekker, New York, 1981.
2 R. T. Parker, R. S. Freedlander and R. B. Dunlap, Anal. Chim. Acta, 119 (1980) 189; 120 (1980) 1.
3 J. L. Ward, G. L. Walden and J. D. Winefordner, Talanta, 28 (1981) 201.
4 T. Vo-Dinh, Room Temperature Phosphorimetry for Chemical Analysis, Wiley-Interscience, New York, 1984.
5 V. P. Senthilnathan, S. M. Ramasamy and R. J. Hurtubise, Anal. Chim. Acta, 157 (1984) 203.
6 C. D. Ford and R. J. Hurtubise, Anal. Lett., 13(A6) (1980) 485.
7 V. P. Senthilnathan and R. J. Hurtubise, Anal. Chem., 56 (1984) 913.
8 R. A. Dalterio and R. J. Hurtubise, Anal. Chem., 56 (1984) 819.
9 R. A. Dalterio and R. J. Hurtubise, Anal. Chem., 56 (1984) 1183.
10 T. R. Griffiths, K. King, St. H. V. A. Hubbard, M. J. Schwing-Weill and J. Meullemeestre, Anal. Chim. Acta, 143 (1982) 163.
11 T. C. O'Haver and G. L. Green, Anal. Chem., 48 (1976) 312.
12 T. Vo-Dinh and R. B. Gammage, Anal. Chim. Acta, 107 (1979) 261.

Analytica Chimica Acta, 170 (1985) 187—198
Elsevier Science Publishers B.V., Amsterdam — Printed in The Netherlands

FLUORESCENCE QUENCHING AND HALIDE-ION NUCLEAR MAGNETIC RESONANCE SPECTROSCOPY AS PROBES FOR METAL BINDING TO PROTEINS

JOSEPH J. PESEK*
Department of Chemistry, San Jose State University, San Jose, CA 95192 (U.S.A.)
ROBERT J. DOWE and JOHN F. SCHNEIDER
Department of Chemistry, Northern Illinois University, DeKalb, IL 60115 (U.S.A.)
(Received 30th March 1984)

SUMMARY

Fluorescence quenching can be used to detect the binding of some metals to proteins at concentrations as low as 10^{-7} M. In many cases the effects of pH can be studied and the stoichiometries of metal complexes can be determined. The technique has potential for studying kinetic processes involving metal/protein complexes. Halide-ion nuclear magnetic resonance n.m.r. can also be used to detect metal binding to proteins, to study the effects of pH on metal/protein complexes, and to determine the stoichiometry of the complex. Two additional parameters about metal/protein systems can be obtained from halide-ion n.m.r. experiments. These are the local correlation time of the metal binding site and the halide-ion exchange rate at the binding site. These parameters give information about local motion at the binding site and the accessibility of the binding site. The two techniques appear to be an effective combination for the study of metal/protein systems, which provides a more complete description of these systems than is available from either technique alone or from many other methods.

Proteins possess intrinsic fluorescence as a result of their complement of aromatic amino acids, i.e., tryptophan, tyrosine and phenylalanine. This phenomenon was first reported by Shore and Pardee in 1956 [1]. Tryptophan produces the most intense fluorescence and is primarily responsible for the intrinsic fluorescence associated with proteins [2—4].

The technique of fluorescence quenching has already been applied to the study of metal/protein interactions. In an early study Rogers [5, 6] reported that silver(I) quenched the fluorescence of glutamate and lactate dehydrogenases. The quenching mechanism in these systems is not completely understood. In sulfhydryl-containing proteins the binding of metal ions produces ultraviolet absorption because of mercaptide bond formation. Overlap of emission and absorption bands causes quenching by the Forster energy-transfer mechanism [7] in which radiationless energy transfers from excited tryptophan residues to the metal. Chen [8] studied the effects of silver(I) on the fluorescence of tryptophan and several proteins and concluded that it

0003-2670/85/$03.30

quenches by at least two mechanisms: collisional quenching and energy transfer to Ag(I)-mercaptide absorption bands. Mercury(II) ions have also been shown to quench the intrinsic fluorescence of proteins [9]. Heavy metal atoms such as Ag(I) and Hg(II) frequently quench by the "heavy metal effect [10]"; the inhomogeneous electric field of a large atom perturbs the spin and orbital motions of the fluorescent molecule. The result is enhanced spin-orbit coupling and easier intersystem crossing between the singlet and triplet states. The effects of Ag(I) and Hg(II) on the fluorescence of tryptophan and proteins have been reviewed by Chen [11]. Fluorescence has been used to study the binding of copper(II) and iron(III) to transferrin [12] and the effect of the metal ion on the quantum yield in some magnesium(II)-containing enzymes [13, 14].

The chlorine-35 line-width technique [15—19] has proved to be a useful method for studying the binding of metals to proteins. Previous studies have utilized protein concentrations of 100 μM or greater and high halide ion concentrations (usually >0.5 M). The advent of the Fourier transform method makes it possible to reduce these concentrations by a factor of ten to approximate more closely physiological conditions.

Quadrupolar relaxation is the predominant relaxation mechanism for nuclei having $I > 1/2$. The spin-lattice decay rate is given by

$$R_1 = 3\pi^2(2I + 3)/10I^2(2I - 1)[e^2qQ/h]\tau_c = k\tau_c \quad (1)$$

where e is the unit electrical charge, q the electric field gradient, Q the quadrupole moment, h Planck's constant, and τ_c the correlation time for reorientation of the field gradient. When the halide-ion exchange rate is fast with respect to τ_c and slow compared to the spin-lattice decay time of the bound halide (T_{1B}), a single composite line is observed. For halide ions covalently bound to proteins, the line width is about 10^5 greater than that of free aqueous halide ions because of the large difference in the field gradient at the nucleus. Therefore, halide ions in the presence of metal/protein complexes at physiological concentrations will produce measurable line broadening.

If the free halide concentration [X] is much greater than the concentration of bound halide [B], the following equation applies:

$$R_2 - R_{1F} = (1/k_2[B] - [X]/R_{1B}[B])^{-1} \quad (2)$$

where $R_2 - R_{1F}$ is the broadening of the halide-ion line width, k_2 the bimolecular exchange rate, and R_{1B} as given by Eqn. 1. If a protein/metal/halide species (PMX) is considered, then $R_2 - R_{1F} = \alpha B$. The parameter α is determined experimentally and is the slope of the relaxation rate (R_2) vs. the concentration of metal bound. Then

$$R_2 - R_{1F} = (1/k_2 - [X]/k\tau_c)^{-1} = \alpha \quad (3)$$

From a plot of free halide concentration vs. α^{-1}, the halide-ion exchange rate, k_2, and the correlation time, τ_c, can be determined. Thus halide ion probes are useful in obtaining two important characteristics about the binding site,

namely the rigidity of the binding site as reflected by τ_c and access to the binding site as reflected by k_2.

Fluorescence spectroscopy and halide-ion (n.m.r.) spectroscopy appear to offer a desirable combination as probes of metal/protein interactions. Fluorescence spectroscopy provides good sensitivity for the detection of such interactions and some information about the binding site, while halide-ion n.m.r. provides additional information about the environment of the binding site.

EXPERIMENTAL

Reagents

Bovine serum albumin (BSA), fraction V, was obtained from General Biochemical. Hen egg conalbumin (Type I), ovalbumin (Grade V), lysozyme (Grade I), insulin, alkaline phosphatase (Type 5), papain and α-chymotrypsin were all obtained from Sigma Chemical Co. Reagent-grade metal salts as chlorides or sulfates were used to prepare 20 mM stock solutions. A stock solution of methylmercury(II) chloride (Apache Chemicals) was prepared by dissolving the salt in 1 M perchloric acid. A *p*-hydroxymercuribenzoate (PMB; Sigma) stock solution was prepared by dissolving the solid in 1 M sodium hydroxide and determining the concentration by measuring the absorbance at 230 nm. All protein and metal ion solutions were prepared with deionized water and used without further purification.

Stock buffer solutions of pH 4.0—5.7 were prepared from acetic acid and sodium acetate. Buffers in the range 6.0—8.5 were prepared from monobasic and dibasic sodium phosphate while those in the pH range 8.7—10 were prepared from sodium carbonate and sodium hydrogencarbonate. Occasionally, tris(hydroxymethyl)aminoethane (Tris) and *N*,*N*-2-hydroxyethylpiperazine-*N'*-2-ethane sulfonic acid (HEPES) were used to study buffer effects. All stock buffer solutions were 0.2 M.

Apparatus

Relative fluorescence intensities and spectra were measured with an Aminco-Bowman spectrofluorimeter equipped with a ratio photometer attachment. The excitation slit width was 1 mm and the emission slit width was 2 mm for all measurements. Excitation and emission monochromators were calibrated by utilizing the fluorimetric standard quinine sulfate. A Corning Model 7 pH meter equipped with either a Fischer combination electrode or combination microelectrode was used for pH measurements.

Chlorine-35 magnetic resonance spectra were obtained at 9.75 MHz on a JEOL PFT-100 spectrometer equipped with a PG-100 pulse programmer. The 90° pulse width was 30 μs and 4K of memory were used in acquiring the spectra. The sample tube was 10 mm in diameter with a 5-mm insert containing D_2O for locking.

Bromine-81 magnetic resonance spectra were obtained on the same spectrometer at 9.75 MHz. The magnetic field was lowered to 8.5 kG. No

locking signal was employed, but field stabilization was utilized. Because of the large line widths involved, magnetic field drift was expected to contribute only slightly to the overall line width. The 90° pulse width for bromine-81 was 12 μs.

Procedures

Fluorescence quenching experiments were done on 5 μM protein solutions. The excitation wavelength was 280 nm and the emission wavelength was 355 nm. Varying amounts of metal ion were added by means of a Gilmont microburet such that the increase in volume was less than 5%. Protein concentrations were determined spectrophotometrically.

Fluorimetric pH titrations of metal/protein complexes were made by adding sodium hydroxide with a microburet to the solutions with an initial pH of 2.0. Volume changes were less than 5% so no correction was made in relative fluorescence for dilution. The reversibility of the system was tested by adding 1 M hydrochloric acid at the end of the titration.

Chlorine-35 and bromine-81 line-broadening experiments were done on solutions containing 10 μM protein and 100 mM halide ion. Metal ions were added by means of a Gilmont microburet as in the fluorescence studies. The pH dependence of the line width was evaluated on these solutions by the procedure described above for fluorescence.

Halide exchange rates and correlation time measurements were done at several metal/protein mole ratios with varying halide ion concentrations. All studies were conducted at pH 7.0 in 10 mM phosphate buffer.

RESULTS AND DISCUSSION

Fluorescence experiments

Metal ions such as copper(II) and mercury(II) have been shown to be very effective quenchers of proteins at all values of pH while ions such as Ni(II), Co(II), Fe(II), Ag(I), and Cr(III) exhibit some quenching effects in the alkaline and neutral pH ranges. Table 1 gives some representative results of fluorescence changes when mercury(II) and copper(II) are added to protein

TABLE 1

Relative fluorescence intensities[a] of proteins[b] in the presence of metal ions

Metal[c]	Relative fluorescence intensity					
	BSA	Lysozyme	Ovalbumin	Conalbumin	Insulin[d]	Papain[d]
Hg(II)	55	52	32	88	48	74
Cu(II)	76	90	93	90	32	75

[a]Normalized to an intensity of 100 in the absence of metal ion. [b]Protein concentrations are 5 μM, pH 7. [c]Metal ion concentrations are 4.0×10^{-5} M. [d]Metal ion concentrations are 5.0×10^{-5} M for papain and insulin.

solutions. This study will concentrate on mercury/protein systems which provide the best and most numerous examples for elucidating the advantages of these two techniques in combination.

The pH dependence of the fluorescence of mercury complexes with BSA, lysozyme, ovalbumin, conalbumin, papain, and insulin was studied. Figure 1 shows some typical examples of these studies. Although the interpretation of these data is complicated by the uncertain relationship between the binding site and tryptophan residues, hydrolysis of metal ions, and complications arising from the use of buffers, some general observations can be made. Abrupt fluctuations can occur at buffer transitions that probably reflect competition between protein and buffer for the metal ions. In general, the pH dependence of the protein itself follows a general pattern. Fluorescence increases initially as the pH is raised from the lowest value to a maximum near neutral pH. Then there is a decrease as the pH is raised further. This latter decrease may be due to a lowering of the quantum yield as energy is transferred to ionized tyrosine residues.

The pH/fluorescence profile of a mercury/protein complex varies considerably because every protein has many potential binding sites. In the case of ovalbumin, ions of mercury, *p*-hydroxymercuribenzoate (PMB) and methylmercury bind to one or more of the free sulfhydryl groups present. At low pH values, mercury combines quite selectively with sulfhydryl groups and shows maximum quenching in the acidic region. The higher pH regions are probably dominated by the formation of hydroxy complexes. For BSA, which has one free sulfhydryl and seventeen disulfide bonds, even the organomercurials still exhibit maximum quenching at low pH values. Mercury(II) shows strongest quenching at a pH of about 7.5. This corresponds to the pK_a of the

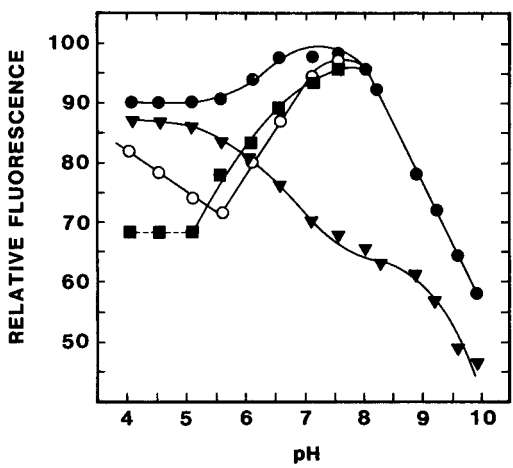

Fig. 1. Relative fluorescence vs. pH of: (•) 9.3 μM lysozyme; 9.3 μM lysozyme in the presence of (▾) 20 μM Hg(II), (○) 74 μM methylmercury; (▪) 74 μM PMB.

imidazole proton, indicating histidine which has been suggested in previous studies [20—22] as a potential binding site. In the absence of free sulfhydryl groups in the proteins lysozyme and conalbumin, mercury(II) exhibits significant quenching over a wide pH range with a maximum occurring at about 7.5. The organomercurials are more efficient quenchers in the acidic region with the formation of hydroxy complexes favored at higher pH values.

Figure 2 shows the relative mole ratios of several metal ions to ovalbumin. At pH 4.1, a 2:1 ratio is obtained for mercury(II) and PMB while methylmercury gives a 3:1 ratio. Spectrophotometrically, Boyer [23] found three sulfhydryl groups in ovalbumin. However Chen [9] only detected the binding of two PMBs per ovalbumin. At pH 7.1, a ratio of 3:1 is obtained for mercury(II) while at pH 9.0 a ratio of 4:1 is obtained. This latter value is consistent with another study [24] that detected four sulfhydryl groups per ovalbumin. The variation in the number of binding sites determined by fluorescence studies may be due to small conformational changes that affect the accessibility of the site, changes in quantum efficiency, and binding to sites other than sulfhydryl groups in ovalbumin.

Insulin exhibits the same variation in the number of binding sites. Figure 3 shows the mercury(II)- and copper(II)-binding curves at pH 8. Both have relatively sharp breaks which indicate two copper(II) per molecule and three mercury(II) per molecule. This difference may be due to the ability of mercury(II) to break a disulfide bond.

The quenching curves for lysozyme, BSA, conalbumin and alkaline phosphatase show considerable rounding and no stoichiometry of mercury binding can be determined. Papain and α-chymotrypsin show relatively little fluorescence quenching in the presence of mercury(II) except at very large excesses of metal ion.

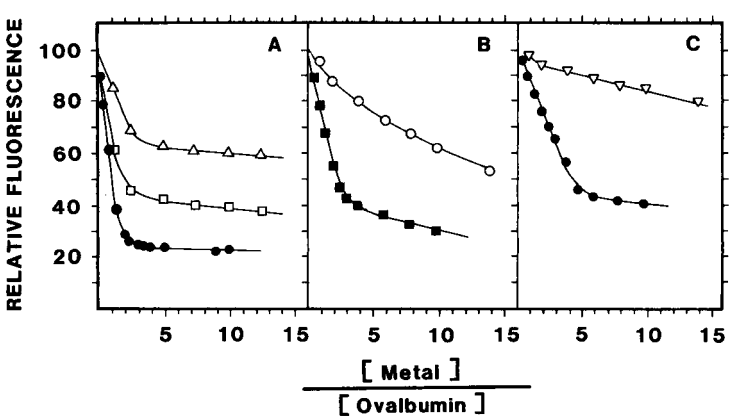

Fig. 2. Relative fluorescence vs. mole ratio of metal ion to ovalbumin (5.1 μM). (A) pH 4.1: (△) methylmercury; (□) PMB; (●) Hg(II). (B) pH 7.1: (○) Cu(II); (■) Hg(II). (C) pH 9.0: (▽) Cu(II); (●) Hg(II).

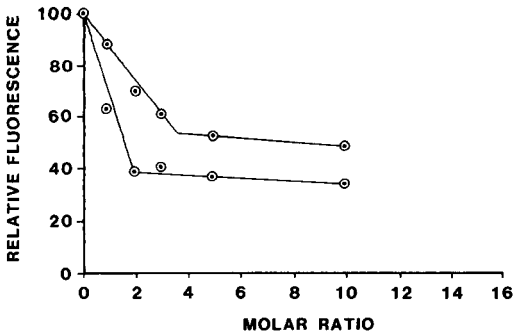

Fig. 3. Relative fluorescence of insulin vs. the mole ratio of copper(II)/insulin (top line) and mercury(II)/insulin (bottom line).

The above examples show that utilization of the native fluorescence of proteins can be useful in obtaining information about mercury/protein systems. The general ability of the protein to bind the metal can be detected and in some cases a metal/protein ratio can be determined. The behavior of the metal/protein complex as a function of pH can also be monitored. The unique feature of the fluorescence experiments is that the binding of metals to proteins can be detected in some systems at protein concentrations of 10^{-7} M. Even with the limitations discussed previously, there is the potential to study other aspects of metal/protein systems such as monitoring the kinetics of any process involving a metal bound to a protein. The relatively low detection limits of fluorescence spectroscopy will be important in such measurements because most of the kinetic processes which might be studied are second order. Therefore, the ability to work at low concentrations makes possible the study of reactions with very large second-order rate constants. In addition, because quenching is generally dominated by the through-space Forster mechanism, small conformational changes which might occur at the binding site during a metalloenzyme reaction and that alter the distance between the metal and the fluorescing amino acid could be detected.

Halide-ion nuclear magnetic resonance

The line width of the ^{35}Cl resonance in 0.1 M sodium chloride is about 16 Hz and is independent of pH. The ^{35}Cl line width is broadened slightly in the presence of lysozyme, insulin, papain, α-chymotrypsin and alkaline phosphatase and significantly in the presence of BSA and conalbumin. Broadening by the latter two proteins is probably due to anion binding at sites such as the protonated imadazole of histidine, the α-amino group of lysine, or the guanidyl sidechain of arginine.

Mercury(II) and PMB in the presence of lysozyme, BSA, conalbumin, papain, insulin, α-chymotrypsin, and alkaline phosphatase resulted in significant broadening of the ^{35}Cl line width. Methylmercury produced significant line broadening with all of the above proteins except α-chymotrypsin and

alkaline phosphatase which exhibited only slight line broadening. All of the mercury species produced only slight line broadening in the presence of ovalbumin. It has already been proposed [25] that mercury binds to sites on ovalbumin at which exchange cannot easily occur. This is consistent with the fluorescence data reported above which indicates strong binding of mercury-(II) to ovalbumin. It is only by combination of these techniques that it can be established that there is strong binding of mercury (by fluorescence quenching) at a site that is sterically crowded (no chlorine-35 line broadening because of the reduction of the halide exchange rate).

Figure 4 shows a typical plot of the chlorine-35 line width as a function of pH for the mercury/insulin complex. There is usually a maximum in the pH range 5—8 for most mercury/protein complexes. The exact location depends on the number of free sulfhydryl groups in the protein and the metal/protein ratio. In general, it can be assumed that metal binding is influenced by proton competition at low pH values and that chloride displacement by hydroxide occurs at high pH values. Both effects will cause the ^{35}Cl line width to decrease as observed. Although these plots are similar in shape to those obtained for fluorescence studies of mercury/protein complexes, the causes are somewhat different and usually more easily explained in the n.m.r. studies.

Figure 5 shows a plot of the ^{35}Cl line width as a function of molar ratio for the mercury(II)/papain system. This plot is analogous to those described in the fluorescence section. Extrapolation of the linear portion of each curve permits the determination of the number of metal ions bound per protein. In the case of papain, there are six binding sites for mercury(II) at pH 7.1. For conalbumin at pH 4.0, there are two binding sites for mercury(II). The number of binding sites found will depend on three factors. First, the type of metal ion is important. The metal ion must have both an affinity for chloride as well as binding sites on the protein. Mercury(II) is a particularly good choice because it exhibits a strong affinity for halide ions. In the case of many weak binding sites on a protein, the mole-ratio curve will increase with no definite break, as in the case of methylmercury with all of the

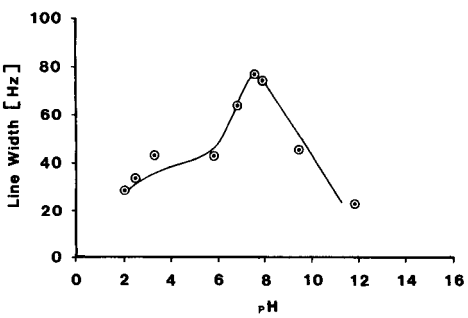

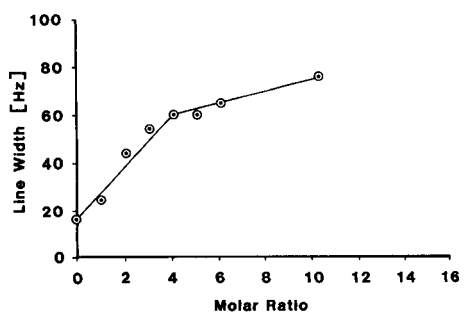

Fig. 4. ^{35}Cl line width of 8:1 mercury(II)/insulin complex vs. pH.

Fig. 5. ^{35}Cl line width vs. the molar ratio of mercury(II)/papain.

proteins studied at pH 7.1 and above. As has already been observed in the fluorescence studies, mole-ratio plots show that the number of binding sites will vary with different metal ions and that there is significant rounding caused by weak binding. Second, the pH is also crucial. At low pH values there are fewer binding sites because of proton competition. In most of the proteins studied, the number of binding sites increases with pH. This may be the result of less proton competition as well as a conformational change in the protein which could make more binding sites available. Third, the halide ion concentration in some cases may be important. An example of such a case is the mercury(II)/lysozyme system shown in Fig. 6. The stoichiometry of this complex can be determined at concentrations of halide between 0.25 and 1.0 M chloride but not at lower concentrations. A similar plot, with sodium bromide instead of chloride, shows the same 4:1 mercury/lysozyme ratio. It is interesting to note that lysozyme has four disulfide bonds. Therefore the stoichiometry of the complex might be explained in the following manner

$$R{-}S{-}S{-}R' + Hg(II) \rightleftharpoons \left[\begin{array}{c} R{-}S{-}S{-}R' \\ \diagdown\ \diagup \\ Hg \end{array}\right]^{2+}$$

Such an intermediate has been proposed in the hydrolytic splitting of disulfide bonds by mercury(II) and silver(I) in alkaline media [26]. Evidence of binding of mercury(II) to disulfide linkages is supported by the difference spectrum which shows absorption resulting from the formation of mercaptide bonds. It should be noted that the stoichiometry of the mercury/lysozyme complex as determined by both the fluorescence and n.m.r. studies is identical.

The unusual aspect of the n.m.r. studies is that information about the environment around the binding site can be obtained. Figure 7 shows a typical plot for the dependence of α^{-1} on the sodium halide concentration. The value of α^{-1} was calculated using Eqn. 3. The values of τ_c, k_2, and T_{1B} were obtained from a least-squares analysis of the data from the plot of R_2 vs. the mole ratio of metal to protein. Error limits represent one standard deviation. Correlation times were calculated by assuming a ^{81}Br coupling constant of 320 MHz and a ^{35}Cl coupling constant of 40 MHz. Table 2 summarizes the results of several mercury/protein systems with both bromide and chloride probes being used in two cases. The correlation times and exchange rates for the tetrahalide complexes of mercury are included for comparison [25]. It has been proposed [25] that the ^{81}Br probe is more sensitive to conformational changes in the protein because of the faster exchange rate of the bromide nuclei. The present study indicates that the ^{81}Br probe results in shorter correlation times and faster free-to-bound exchange rates than the corresponding chloride probe.

Analysis of the slopes after the end point are summarized in Table 3. The end point corresponds to a decrease in slope as the relatively long τ_c values

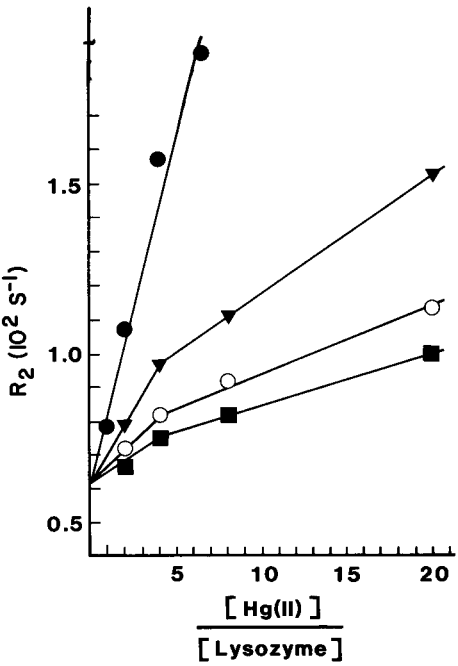

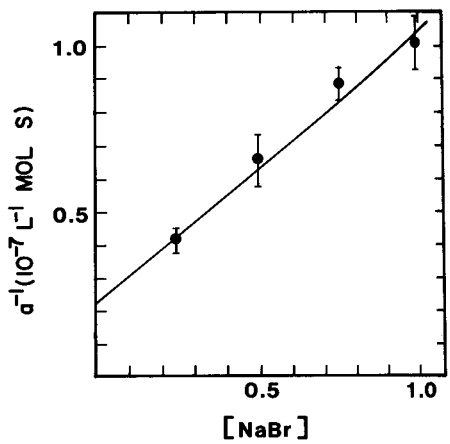

Fig. 6. Transverse decay rate, R_2 (s^{-1}) vs. the ratio of Hg(II) concentration to the concentration of lysozyme (9.2 μM) at pH 7.0 and various NaCl concentrations: (•) 0.10 M; (▾) 0.25 M; (○) 0.50 M; (▪) 1.0 M.

Fig. 7. α^{-1} (l^{-1} mol s^{-1}) vs. NaBr concentration for lysozyme. Bars represent the error of the individual values of α and the line represents the least squares fit to the data.

TABLE 2

Experimental values of τ_c, k_2 and T_{1B}

	Halide ion	τ_c (10^{-10} s)	k_2 (10^7 mol^{-1} s^{-1})	T_{1B} (10^{-8} s)
BSA	^{81}Br	0.44 ± 0.13	6.7 ± 4.9	5.6 ± 1.6
	^{35}Cl	1.6 ± 0.6	3.4 ± 10	97 ± 10
Lysozyme	^{81}Br	0.30 ± 0.07	4.5 ± 2.2	8.3 ± 1.8
	^{35}Cl	0.56 ± 0.22	3.2 ± 0.7	280 ± 11
$HgBr_4^{2-}$		0.036	4	69
$HgCl_4^{2-}$		0.079	1	2000

associated with the protein-bound halide change to the shorter correlation times for the tetrahalo complexes. Because the correlation times measured are longer than those expected for the tetrahalo complexes, it appears that secondary (weak) binding sites are available. The presence of additional weak

TABLE 3

Experimental values of τ_c after the end point

	Halide ion	τ_c (10^{-12} s)
BSA	^{81}Br	13
	^{35}Cl	5.8
Lysozyme	^{81}Br	6.4
	^{35}Cl	39
$HgBr_4^{2-}$		3.6
$HgCl_4^{2-}$		7.9

binding sites on these proteins has been confirmed in the fluorescence mole-ratio studies.

The ^{35}Cl and ^{81}Br studies measured correlation times of approximately 5×10^{-11} s. Correlation times for both lysozyme and BSA have been measured by fluorescence polarization studies. Weber [27] used 1-dimethylaminopthalene-5-sulfonyl chloride to measure a rotational correlation time of 127 ns for BSA. Measurements with fluorescein isothiocyanate gave a correlation time of 25 ns for lysozyme [28]. Because the correlation times obtained by the ^{35}Cl and ^{81}Br n.m.r. methods are shorter by 2—3 orders of magnitude than those measured by fluorescence depolarization, the τ_c in the present study reflects motion at the metal-binding site rather than motion of the entire molecule.

The halide exchange rates, k_2, of the protein-bound mercury(II) are close to the exchange rates for the tetrahalo complexes; the latter rates approaching the theoretical diffusion limit. The magnitude of k_2 should reflect the environment around the binding site including such factors as steric effects, electrostatic effects, and accessibility of the binding site. The halide exchange rates determined in the present study would indicate that the mercury(II)-binding sites examined, with the exception of ovalbumin, are quite accessible to halide ions and quite possibly to other molecules in solution.

In conclusion, the use of fluorescence spectroscopy and halide-ion n.m.r. spectroscopy appears to be an effective combination for the study of metal/protein systems. Fluorescence spectroscopy provides high sensitivity for detecting binding to proteins without the use of an external probe to perturb the system. In addition, fluorescence spectroscopy can also provide valuable information about the stoichiometry and the pH behavior of metal/protein complexes and has the potential to gather kinetic information about reactions involving metal/protein systems. The use of the Fourier transform technique has made halide-ion n.m.r. a more useful tool for the study of these systems. Halide-ion n.m.r. spectroscopy can be most effectively used to provide information about metal-binding sites. The local motion of the binding site can be determined from the τ_c values and the accessibility of the binding site

can be determined from the halide exchange rates. The combination of these two techniques provides both complementary and confirmatory information about metal/protein interactions and appears to be a useful alternative for studying such systems.

One of the authors (J. J. P.) acknowledges a University Foundation Research Grant for partial support of this work.

REFERENCES

1 V. G. Shore and A. B. Pardee, Arch. Biochem. Biophys., 60 (1956) 100.
2 S. Udenfriend, Fluorescence Assay in Biology and Medicine, Academic Press, New York, 1969.
3 S. Udenfriend, Fluorescence Assay in Biology and Medicine, Vol. II, Academic Press, New York, 1969.
4 G. G. Guilbault, Practical Fluorescence, M. Dekker, New York, 1973.
5 K. S. Rogers, Enzymologia, 36 (1969) 153.
6 K. S. Rogers, Enzymologia, 37 (1969) 174.
7 T. Forster, Fluoreszenz Organischer Verbindugen, Vandenboeck and Rupprecht, Gottingen, 1951.
8 R. F. Chen, Arch. Biochem. Biophys., 158 (1973) 605.
9 R. F. Chen, Arch. Biochem. Biophys., 142 (1971) 552.
10 R. F. Chen, Arch. Biochem. Biophys., 166 (1975) 584.
11 R. F. Chen, Fluoresc. News, 9 (1975) 9.
12 S. S. Lehrer, J. Biol. Chem., 244 (1969) 3613.
13 C. Helene, F. Brun and M. Yaniv, J. Mol. Biol., 58 (1971) 349.
14 R. T. Kuczenski and C. H. Suelter, Biochemistry, 10 (1971) 2862.
15 T. R. Stengle and J. D. Baldeschwieler, Proc. Natl. Acad. Sci. U.S., 55 (1967) 1020.
16 T. R. Stengle and J. D. Baldeschwieler, J. Am. Chem. Soc., 89 (1967) 3045.
17 W. D. Ellis, H. B. Dunford and J. S. Martin, Can. J. Biochem., 47 (1969) 157.
18 R. G. Bryant, J. Am. Chem. Soc., 91 (1969) 976.
19 J. L. Sudmeier and J. J. Pesek, Anal. Biochem., 41 (1971) 39.
20 M. S. Rao and H. Lal, J. Am. Chem. Soc., 80 (1958) 3222.
21 H. Holeysovska, Collect. Czech. Chem. Commun., 26 (1961) 3074.
22 I. M. Kolthoff, W. Stricks and L. Morren, Anal. Chem., 26 (1954) 366.
23 P. D. Boyer, J. Am. Chem. Soc., 76 (1954) 4331.
24 R. Cecil and J. R. McPhee, Biochem. J., 66 (1957) 538.
25 T. R. Collins, Z. Starcule, A. H. Burr and E. J. Wells, J. Am. Chem. Soc., 95 (1973) 1649.
26 I. M. Klotz and B. J. Campbell, Arch. Biochem. Biophys., 80 (1962) 96.
27 G. Weber, Biochem. J., 51 (1952) 155.
28 R. Irwin and J. E. Churchich, J. Biol. Chem., 246 (1971) 5329.

Analytica Chimica Acta, 170 (1985) 199—207
Elsevier Science Publishers B.V., Amsterdam — Printed in The Netherlands

DETERMINATION OF CHOLESTEROL WITH A MICROPOROUS MEMBRANE CHEMILUMINESCENCE CELL WITH CHOLESTEROL OXIDASE IN SOLUTION

NATHAN L. MALAVOLTI, DAVID PILOSOF[a] and TIMOTHY A. NIEMAN*
School of Chemical Sciences, University of Illinois, Urbana, IL 61801 (U.S.A.)
(Received 12th October 1983)

SUMMARY

A reagent solution, containing cholesterol oxidase buffered at pH 7, is contained in a pressurized reservoir and forced through a microporous membrane at 2—5 μl min^{-1} into a stream flowing at 2—10 ml min^{-1} which contains injected slugs of cholesterol as the analyte. The hydrogen peroxide produced then reacts with luminol in pH 9.0 Tris buffer, catalyzed by horseradish peroxidase, to produce chemiluminescence, the intensity of which is related to the cholesterol concentration. The working range is 0.4—40 mg dl^{-1}; precision is 1—4% over this range. The detection limit is 0.2 mg dl^{-1} or 5 μM. Sample throughput is 60 h^{-1}, and only 0.01 unit of enzyme is consumed per sample. Blood serum samples may be analyzed for either free or total cholesterol by using standard addition and pre-treatment with Somogyi reagents for removal of reducing species.

Cholesterol assay plays a significant role as a diagnostic tool for a number of diseases. The normal range of serum total cholesterol in adults varies from 100 to 400 mg dl^{-1}, and is affected by the age, sex and diet of the individual [1]. Several nonenzymatic methods have been used extensively for routine cholesterol assay [1, 2], but because of the many advantages provided by enzymatic methods, most current assays utilize cholesterol oxidase (E.C. 1.1.3.6) in conjunction with cholesterol esterase (E.C. 3.1.1.13) [2—4]. Although cholesterol esters can be hydrolyzed in strong base, the enzymatic approach with cholesterol esterase is faster and eliminates the need to use corrosive chemicals. The reaction between cholesterol and cholesterol oxidase produces hydrogen peroxide. The peroxide can then be determined by absorption, fluorescence, electrochemical or chemiluminescence methods.

Chemiluminescence has been widely used analytically because of its high sensitivity, extended dynamic range, and inexpensive instrumentation [5]. However, because of the intrinsic lack of selectivity of many chemiluminescent reactions, the most successful determinations couple the sensitivity of the chemiluminescence measurement with a step that provides a high degree

[a]Present address: Procter and Gamble Co., Sharon Woods Technical Center, 11511 Reed Hartman Highway, Cincinnati, OH 45241 U.S.A.

0003-2670/85/$03.30

of selectivity, such as an enzyme reaction. Chemiluminescent determinations of enzymatically generated hydrogen peroxide have been reported for a variety of substrates [5—7].

The use of microporous membrane flow cells for chemiluminescent determinations was reported earlier [8—12]. In this method, the reagent solution contained in a pressurized reservoir is forced to flow through a microporous membrane (at a few μl min^{-1}) into a stream carrying an injected analyte slug, continuously flowing at a few ml min^{-1}. This flow rate ratio creates an efficient dilution which minimizes reagent consumption, avoids significant sample contamination, and produces the emission in a region localized close to the surface of the membrane [9—11]. The technique is simple and inexpensive to use. In addition, when used in combination with an enzymatic reaction in which hydrogen peroxide is generated, the microporous membrane flow cell can create a stable pH gradient in which both reactions (the enzymatic reaction generating the hydrogen peroxide and the chemiluminescent reaction detecting the hydrogen peroxide) can proceed under their optimum conditions [10, 11]. The general scheme is indicated in Fig. 1. Previous papers reported on such a method for determination of glucose [10, 11]. In the present paper, this technique is extended to the determination of cholesterol in both aqueous-micellar cholesterol standards and in actual blood serum samples.

EXPERIMENTAL

Apparatus

The microporous membrane flow system and instrumentation for measurement of chemiluminescent emission intensities were the same as that de-

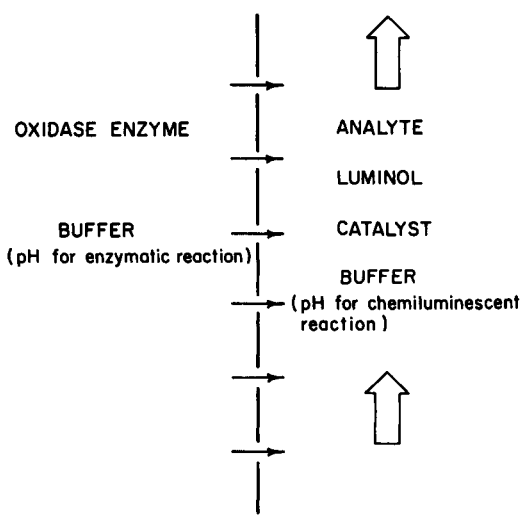

Fig. 1. Schematic diagram of microporous membrane flow cell. The left side is the reagent chamber, the right side is the analyte flow stream, and the dashed line is the membrane.

scribed earlier [10, 11]. The 110-μl analyte chamber of the flow cell is separated from a 1-ml reagent reservoir by a 1-cm^2 microporous membrane (Nylon-66 with 0.2-μm pores; Rainin). The flow rate of reagent through the membrane was typically 2—5 μl min^{-1} (Sage 355 syringe pump). The flow rate in the analyte channel was 2—10 ml min^{-1} (Rainin peristaltic pump), and 1-ml sample volumes were injected (Rheodyne 5020 low-pressure teflon injection valve).

Reagents

Cholesterol oxidase (E.C. 1.1.3.6) and cholesterol esterase (E.C. 3.1.1.13) were obtained as powders, readily soluble in water or aqueous buffers (Sigma Chemical Co.). The cholesterol oxidase was from *Pseudomonas* species, and the optimal pH has been reported as 7.0 with a 0.1 M phosphate buffer solution [13]. Cholesterol oxidase solutions (0.3 mg ml^{-1}; 2 units ml^{-1}) were prepared in the buffer described above. For cholesterol oxidase, one unit converts 1 μmol of cholesterol to 4-cholesten-3-one per minute at pH 7.5 at 25° C. The cholesterol esterase was from bovine pancreas, and the optimal pH for hydrolysis of cholesterol esters has been reported as 6.6 with 0.154 M phosphate buffer [14]. A cholesterol esterase stock solution was prepared by dissolving the solid enzyme in 0.1 M phosphate buffer at pH 6.6 to obtain an activity of 5 units ml^{-1}. For cholesterol esterase, one unit will hydrolyze 1 μmol of cholesteryl oleate to cholesterol and oleic acid per minute at pH 7.0 and 37°C in the presence of taurocholate.

Luminol (Aldrich), cholesterol (Aldrich), water-soluble polyethoxyethanyl-cholesteryl adipate (Sigma), Triton X-100 (Sigma), tris(hydroxymethyl)-aminomethane (Tris; Sigma), sodium cholate (Sigma), and other chemicals were reagent-grade and were used without further purification. The horseradish peroxidase (HRP; E.C. 1.11.1.7) was obtained from Sigma as type I with a specific activity of 100 000 units g^{-1}. The peroxidase reagent was buffered with a 0.2 M Tris buffer at pH 9.0. The control serum standards (American Dade) were Monitrol ES Level I Chemistry Control, (Lot No. LTS-16) and the listed assay values were from 215 to 269 mg dl^{-1} total cholesterol. All solutions were prepared with water from a Continental/Millipore Milli-Q reagent-grade system.

Cholesterol aqueous standards

A problem associated with the determination of cholesterol in aqueous solution is its limited solubility. In the method proposed by Richmond [4] Triton X-100 is added to provide water solubility. In a simplification of this procedure, solid cholesterol was added to a hot measured amount of Triton X-100 while the solution was agitated in an ultrasonic bath. By adding hot water to volume, the highest concentration obtained was 400 mg dl^{-1} in 10% (v/v) Triton X-100. Cholesterol precipitation was observed after several days of standing at 4°C, but the white solid redissolved on gentle heating and ultrasonic vibration.

A water-soluble cholesterol derivative, polyethoxyethanyl-cholesteryl adipate (Sigma) is based on a synthesis reported by Proksch and Bonderman [15]. This derivative is prepared by esterifying cholesterol with adipic acid; the cholesterol hemiadipate formed is then treated with polyethylene glycol. This product reacts quantitatively in most total cholesterol assays, including the present one and other enzymatic procedures [15]. However, because standards prepared from this cholesterol ester would have to be hydrolyzed to yield free cholesterol, it seemed simpler to use the micellar standards instead. These micellar standards gave good results, suggesting no real need for the water-soluble derivative.

The necessary reagents for the chemiluminescent reaction were added to each of the cholesterol analyte solutions prior to injection. The reagent concentrations used were: 1×10^{-3} M luminol, 0.040 mg ml^{-1} HRP, and 0.2 M Tris at pH 9.0. In order to insure similar chemical and physical properties for all cholesterol analyte solutions prepared by dilution from stock solution containing Triton X-100, sufficient Triton X-100 was added to all solutions to make them 2.5% (v/v) in the surfactant.

Procedure for serum

Cholesterol, both free and esterified, is maintained in solution in blood serum by micellar association with phospholipids, proteins, and triglycerides. In this procedure, the surfactant Triton X-100 fulfils a dual role by disrupting serum lipoprotein complexes and by holding the free cholesterol thus released in micellar solution in a form suitable for enzymatic oxidation. The reaction scheme is given below.

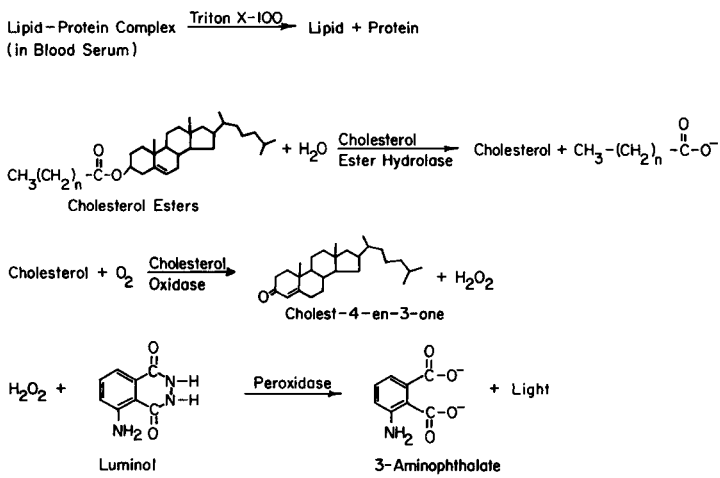

A 1.50-ml aliquot of the raw serum was added to 1.0 ml of 25% (v/v) Triton X-100 and agitated for 10 min to insure complete breakdown of the lipoprotein complexes. When total cholesterol was assayed, the treated serum sample was then added to 0.5 units of cholesterol esterase from the 5 unit ml^{-1}

stock solution and 6 mM sodium cholate, which is required for efficient hydrolysis of cholesterol esters by cholesterol esterase [3]. This mixture was incubated at 37°C for 60 min, although 15 min has been reported [16] as satisfactory for the complete conversion of cholesterol esters to free cholesterol with this concentration of cholesterol esterase. Otani et al. [17] found the optimum concentration for sodium cholate to be 4—8 mM; 6 mM cholate was used here. After the sample mixture had been incubated, it was deproteinated with equimolar portions of barium hydroxide and zinc sulfate (0.1 M in each case) to form the Somogyi precipitate. From this 10-ml volume, which was then centrifuged for 30 min, 5 ml of the centrifugate was diluted with 5 ml of the chemiluminescence reagents and enough Triton X-100 to make the final sample 2.5% (v/v) in the surfactant, uniform with the cholesterol standards. When only free cholesterol was to be assayed, the addition of cholesterol esterase and sodium cholate plus subsequent incubation was not done, but the remaining procedure was the same.

RESULTS AND DISCUSSION

Results for micellar cholesterol standards

Chemiluminescent response was measured for cholesterol concentrations of 0.4—40 mg dl^{-1} (10^{-5}—10^{-3} M) prepared from the surfactant-containing stock. Signals obtained for triplicate injections of 2 mg dl^{-1} and 30 mg dl^{-1} cholesterol are shown in Fig. 2 (A and B). The peak shape for these standards is similar to that seen for glucose [10, 11]; the decay to baseline is fast, and the width at half-maximum is 25 s; samples may be injected at 1-min intervals.

Figure 3 shows a calibration graph for the cholesterol standards mentioned above. The plot is linear (on a log-log scale) over the entire range of 0.4—40 mg dl^{-1}. Precision in this region ranged from 0.68% to 3.69% relative

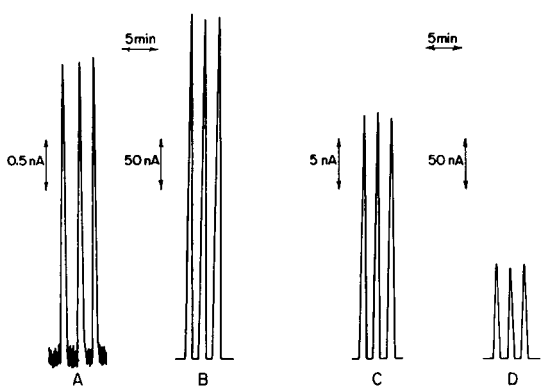

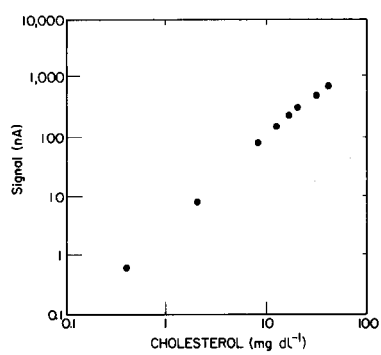

Fig. 2. Typical chemiluminescent signals: (A) 2 mg dl^{-1} standard; (B) 30 mg dl^{-1} standard; (C) serum sample for free cholesterol; (D) serum sample for total cholesterol.

Fig. 3. Calibration plot for cholesterol standards in 2.5% (v/v) Triton X-100.

standard deviation (r.s.d.) with an average of 2.04%; this is comparable to most assays using flow-injection systems. The slope of the working curve, 1.58 ± 0.03 (correlation coefficient = 0.999), is only slightly higher than that observed for glucose determinations with glucose oxidase also with HRP as the catalyst for the luminol luminescence reaction [11]. The emission intensities observed here for cholesterol are similar to those noted for glucose (with the appropriate enzymes in each case and in the continuous flow mode) and yield a detection limit of 0.2 mg dl^{-1} (ca. 5 μM). The dynamic range is more than adequate for clinical samples in which cholesterol only varies over a four-fold concentration range, and the detection limit is low enough to allow a serum sample to be diluted by a factor of 100. Because of the higher cost of cholesterol oxidase, only 2 units ml^{-1} was used for this work as opposed to 290 units ml^{-1} glucose oxidase employed in the glucose studies. Thus, if lower cholesterol detection limits were needed, they could be obtained by using higher enzyme concentrations at proportionately higher cost.

Application to blood serum samples

Initial efforts to apply the method to blood sera involved no sample pretreatment, but merely dilution of the serum sample with the chemiluminescence reagents and adequate Triton X-100. However, no emission signals were observed (for samples diluted 2—10 fold). Seitz [7] stated that reducing components in biological samples may consume hydrogen peroxide before it can react with luminol, and thus cause reduced chemiluminescence intensity. Bostick and Hercules [18, 19] used the Somogyi precipitate obtained by adding equimolar portions of barium hydroxide and zinc sulfate to remove practically all reducing substances (primarily uric acid) from blood. Williams et al. [20] later used this deproteination method on urine samples for the same reason. In each case, the luminol/H_2O_2 system was used with hexacyanoferrate(III) catalyst to quantify glucose. To examine possible interference from uric acid, a cholesterol standard without any uric acid and that same standard containing 5 mg dl^{-1} of uric acid (the approximate level present in blood sera) was injected and the emission intensity was observed. The uric acid completely eliminated the emission from the cholesterol sample. Bostick and Hercules [19] showed that luminol chemiluminescence is affected by as little as 0.001 mg dl^{-1} uric acid. Thus, serum samples would have to be diluted by a factor of 10^4 before uric acid would have no effect on this procedure, but such dilutions would reduce the cholesterol concentration below the detection limit of the technique. Thus the Somogyi treatment seems necessary to remove at least the uric acid interference.

Before the procedure described under Experimental was chosen, other deproteination methods were investigated. First, deproteination with trichloroacetic acid and subsequent centrifugation, similar to the procedure described previously for glucose [10], was examined; the centrifugate was treated with cholesterol esterase and sodium cholate to hydrolyze the cholesterol esters to free cholesterol and the overall dilution before injection was 20-fold. The

second method was the use of the Centrifree Micropartition system (Amicon Corp., Danvers, MA) in which a protein-free filtrate is obtained by filtration of a sample through an anisotropic, hydrophilic YMT ultrafiltration membrane driven by centrifugation at 1000—2000*g*. This filtrate (after incubation with the hydrolyzing reagents) was added to the chemiluminescence reagents with a 10-fold dilution before injection. The sample was a control serum (Monitrol ES Level I), and both methods were used to analyze it for total cholesterol. The trichloroacetic acid procedure yielded a cholesterol concentration that was 134% of the theoretical value, while the ultrafiltration scheme gave a value only 3.7% of that expected. (The theoretical value taken for the total cholesterol assay of Monitrol ES Level I was 238 mg dl^{-1} which is the average of the results for 12 enzymatic methods listed by the manufacturer ranging from 215 to 260 mg dl^{-1}. The theoretical value for the free cholesterol assay was obtained by multiplying 238 by 0.3 to yield 71.4 mg dl^{-1}, as Bertrand et al. [21] stated that free cholesterol represents 20—40% of total cholesterol. The widest acceptable range of free cholesterol in this control serum is 43—104 mg dl^{-1}.) As both of these deproteination methods seemed to have inherent problems, it was decided to concentrate on the Somogyi treatment.

The Somogyi procedure was tried on the same control serum sample for determination of both free and total cholesterol. The emission signals recorded for triplicate injections of each treated sample are shown in Fig. 2 (C and D). The peak shapes are not significantly different from those of the cholesterol standards (A and B). Precision was 1.07% and 2.86% r.s.d. for the free and total cholesterol injections, respectively, which were both in the range mentioned above for the micellar standards. However, when the observed emission intensities were inserted into the least-squares equation for the calibration graph (Fig. 3), the corresponding cholesterol concentrations were 72.7% and 50.9% of the theoretical values for the free and total cholesterol assays, respectively.

As the serum seemed to be still causing adverse effects on the chemiluminescent signals, the standard addition method was used to determine the unknown concentration. For the free cholesterol assay, spikes of 5 and 10 mg dl^{-1} from the surfactant-containing stock were added before the Somogyi treatment, as the approximate free cholesterol concentration for most serum samples after final dilution should be about 2—10 mg dl^{-1}. In a similar fashion for the total cholesterol assay, spikes of 15 and 30 mg dl^{-1} were added before both the hydrolysis step and Somogyi treatment, to insure that the cholesterol standard was subjected to all the same treatment that the serum sample was. Because the linear calibration is a log-log plot, it is necessary to use a non-linear regression routine which minimizes calculated residual values by adjusting the unknown concentration values, given an experimental value for the calibration slope and also initial estimates of the concentrations. Good results were obtained. For the Monitrol serum, the free cholesterol assay yielded a value of 75.0 mg dl^{-1}, which is in the middle

of the expected 43—104 mg dl^{-1} range; the total cholesterol assay gave a value of 247 mg dl^{-1}, also within the expected 215—260 mg dl^{-1} range. By use of standard addition and Somogyi treatment of the sera samples, this chemiluminescence method can quantify both free and total cholesterol in blood serum with good accuracy and precision.

Conclusion

Major strengths of this technique are the speed and the small amount of enzyme required. At 1 min or less per sample, the method is equivalent to other standard continuous flow methods for cholesterol [22]. At a reagent flow rate of 5 μl min^{-1} and samples at 1 min^{-1}, only 0.01 unit of the oxidase is used per sample. This compares with 0.2—0.25 units per sample for conventional continuous flow or discrete methods [22, 23].

In the only other chemiluminescent method proposed to date for cholesterol [24], immobilized cholesterol oxidase (3600 units) and cholesterol esterase were contained in separate glass-bead reactors. After several minutes of incubation in each reactor (around 15 min overall), the generated hydrogen peroxide was determined by chemiluminescence with bis(3,4,6-trichlorophenyl)oxalate as reagent in a dioxan solvent. The method described here has 15-fold greater throughput. Comparison of the enzyme consumption is even more dramatic. The immobilized enzyme reactor would need to be in continuous use for several years to yield as low a value for oxidase enzyme consumption per sample as we report here.

This research was supported in part by the National Science Foundation (CHE-81-08816).

REFERENCES

1 N. W. Tietz, Fundamentals of Clinical Chemistry, Saunders, Philadelphia, PA, 1976.
2 B. Zak, Clin. Chem., 23 (1977) 1201.
3 C. C. Allain, L. S. Poon, C. W. S. Chan, W. Richmond and P. C. Fu, Clin. Chem., 20 (1974) 270.
4 W. Richmond, Clin. Chem., 22 (1976) 1579.
5 W. R. Seitz, CRC Crit. Rev. Anal. Chem., 13 (1981) 1.
6 F. Gorus and E. Schram, Clin. Chem., 25 (1979) 512.
7 W. R. Seitz, Methods Enzymol., 57 (1978) 409.
8 V. J. Nau and T. A. Nieman, Anal. Chem., 51 (1979) 424.
9 D. Pilosof and T. A. Nieman, Anal. Chem., 52 (1980) 662.
10 D. Pilosof and T. A. Nieman, Anal. Chem., 54 (1982) 1698.
11 N. L. Malavolti, D. Pilosof and T. A. Nieman, Anal. Chem., 456 (1984) 2191.
12 R. B. Smart, Anal. Lett., 14 (1981) 189.
13 W. Richmond, Clin. Chem., 19 (1973) 1350.
14 J. Hyun, H. Kothari, E. Herm, J. Mortenson, C. R. Treadwell and G. V. Vahouny, J. Biol. Chem., 244 (1969) 1937.
15 G. J. Proksch and D. P. Bonderman, Clin. Chem., 24 (1978) 1924.
16 H. Huang, J. W. Kuan and G. G. Guilbault, Clin. Chem., 21 (1975) 1605.

17 T. Otani, K. Ishimaru, S. Nakamura, T. Kamei and H. Suzuki, Chem. Pharm. Bull., 25 (1977) 1452.
18 D. T. Bostick and D. M. Hercules, Anal. Lett., 7 (1974) 347.
19 D. T. Bostick and D. M. Hercules, Anal. Chem., 47 (1975) 447.
20 D. C. Williams, G. F. Huff and W. R. Seitz, Clin. Chem., 22 (1976) 372.
21 C. Bertrand, P. R. Coulet and D. C. Gautheron, Anal. Lett., 12 (1979) 1477.
22 R. F. Lie, J. M. Schmitz, K. J. Perre and N. Gochman, Clin. Chem., 22 (1976) 1627.
23 A. C. Deacon and P. J. G. Dawson, Clin. Chem., 25 (1979) 976.
24 V. I. Rigin, Zh. Anal. Khim., 33 (1978) 1623.

Analytica Chimica Acta, 170 (1985) 209—216
Elsevier Science Publishers B.V., Amsterdam — Printed in The Netherlands

OPTICAL SENSOR FOR THE DETERMINATION OF MOISTURE

A. P. RUSSELL and K. S. FLETCHER*
Corporate Research, The Foxboro Company, Foxboro, MA 02035 (U.S.A.)
(Received 28th August 1984)

SUMMARY

Cobalt(II) chloride in gelatin is cast as films on the surface of 600-μm optical fibers. The absorption of these films at 680 nm is measured through the fiber by internal reflection spectroscopy to determine the relative humidity of air between 40% and 80%. The spectrum of cobalt chloride on the fiber is similar to a transmission spectrum rather than an attenuated total reflection (a.t.r.) spectrum because of the refractive index of the film, which is slightly greater than that of the fiber. Consequently, the spectrum is less sensitive to measurements near the critical angle, and to refractive index changes than is the case with an a.t.r. spectrum. The uptake of water by cobalt chloride at different humidities suggests that the spectral change is due to the formation of hydrates having molecules of bound water similar to those shown by the free salt.

Chemical sensors based on optical fibers represent a new, exciting, and active area of research. The activity has recently been reviewed by Seitz [1]. Sensors based on absorption or fluorescence changes of chromophoric materials deposited on or entrapped near the surfaces of optical fibers have been described for ammonia [2], pH [3, 4], oxygen [5, 6] and others. Milanovich and Hirschfeld [7] have described a different approach based on remote fluorimetry. They used optical fibers to transmit light to a sample in contact with the fiber. If the sample fluoresces, the emitted light is transmitted back through the fiber to yield the analytical result. The work reported here describes an optical sensor with a bonded reagent on its surface which changes color when exposed to gaseous moisture.

Water, in various chemical and physical forms, is ubiquitous in the environment and its detection and determination are often critical parameters in many processes. Analytical methods for water, though usually restricted to specific applications, can be found in great numbers, right back through the earliest literature. An excellent review of this topic is available [8].

The sensor described herein uses the well-known colorimetric interaction of cobalt(II) chloride with water vapor. The anhydrous salt is blue, and turns pink as water of hydration converts the salt to the hexahydrate. This observation was first reported by Winkler [9] and subsequently has been studied and utilized extensively for the detection of water. Cobalt chloride is immobilized here on the surface of silica optical fiber. Light from a monochromator

0003-2670/85/$03.30

passes into one end of the fiber. The multiple internal reflections of the light with the silica-cobalt chloride interface, as it transits the fiber, leads to the spectrometric determination of the blue-pink equilibrium of cobalt chloride with moisture in the atmosphere to which the fiber is exposed. The quantitative result is obtained by photodetection of the light emerging from the fiber.

EXPERIMENTAL

Equipment

Plastic-clad silica fiber (EOTec Corporation, West Haven, CT) with a 0.6-mm silica core was used. Lengths (60 cm) of the fiber were stripped of cladding at the center for lengths of 12 cm. Stripping was done with a razor blade to remove the bulk of the silicone polymer cladding, which was further removed by rubbing the silica core with a plastic scraper. Traces of plastic and grease were removed by heating the stripped silica fiber in a flame. For convenience of use, fibers were bent in the middle into a 5-mm diameter U-shape by softening the silica in a propane flame.

The bared silica of the probes was coated with cobalt chloride by dipping into an aqueous solution of 4% gelatin and 2% cobalt chloride hexahydrate by weight. After excess solution had been drained, probes were dried either in an oven or in room air with a humidity below 50%.

Film thickness on the probe was measured by a Sloan Dektak surface profile measuring system (Sloan Technology Corp., Santa Barbara, CA) and found to be nominally 100-nm thick. This instrument was also used to measure the thickness of films on flat glass plates used in the transmission experiments. The refractive index of the dry gelatin was found to be 1.5 by ellipsometry (Gaertner Production Ellipsometer L117; Gaertner Scientific Co., Chicago, IL).

The probes were attached to the optical system by placing one end of the fiber at the exit slit of a visible-light monochromator (ISA Inc.; Model H10, bandwidth 12 nm mm^{-1}), and the other end against a photodetector (United Detector Technologies, Model 455HS).

Transmission spectrometry was performed with a Cary Model 17 spectrophotometer.

Samples and standards

Air of known dew point was obtained by pumping room air into chilled water through a coarse-porosity glass frit. The temperature of the chilled water was maintained ($\pm 0.02^{\circ}C$) by a refrigerated water bath. The humidified air was filtered through glass wool to remove entrained water droplets, and then brought to 25°C by running it through coiled 1/8-in. copper tube immersed in a 25°C water bath to ensure that no loss of water from the sample by condensation occurred and to establish the reference temperature for the relative humidity calculation. The relationship between the dew point and percent relative humidity (%RH) was taken from tabulated sources [10].

In some of the experiments, humid atmospheres were obtained with saturated salt solutions. The salts and their equilibrium percent relative humidities were: NH_4Cl, 79.3% at 25°C; $NaNO_3$, 66% at 20°C; $Ca(NO_3)_2 \cdot 4H_2O$, 51% at 24.5°C; and $CaCl_2 \cdot 6H_2O$, 31% at 24.5°C [10]. Air dried to less than 1% relative humidity was obtained by using anhydrous calcium sulfate in a closed container.

RESULTS AND DISCUSSION

Cobalt chloride forms several hydrated salts having 1 to 6 molecules of bound water [11]. The anhydrous form is bright blue and has high optical absorption between 550 and 750 nm. It can be obtained by heating the hydrated salt to 120°C. The hydrated pink form with six waters of crystallization has an absorption maximum near 500 nm with a molar absorptivity which is about 50 times lower than that of the blue form [12]. It is the loss of the intense blue color which is most noticeable during the hydration of cobalt chloride.

The use of cobalt chloride on an optical fiber detector requires that it be suspended in an optically transparent bonding medium, because by itself cobalt chloride forms salt crystals which adhere poorly to the silica surface. Further, it is necessary to avoid formation of discrete crystals on the fiber surface because these would scatter light and lead to loss of signal. Photographic gelatin was found to be a satisfactory carrier material because the salt dissolves readily in the gelatin solution and dries to a transparent crystal-free film on the fiber. Other polymer carriers examined, such as polyvinyl alcohol, polymethylmethacrylate, and nitrocellulose turned opalescent when exposed to high humidities. This can be attributed to separation of the cobalt/water phase from the polymer, resulting in scattering of light. Gelatin, which is hydrophilic, does not do this.

A preliminary examination of cobalt chloride in gelatin placed either on a flat internal reflection plate, or on a glass fiber, demonstrated that the salt responded to humidity with a change in the spectrum which was most pronounced from 600 to 700 nm. Initially, it was thought that the spectrum of cobalt chloride on the fiber surface was measured by attenuated total reflection (a.t.r.) spectrometry. It is known that a.t.r. spectra, if measured near the critical angle for reflection, as occurs in these fibers, are distorted, and exhibit a pronounced red shift. This distortion is sensitive to changes in the refractive index in the medium outside the fiber, and consequently to temperature [13].

In order to establish the validity of this hypothesis, the absorption spectra of the cobalt chloride/gelatin films were measured by internal reflection with a fiber, and by transmission through a glass plate. Because transmission spectra are not subject to the red shift distortion seen in a.t.r. spectra, this comparison should indicate the degree of red shift introduced to the cobalt chloride spectra by the fiber optic configuration. The coated fiber optic

probes were equilibrated with humidified air for 5 min prior to spectral measurements. The films on glass plates were much thicker (5—10 μm) and required about an hour for equilibration. A gelatin-coated plate without cobalt chloride was used as a reference for the transmission experiment. In order to obtain a reference for the fiber optic probe, after measurements of the spectra of cobalt chloride, the probe was cleaned, and recoated with gelatin without cobalt chloride. Reference spectra were then obtained in the humidified airs. Values of absorbance (A) were calculated as log I_0/I where I_0 values are the reference values obtained for cobalt chloride-free films and I values are those obtained with dissolved cobalt chloride. The spectra are compared in Fig. 1. The broad band of absorption between about 550 and 750 nm, which corresponds to the blue form of cobalt chloride, decreases with increasing humidity. The peak corresponding to the pink form near 510 nm is visible at 79% RH. No difference in wavelength of absorption maxima for the spectra recorded by the two techniques is apparent.

On this basis, it is suggested that the spectra measured with the fiber are

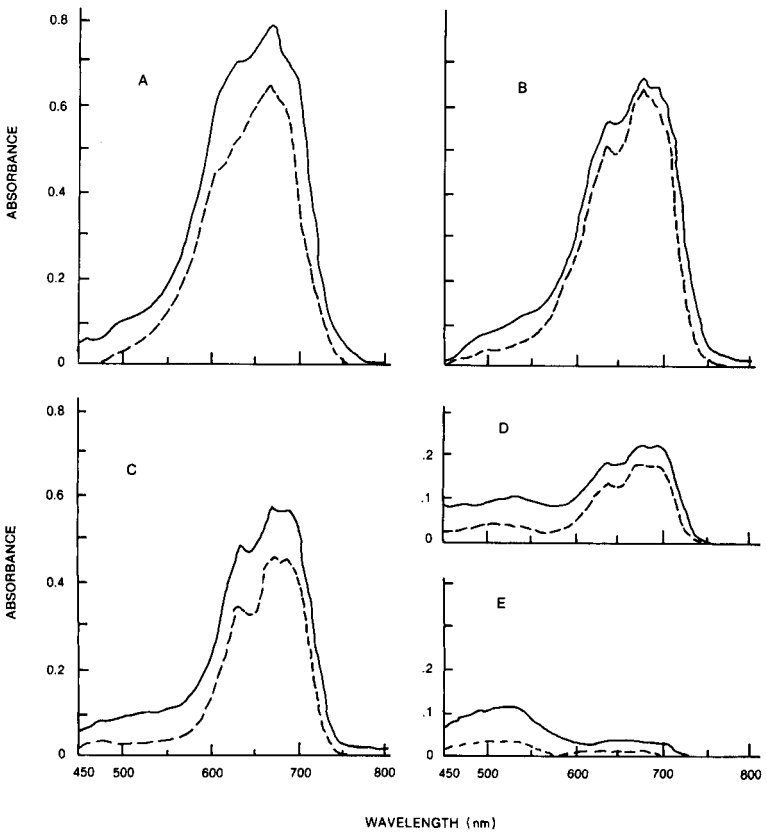

Fig. 1. The absorption spectra of cobalt(II) chloride in gelatin at different percent relative humidities: (—) measured on an optical fiber; (---) measured by transmission. Relative humidity: (A) 10%; (B) 31%; (C) 51%; (D) 66%; (E) 79%.

actually transmission spectra rather than a.t.r. spectra. A.t.r. spectrometry depends on refractive index differences of surfaces. By ellipsometry, the refractive index of the gelatin film was measured as 1.50, while the refractive index of the fiber is 1.45. It is concluded that light passes from the quartz fiber through the gelatin film and reflects from the air/gelatin interface. During passage through the gelatin film, light is absorbed by the cobalt chloride in a manner similar to the transmission experiment. It is also interesting to note that light within the fiber interacts with the gelatin/cobalt chloride film on the surface many times as it reflects down the fiber so that the effective pathlength is greater than found in the transmission experiment. Clearly, a much greater surface area of film can be exposed when the fiber is used, resulting in increased signal and faster response time compared to the transmission case for which an increase in pathlength can be obtained only by increasing film thickness.

Further evidence to support this was obtained by studying cobalt chloride dissolved in acetone to provide a medium with a refractive index lower than that of the fiber. In dry acetone, cobalt chloride is soluble and the solution exhibits the color characteristic of the anhydrous salt. As water is added to the solution, the color change from blue to pink occurs in a fashion analogous to that observed for the gelatin film [11]. The spectral properties of one of these solutions were measured by transmission through the solution and by using a bare fiber immersed in the solution. The spectrum measured with the fiber was shifted 10 nm toward longer wavelengths compared with the transmission spectrum. This shift is typical of a.t.r. spectra and is due to a decrease in reflectivity of the light at the acetone/glass interface near the critical angle. The decrease is a result of a change in refractive index of this interface near an absorption band. This well known effect, termed anomalous dispersion, shifts absorption spectra toward longer wavelengths [13]. Because the spectrum of cobalt chloride in gelatin on the fiber does not show this effect, reflection of light from the fiber surface must take place at the gelatin/air interface and not at the fiber/gelatin interface. Furthermore, because air does not have absorbing bands at visible wavelengths, anomalous dispersion is not possible, and reflectivity is not lost.

From these results, it is concluded that it is possible to measure an undistorted transmission spectrum of material on the surface of a fiber, if it is embedded in a thin film with a refractive index equal to or greater than that of the fiber. Such a system should be free of errors associated with temperature-dependent alterations in the refractive index of the external medium, provided that the index is lower than that of the fiber or surface film. Other variables which might affect the spectrum, such as the length and diameter of the fiber, were not examined.

It was of interest to investigate the weight change of cobalt chloride as it hydrated in the films because hydrated salts other than the hexahydrate have been reported [11]. To do this, 5—10-μm films were deposited on weighed microscope cover glasses and their dry weights were accurately determined.

After equilibration with atmospheres of known humidity for 1 h, the glasses with films were reweighed. To permit correction for water uptake by the gelatin alone, similar measurements were made on films without cobalt chloride. The same experiment and procedure were used for cobalt chloride deposited on filter paper as a control to determine whether gelatin affected the cobalt chloride/water equilibrium.

The mole ratio of water to cobalt chloride at each relative humidity tested was calculated; the results are shown in Fig. 2. There appears to be less water taken up at each humidity by cobalt chloride in gelatin than by cobalt chloride on paper. This is in agreement with other work that shows that polar organic compounds and hydroscopic salts alter the response of cobalt chloride to humidity [14]. It is noted that in each case there is little or no water taken up from 30—50% RH, while about 6 mol of water is taken up between 70% and 80% RH. In extensive kinetic weight-gain and optical studies of cobalt chloride dried on cellulose film (cellophane) exposed to humid air, Holland and Santangelo [15] reported that below 23% RH, no water is taken up. At higher humidities, 6 mol of water is taken up per mole of cobalt chloride and the optical absorbance at 690 nm becomes zero. The present results are in substantial agreement. A cobalt chloride/gelatin film was also exposed to a water-saturated atmosphere and weighed immediately after the absorbance at 690 nm became zero. The weight gain represented 6.4 mol of water per mole of cobalt chloride, in near agreement with their findings. On the basis of this and the smooth change of absorption with humidity, no evidence for the presence of salts beyond the hexahydrate up to about 80% RH is apparent. However, the hexahydrate is deliquescent and above 80% RH it absorbs additional water. A mole ratio of 12 is obtained after exposure to a relative humidity of 78% for 14 h (Fig. 2). If crystals of cobalt chloride are left in a water-saturated atmosphere for a few hours, sufficient water is taken up to form a solution. However, at lower humidities and a constant temperature, the mole ratio of bound water to cobalt chloride increases to 6 with the smooth and continuous change in optical absorbance noted in Fig. 3.

The response characteristics of these sensors were tested by using a 10-cm length of fiber coated with a 100-nm thick film. It was placed in a stream of humidified air flowing at 10 $cm^3\ s^{-1}$, and at a temperature of 26°C. The temperature of the dew-point water bath was started at 15°C (50.7% RH at 26°C) and increased at a rate of 0.1°C min^{-1}. No change in light absorption by the cobalt chloride film was seen until the dew point of the air had reached 17°C (57.6% RH). The absorbance then decreased as the dew point was raised, and reached a minimum at 23.5°C (86% RH), then increased slightly at 24°C (88.8% RH). The intensity of light at 680 nm passing through the fiber at different humidities was converted to absorbance by using the relationship $A = \log I_0/I$, where I_0 is the minimum intensity, noted at a dew point of 23.5°C, and values of I are the intensities at other dew points. The results, absorbance at 680 nm vs. dew point and %RH, are shown in Fig. 3. The

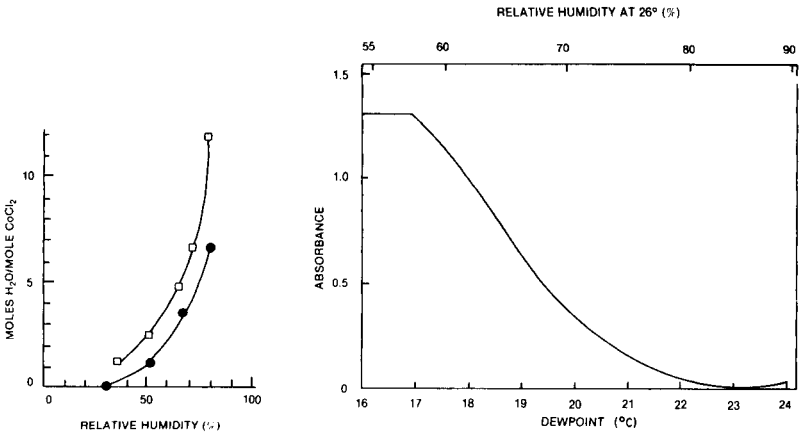

Fig. 2. The number of moles of water bound per mole of cobalt chloride dried on filter paper (□) and in gelatin (•) at various percent relative humidity at 25°C. Equilibration time for cobalt chloride in gelatin was 1 h. Equilibration time for cobalt chloride on filter paper was 2 h, except the point at 79% RH, which was allowed to equilibrate for 14 h.

Fig. 3. The absorption of light at 680 nm vs. dew point of humidified air, measured by an optical fiber with cobalt chloride in gelatin on the surface. The percent relative humidity at 26°C corresponding to the dew points is indicated.

absorption of light at 680 nm decreases smoothly from a dew point of 17°C to the minimum at 23.5°C. The upturn at the higher dew point and humidity was observed in several measurements, and may relate to the deliquescence of cobalt chloride noted earlier. Absorption of water causes the gelatin film to swell and the refractive index to decrease. Even when taken to higher humidities, the curve is reversible. Repeated cycling of the fiber between different humidities in the flowing air stream, or in atmospheres of different humidity over solutions of salts, show a reproducibility between absorbance and humidity of ±2% RH. Further, the system equilibrates rapidly after an abrupt change in humidity; 90% of the optical change occurs in 30 s and the system comes to equilibrium within 1 min.

In practical applications, optical sensor probes of the type described would require reproducibility in the thickness of the indicator film and long-term stability. Because the goal of the work was to study the interaction between light in a fiber with a surface indicator film, these questions were not specifically studied. However, it was observed that the gelatin films do not deteriorate over a period of four months at room humidities. For films based on other polymers, it was found that deterioration, such as peeling or clouding, results in a loss of light transmission through the fiber at all wavelengths because of scattering from the surface. Irregularities in film thickness or in indicator concentration may in part be compensated by measurements at two wavelengths, as recommended by Seitz [1].

In summary, utilization of cobalt chloride in gelatin on the surface of

optical fiber results in sensors for humidity over a range of about 40—80% RH. Although the interaction of light in an optical fiber with surface films is complex, it was found that if the refractive index of the film is near that of the fiber core, the absorption spectrum of a material in the film resembles a transmission spectrum, whereas the absorption spectrum of a material in a low-index medium is distorted, and would be sensitive to temperature and refractive index changes of the outside medium. Further, the unique geometry presented by the fiber optic configuration leads to a substantial increase in pathlength relative to that possible for transmission through a film. The change in the absorption spectrum of cobalt chloride in gelatin with humidity appears to be a result of the formation of cobalt chloride hydrates similar to those known for free cobalt chloride.

We thank A. C. Gilby and G. S. Maurer for helpful discussions on a.t.r. spectroscopy, D. E. Ihnat and R. D. Driver for optical design help and W. F. Vallett for general experimental assistance.

REFERENCES

1 R. W. Seitz, Anal. Chem., 56 (1984) 16A.
2 J. F. Giuliani, H. Wohltjen and N. L. Jarvis, Optics Lett., 8 (1983) 54.
3 L. A. Saari and W. R. Seitz, Anal. Chem., 54 (1982) 821.
4 J. I. Peterson, S. R. Goldstein, R. V. Fitzgerald and D. K. Buckhold, Anal. Chem., 52 (1980) 864.
5 T. M. Freeman and W. R. Seitz, Anal. Chem., 53 (1981) 98.
6 J. I. Peterson, R. V. Fitzgerald and D. K. Buckhold, Anal. Chem., 56 (1984) 62.
7 F. P. Milanovich and T. Hirschfeld, Instrument Society of America meeting, October 1983, Houston, TX.
8 J. Mitchell, Jr. and D. M. Smith, Aquametry. Parts I—III. A Treatise on Methods for the Determination of Water, 2nd edn., Wiley, New York, 1977—1982.
9 C. Winkler, J. Prakt. Chem., 91 (1864) 209.
10 CRC Handbook of Chemistry and Physics, Vol. 60, R. C. Weast (Ed.) and M. J. Astle (Assoc. Ed.), CRC Press, Inc., Boca Raton, FL, E 44, 46, 1980.
11 L. I. Katzin and J. R. Ferraro, J. Am. Chem. Soc., 74 (1974) 2752.
12 F. A. Cotton and G. Wilkinson, Advanced Inorganic Chemistry, 4th edn., Wiley, New York, 1980.
13 N. J. Harrick, Internal Reflection Spectroscopy, Harrick Scientific, Croton Dam Road, Ossining, NY 10562, 1979.
14 V. M. Yarygin, M. M. Alekseev, N. I. Volynkin and O. K. Nikolaev, Moisture Sensor for Gases, Patent, USSR SU 381012, 1973.
15 R. V. Holland and R. A. Santangelo, J. Appl. Polym. Sci., 27 (1982) 1681.

Analytica Chimica Acta, 170 (1985) 217—224
Elsevier Science Publishers B.V., Amsterdam — Printed in The Netherlands

DETERMINATION OF SELENIUM BY ATOMIC ABSORPTION SPECTROMETRY WITH MINIATURIZED SUCTION-FLOW HYDRIDE GENERATION AND ON-LINE REMOVAL OF INTERFERENCES

MASAHIKO IKEDA

Nippon Jarrell-Ash Company, 28, Joshunga mae-cho, Shimotoba, Fushimiku, Kyoto 612 (Japan)

(Received 28th June 1984)

SUMMARY

On-line removal of transition metal interferences in microscale suction-flow hydride generation atomic absorption spectrometry is described for the determination of selenium at $\mu g\ l^{-1}$ levels. A mini-column of a chelating resin with iminodiacetate groups is used. Selenium in solutions containing ≤ 2.5 mg of copper or nickel was determined at a rate of 30 samples per hour; the detection limit was 0.1 ng of selenium. The relative standard deviation for ten replicate measurements of 5 ng of selenium was 3.8%. The method was applied successfully to the determination of selenium in standard copper alloys and nickel sponge.

Hydride-generation atomic absorption spectrometry (a.a.s.) has been widely used for the determination of several elements, though the technique has some disadvantages [1, 2]. Transition metals decrease the efficiency of hydride generation, and there are mutual interferences from other hydride-forming elements (arsenic, antimony, bismuth, germanium, lead, tellurium and tin). Also, there is a difference in sensitivity between different oxidation states of the analyte (e.g., arsenic(III, V), selenium(IV, VI)), although this can be used for their selective determinations. Transition metal interference is the most serious of these problems. Therefore, various methods of circumventing the interferences have been reported, including removal of the interferent by precipitation with sodium hydroxide [3], coprecipitation with lanthanum hydroxide [4, 5] or zirconium hydroxide [6], flotation and coprecipitation with hydrated iron oxide [7] and ion-exchange resin separation [8—11]. Chelating resins strongly sorb transition metals, whereas hydride-forming elements (except for bismuth and lead) and the alkali and alkaline earth metals are only slightly retained. However, the use of such resins is time-consuming in batch systems.

Recently, the combination of conventional flame a.a.s. with flow injection analysis has been developed for on-line preconcentration of cadmium, lead, copper and zinc from sea water on a mini-column of chelating resin [12], and for on-line removal of interferences from phosphate and sulfate in the determination of calcium, on an anion-exchange resin column [13].

0003-2670/85/$03.30

In this paper the on-line removal of some interferences is described for suction-flow hydride-generation a.a.s. [14] by use of a mini-column of a chelating resin. The method permits simpler operation and faster determinations of selenium than any other pre-separation technique for hydride-generation a.a.s. The performance of this technique was evaluated by its application to the determination of selenium in nickel and copper metals.

EXPERIMENTAL

Apparatus and reagents

Figure 1 is a schematic diagram of the instrumentation, all components of which are the same as previously described [14] except for the column of chelating resin (see below). A pH meter model HM-5ES (TOA Electronics, Tokyo), a Pipetman P-1000 (Gilson, France), a Hamamatsu selenium hollow-cathode lamp (L233-34NQ) and a strip-chart recorder were used.

Resin column. Muromac A-1 (Muromachi Chemicals Co., Tokyo), a styrene-divinylbenzene copolymer matrix chelating resin, containing paired imino-diacetate groups, was used to fill the column. The nominal exchange capacity was 50 mg Cu ml^{-1}. (The resin was purified from Dowex A-1 chelating resin by the supplier.) Muromac A-1 was confirmed to have almost the same exchange capacity for copper as the Chelex-100 (Bio-Rad Laboratories, Richmond, CA) which was used in preliminary experiments. The preferred

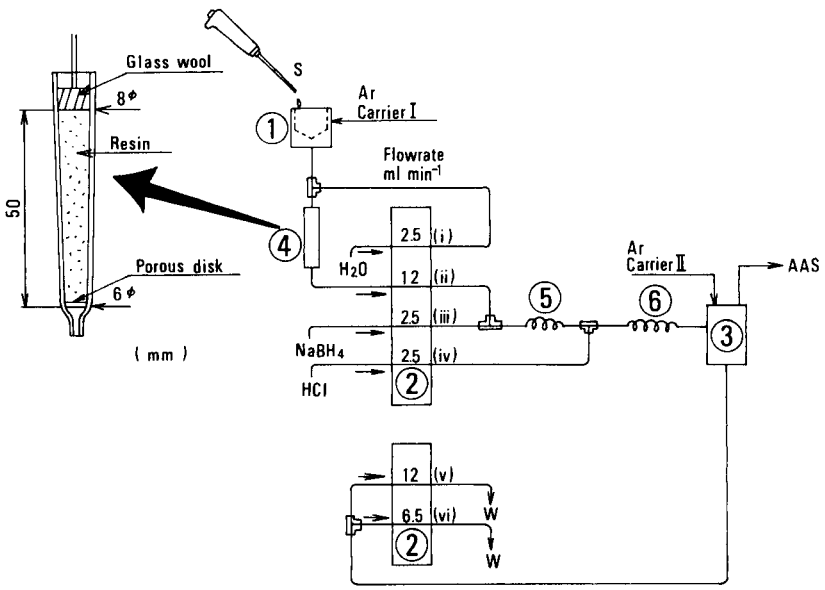

Fig. 1. On-line removal of interferences for the suction-flow hydride-generation a.a.s. manifold: (1) teflon suction cup; (2) peristaltic pump; (3) gas-liquid separator; (4) flow-through column; (5) pre-mixing coil; (6) reaction coil; (S) sample solution; (W) waste.

particle size was 100—200 mesh. Before its packing into the column, the resin was preconditioned by soaking in 2 M nitric acid overnight, washing with pure water 5—6 times, converting to the sodium form by standing overnight in 2 M sodium acetate and washing 2—3 times with pure water. About 2 ml of resin was packed into a plastic column, as shown in Fig. 1. A sintered-glass disk (nominal pore size 50 μm) was provided as the bottom fitting to the column, and glass wool was placed on top of the resin.

Reagents. All reagents used were of analytical-reagent grade. Pure water from a Millipore Milli-Q water system was used throughout. Sodium tetrahydroborate solution was freshly prepared and made alkaline with 0.5% sodium hydroxide solution. A stock solution (1000 mg l^{-1}) of selenium was prepared by dissolving selenium in the minimum amount of concentrated nitric acid and diluting with 1.2 M hydrochloric acid. Working solutions were prepared by serial dilution of the stock solution with water. Clark-Lubs buffer solutions (potassium hydrogenphthalate/hydrochloric acid) were used to adjust the pH.

Procedures

A 500-μl sample was injected into a teflon suction cup from a Pipetman P-1000. The sample was carried to the top of the column with a continuous flow of water. The effluent was introduced into the tetrahydroborate solution and mixed with hydrochloric acid in the reaction coil. The solution, argon carrier gas I, evolved hydrogen and hydrogen selenide were introduced into the gas-liquid separator. The separated hydride was swept by argon carrier gases I and II into an electrically heated quartz cell. The peak height of the transient absorbance signal was measured from the strip-chart recorder. The signal began to appear 15 s after the sample was dropped into the suction cup.

Digestion procedure for nickel samples. Weigh 0.5 g of sample accurately into a beaker. Add an acid mixture (6 ml of 12 M hydrochloric acid, 4 ml of 18 M nitric acid and 5 ml of water), cover the beaker, and evaporate to near dryness on a hot plate. Add 10 ml of 6 M hydrochloric acid and heat the solution in a boiling water bath for 15 min. Adjust the pH to 3.5 with buffer, ammonia, or dilute hydrochloric acid as required, using a pH meter. Dilute to 100 ml with water and determine selenium in this solution.

Digestion procedure for copper alloys. Weigh 0.5 g of sample accurately into a beaker, add 10 ml of 8 M nitric acid, cover the beaker, and evaporate to near dryness on a hot plate. Add 10 ml of 6 M hydrochloric acid and heat the solution in a boiling water bath. Dilute to 100 ml. Dilute further with water if necessary, and adjust the pH (pH meter) to 3.5. Then determine selenium in this solution.

RESULTS AND DISCUSSION

Optimization of conditions

The effect of the sampling tube diameter ((ii) in Fig. 1) on the signal shape is shown in Fig. 2. A 3.2-mm i.d. tube gave the sharpest peak. The peak height increases with increasing sample volume up to ca. 1 ml; thereafter, the signal reaches a plateau. A 500-μl sample gives ca. 80% of the plateau signal obtained with a 2-ml sample.

The influence of pumping speed, flow rate of argon carrier gas and furnace temperature were studied with a solution containing 10 ng of selenium. A pumping speed of 6 (2.5 ml min^{-1}) was a good compromise between sensitivity and reagent consumption rate. The introduction of air into the system from the sampling tube decreased the reproducibility [15], but the use of argon carrier gas I minimized the intake of air. Changes in the flow rate of this carrier gas in the range 0.03—3 l min^{-1} did not affect the sensitivity. For practical convenience, carrier gas I was set at 0.1 l min^{-1}. The flow rate of carrier gas II was not critical provided that it was in the range 0.3—0.6 l min^{-1}. Thus a flow rate of 0.4 l min^{-1} was used in the following study. Temperatures of the furnace for the quartz cell in the range 900—1200°C were satisfactory, so 1000°C was selected.

The sensitivity decreased with an increase in sodium tetrahydroborate concentration above 1.5%, mainly because of the production of a large amount of hydrogen. Therefore, a 1% tetrahydroborate solution was chosen.

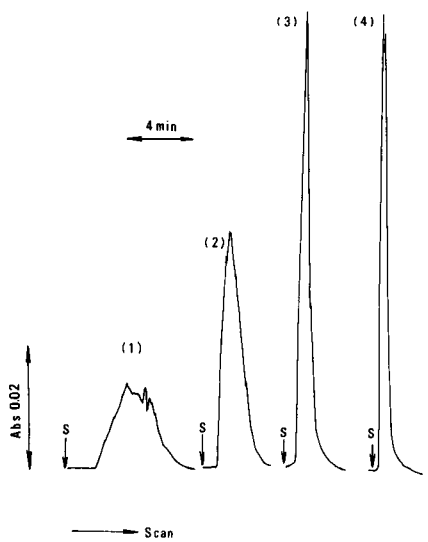

Fig. 2. Influence of sampling tube inner diameter and flow rate on absorbance signal for 10 ng of selenium in 500 μl of solution: (1) 1.6 mm i.d., 2.5 ml min^{-1}; (2) 2.4 mm i.d., 6.5 ml min^{-1}; (3) 3.2 mm i.d., 12 ml min^{-1}; (4) with two tubes of 3.2 mm i.d. in parallel, 24 ml min^{-1}; (S) sample injection.

Increasing the hydrochloric acid concentrations up to 8 M gave higher sensitivity; the Tygon tube used in the peristaltic pump swelled in the presence of concentrated hydrochloric acid, and 6 M hydrochloric acid was chosen. With respect to the effect of particle size of the resin on sensitivity, there was no difference in sensitivity for 20—50 mesh, 50—100 mesh and 100—200 mesh particles. However, there was more noise when the 20—50 mesh resin was used, presumably because the amount of solution added was insufficient to occupy the entire void volume of the column. As a result, a resin of 100—200 mesh particle size is recommended, to give a higher exchange capacity and greater reproducibility. The optimized operating conditions are summarized in Table 1.

Effect of sample pH on the break-through capacity of the resin

Under the experimental conditions used, the break-through capacities of the resin for copper and nickel, expressed as the maximum weights (mg) of metals found to have no break-through, were measured by repeated injections of a 500-μl sample containing 10 ng of selenium and 2.5 mg of copper or nickel. Break-through was considered to have occurred when the selenium signal was suppressed by more than 10% from that for the first measurements. At pH 2.8, the break-through capacities were 50 mg for copper and 38 mg for nickel; at pH 3.5, the values were 75 and 87 mg, respectively. These general trends are to be expected, because the distribution coefficient for nickel [16] is larger than that for copper at pH 3.5. Also nickel is more readily tolerated than copper in the hydride-generation of selenium a.a.s. [11, 17, 18]. In contrast, the distribution coefficient for nickel at pH 2.8 is smaller than that for copper [16], and therefore the break-through capacity for nickel is, as expected, less than that for copper. The pH of the sample should be kept at $\geqslant$3.5, because of its greater capacity for both metals at such pH values. In general, a column packed with resin was replaced by a new one after every 25 measurements of a sample containing 2.5 mg of copper or nickel.

TABLE 1

Recommended operating conditions

Wavelength	Se 196.0 nm	Tube sizes (mn)	
Lamp current	12 mA	(i) Rinse	1.6 i.d./3.2 o.d.
Time constant	2.2 s	(ii) Sample	3.2 i.d./4.8 o.d.
Spectral bandwidth	1.3 nm	(iii) $NaBH_4$	1.6 i.d./3.2 o.d.
Quartz cell temperature	1000°C	(iv) HCl	1.6 i.d./3.2 o.d.
Pumping speed	6	(v) Waste	3.2 i.d./4.8 o.d.
Muromac A-1 column	2 ml, 100—200 mesh	(vi) Waste	2.4 i.d./4.0 o.d.
Sample size	500 μl	Argon flow rates	I, 0.1 l min^{-1}
Reducing reagent	1%(w/v) $NaBH_4$ in 0.5% w/v NaOH		II, 0.4 l min^{-1}
Acid	6 M HCl		

Sensitivity and precision

A linear calibration graph was obtained by using freshly prepared standard solutions of up to 100 ng of selenium. The 3σ detection limit [19] for selenium was found to be 0.1 ng for a 500-μl sample (corresponding to 40 ng Se g^{-1} in alloys). The relative standard deviation for 10 replicate measurements was 3.8% for 5 ng of selenium. The sample throughput was 30 h^{-1}.

Effect of foreign ions

Hydride-generation a.a.s. is well known to be susceptible to interferences from many elements [1, 2, 10, 11, 14, 17, 18, 20, 21]. The extent of the interference can depend upon not only the concentration of interferent [17, 22], but also on the experimental conditions and the apparatus [20].

Table 2 shows the effect of various ions on the determination of selenium. Many elements interfered, especially those which reacted with sodium tetrahydroborate in acidic media to form volatile hydrides, or elements in Periodic groups IB, IIB and VIII [23]. The permissible amounts reported are the maximum amounts of interferences that can be tolerated, expressed as weight ratios to selenium. The usefulness of the mini-column of chelating resin for on-line removal of interferences in Periodic groups IB, IIB and VIII, e.g., copper and nickel up to 500 000-fold (5 mg), and platinum metals and cobalt up to 50 000-fold (500 μg) can clearly be seen. Alkali and alkaline earth metals, iron, cadmium and manganese did not affect the sensitivity of selenium up to 50 000-fold (500 μg) without the resin column. However, the depressing interferences from other hydride-forming elements, except for bismuth and lead, could not be eliminated.

TABLE 2

Comparison of maximum permissible amounts of foreign ions in the determination of 10 ng of selenium with and without on-line removal of interferences on the resin column[a]

Ion	Limiting ion/Se (w/w)		Ion	Limiting ion/Se (w/w)	
	Without column	With column		Without column	With column
Cu^{2+}	500	500 000	Rh^{3+}	1000	N
Ni^{2+}	1000	500 000	Pb^{2+}	1000	N
Co^{2+}	1000	N[b]	As(III)	1000	1000
Ag^{+}	50	N	Sb(III)	5000	5000
Au^{3+}	100	N	Bi(III)	2500	N
Hg^{2+}	500	N	Ge(IV)	1000	1000
Pd^{2+}	50	N	Sn^{2+}	150	150
Pt^{4+}	250	N	Te(IV)	1000	1000

[a]The following are tolerable (50 000-fold excess) without the resin column: Cd^{2+}, Fe^{3+}, Mn^{2+}, Ba^{2+}, Ca^{2+}, Sr^{2+}, Mg^{2+}.

[b]N, no interference with 500 μg (50 000-fold excess).

TABLE 3

Recovery of selenium spiked in sponge nickel (0.5 g)

Amount of selenium (μg)		Recovery (%)
Added[a]	Found[b]	
0.00	0.06	—
0.25	0.32	104
0.50	0.60	108
0.75	0.83	103
1.00	1.00	94
2.50	2.50	98

[a]Added as selenium(IV) prior to digestion. [b]Average of duplicate digestions.

Recovery of selenium from nickel sponge and determination of selenium in copper alloys

Trace amounts of selenium markedly affect the conductivity and softening temperature of electrolytic copper [24], and the mechanical working properties of nickel-base alloys [3]. It is desirable, therefore, to have a reliable method for the determination of traces of selenium in copper- or nickel-base alloys. The digestion procedure outlined under Experimental was adapted from the literature [3, 25] for the recovery study of nickel sponge. Selenium recoveries were evaluated by adding to sponge nickel a known amount of selenite in solution prior to the dissolution procedure. The results obtained are shown in Table 3.

This method was also applied to the determination of selenium in Johnson-Matthey copper alloy reference materials. The digestion procedure given under Experimental was adapted from the literature [24—26]. The analytical results obtained by this method agree well with the certified values. They were 0.0015% (duplicate measurement) for CC-4 as compared with a certified value of 0.0016% and 0.00075% (duplicate measurements) for CC-5 (Johnson-Matthey CC second series) compared with a certified value of 0.0008%.

The author thanks Professor Yuroku Yamamoto and Professor Takahiro Kumamaru of Hiroshima University for their helpful advice and suggestions.

REFERENCES

1 T. Nakahara, Prog. Anal. Atom. Spectrosc., 6 (1983) 163.
2 R. G. Godden and D. R. Thomerson, Analyst (London), 105 (1980) 1137.
3 B. Welz and M. Melcher, Anal. Chim. Acta, 153 (1983) 297.
4 M. Bedard and J. D. Kerbyson, Can. J. Spectrosc., 21 (1976) 64.
5 J. Azad, G. F. Kirkbright and R. D. Snook, Analyst (London), 104 (1979) 232.
6 S. Nakashima and M. Yagi, Bunseki Kagaku, 31 (1982) E431.
7 S. Nakashima, Analyst (London), 103 (1978) 1031.

8 T. Yamashige, Y. Ohmoto and Y. Shigetomi, Bunseki Kagaku, 27 (1978) 607.
9 J. W. Jones, S. G. Capar and T. C. O'Haver, Analyst (London), 107 (1982) 353.
10 T. Nakahara, T. Wakisaka and S. Musha, Spectrochim. Acta, 36B (1981) 661.
11 H. Narasaki and M. Ikeda, Anal. Chem., 56 (1984) 2059.
12 S. Olsen, L. C. R. Pessenda, J. Růžička and E. H. Hansen, Analyst (London), 108 (1983) 905.
13 O. F. Kamson and A. Townshend, Anal. Chim. Acta, 155 (1983) 253.
14 M. Ikeda, Anal. Chim. Acta, 167 (1985) 289.
15 M. Ikeda, H. Nakata, H. Matsuo and T. Kumamaru, Bunseki Kagaku, 33 (1984) 416.
16 D. E. Leyden and A. L. Underwood, Phys. Chem., 68 (1964) 2093.
17 P. N. Vijan and D. Leung, Anal. Chim. Acta, 120 (1980) 141.
18 P. N. Vijan and G. R. Wood, Talanta, 23 (1976) 2294.
19 IUPAC, Anal. Chem., 48 (1975) 300.
20 O. Åstrom, Anal. Chem., 54 (1982) 190.
21 Y. Yamamoto and T. Kumamaru, Fresenius Z. Anal. Chem., 281 (1976) 353.
22 B. Welz and M. Melcher Spectrochim. Acta, 36B (1981) 439.
23 T. Nakahara, Anal. Chim. Acta, 131 (1981) 73.
24 T. W. Hamilton, J. Ellis and T. M. Florence, Anal. Chim. Acta, 110 (1979) 87.
25 G. A. Cutter, Anal. Chim. Acta, 98 (1978) 59.
26 M. Bedrossian, Anal. Chem., 56 (1984) 311.

Analytica Chimica Acta, 170 (1985) 225—235
Elsevier Science Publishers B.V., Amsterdam — Printed in The Netherlands

PRECONCENTRATION OF COPPER, LEAD, CADMIUM AND ZINC IONS FROM WATER WITH 2-MERCAPTOBENZOTHIAZOLE LOADED ON GLASS BEADS WITH THE AID OF COLLODION

KIKUO TERADA*, KEN MATSUMOTO and TOHRU INABA

Department of Chemistry, Faculty of Science, Kanazawa University, 1-1 Marunouchi, Kanazawa, Ishikawa 920 (Japan)

(Received 4th July 1984)

SUMMARY

2-Mercaptobenzothiazole (MBT) loaded on glass beads with the aid of collodion was prepared and used for selective preconcentration of $\mu g\ l^{-1}$ levels of copper(II) and lead from aqueous solutions. Copper and lead were quantitatively retained on the loaded beads from solutions of pH 5.0—6.0, and >5.0, respectively, while cadmium(II) and zinc(II) were retained at ≥pH 6.0 and 7.0, respectively. The retention capacity of the loaded beads was ca. 108 μg Cu g^{-1} (1.7 $\mu mol\ g^{-1}$) at pH 5.5 for beads of 0.3—0.4 mm diameter. The mole ratios of MBT to copper(II) and lead(II) were ca. 10 and 45, respectively, regardless of the amount of MBT loaded on the beads. Copper was completely retained on the column at a high flow rate (21.7 ml min^{-1} cm^{-2}) and lead(II) at up to 12.7 ml min^{-1} cm^{-2}. Cadmium(II) and zinc(II) were not retained quantitatively even at low flow rates (<1.2 ml min^{-1} cm^{-2}). Thus, selective preconcentration of copper and lead was achieved by passing the sample through the column at high flow rate at pH 6.5. The copper and lead retained on the column were completely eluted together with the collodion with 5 ml of MIBK by batch-mode elution, and determined directly by one-drop atomic absorption spectrometry. Copper(II) and lead(II) in several kinds of water were determined.

Several kinds of exchange materials have been prepared in this laboratory by loading water-insoluble inorganic exchangers and complexing precipitants on silica gel, and rapid methods for preconcentration and determination of several trace metals in natural waters have been established by using columns packed with these materials [1—8]. These columns are superior to conventional exchanger columns, because of their high sorption efficiency for trace metals even at high flow rates. However, the method in which silica gel serves as the support for these reagents has some disadvantages. The preparation of the materials is time-consuming, and, because loading of complexing agents is principally by physical adsorption onto the gel, the reagent tends to be released resulting in a decreased complexing capacity. Moreover, the porous surface of silica gel make it difficult completely to elute the metals retained within the pores.

0003-2670/85/$03.30

After some investigations to overcome these disadvantages, it was found that glass beads loaded with complexing agent with the aid of collodion were excellent collectors of trace metals from water samples. The loaded beads can be prepared very simply and rapidly. Cellulose nitrate, which is the main component of collodion, can be dissolved in a small amount of 4-methylpentan-2-one, thus releasing the metal complex so that the eluate can be directly introduced into an atomic absorption spectrometer. Because the complexing agent is incorporated in the collodion, the reagent is protected from oxidation by air, so that degradation of the material is not appreciable. Finally, the glass beads can repeatedly be used as a support.

In the present study, 2-mercaptobenzothiazole (MBT) was chosen as a complexing agent; MBT loaded on silica gel (MBT/SG) has proved to be useful for rapid and convenient preconcentration and determination of several heavy metals in natural waters [2, 3, 7]. Copper, lead, cadmium and zinc were chosen as representative metal ions of interest. Retention behaviour at various pH, the reaction rate between the reagent and the metal ions, preconcentration and recovery of the metals from dilute solutions and the effects of various ions and organic substances were investigated in order to establish a rapid and convenient preconcentration method for these metals.

EXPERIMENTAL

Reagents

Standard solutions (1000 μg ml^{-1}) of each metal were prepared by dissolving pure copper or lead in nitric acid, and pure cadmium or zinc in hydrochloric acid, and diluting with deionized water. Deionized water was prepared by passing distilled water through the Nanopure system (Barnstead Ltd.) and was used in all experiments.

Commercially available glass beads (Toshinriko Co.; No. 1, 0.99—1.39 mm; No. 0.6, 0.49—0.70 mm; No. 0.4, 0.29—0.49 mm in diameter) were soaked in (1 + 1) nitric acid for 3 days, washed with deionized water, soaked in hydrofluoric acid (ca. 11.5%) for 5 min with continuous stirring and washed with deionized water. Finally, the beads were soaked in (1 + 1) nitric acid for 2 days and after being washed with deionized water, were dried in an oven at 90° C. The purified beads were stored in a desiccator. Used glass beads can be purified as follows. The beads were washed with ethanol and acetone to remove collodion and MBT, and then soaked in (1 + 1) nitric acid for 2 days, washed with deionized water and dried at 90° C for 12 h.

Distilled ethanol and acetone were used. 4-Methylpentan-2-one (MIBK) was of atomic absorption spectrometric grade. The collodion containing 5.0—5.5% cellulose nitrate was of extra-pure grade. 2-Mercaptobenzothiazole (MBT) was of analytical-reagent grade. For buffering, the aqueous solution was adjusted with sodium acetate and hydrochloric acid (pH 1—5), potassium hydrogenphthalate and sodium hydroxide (pH 6) and boric acid, sodium borate and sodium chloride (pH 7—10). For lead, 0.025 mol l^{-1} sodium

acetate and aqueous ammonia were used for buffering to prevent adsorption of lead on the vessels.

Preparation of MBT loaded on glass beads with the aid of collodion (MBT/CGB). About 100 g of purified glass beads were put into a glass column (20 mm i.d., 210 mm long), and MBT/collodion solution [10 ml of acetone containing 1.0 g of MBT mixed with 10 ml of commercial collodion solution (5%)] was added. After 7—8 ml of the effluent had drained off, dry air was introduced into the column, via a U-tube packed with anhydrous calcium chloride, by gentle suction for 15 min. Finally, the dry glass beads adhering to each other in the column were gently detached with a glass rod, and all were transferred to a bottle. The MBT/CGB was stored in a darkened desiccator.

Apparatus

A Shimadzu Model AA-646 atomic absorption spectrometer with Hamamatsu Photonics hollow-cathode lamps was used for the determination of the metals. The pH of the aqueous solution was measured by a TOA Model IM-20E ion meter with a combined glass electrode. A Jasco Unidec-505 u.v.-visible recording digital spectrophotometer with a 1-cm quartz cell was used for the measurement of spectra of MBT and collodion. A Shimadzu Model UV-120-02 digital spectrophotometer was used for the determination of MBT. A Taiyo Model SR-11 electric reciproshaker was used for batch experiments. A Tokyo Rikakikai Model MP-3 peristaltic pump and a Toyo Model SF-160K balance-operated fraction collector were used for column experiments. The columns were glass tubes (10 mm or 20 mm i.d., 140 mm long) with a coarse sintered glass disc and stopcock at the bottom.

Procedures

Batch experiments. A 10-ml portion of each metal solution (1.5 $\mu g\ ml^{-1}$), 5 ml of buffer solution and 4 g of MBT/CGB were put into a 50-ml glass-stoppered centrifuge tube. The contents were shaken at 300 strokes min^{-1} for a definite time at room temperature. After the beads had settled, the supernatant liquid was filtered through a dry sheet of Toyo No. 5C filter paper. The metal concentration in each solution was measured with an atomic absorption spectrometer, and the percent retention was calculated. At the same time, the pH of the solution was measured.

Column experiments. A glass column (10 mm or 20 mm i.d.) was filled with a water slurry of a defined amount of the water-washed MBT/CGB and washed with deionized water so that any air bubbles adhering to the surface of the beads were expelled. In most experiments, the bed length was 6—10 cm. A given volume of sample solution containing the individual metal ion was adjusted to a suitable pH and percolated through the column at various flow rates adjusted by using the MP-3 pump. The effluent was collected by a fraction collector and the concentration of each metal was measured as described above. In the case of very low concentration of metals, after the column re-

taining the metal had been washed with a small portion of deionized water, dry air was passed through the column in a similar manner to that described for the preparation of MBT/CGB. A given volume of MIBK was passed through the column, and the metal eluted was determined by atomic absorption spectrometry (a.a.s.).

Determination of the amount of MBT loaded on the glass beads. The amount of MBT loaded on the glass beads was determined as follows. A 1-g portion of dried MBT/CGB was put into the column tube, and 6 ml of acetone was passed through to remove the reagent and collodion completely from the column. The effluent was diluted with ethanol to the desired volume and the absorbance of the solution was measured at 325.6 nm against ethanol as a reference.

RESULTS AND DISCUSSION

The amount of MBT loaded on glass beads

The absorption spectra of MBT and collodion dissolved in ethanol are shown in Fig. 1; MBT shows maximum absorption at 325.6 nm [1], but collodion has no peak at this wavelength. Furthermore, the spectrum of a mixture of MBT and collodion is quite similar to that of MBT. Therefore, the spectrophotometric determination of MBT was not affected by the presence of collodion.

Because the surface of the commercial glass beads was very smooth, in order to increase the active surface of the beads, etching with hydrofluoric acid was examined by immersing the beads in 11.5% hydrofluoric acid for

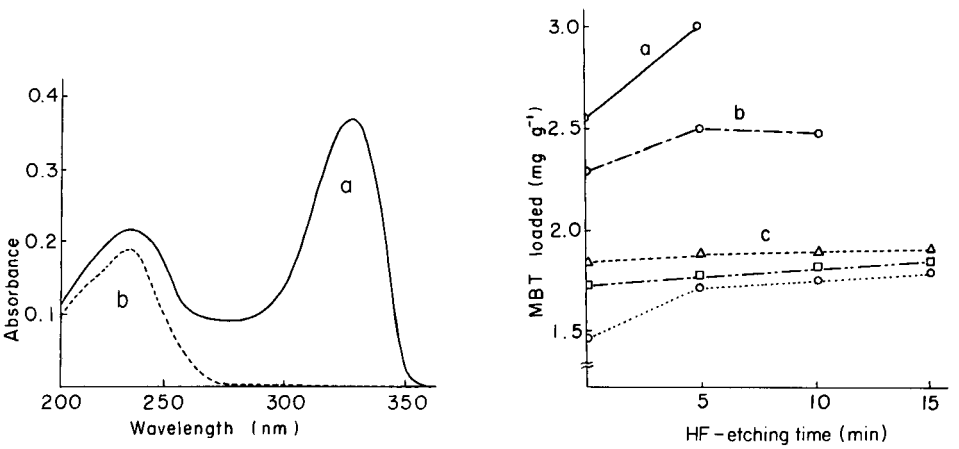

Fig. 1. Absorption spectra of MBT (a) and collodion (b), dissolved in ethanol and measured against ethanol.

Fig. 2. Relationship between etching time and amount of MBT loaded on glass beads. Bead size: (a) No. 0.4, (b) No. 0.6; (c) No. 1. Loading material: (○) MBT 5%, collodion 2.5%; (□) MBT 6%, collodion 2.0%; (△) MBT 7%, collodion 1.5%.

definite times. Figure 2 shows the effect of etching time and size of the beads on the amount of MBT at various mixing ratios of MBT and collodion. As can be seen, the amount of MBT retained on the glass beads increased with etching time for all glass beads. Optical microscopic observation of etched beads proved that the smooth surfaces became rougher after treatment. The results show that etching for 5 min was sufficient. Longer treatment is undesirable because it decreases the size of the bead. Furthermore, it was found that with an increasing proportion of MBT to collodion, larger amounts of the reagent were retained on the glass beads. However, when the MBT/CGB were prepared with insufficient collodion, the membrane on the beads was liable to release reagent. As a result the reagent mixture of 10 ml of acetone containing 1.0 g of MBT and the same volume of commercial collodion solution (5%) was most suitable.

Retention capacity of MBT/CGB

The retention capacities of MBT/CGB for copper(II) and lead were measured by the break-through method. As shown in Table 1, for No. 1 beads, no appreciable difference in the capacity was observed for each MBT/CGB sample prepared from reagent mixtures of different MBT concentrations, while the beads of smaller size (Nos. 0.6 and 0.4) revealed higher retention capacities than the larger ones.

The mole ratios of MBT to copper and lead were about 10.4 and 45, respectively, which are higher than the theoretical value of 2 [7, 9]. This indicates that a large proportion of MBT may not react with these metals, perhaps because of rather low capacity of MBT on the surface of the beads. Most of the MBT is within the collodion coating, and thus may be restricted in its ability to react with both metals. Therefore, the data in the Table indicate that the retention capacity of the beads for copper(II) and lead(II) may mainly depend on the active area of the beads but is independent of the amount of MBT loaded. No difference in percolation characteristics was observed among three kinds of beads, therefore, No. 0.4 beads seemed to be more adequate as a supporting material.

TABLE 1

Retention capacity of MBT/CGB and mole ratio to copper(II)

MBT concentration[a] (% w/v)	Retention capacity[b] ($\mu g\ g^{-1}$)	Mole ratio (MBT:Cu)
5	68 ± 3	9.8 ± 0.8
5[c]	89 ± 3	10.4 ± 0.4
5[d]	108 ± 3	10.6 ± 0.4
6	63 ± 3	10.3 ± 1.1
7	56 ± 4	12.6 ± 1.6

[a]3.0 g of MBT/CGB. [b]1 $\mu g\ Cu^{2+}\ ml^{-1}$. [c]No. 0.6 glass beads. [d]No. 0.4 glass beads.

Effect of pH and shaking time on retention of metals

The recovery of each metal ion from an aqueous solution at various pH values was examined by the batch method. The results are shown in Fig. 3. Copper(II) was quantitatively retained on the material at pH 4—6 and the retention curve descended on the alkaline side. This is probably due to the formation of the hydroxide which is known to form at above pH 5.3. Lead, cadmium and zinc were retained completely at pH 5, pH 6 and pH 7, respectively. The retention behaviour of these elements with MBT/CGB is similar to that observed with MBT/SG [2, 7]. Therefore, the supporting material seems to have no effect on the recoveries of these metals. Complete retention of lead, cadmium and zinc is achieved at pH values above which the hydroxides form.

The effects of shaking time on retention of metal ions are shown in Fig. 4. Copper(II) was completely collected on the beads within 30 s at pH 5.0, and lead at pH 6.5. But cadmium and zinc required at least 10 min for quantitative retention even at pH 7.0.

Effect of flow rate on retention of metals by the column method

Retention of each metal was also examined at various flow rates by the column method. The results are illustrated in Fig. 5. It is clear that copper was quantitatively retained on the column even at a high flow rate (21.7 ml min^{-1} cm^{-2}) and that lead was retained at a practical flow rate (12.7 ml min^{-1} cm^{-2}). In contrast, cadmium and zinc were not retained quantitatively even at low flow-rates (<1.2 ml min^{-1} cm^{-2}). These results are different from those obtained with MBT/SG [2], for the following possible reasons. The collodion coating, which has a micellar structure of cellulose nitrate, is hydrophobic and inhibits close contact between the aqueous solution and complexing agent on the collodion surface. The nature of the collodion is similar to that of polytrifluorochloroethylene and also activated carbon, which have been examined as support materials of MBT for preconcentrating

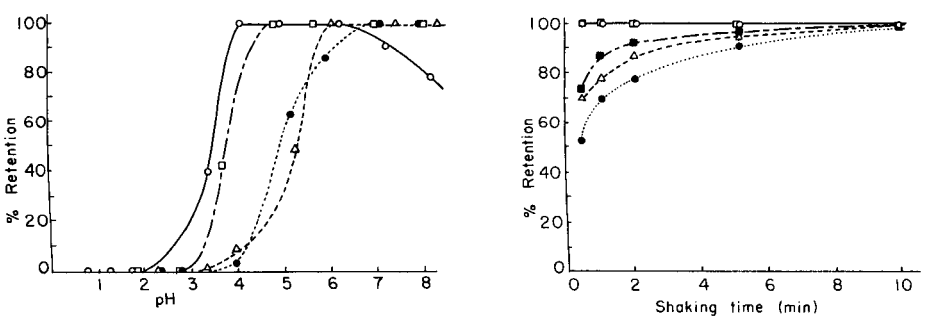

Fig. 3. Effect of pH on retention: (○) copper; (□) lead; (△) cadmium; (●) zinc.

Fig. 4. Effect of shaking time on retention: (○) copper; (□) lead at pH 6.5; (■) lead at pH 5.0; (△) cadmium; (●) zinc.

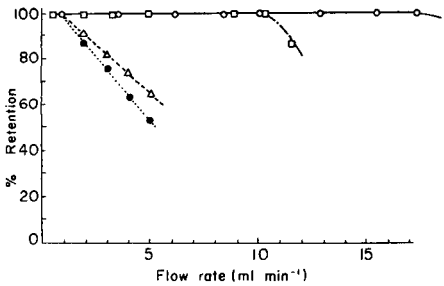

Fig. 5. Relationship between flow rate and retention (10 mm i.d. column): (○) copper; (□) lead; (△) cadmium; (●) zinc.

copper(II) [7]. It is known that among most doubly charged metal cations, copper forms a more stable complex with chelating reagents containing oxygen, nitrogen and sulphur as ligand atoms than any of the other ions studied [10]. Lead forms a less stable complex, and cadmium and zinc form moderately stable complexes with organic reagents which contains polarized nitrogen and sulphur as ligand atoms, and react reversibly with such reagents. These tendencies are revealed by the elution behaviour of these metals from a MBT/SG column [2]. About 30—40% of lead retained on a MBT/SG column was released with (1 + 99) hydrochloric acid but copper was not released. Zinc was eluted completely with a pH 4 buffer. Thus the order of affinity for MBT/CGB is Cu > Pb > Cd ≃ Zn. Therefore, selective preconcentration of copper and lead ions from aqueous solution can be achieved by passing the sample through the MBT/CGB column at a rather high flow rate at pH 6.5.

Elution of metals

Elution of each metal retained on MBT/CGB was achieved by dissolving off the collodion with suitable organic solvent. First, acetone was examined for the dissolution of the MBT/collodion membrane and direct introduction of the eluate into the atomic absorption spectrometer. However, acetone is volatile and the volume is apt to change over rather a short period, giving poorly reproducible results. In addition, deposition of collodion occurred in the burner.

Next, MIBK was examined and the eluate was directly introduced into the flame by decreasing the suction rate and using an air/acetylene ratio of 1:1. However, it was difficult to obtain reproducible results because of imperfect dissociation of the MBT-metal complex in the flame. Therefore, the one-drop method [11] for a.a.s. was employed, in which 100 μl of the eluate was injected with a micropipette into the flame from a small teflon funnel. Flow rates of air and acetylene were controlled at 10 l min^{-1} and 1 l min^{-1}, respectively. Because only a very small volume of sample was introduced into the flame, the metal-MBT complex was completely dissociated and reproducible

peaks were obtained. However, complete elution of metals could not be achieved with MIBK from the column even at a very low flow rate. Therefore, elution was done by a batch process. The column was washed with a small portion of deionized water and dry air was passed through the column as described in the preparation of MBT/CGB. The MBT/CGB was then transferred to a 50-ml centrifuge tube and a known volume of MIBK was added. The contents were shaken by an electric shaker for 15 min. The metal content in the supernatant solution was determined by one-drop a.a.s. Complete elution of 10 μg of copper retained on 10 g of MBT/CGB was achieved by using more than 5 ml of MIBK. In the one-drop method, a very small sample is required for the measurement, therefore the volume of MIBK should be as small as possible to obtain a high concentration factor.

Preconcentration of copper and lead

To examine the retention of copper and lead on a MBT/CGB column, several test solutions (aqueous and 3.3% sodium chloride solutions and sea water) containing copper (pH 5.0) or lead (pH 6.5) in various concentrations were passed through the column (10 mm or 20 mm i.d., 140 mm long) at different flow rates. The metal contents were measured after elution with 5 ml of MIBK as described above. The results are shown in Table 2. Quantitative retention was obtained for copper and lead in the range 1—100 μg l^{-1} at flow rates of 12.7 ml min^{-1} cm^{-2} for copper and 3.8—6.4 ml min^{-1} cm^{-2} for lead. Although such high flow rates of the sample as were attained with a MBT/SG column were not practical with MBT/CGB, batch-mode elution of the metal with a smaller amount of MIBK could compensate for this disadvantage.

TABLE 2

Preconcentration of copper or lead

Metal concentration (μg l^{-1})	MBT/CGB (g)	Copper recovery[a] (%)	Lead recovery (%)
100	7	100	100[b]
40	10	100	—
20	10	100	100[b]
10	10		91[b]
10	10		100[c]
5	10	99	—
1	15	98	97[c]
5[d]	15[f]	99	98[c]
1[d]	15[f]	97	96[c]
5[e]	15[f]	99	98[c]
1[e]	15[f]	98	97[c]

[a]Flow rate 12.7 ml min^{-1} cm^{-2}. [b]Flow rate 6.4 ml min^{-1} cm^{-2}. [c]Flow rate 3.8 ml min^{-1} cm^{-2}. [d]3.3% NaCl matrix. [e]Sea water. [f]20 mm i.d. column.

Effect of various ions and organic substances

Several ions thought to react with MBT (cobalt(II), iron(III) and nickel) were investigated for their effect on the preconcentration or recovery process. In the experiments, 200 ml of a test solution containing 50 $\mu g\ l^{-1}$ copper or lead as well as one other ion in the concentration range 0.1—10 $\mu g\ ml^{-1}$ was prepared. This solution was passed through a column containing 10 g of MBT/CGB at a flow rate of 6.4 ml min^{-1} cm^{-2} for copper and 3.8 ml min^{-1} cm^{-2} for lead. At the same time, mutual effects of the four ions of interest were also examined at various concentrations. The results are shown in Table 3. At 10 $\mu g\ ml^{-1}$, almost all metals decreased the recoveries of copper and lead but mutual interference of copper and lead was not observed because copper and lead react with MBT at different pH values. At the 1 $\mu g\ ml^{-1}$ level, retention of copper on the beads was scarcely influenced by other metal ions, because the copper chelate was formed at pH 5.0, and other metal ions did not react rapidly with MBT at this pH value. The retention of lead was significantly decreased by cadmium, cobalt(II) and iron(III). However, these effects were less than with MBT/SG. This may be because silica gel itself adsorbs iron(III) at higher pH values, while the collodion coating does not. On the whole, lead tends to be influenced by other metal ions because of the rather low stability of its complex. Furthermore, when 20 $\mu g\ l^{-1}$ of each metal ion was added to a solution containing 50 $\mu g\ l^{-1}$ of copper or lead, both metals were recovered quantitatively. As 1 l of sea water usually contains about 0.3 μmol of total heavy metals, which requires only 0.15 g of MBT/CGB, the interferences of heavy metal ions on the adsorption of copper and lead from sea water may be neglected.

The effects of some organic complexing agents (EDTA, citric acid and tartaric acid) were also investigated. Each organic compound was added in the concentration range 10^{-7}—10^{-4} mol l^{-1} to the test solution. The results are shown in Table 4. EDTA, especially, considerably decreased retention

TABLE 3

Effect of various ions on the recovery of copper and lead[a]

Ion	Concentration ($\mu g\ ml^{-1}$)	Recovery (%)		Ion	Concentration ($\mu g\ ml^{-1}$)	Recovery (%)	
		Cu	Pb			Cu	Pb
Co(II)	10	100	54	Cu(II)	5	—	100
	1	100	75		1	—	100
Fe(III)	10	55	23	Pb(II)	10	100	—
	1	95	64		1	100	—
	0.1	95	85	Cd(II)	10	24	65
Ni(II)	10	96	74		1	100	70
	1	100	100	Zn(II)	10	87	71
					1	100	100

[a]10 g of MBT/CGB; 50 $\mu g\ ml^{-1}$ each of copper and lead ions; flow rates 6.4 ml min^{-1} cm^{-2} for copper and 3.8 ml min^{-1} cm^{-2} for lead.

TABLE 4

Effect of organic complexing agents on the recovery of metal ions (conditions as Table 3)

Organic substance	Concentration (mol l^{-1})	Recovery (%)	
		Cu	Pb
EDTA	1×10^{-5}	1.5	0
	1×10^{-6}	2.3	0
	1×10^{-7}	100	76
Citric acid	1×10^{-4}	79	48
	1×10^{-5}	100	61
	1×10^{-6}	100	100
Tartaric acid	1×10^{-4}	94	46
	1×10^{-5}	100	57
	1×10^{-6}	100	100

TABLE 5

Copper and lead content determined in various water samples (ng kg^{-1})

Sample water	Cu	Pb
Pacific Ocean (100 m)	170[b]	<250[b]
Ootebori-Pond (0 m)	396[c]	<250[b]
Tap water (Marunouchi)	711[c]	<250[b]

[a]15 g of MBT/CGB in a 20 mm i.d., 35 mm column. [b]2000-ml sample. [c]1000-ml sample.

of both metals at concentration above 10^{-6} mol l^{-1}. However, in natural water, especially sea water, these organic substances are never found in such high concentration and the influence of these substances will be negligible in practice.

Analysis of water samples for copper and lead

The present method was applied to several kinds of water samples. A seawater sample was collected 100 m deep in the Pacific Ocean on The Hakuho Maru cruise KH-82-1 (Station 8, 12°45′N, 173°14′E). It was acidified by adding 2 ml of sub-boiled hydrochloric acid (1 + 1) to every 1 l of sample. The sample was adjusted to pH 6.5 with aqueous ammonia and passed through the column for preconcentration by a factor of 200. The results obtained are shown in Table 5. The detection limits for one-drop a.a.s. are 0.04 and 0.1 μg ml^{-1} for copper and lead, respectively.

This work was partially supported by a Grant-in-Aid for Scientific Research from the Ministry of Education, Japan (No. 57340032).

REFERENCES

1 K. Terada, H. Hayakawa, K. Sawada and T. Kiba, Talanta, 17 (1970) 955.
2 K. Terada, A. Inoue, J. Inamura and T. Kiba, Bull. Chem. Soc. Jpn., 50 (1977) 1060.
3 K. Terada, K. Morimoto and T. Kiba, Bull. Chem. Soc. Jpn., 53 (1980) 1605.
4 K. Terada, K. Morimoto and T. Kiba, Anal. Chim. Acta, 116 (1980) 127.
5 K. Terada and K. Nakamura, Talanta, 28 (1981) 123.
6 K. Terada, K. Matsumoto and Y. Taniguchi, Anal. Chim. Acta, 147 (1983) 411.
7 K. Terada, K. Matsumoto and H. Kimura, Anal. Chim. Acta, 153 (1983) 237.
8 K. Terada, K. Matsumoto and T. Inaba, Anal. Chim. Acta, 158 (1984) 207.
9 F. Feigl, Chemistry of Specific, Selective and Sensitive Reactions, Academic Press, New York, 1949, p. 236.
10 Z. Holzbecher, L. Divis, M. Kral, L. Sucha and F. Vlacil, Handbook of Organic Reagent in Inorganic Analysis, Wiley, New York, 1976, p. 30.
11 C. Iida, Bunseki, (1983) 531.

Analytica Chimica Acta, 170 (1985) 237—243
Elsevier Science Publishers B.V., Amsterdam — Printed in The Netherlands

EVOLVED-GAS ZEEMAN FLAME ATOMIC ABSORPTION SPECTROMETRY FOR THE DETERMINATION OF ARSENIC COMPOUNDS

T. SAKAI[a], S. HANAMURA and J. D. WINEFORDNER*
Department of Chemistry, University of Florida, Gainesville, FL 32611 (U.S.A.)
(Received 19th September 1984)

SUMMARY

An evolved-gas separation/flame Zeeman atomic absorption spectrometric approach is demonstrated for the speciation and determination of arsenic in oyster tissue. No digestion is needed and separation of inorganic arsenic compounds having similar boiling points is achieved. A stoichiometric or air-rich acetylene/air flame for atomic absorption spectrometry is not generally suitable for arsenic determination because of severe ultraviolet absorption interference at 193.7 nm and low sensitivity; polarized flame Zeeman atomic absorption spectrophotometry with a fuel-rich flame is suitable for the detection of traces of arsenic. The evolved-gas separation/Zeeman atomic absorption approach is simple, based on commercially available instrumentation, and useful for the selective determination of major arsenic compounds. Data are given to demonstrate optimal conditions and to show application to oyster tissue.

Arsenic is an environmental toxic agent and is accumulated in numerous vegetables, grains, fruits, seafood and meat. Fruits and vegetables sprayed with arsenicals may also accumulate the element. In addition, arsenic is concentrated from the marine environment by fish and shellfish. Therefore, its measurement and assessment in environmental and biological samples is very important.

Numerous investigations have been reported on the determination of arsenic with flame atomic absorption spectrometry (a.a.s.) with hydride generation [1—4], atomic emission spectrometry based on a cold-trap method [5], graphite-furnace a.a.s. with liquid-liquid extraction [6] and gas chromatography with microwave emission spectrometry [7]. Most of these methods provide nanogram sensitivity for total arsenic, but these procedures have involved sample digestions. Accordingly, volatile arsenic may be lost during digestion and sample preparation of solid samples.

Four different digestion methods were compared by Yanagi and Abe [8] in order to determine arsenic in biological samples and a significant loss of arsenic (15—30%) was found when using a nitric/sulfuric/hydrofluoric acid

---

[a]On leave: Gifu College of Dentistry, Department of Chemistry, 1851 Takano Hozumicho, Motosu-gun, Gifu Prefecture, Japan.

0003-2670/85/$03.30

mixture for sample preparation. Therefore, a procedure based on evolved gas analysis for volatile species in solid samples has been developed here.

Although inorganic arsenic species, arsenite and arsenate, exist in nature, the arsenicals formed by the interaction of the inorganic form with bacteria are thought to account for the changes in oxidation state and the major chemical forms of arsenic. Therefore, it is very important to recognize the arsenic chemical forms and their quantities in the evaluation of arsenic in the environment. Recently, the speciation of inorganic and organic-bound arsenic has been achieved by thermal vaporization separation atomic spectrometric measurement [9—13]. However, these methods depend on special detection systems and instrumentation.

The present approach involves the determination and speciation of inorganic arsenic compounds by the simple and easily constructed method of evolved gas analysis/flame Zeeman atomic absorption spectrometry. The evolved gas separation has been described by Hanamura et al. [13].

EXPERIMENTAL

Apparatus and reagents

A Hitachi Model 180-80 polarized Zeeman atomic absorption spectrometer equipped with a 10-cm slot burner for air/acetylene (Modal 180-0690) and an arsenic hollow-cathode lamp (Hamamatsu TV Co.) was used for absorbance measurements. Signals were recorded with a Hitachi Model 056 chart recorder. The furnace vaporizer described previously [13] was combined with the polarized Zeeman atomic absorption spectrometer. The sample in the crucible was heated by a resistance heater from 50°C to 400°C. The temperature of the sample crucible was measured by a platinum resistance thermometer. The temperature was increased at a rate of 25°C min^{-1}. The volatile constituents were introduced into the nebulizer chamber by nitrogen carrier gas through the auxiliary gas port on the chamber.

An arsenic standard solution (1006.6 mg l^{-1}) in 4% (v/v) nitric acid was prepared by dissolving 0.3323 g of arsenic trioxide in 10 ml of distilled nitric acid and diluting to 250.0 ml with distilled water. The solution was stored in a polyethylene bottle.

Procedures

The instrumental operating conditions used for arsenic determination were as follows: lamp current, 10 mA; wavelength, 193.7 nm; monochromator slit width, 2.6 nm; burner height, 9 mm from burner top; flow rate of acetylene, 3.1 l min^{-1}; flow rate of air, 9.4 l min^{-1}; flow rate of nitrogen, 150 ml min^{-1}; heating rate for sample vaporization, 25°C min^{-1}; time constant, 5 s; scale expansion, 20×; recorder chart speed, 20 mm min^{-1}; recorder full scale, 10 mV.

For the analysis of oyster tissue, 0.2500 g of dried sample containing about 13 ng of arsenic was placed in a quartz crucible. The sample thickness should

be less than 3 mm to minimize tailing of the peaks. After ignition of the acetylene/air flame, the sample in the crucible was heated at a rate of 25°C min^{-1} and the absorbance signal at 193.7 nm was recorded. The signal area was measured by cutting out the absorption peak and weighing it.

RESULTS AND DISCUSSION

Analytical conditions

The effect of the time constant for the absorption signals was investigated at 0.5, 1, 2, 5 and 20 s. A time constant of 5 s (also 20 s) gave the largest signal-to-noise ratio. In Fig. 1, the variation is given in the Zeeman background-corrected atomic absorption for an arsenic standard with variation in acetylene flow rate and burner height. The optimum acetylene flow rate and burner height were 3.3 l min^{-1} and 9 mm, respectively. In unpublished work, the enhancement in the sensitivity under fuel-rich conditions was 4.2× compared to that in the fuel-lean flame. In this work, a flow rate of 3.1 l min^{-1} is recommended for the sensitive determination of arsenic with the air-acetylene flame because of the greater signal reproducibility and stability even though the signal-to-noise ratio is slightly less than at 3.3 l min^{-1}. Because the

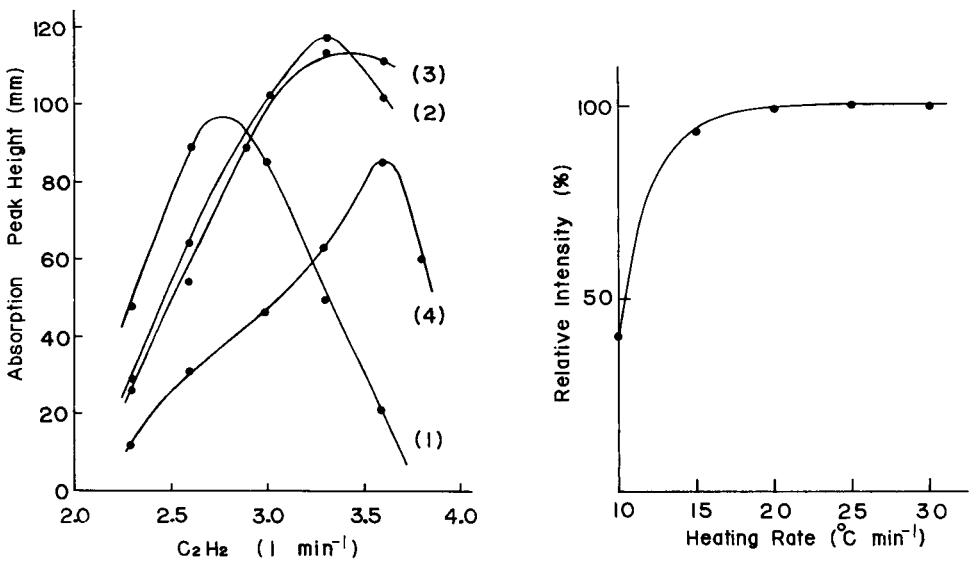

Fig. 1. Variation of atomic absorption peak height with acetylene flow rate and burner height (observation height from burner tip) for arsenic (20.13 μg ml^{-1}). Air flow rate 9.4 l min^{-1}; wavelength 197.7 nm; spectral slit width 2.6 nm.

Fig. 2. Effect of heating rate in sample crucible for evolution of arsenic (10.07 μg) from a solid sample. Time constants 5 s; nitrogen flow rate 150 ml min^{-1}; acetylene flow rate 3.1 l min^{-1}, spectral slit width 2.6 nm.

vaporized molecular species introduced into the flame appeared at characteristic temperatures dependent upon their molecular form, a constant heating rate and sufficiently high final temperature are required to evolve the arsenic species from the solid sample. In Fig. 2, the effect of thermal vaporization of arsenic trioxide solution is shown as a function of heating rate. The absorption intensity was maximal and constant at heating rates in the range 20—30°C min^{-1} (30°C min^{-1} was the highest practical rate with the heater used). When the heating rate was less than 15°C min^{-1}, the absorption area decreased. Because a slower heating rate results in an absorption peak which is broader and a signal-to-noise ratio (S/N) which is smaller, and a heating rate higher than 30°C min^{-1} destroys the heater wire, a 25°C min^{-1} heating rate was used for all studies.

Transfer line temperature. If the temperature of the sample gas transfer line between the evolved gas system and the nebulizer chamber is too low, the vaporized gas species condense and deposit on the line and/or are adsorbed, resulting in losses and contamination in future determinations. Consequently, the absorption peak shape may be distorted, broadened and tailed. In this work, the transfer line was maintained at about 200°C by heating tape. However, disassembly and cleaning of the transfer line were still required after every 5 determinations to avoid memory effects. Also, after each measurement, the temperature of the transfer line was raised to about 350°C for a few seconds.

Effect of nitrogen carrier flow rate. The carrier gas is important to sweep the vaporized arsenic molecules into the nebulizer chamber. The absorption intensity was maximum and constant for a nitrogen flow rate of 100—200 ml min^{-1}. When the flow rate was more than 300 ml min^{-1}, the intensity decreased because the temperature in the sample crucible decreased owing to the fast gas flow. The flow rate recommended for measurements is therefore 150 ml min^{-1}.

Calibration graph and precision

Under the optimum experimental conditions, the calibration graph was prepared with an arsenic trioxide standard solution. Volumes (3—5 μl) of 1006.6 μg ml^{-1} arsenic standard solution were placed in the crucible with a micropipette. Several profiles of absorption signals for the determination of arsenic are shown in Fig. 3.

The relationship between the signal area and amount of arsenic was linear in the range 0—9 μg but the signal-to-noise ratio was only suitable in the range 3—9 μg. The linearity became poor when the amount of arsenic was less than 3 μg because of the small S/N ratio. As can be seen in Fig. 3, the absorption intensity is linear, but the absorption signal shape varies with the amount of arsenic. Accordingly, measurements of peak areas are required rather than the peak heights. The relative standard deviation (12 determinations) was estimated to be 5.2% for 5 μg of arsenic and the limit of detection was 0.5 μg. This limit was almost the same with Zeeman atomic absorption spectrometry using an aqueous standard solution (0.4 μg).

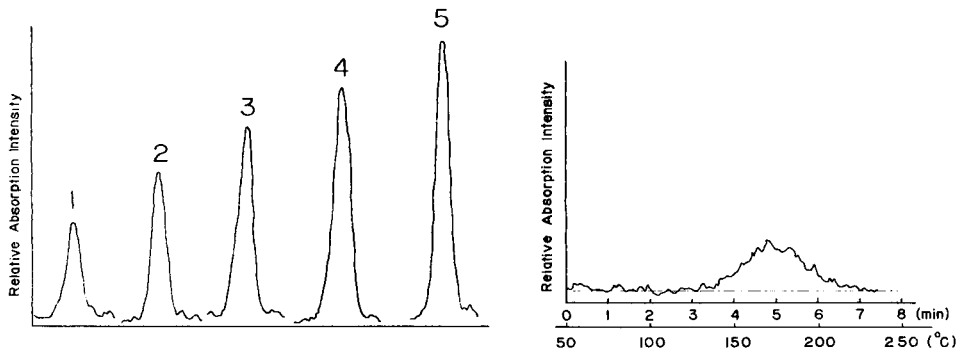

Fig. 3. Profiles of absorption signals for calibration graph. Arsenic concentrations: (1) 4.03 μg; (2) 5.03 μg; (3) 6.04 μg; (4) 7.05 μg; (5) 8.05 μg. Heating rate 25° C min^{-1}; carrier gas flow rate 150 ml min^{-1}.

Fig. 4. Absorption profile of arsenic from standard oyster tissue. Time constant 5 s; heating rate 25° C min^{-1}; carrier gas flow rate 150 ml min^{-1}.

Application to arsenic determination

Absorption profiles of arsenic in oyster tissue (NBS SRM-1566 oyster tissue) are shown in Fig. 4. The heating rate of the sample was 25° C min^{-1} and carrier gas flow rate was 150 ml min^{-1}. Although arsenic absorption signals from standard solutions appeared at about 3 min, the signal from oyster tissue occurred at about 5 min, which was probably caused by a matrix effect between the arsenicals and the tissues. Arsenic in NBS SRM-1566 oyster tissues was determined from the calibration graph (using least squares). The result obtained was 13.9 ± 0.52 μg g^{-1} for 4 determinations (NBS value is 13.4 ± 1.9 μg g^{-1}).

In order to assess the capability of this method, recovery experiments were done on mixtures of standard oyster tissue and arsenic trioxide standard solutions. Here, 5.03 μg and/or 8.06 μg of arsenic as the standard solution was added to 0.35 g of the oyster tissue. The results obtained are shown in Table 1. The recovery of arsenic by this method was highly successful.

In other analytical procedures for biological samples, the samples are usually decomposed with some kind of acid under heated conditions. Accordingly, volatile components, such as arsenic and mercury, are lost during this preparation. However, with the proposed method, volatile elements are determined by direct evolution of the gaseous species into the detection system. Also, great selectivity occurs because of the different boiling points of potentially interfering species.

Speciation with Zeeman atomic absorption spectrometry

Typical absorption profiles for pure arsenic triiodide and arsenic trioxide are shown in Fig. 5. Although the boiling points of arsenic triiodide and arsenic trioxide are similar, the signal of arsenic triiodide appeared at 93° C

TABLE 1

Recovery tests of arsenic in NBS SRM-1566 standard oyster tissue

As added (μg)	As found (μg)[a]	Recovery (%)
0	3.48	—
5.03	8.88	107
8.06	11.56	100

[a]The results given are the means of 3 determinations and these values were obtained by the least-squares method.

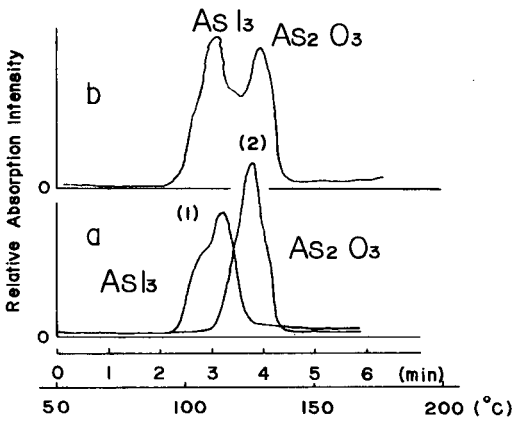

Fig. 5. Evolution profiles of arsenic compounds and the mixture. (a) Single compounds: (1) AsI_3; (2) As_2O_3. (b) AsI_3/As_2O_3 mixture, 50%/50%. Heating rate 20° C min^{-1}; spectral slit width 1 nm; carrier gas flow rate 150 ml min^{-1}.

and that of arsenic trioxide appeared at 115° C (the heating rate was 20° C min^{-1}). The absorption peaks obtained from mixtures of the two compounds are also shown in Fig. 5. However, in this work, the profiles of other arsenicals and other organometallic compounds could not be obtained because of the limited upper temperature of the furnace.

The evolved gas/Zeeman atomic absorption method has excellent background correction and few interferences from other elements because of the characteristic thermal vaporization of arsenicals and allows the sampling of large amounts of solid sample (250 mg—1 g) to avoid heterogeneity problems.

This work was supported by AF-AFOSR-49620-84-C-0002DEF and EPA-R-810387-01-1.

REFERENCES

1 W. Holak, Anal. Chem., 42 (1969) 1713.
2 J. S. Edmonds and K. A. Francesconi, Anal. Chem., 48 (1976) 2019.

3 R. Tsujino, H. Yamamoto, S. Ueda, T. Sudo and Y. Sawasaki, Bunseki Kagaku, 23 (1974) 1378.
4 Y. Yamamoto, T. Kumamaru, T. Edo and J. Takemoto, Bunseki Kagaku, 25 (1976) 770.
5 R. S. Braman, D. L. Johnson, C. C. Foreback, J. M. Ammous and J. L. Bricker, Anal. Chem., 49 (1977) 621.
6 Y. Odanaka, O. Matano and S. Goto, Bunseki Kagaku, 28 (1979) 517.
7 Y. Talmi and D. T. Bostick, Anal. Chem., 47 (1975) 2145.
8 K. Yanagi and M. Abe, Bunseki Kagaku, 30 (1981) 209.
9 A. U. Shaikh and D. E. Tallman, Anal. Chim. Acta, 98 (1978) 251.
10 J. W. Robinson and L. J. Rhodes, Spectrosc. Lett., 13 (1980) 253.
11 C. F. Bauer and D. F. S. Natusch, Anal. Chem., 53 (1981) 2020.
12 E. R. Prack and G. J. Bastiaans, Anal. Chem., 55 (1983) 1654.
13 S. Hanamura, B. W. Smith and J. D. Winefordner, Anal. Chem., 55 (1983) 2026.

Analytica Chimica Acta, 170 (1985) 245—253
Elsevier Science Publishers B.V., Amsterdam — Printed in The Netherlands

ESTIMATION OF INDIVIDUAL ULTRAVIOLET SPECTRA IN INCOMPLETE TWO-COMPONENT SEPARATIONS BY HIGH-PERFORMANCE LIQUID CHROMATOGRAPHY

J. H. VAN TONGEREN, J. W. WEYLAND, H. VAN DER VOET* and P. M. J. COENEGRACHT

Chemometrics Research Group, Pharmaceutical Laboratories, State University, Anton Deusinglaan 2, 9713 AW Groningen (The Netherlands)

(Received 9th July 1984)

SUMMARY

A method is described for the estimation of spectral features in a two-component chromatographic peak by means of a u.v. diode-array detector. The calculation relies on the assumption that the front of a fused chromatographic peak contains a single pure component. The spectrum of this component is used in calculating the concentration profile of the other component, thus allowing the determination of a solution band for the spectrum of the second component. The boundaries of the solution band are based on non-negativity restrictions of chromatographic and spectral features. The method does not require the use of principal components analysis.

Principal component analysis is a powerful technique for the manipulation of large data sets. It is useful for the improvement of signal/noise ratios [1], and for estimation of pure spectra from spectra of mixtures [2—7]. This paper describes an alternative method for the estimation of unknown spectra in the case of a two-component fused peak in high-performance liquid chromatography (h.p.l.c.) with a u.v. detector. Unlike some other methods, this method does not require the use of principal component analysis. The main assumption is that the front of a fused chromatographic peak contains a pure component and that neither component can contribute to negative absorbance values. If one of the components is nowhere eluted in a pure state, then no estimation methods will derive an exact solution but a solution band, based on the reasonable assumptions that a spectrum is always non-negative and that all measured spectra are positive linear combinations of the pure spectra. The width of the solution band becomes smaller when the pure spectra have values near zero. When u.v. detection is used rather than mass spectrometry, it is probable that the pure spectra do not contain values near zero. This results in a broad non-negativity restriction in the solution band. However, u.v. detection is widely used, and many routine laboratories are interested in fast, easily applicable methods of estimating unknown spectra.

0003-2670/85/$03.30

THEORY

General aspects

An arbitrary absorbance, $A^{AB}(\lambda_i, t_j)$, measured at wavelength λ_i and time t_j can be described as the summation of the individual absorbances of the components at that wavelength and time

$$A^{AB}(\lambda_i, t_j) = \epsilon^A(\lambda_i)c^A(t_j) + \epsilon^B(\lambda_i)c^B(t_j) \quad (1)$$

where $\epsilon(\lambda_i)$ is the absorptivity of component A or B as indicated by the superscript at wavelength λ_i, and $c(t_j)$ is the concentration of the component at time t_j.

A spectrum measured at a fixed time t_j can be represented as

$$A^{AB}(\lambda, t_j) = \epsilon^A(\lambda)c^A(t_j) + \epsilon^B(\lambda)c^B(t_j) \quad (2)$$

where $\epsilon(\lambda)$ is the spectral profile of the component indicated by the superscript. Analogously, a chromatogram measured at fixed wavelength λ_i can be represented as

$$A^{AB}(\lambda_i, t) = \epsilon^A(\lambda_i)c^A(t) + \epsilon^B(\lambda_i)c^B(t) \quad (3)$$

where $c(t)$ is the concentration profile of the component indicated by the superscript. The magnitude of these profiles is not of interest for qualitative work. The only requirement is that the product of the spectral and concentration profiles of the component, i.e., the individual contribution to the measured data, remains the same.

As indicated by Eqn. 1, all measured absorbances can be described as the summation of the individual contributions of components A and B. Neglecting the effects of noise, neither component contributes negative values, for both the spectral and the concentration profiles have positive or zero values, i.e., $\epsilon^A(\lambda)c^A(t) \geqslant 0$ and $\epsilon^B(\lambda)c^B(t) \geqslant 0$ where $\epsilon(\lambda) \geqslant 0$ and $c(t) \geqslant 0$. These are the only restrictions imposed on the estimations; they can be interpreted as non-negativity of the spectrum of the second component at a certain time and of the chromatogram of the first component at a certain wavelength (see below).

Estimation of the concentration profile of the second component

The derivative of Eqn. 3 with respect to wavelength is

$$\partial A^{AB}/\partial\lambda(\lambda_i, t) = c^A(t)d\epsilon^A(\lambda_i)/d\lambda + c^B(t)d\epsilon^B(\lambda_i)/d\lambda \quad (4)$$

If the spectrum of component A has a maximum (or a minimum) at wavelength λ_m (so that $d\epsilon^A(\lambda_m)/d\lambda = 0$), Eqn. 4 simplifies to

$$\partial A^{AB}/\partial\lambda(\lambda_m, t) = c^B(t)d\epsilon^B(\lambda_m)/d\lambda \quad (5)$$

Because the derivative term on the right-hand side is a constant with respect to time, the derivative on the left-hand side is directly proportional to the concentration profile of component B. Depending on the sign of the

slope of the spectrum of component B at wavelength λ_m the derivative $\partial A^{AB}/\partial\lambda(\lambda_m, t)$ will be either positive or negative. Therefore it may be necessary to convert all values to the opposite sign if the peak turns out to consist of negative values. If it can be assumed that the front of the fused peak contains the pure component A, a maximum of its spectrum can be determined and the concentration profile of component B can be calculated up to a proportionality constant.

Estimation of the spectral profile of the second component

A chromatogram of a mixture measured at wavelength λ_m contains both the first and second components. The chromatogram of the first component $A^A(\lambda_m, t)$ is found by subtraction of the contribution of component B from $A^{AB}(\lambda_m, t)$. Substitution of Eqn. 5 into Eqn. 3 and rearrangement results in

$$A^A(\lambda_m, t) = A^{AB}(\lambda_m, t) - K\partial A^{AB}/\partial\lambda(\lambda_m, t) \tag{6}$$

with $K = \epsilon^B(\lambda_m)/[d\epsilon^B(\lambda_m)/d\lambda]$. The value of K cannot be determined exactly. It is, however, possible to restrict the range of possible values of K to a certain interval (i.e., a solution band). The upper boundary for K is found by varying K and constantly checking whether any point of the estimated chromatogram $A^A(\lambda_m, t)$ becomes more negative than the noise level. (In the following, this upper boundary for K is referred to as the non-negative chromatogram (NNC) boundary.) The lower boundary for K is characterized by a restriction imposed on the spectrum of component B, and will therefore be referred to as the non-negative spectra (NNS) boundary.

The spectrum of the pure component A is measured at the leading flank of the chromatographic peak at time t_1

$$A^A(\lambda, t_1) = \epsilon^A(\lambda)c^A(t_1) \tag{7}$$

Substitution of Eqn. 7 into Eqn. 2 and rearrangement gives the expression for the spectrum $A^B(\lambda, t_m)$ of component B at time t_m

$$A^B(\lambda, t_m) = A^{AB}(\lambda, t_m) - A^A(\lambda, t_1)c^A(t_m)/c^A(t_1) \tag{8}$$

or

$$A^B(\lambda, t_m) = A^{AB}(\lambda, t_m) - A^A(\lambda, t_1)\epsilon^A(\lambda_m)c^A(t_m)/[\epsilon^A(\lambda_m)c^A(t_1)] \tag{8a}$$

The value of $\epsilon^A(\lambda_m)c^A(t_1)$ is known from the spectrum of component A (Eqn. 7) and $\epsilon^A(\lambda_m)c^A(t_m) = A^A(\lambda_m, t_m)$ is the absorbance of component A at wavelength λ_m and time t_m, which can be calculated from Eqn. 6. Substitution of Eqn. 6 into Eqn. 8a and rearrangement gives

$$A^B(\lambda, t_m) = A^{AB}(\lambda, t_m) - A^A(\lambda, t_1)\{[A^{AB}(\lambda_m, t_m)/A^A(\lambda_m, t_1)] - [K/A^A(\lambda_m, t_1)][\partial A^{AB}/\partial\lambda(\lambda_m, t_m)]\} \tag{9}$$

From Eqn. 9, the NNS boundary can be found by decreasing K and checking

whether any point of the estimated spectrum $A^B(\lambda, t_m)$ becomes more negative than the noise level.

By substitution of both the upper and lower boundary for K into Eqn. 9, a solution band for the unknown spectrum of component B is found.

Search areas and noise levels

Because all calculations are based on the variation of the magnitude of the concentration profile of the second component $\partial A^{AB}/\partial\lambda(\lambda_m, t)$, it is necessary to check only those calculated absorbances where the second component is present. The search area for the NNS boundary is restricted further to time t_m (where the concentration is the largest), for that spectrum is influenced the most by variation of K. When K is chosen too small, it is the largest concentration of the second component that accounts for the most negative $A^B(\lambda, t_m)$.

From a similar point of view, the search area for the NNC boundary is restricted to a single calculated chromatogram of component A. This chromatogram should be that chromatogram where the absorptivity of component A is the largest, for this chromatogram will produce the most negative values of $A^A(\lambda_m, t)$. Furthermore, only that area of the chromatogram need be investigated where the influence of component B is present, as noted above.

Normally, restrictions are based on non-negativity of the individual contributions. However, in practice, negative elements may be measured, because of noise and the level of the baseline. Therefore it will be more useful to base restrictions on baseline noise of the individual contributions rather than the customary non-negativity. If white noise is present on a constant baseline level, the restriction for the individual contributions can be written as $A(\lambda_i, t_j) > M - 2SD$, where $A(\lambda_i, t_j)$ is the calculated absorbance of either component A or B, M is the mean of the calculated baseline, and SD is the standard deviation of the calculation baseline.

In most cases, the proposed restriction will differ little from a non-negativity restriction, but small negative values are now tolerated. When the NNC boundary is searched for the constant K (Eqn. 6), the baseline noise is calculated from the values $A^A(\lambda_m, t)$ from the beginning of the chromatogram up to a time t_0, which is chosen somewhere before the leading flank in order to make certain that the calculations are made on true baseline values (here, t_0 was taken as 4 arbitrary time units before t_1). When the NNS boundary is searched for K, the noise level is estimated from an arbitrary baseline "spectrum" $A^B(\lambda, t_{ar})$. Figure 1 is a schematic representation of the measured data, the individual contributions of components A and B, and the search areas.

EXPERIMENTAL

Data

The technique was tested on simulated and real h.p.l.c. outputs. Simulated separations were constructed from digitized spectra of sulfafurazole and

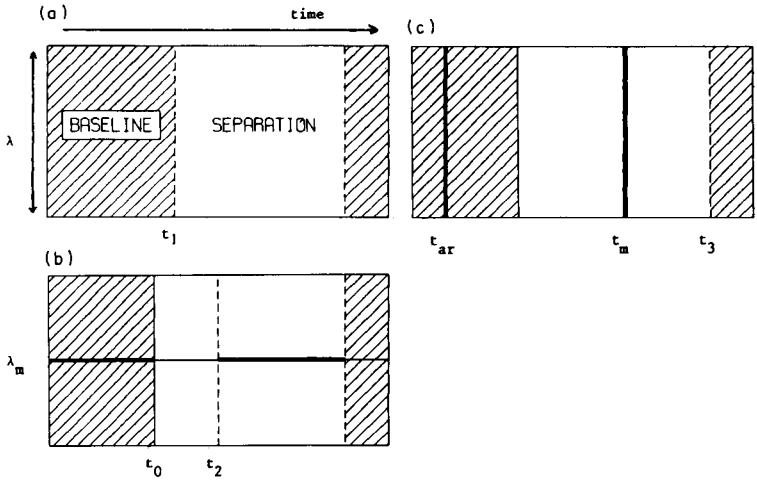

Fig. 1. Schematic representation of: (a) measured data; (b) contribution of component A; (c) contribution of component B. The indicated points of time (arbitrary units) are: t_1, initial spectrum; $t_0 = t_1 - 4$; t_2, peak front B; t_m, concentration maximum B; t_3, peak end B; t_{ar}, arbitrary point of time in the baseline area. The spectral maximum of A is indicated as λ_m. Appropriate areas for noise-level calculation and search areas are indicated by bold lines.

sulfathiazole. The concentration profiles were modelled as Gaussian peaks with standard deviations of three or four arbitrary units on the time axis. Noise was simulated by superimposing Gaussian distributed noise with zero mean and a standard deviation of 0.0002 absorbance. This amount of noise was chosen in order to achieve the same signal/noise ratio as in real separations.

The h.p.l.c. system comprised a Waters solvent-delivery system (M-45), an injection loop (10-μl capacity), a 200 × 46-mm stainless steel column packed with Nucleosil RP8 5 μm, and a Hewlett-Packard diode-array spectrophotometric detector (8450A). The concentrations of the investigated components, succinylsulfathiazole and sulfamerazine, were approximately 40 μg ml^{-1}. The amount of peak overlap was established by varying the composition of the eluent water/acetonitrile/acetic acid; the ratios used were 79:20:1 (I) and 79.5:19.5:1 (II) [8]. The flow rate was 1.0 ml min^{-1}.

Computations

Programs for the determination of the front of the chromatographic peak, a maximum for the spectrum of the first component, the concentration profile of the second component, and the estimation of its spectrum were written in PASCAL. Peak start was determined by calculating a mean chromatogram from the measured chromatograms and following increasing tangent search with second derivative check, as discussed by Woerlee and Mol [9]. Subroutines from the NAG-package library were used for 5-point least-squares

parabolic curve-fitting round the maximum of the spectrum of the first component. All calculations were done with the Cyber 170/760 of the State University of Groningen. Plotted spectra were standardized to equal area under the curve in order to make comparison of the relative shapes possible.

RESULTS AND DISCUSSION

Reproducibility

The concentration profiles of a simulated separation were modelled as Gaussian peaks with a standard deviation of three time units. For sulfafurazole, a maximum was placed at time 26 while the maximum of sulfathiazole was placed at time 30. This separation has a fairly large amount of chromatographic peak overlap but the front still contains pure sulfafurazole.

In order to demonstrate the reproducibility of the proposed method, random Gaussian noise was added and the calculations were done. The results of five such simulations are given in Table 1. Although the same amount of noise was added to the simulation, the peak-start and peak-end detection fluctuated somewhat. This, however, does not appear to have major consequences on the values of the NNS and NNC boundaries for K.

Figure 2 shows a graphical representation of the estimated spectra for a typical boundary set, compared with the pure spectrum of sulfathiazole. As can be seen, the NNC boundary clearly gives a better estimate of the pure spectrum than does the NNS boundary. This indicates that the simulation contains an area of pure sulfathiazole (as expected), for an area in the mixture chromatogram $A^{AB}(\lambda_m, t)$ consisting of the pure second component, gives a remainder (see Eqn. 6) that reaches the noise level restriction at an earlier stage than a mixture area. Moreover, the measured spectrum that best resembles the real spectrum of the second component is actually the NNC estimate of the spectrum of the second component. The NNS boundary is a poorer estimate because it is forced through zero, whereas in this case the real spectrum does not contain zero values.

TABLE 1

Influence of superimposed Gaussian noise (mean = 0, SD = 0.0002; peak front and peak end are expressed in arbitrary time units)

	Front A	Front B	End	NNS boundary for K	NNC boundary for K
1	20	23	38	5.45	11.2
2	20	23	37	6.12	10.5
3	20	23	38	5.68	11.7
4	20	24	37	6.06	11.9
5	20	22	37	5.97	11.4
Mean	20	23	37	5.86	11.3

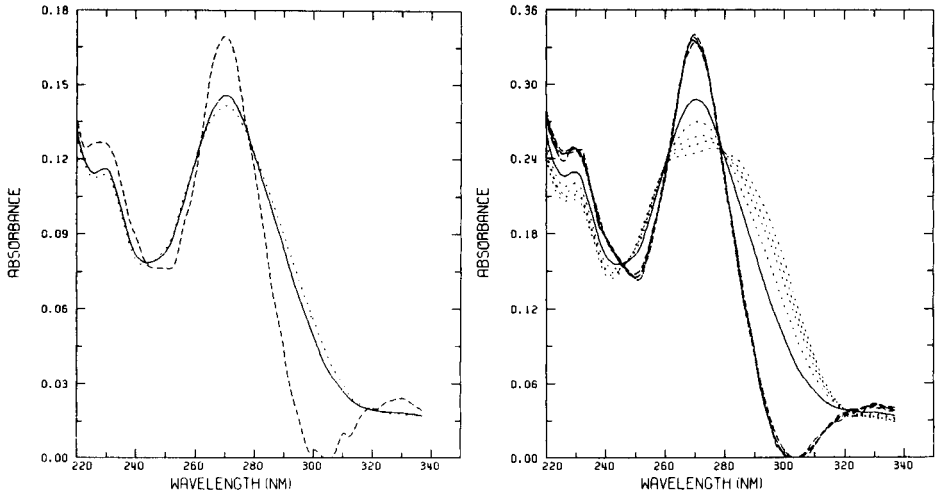

Fig. 2. Representation of spectral estimations of sulfathiazole from a simulated separation: (---) NNS boundary; (···) NNC boundary; (—) real spectrum.

Fig. 3. Influence of amount of peak overlap on spectral estimations: (—) real spectrum of sulfathiazole; (---) NNS boundary; (···) NNC boundary. Less resemblance to the real spectrum corresponds to a greater amplitude ratio A:B.

Simulations with total overlap of the second component

In order to achieve simulations containing no pure spectrum of the second component, the concentration profile of the first component was widened by modelling it as a Gaussian peak with a standard deviation of four time units rather than three. The positions of the maxima remained the same, namely, at times 26 and 30. Furthermore, the amplitude of the first component relative to the second component was varied. The parameters of the concentration profiles and the results of four simulated separations are listed in Table 2. For all four separations, the spectrum at time unit 20 was chosen as the pure spectrum of the first component, in spite of the front being de-

TABLE 2

Influence of amount of overlap and amplitude ratio, component A: mean = 26, SD = 4 in arbitrary time units; component B: mean = 30, SD = 3 in arbitrary time units

	Amplitude ratio	NNS boundary for K	NNC boundary for K
1	1	5.92	13.9
2	2	5.87	17.0
3	3	6.04	19.6
4	4	5.97	23.2

tected at an earlier time. This was done so that all differences between the results could be attributed to amplitude variation of the concentration profile of the first component.

Because there is no area in the simulation consisting of pure second component, a greater amount of the concentration profile of the second component has to be subtracted from the mixture chromatogram (Eqn. 6) before the imposed restriction is reached. Moreover, the NNC boundary will vary with the amplitude of the concentration profile of the first component, i.e., the amount of overlap. Figure 3 gives a graphical representation of the real spectrum of sulfathiazole compared with the spectra based on the estimations for K listed in Table 2. The NNS boundary remains practically the same for each separation because it is based on restrictions imposed on a spectrum and not on a chromatogram. Therefore, it is independent of the amount of chromatographic peak overlap.

Real separations

Graphic representations of two real separations are given in Fig. 4. The mobile phases used are given under Experimental. Both separations contain pure spectra of the first component (succinylsulfathiazole), making application of the proposed method possible. The spectral estimations of sulfamerazine are given in Fig. 5. Although there is a large difference in the amount of chromatographic peak overlap (Fig. 4), Fig. 5 shows only a small difference in the width of the solution band.

The NNC solution does not coincide with the pure spectrum. This means that a pure spectrum of sulfamerazine was not measured because of tailing of the succinyl-sulfathiasole peak.

Conclusions

A solution band of the spectrum of the second component can be determined with the use of restrictions based on the noise level in estimated indi-

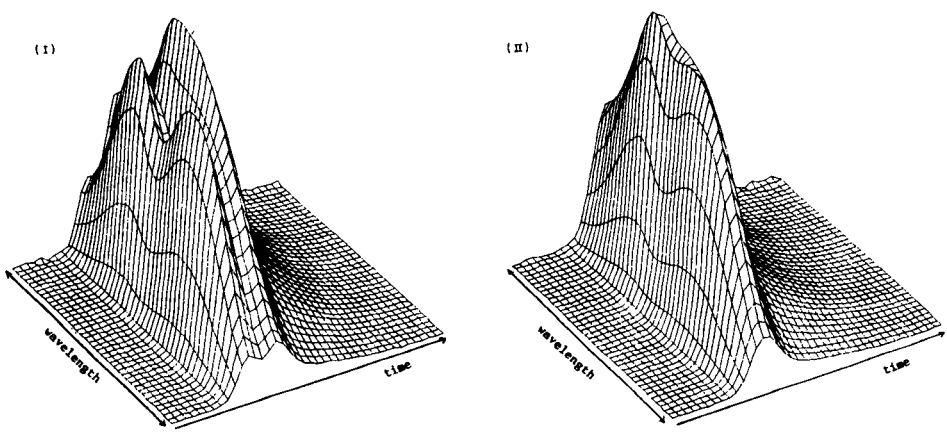

Fig. 4. Graphic representations of real h.p.l.c. separations done with different mobile-phase compositions (for I and II, see text).

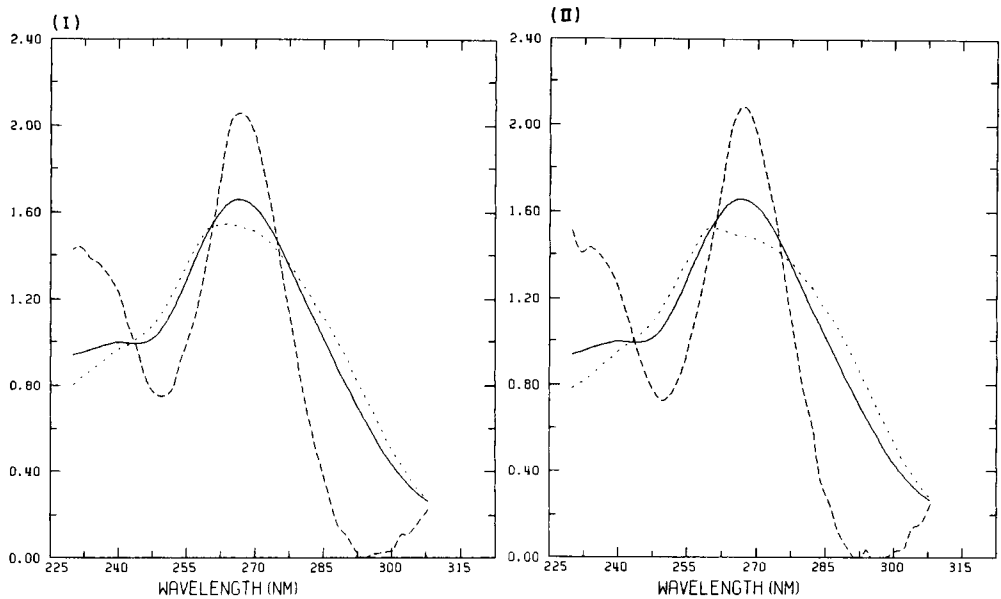

Fig. 5. Spectral estimations of sulfamerazine for two real h.p.l.c. separations: (---) NNS boundary; (···) NNC boundary; (——) real spectrum of sulfamerazine (see text).

vidual contributions. The NNC boundary of the solution band is that measured spectrum that best resembles the real spectrum. The NNS boundary of the solution band contains values near zero. Therefore, if the real spectrum also contains zero absorbance values, the lower boundary approaches the real spectrum. Accordingly, it is recommended to measure all spectra over a wavelength interval in which the second component is expected to have zero absorbances somewhere.

Considering the small amount of calculation needed, the proposed method should be suitable for implementation on microcomputers.

REFERENCES

1 E. R. Malinowski and D. G. Howery, Factor Analysis in Chemistry, Wiley, New York, 1980, Ch. 4.
2 P. C. Gillette, J. B. Lando and J. L. Koenig, Anal. Chem., 55 (1983) 630.
3 W. H. Lawton and E. A. Sylvester, Technometrics, 13 (1971) 617.
4 M. A. Sharaf and B. R. Kowalski, Anal. Chem., 53 (1981) 518.
5 M. A. Sharaf and B. R. Kowalski, Anal. Chem., 54 (1982) 1291.
6 J. Chen and L. Hwang, Anal. Chim. Acta, 133 (1981) 271.
7 C. H. Lin and L. C. Lin, Proc. Natl. Sci. Counc. ROC, 3 (1979) 11.
8 J. W. Weyland, C. H. P. Bruins and D. A. Doornbos, J. Chromatogr. Sci., 22 (1984) 31.
9 E. F. G. Woerlee and J. C. Mol, J. Chromatogr. Sci., 18 (1980) 258.

Analytica Chimica Acta, 170 (1985) 255—264
Elsevier Science Publishers B.V., Amsterdam — Printed in The Netherlands

USE OF FACTOR ANALYSIS AND LIQUID CHROMATOGRAPHY TO DETERMINE THE NUMBER OF SPECIES IN REACTIONS OF POTASSIUM IONS WITH SELECTED POLYETHERS

MARIUS D'AMBOISE* and DENIS NOEL[a]

Department of Chemistry, University of Montreal, P.O. Box 6210, Station A, Montreal H3C 3V1 (Canada)

(Received 4th September 1984)

SUMMARY

Abstract factor analysis is used to determine the number of species in chemical systems from data obtained by high-performance liquid chromatography. Retention data for the systems involving the reaction between potassium ions and three polyethers, benzo-5-crown-5, dibenzo-18-crown-6, and dibenzo-24-crown-8, were obtained in methanol at room temperature. The experimental data were factor-analyzed in order to yield the number of species in the reacting system. In addition to the usual criteria, it is proposed that three-dimensional graphs of calculated data be compared to three-dimensional graphs of raw data in order to evaluate the factor space. It is also suggested that the three-dimensional graphs showing the residual error matrix be examined as a tool in the evaluation of the factor space. Two species were found from the reaction between benzo-15-crown-5 and potassium, one from dibenzo-18-crown-6, and three from dibenzo-24-crown-8 in methanol.

The study of chemical reactions involves determination of the number of reacting species as well as their identity and evaluation of equilibrium constants for the reactions linking them together. High-performance liquid chromatography (h.p.l.c.) can generate data that can be used for the resolution of chemical systems [1]. Abstract factor analysis, a.f.a., [2] and matrix rank analysis, m.r.a., have been used [3—5] with spectrophotometric data in order to establish the number of species in a solution. From a mathematical point of view, the rank of a data matrix corresponds to the number of species in a system; therefore, simple m.r.a. should suffice to answer the question. However, because experimental data are not exact, one must take into account the experimental error. This complicates the task of extracting the number of species from a set of data. The observed data matrix, [D], is the result of a pure data matrix, [D*], intertwined with an error matrix, [E]. The mathematical tool best suited to solve the problem is factor analysis [6].

---

[a]Present address: Conseil national de recherches Canada, Institut de génie des matériaux, 75, boul. De Mortagne, Boucherville, QC, J4B 6Y4, Canada.

0003-2670/85/$03.30

The present paper illustrates how liquid chromatographic retention data can be used to evaluate the number of chemical species present in a reacting system by means of a.f.a. The chemical systems studied consisted of the reactions between three polyethers and potassium ions in methanol. The polyethers were benzo-15-crown-5, dibenzo-18-crown-6 and dibenzo-24-crown-8. The nomenclature used in the present paper is that of Pedersen [7]; the compounds are abbreviated to B15C5, DB18C6 and DB24C8, respectively.

THEORY

Factor analysis

Factor analysis is one of the most powerful tools of chemometrics [8]. Essentially, it provides information on the number of factors responsible for a given set of observables and the identify of those factors. Abstract factor analysis provides the answer to the first problem, whereas target factor analysis (t.f.a.) may answer the second. The experimental data matrix, consisting of r rows and c columns, yields a set of abstract eigenvectors and an associated set of abstract eigenvalues. The magnitude of an eigenvalue indicates the relative importance of the corresponding eigenvector. The presence of experimental errors produces as many eigenvectors as there are columns or rows, whichever is smaller, in the data matrix. In this work, the number of rows always exceeded the number of columns. Eigenanalysis will thus generate c factors from which one must select the n principal factors responsible for the data. In a chemical system, a factor may correspond to a chemical entity; it is characterized by its eigenvector. In the abstract solution, the eigenvector itself is meaningless. However, t.f.a. may transform it into a meaningful vector such as the spectrum of a chemical species or the chromatogram of a pure compound.

Factor analysis yields a row matrix, $[\mathbf{R}]$, and a column matrix, $[\mathbf{C}]$, which lead to factor compression accomplished by dropping unwanted eigenvectors (i.e., those characterizing experimental errors). Factor compression generates a new calculated data matrix, $[\mathbf{D}^{\ddagger}]$: $[\mathbf{D}^{\ddagger}] = [\mathbf{R}^{\ddagger}][\mathbf{C}^{\ddagger}]$. The superscript indicates that factor compression has been applied. From a practical point of view, new data matrices are calculated using 1, 2, 3 ... c factors. After every consecutive step, the corresponding $[\mathbf{D}^{\ddagger}]$ matrix is compared to the raw data matrix, $[\mathbf{D}]$. The number of principal factors, n, is the minimum number of factors necessary to reproduce the raw data matrix within experimental errors. Omitting the secondary set of factors is merely omitting terms consisting of pure errors and produces data improvement [8].

Treatment of errors

It should be clear that correct deduction of the number of principal factors depends on the correct evaluation or measurement of experimental errors. Various workers [8—10] have discussed the basic concepts behind the effects of experimental errors in factor analysis.

The residual standard deviation is given by $RSD = (\Sigma_1^r \Sigma_1^c e_{ij}^2/rc)^{1/2}$ where e_{ij} is the difference between the raw data and the a.f.a.-calculated data; r and c, as in subsequent equations, refer to the number of rows and columns, respectively. The *RSD* also corresponds to the real error, *RE*, which measures the difference between the raw data and pure data possessing no experimental error.

By dropping the secondary set of factors, some errors are extracted from the raw data. This extracted error, *XE*, is given by $XE = RSD[1 - (n/c)]^{1/2}$. The extracted error is equivalent to the root-mean-square error, *RMS*, and is a measure of the difference between raw data and data regenerated by factor analysis.

Intertwined with the contributions of the principal factors, there remains a certain amount of experimental error in the calculated data. This is the imbedded error, *IE*. The proportion of imbedded error in a calculated matrix depends on the number of factors. It is easily shown that $(IE/RE) = (n/c)^{1/2}$. Hence, increasing the number of columns of the raw data matrix diminishes the imbedded error, all other things being equal.

The tests used to determine the number of principal factors, n, generally belong to two categories, depending on whether or not prior knowledge of error is available. For instance, one may examine the behavior of *IE* as the number of factors varies; it sometimes permits the correct evaluation of n. Similarly, the percent variance contained in the eigenvalue and the residual variance also give useful indications. Various criteria or functions can be used, but none is perfectly satisfactory. Therefore, one should not rely on a single test. In the present paper, criteria that do not require a knowledge of experimental error are applied. The average eigenvalue, in which all factors having eigenvalues larger than or equal to the average eigenvalue are retained, was applied. Further, the cumulative percent variance, *CPV*, was applied. This is given by

$$CPV = 100 \left(\sum_1^r \sum_1^c d_{ik}^{\ddagger 2} \Big/ \sum_1^r \sum_1^c d_{ik}^2 \right)$$

where $d_{ik}^{\ddagger}$ refers to the a.f.a.-reproduced data and d_{ik} refers to the raw data; the summations are taken over all data points. When this criterion is used, it is necessary to decide arbitrarily the value of *CPV* which draws the frontier between principal and secondary factors sets. The *CPV* measures the proportion of total variance in the data that is accounted for by a.f.a. whereas residual variance is due to pure error only. Exner's Ψ function [8, 11] is another criterion that seems useful. For a chromatographic data matrix, it is given by

$$\Psi = \left\{ \left[\sum_1^r \sum_1^c (d_{ik} - d_{ik}^{\ddagger})^2 \Big/ \sum_1^r \sum_1^c (\mathrm{d}_{ik} - \bar{\mathrm{d}})^2 \right] [rc/(rc - n)] \right\}^{1/2}$$

where $\bar{d}$ is the grand mean of the experimental data; the other parameters are as previously defined. Clearly, the larger the number of factors, the smaller

the value of Ψ. It has been suggested [8] that a value of $\leqslant 0.1$ corresponds to excellent agreement between theory and experimental data and a value of 0.1—0.3 to good agreement, whereas a value of 0.5 is the utmost admissible limit permitting one to say that there is a relationship between theory and experiment.

The number of principal factors can also be obtained by examining the correspondence between raw experimental data and calculated data using three-dimensional (3-D) plots. This is achieved by comparing a 3-D representation of raw data to the 3-D representation of data obtained by using successively 1, 2, 3 . . . c factors. It is usually possible to detect the correct number of principal factors required by the system through this approach.

The $[e^0]$ matrix elements were also examined to show the differences between raw data and calculated data. With the correct number of factors, positive and negative differences should be randomly distributed, and in more or less the same quantity; also, the sum of positive elements should equal the sum of negative elements. Furthermore, one can also plot 3-D graphs of these differences between raw and calculated data using 1, 2, 3 . . . c factors. Visual examination of these plots often permits an unambiguous decision concerning the number of factors. The $[e^0]$ matrices were computed, and for each, elements were classified as described above: positive, negative and zero values and the 3-D graph were plotted.

Liquid chromatographic signal

In order to have a mathematical treatment which is meaningful, matrix elements should be changing continuously as the proportion of reactants is modified. A chromatographic peak can be described by an exponentially modified gaussian model, in which the response is a function of the eluted volume V_E [12]. Usually, the chromatographic response, H, is taken at the peak maximum; sometimes, peak areas are calculated. For analytical purposes, these parameters suffice if the retention of the species under investigation is constant. In studies of equilibria such as those reported in the present paper, the chromatographic response must be corrected for the changes in dilution arising from changes in retention volumes. By using the dilution formula [13] that applies to chromatographic peaks, it is possible to show that a chromatographic response, R, given by $R = H/V_E$, is linearly related to the solute concentration C. Thus, the data matrix was constructed using the ratios H/V_E as a function of V_E and of the composition of solutions. The resulting matrix was submitted to factor analysis and to matrix rank analysis in order to determine the number of species responsible for the data. The matrices obtained with chromatographic retention data may sometimes contain a large number of zeros; in such cases, factor analysis may be applied to submatrices in order to decrease the number of zeros.

EXPERIMENTAL

Apparatus and reagents

The liquid chromatograph consisted of an Altex pump (Model 100; Altex Scientific, Berkeley, CA) coupled to a Perkin-Elmer LC-55 variable wavelength detector. An Altex Model 905-19 universal injector was used. The chromatograms were recorded with a linear recorder (Model 2541; Brinkman Instrumentals, Westburg, NY 11950). The stainless steel column (15-cm long, 4.2-mm i.d.) was packed with Lichrosorb RP-18 (10 μm; Merck) by a balanced density slurry method. It was thermostatted by a water jacket at 25° C.

Factor analysis was done with an Apple-II+ microcomputer, which had 64K RAM memory and was equipped with two floppy disk drives and an Apple dumpling-64 interface (Microtek, San Diego, CA 92123). The results were printed on an Epson FX-80 dot matrix printer.

Dibenzo-18-crown-6 was from Aldrich Chemical Co.; benzo-15-crown-5 and dibenzo-24-crown-8 were from Strem Chemicals (Newburyport, MA). The compounds were recrystallized from acetone. Potassium chloride was Fisher analytical reagent and methanol was Fisher h.p.l.c. solvent.

Procedures

Methanol containing various concentrations of potassium chloride (1.00×10^{-5}—1.00×10^{-4} M) was used as eluent in the chromatographic systems. Stock 1.00×10^{-4} M crown-ether (CE) solutions were prepared in methanol, and aliquots of these solutions were mixed with potassium chloride in methanol in proportions such that the sum of reactant concentrations, before reaction, remained constant ($C_T = C_{CE} + C_{KCl} = 1.00 \times 10^{-4}$ M). In every case, C_{KCl} in the eluent was the same as C_{KCl} in the mixed sample. Fifteen solutions were prepared with molar ratios $[CE/C_T]$ ranging between zero and 1.00. A constant volume (20 or 50 μl) was injected at the column head and the chromatogram was recorded. Detector response was measured at 274 nm for various elution volumes along the chromatogram by using a Gradicon digitizer. The value of the signal was divided by the retention volume and arranged as a data matrix in which the columns represented the various solutions.

Retention matrices were factor-analyzed using a series of programs written in Softbasic for an Apple-II+ system. Covariance about the origin was used in the treatment. More information concerning the programs can be obtained from the authors. The three-dimensional graphs were plotted by using Penguin Software's Complete Graphic System II, written for the Apple-II+ by Mark Pelczarski (Penguin Software, Geneva, IL).

RESULTS AND DISCUSSION

Principal component analysis is possible only if the set of principal factors can be separated from the set of secondary factors. This operation is by far

the most difficult of a.f.a.; it is even more complicated when retention data are used because of the large quantity of zeros in the raw data matrix. In order to arrive at the correct number of species in the reactions which were studied here, various sets of data from each system were submitted to a.f.a. Table 1 shows the normalized eigenvalues for a representative set of data for each system.

The average eigenvalue, the so-called eigenvalue-1 criterion, was applied to all systems; the number of factors found is given in Table 2. Similarly, the cumulative percent variance (*CPV*) in the eigenvalue was calculated; the number of factors obtained using 95 and 98% variance in the eigenvalue is given in Table 2. The table also reports the number of factors obtained by using various levels of Exner's Ψ function as well as the factor space obtained by using m.r.a. In addition to these criteria, the table also reports the number of factors obtained when the three-dimensional plots of the calculated data matrix are compared with that of the raw data matrix. An example of this approach is given in Fig. 1 for DB24CB. The example shows clearly that at least four factors are required to cover the factor space properly. Visual inspection whereby the 3-D representation using 1, 2, . . . *c* factors is superimposed on the 3-D representation of the raw data, is very instructive. Although small differences may be observed between raw and 4-factor data graphic representations, these are thought to be within limits of acceptable error. Also given in Table 2 is the number of factors obtained by examining discrepancies between 3-D representation of raw and calculated data. Figure 2 shows these differences, e^0, from a representative set of data of the B15C5-KCl system using 1, 2, 3, and 4 factors. The diagram represents a view

TABLE 1

Normalized eigenvalues

n	B15C5-KCl	DB18C6-KCl	DB24CB-KCl
1	12.2	6.01	6.86
2	3.45	1.42	4.88
3	1.01	0.84	2.20
4	0.26	0.40	0.77
5	0.05	0.23	0.23
6	4×10^{-3}	0.06	0.04
7	7×10^{-4}	0.03	0.01
8	5×10^{-4}	2×10^{-3}	4×10^{-3}
9	3×10^{-4}	6×10^{-4}	2×10^{-3}
10	2×10^{-4}		6×10^{-4}
11	1×10^{-4}		2×10^{-4}
12	4×10^{-5}		2×10^{-4}
13	2×10^{-5}		5×10^{-5}
14	1×10^{-5}		2×10^{-5}
15	7×10^{-6}		1×10^{-5}
16	2×10^{-6}		
17	5×10^{-7}		

TABLE 2

Summary of principal factors

Method	B15C5-KCl	DB18C6-KCl	DB24-KCl
Eigenvalue-1	3	2	3
CPV (95%)	2	3	3
CPV (98%)	3	3	4
Exner function:			
$\Psi = 0.5$	2	2	3
$\Psi = 0.3$	3	3	3
$\Psi = 0.1$	3	5	4
Matrix rank analysis	3	2	3
Three-D plots:			
(a) $[D^{\ddagger}]$	3	2	4
(b) $[e^{o}]$	3	2	4
Dist. of values	3	2	4
Size of matrix	18 x 17	28 x 9	33 x 15

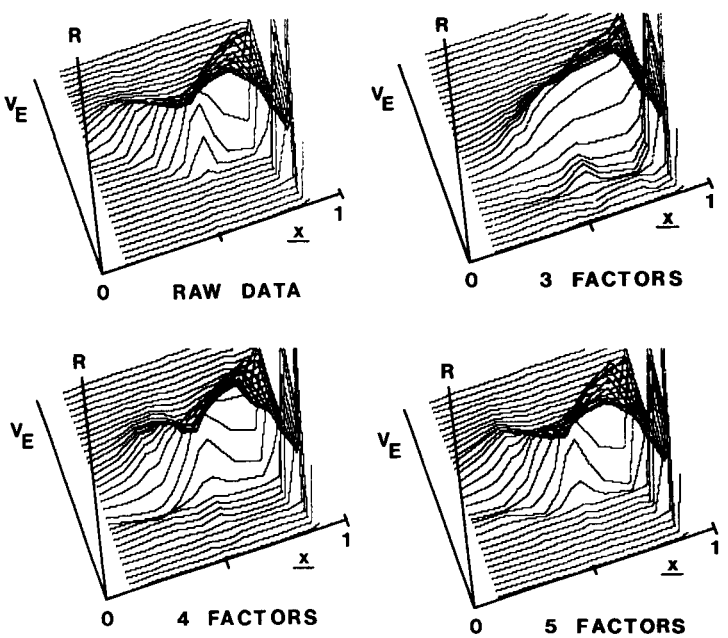

Fig. 1. Three-dimensional graph giving the calculated data matrix using 3, 4 and 5 factors and the raw data matrix for the system DB24C8-KCl in methanol. V_E, volume eluted; R, chromatographic response; x, mole ratio, [DB24C8/(DB24C8+KCl)].

perpendicular to the composition axis. It is evident from the graph that the system requires at least three factors to cover the factor space properly. The distribution of differences, as positive, negative and zero values, obtained by using 1, 2, 3 and 4 factors, led to a value for the factor space. It is given in

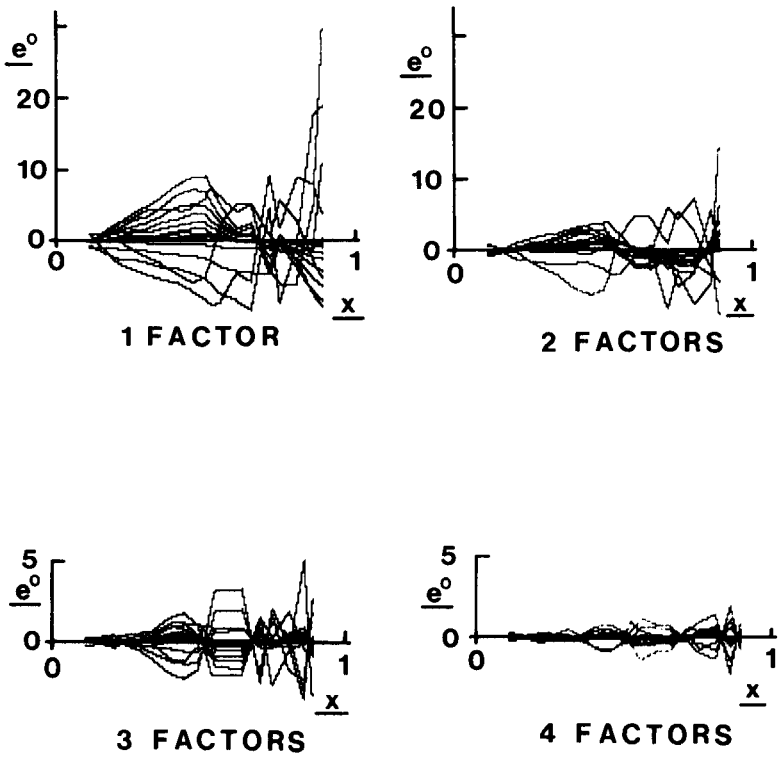

Fig. 2. Three-dimensional representation of the residual error matrix for the system B15C5-KCl in methanol. View perpendicular to the composition axis; x, mole ratio, [B15C5/(B15C5+KCl)]; $e^0 = d - d^{\ddagger}$.

Table 2. Similarly, the factor space derived from the sum of negative and positive values is also given in the table.

Eigenvalue-1, *CPV*, Exner's Ψ function and m.r.a. all produce a number of factors based on some arbitrary choice. They provide a good estimate of the factor space. However, it seems probable that the number of factors obtained from the 3-D plots is more accurate because it does not derive from any arbitrary parameter. The differences between each successive 3-D representation and the 3-D representation of raw data are sufficiently large to provide an unambiguous choice for the minimum number of factors. In contrast, Exner's function requires that the e^0 values be normally distributed with mean value equal to zero [11], a condition which was not fulfilled with the data (e.g., Fig. 2). Therefore the number of factors obtained by the 3-D graph methods was retained. The values given in the table for the system DB18C6-KCl present a larger variation for the reported set of data. This illustrates that a small number of columns, 9, generates a large imbedded error, as indicated by the equation $(IE/RE) = (n/c)^{1/2}$.

It is noteworthy that in the 3-D graph of Fig. 2 the distribution of values for e^0_{ij} becomes more and more symmetrical about the C-axis as the number

of factors increases. Also, a maximum-minimum pattern occurs as the proportion of reactants is changed. The various maxima-minima patterns produce near-nodal points where errors are at minimum values. These quasi-nodal points were observed in every system studied. They correspond to relative maximum values of the signal along the composition axis. Generally, the absolute value of error increases with the value of the signal; this is not the case when the signal is measured along a sharp chromatographic peak. In such a case, the value measured at the top of a peak is much more accurate than the value on either side of the peak. Error, absolute or relative, is not constant with chromatographic data; it does not increase constantly with the value of the signal. The quasi-nodal points represent the errors at the top of chromatographic peaks, and their positions along the *C*-axix give the composition of the corresponding chemical species. The error at the top of the peaks is about 5%; it increases rapidly on each side of the peaks (20—25%), and, as shown in Fig. 2, decreases again as the signal levels off. This behavior of the error function renders the use of the RE function hazardous for factor space determination. Similarly, the use of the number of factors and the corresponding value of *RE* to assess the experimental error does not seem appropriate in dealing with chromatographic peaks. Finally, Malinowski's factor indicating function [8] could not be used with the present data.

The various methods used to establish the number of factors led to postulation of a minimum of three factors for B15C5-KCl, two for DB18C6-KCl, and four for the DB24C8-KCl system. These factors may be attributed to the various chemical species present in each system, provided that the detector responds to all species. Thus, because potassium chloride is not active at the detector, there are respectively, 2, 1, and 3 new species in the systems studied. Therefore, the following species are likely to be present in these systems.

(1) Benzo-15-crown-5-KCl: B15C5, B15C5.KCl and B15C5.KCl.B15C5
(2) Dibenzo-18-crown-6-KCl: DB18C6 and DB18C6.KCl
(3) Dibenzo-24-crown-8-KCl: DB24C8, DB24C8.KCl, KCl.DB24C8.KCl and DB24C8.KCl.DB24C8.

These findings for the system B15C5-KCl and for the system DB18C6-KCl are in agreement with earlier data [7, 14] based on different experimental approaches. No literature data are available for the system DB24C8-KCl. A forthcoming paper will deal with the specific identification of the species reported in the present paper as well as with the evaluation of their formation constants.

The Natural Sciences and Engineering Research Council of Canada is acknowledged for financial support (grant A-1302). One of us (D.N.) is also grateful to the Aluminum Company of Canada for a scholarship.

REFERENCES

1 W. R. Melander and C. Horvath, in C. Horvath (Ed.), High-Performance Liquid Chromatography, Advances and Perspectives, Vol. 2, Academic Press, New York, 1980.
2 P. H. Weiner, Chemtech, May (1977) 321.
3 D. Katakis, Anal. Chem., 37 (1965) 876.
4 J. S. Coleman, L. P. Varga and S. H. Mastin, Inorg. Chem., 39 (1967) 1101.
5 R. M. Wallace and S. M. Katz, J. Phys. Chem., 68 (1964) 3890.
6 E. M. Magar, Biopolymers, 11 (1972) 2187.
7 C. J. Pedersen, J. Am. Chem. Soc., 89 (1967) 7017.
8 E. R. Malinowski and D. G. Howery, Factor Analysis in Chemistry, Wiley-Interscience, New York, 1980.
9 D. L. Duewer, B. R. Kowalski and J. L. Fasching, Anal. Chem., 48 (1976) 2002.
10 B. A. Roscoe and P. K. Hopke, Anal. Chim. Acta, 132 (1981) 89.
11 O. Exner, Collect. Czech. Chem. Commun., 31 (1966) 3222.
12 W. W. Yau, Anal. Chem., 49 (1977) 395.
13 A. M. Krstulović and P. R. Brown, Reversed Phase High Performance Liquid Chromatography, Wiley-Interscience, New York, 1982.
14 C. J. Pedersen and H. K. Frensdorff, Angew. Chem. Int. Ed. Engl., 11 (1972) 16.

Analytica Chimica Acta, 170 (1985) 265—278
Elsevier Science Publishers B.V., Amsterdam — Printed in The Netherlands

STATE ESTIMATION IN DISCRETE TITRATIONS WITH KALMAN FILTERING AND FIXED-INTERVAL SMOOTHING

P. C. THIJSSEN*, N. H. M. DE JONG and G. KATEMAN

Department of Analytical Chemistry, University of Nijmegen, Toernooiveld, 6525 ED Nijmegen (The Netherlands)

H. C. SMIT

University of Amsterdam, Laboratory for Analytical Chemistry, Amsterdam (The Netherlands)

(Received 10th September 1984)

SUMMARY

The suitability of a state space model for processing titration curves and their derivatives is described. The Kalman filter gives a systematic deviation in the evaluated inflection points, which is removed completely by subsequent fixed-interval smoothing. The estimation procedures can be used for on-line control in order to obtain equidistant measurements with variable volume increments. The precision is shown to depend on the minimal delivery of the buret and on the noise variance of the detector. The algorithms are illustrated with a simulated example and applied successfully in practice.

In titrimetry, concentrations of unknown samples are evaluated by adding a titrant of known concentration until an equivalence point corresponding to a stoichiometric reaction or an empirically established end-point has been reached. The equivalence point (or end-point) is indicated by the change of a suitable physical property such as colour, absorbance, potential, current or conductance. Its ease of operation, accuracy and precision make the titration a widely used analytical method. Recent improvements have been centred around the development of computerized instruments with data-handling techniques. Many titrators now utilize microcomputers for control purposes and for data acquisition and processing [1—3]. The present paper describes the application of advanced estimation techniques in automated titration systems.

It is well known that the equivalence point and the inflection point do not always coincide in potentiometric titrations. Derivatives are often used to pinpoint maximum inflections in the curves but are less effective for detailed work than curve-fitting methods. In automatic titrations, continuous addition of titrant can lead to systematic error if the reaction or electrode involved is slow. If the titrant is added stepwise and equilibrium potentials are measured, accuracy is achieved. To obtain maximal precision within minimal time, the use of equidistant potentials is often preferred. Control

0003-2670/85/$03.30

algorithms have been proposed for collecting equidistant measurements in a titration curve [4—6]. Interpolation methods have also been developed to adjust the inflection point to the accurate equivalence point [7—9]. Because the computation of differentiated curves amplifies noise, smoothing techniques and weighted digital filtering have been used [5, 10—13]. All these techniques require equal volume additions.

In this paper a state space model is designed to predict and estimate the titration curve and its derivatives. The Kalman filter establishes a systematic deviation in the estimated state and the location of the evaluated inflection points, which is reduced completely by the off-line fixed interval smoother. To provide equidistant measurements with variable volume increments, a control algorithm may be integrated in the prediction and filtering equations of the Kalman filter. Hereafter, fixed interval smoothing yields accurate and precise results. The proposed theory is demonstrated for simulations of the potentiometric titration of phosphoric acid with sodium hydroxide and successfully applied in practice with use of a computer-controlled titration system. Although only one example is presented, the proposed theory should be generally valid for discrete titrations, especially when the inflection point (end-point) is used for the evaluation of titration curves.

THEORY

A linear dynamic system

The internal structure of a system can be described via the concept of state, which is defined as a set of variables with numerical values that are sufficient to describe the behaviour of the system completely; a state need not represent a physical or chemical quantity. The physical variables are the inputs and outputs of the system, which can be measured. Chemical models of titrations are based on the conservation laws for mass or electric charge and on equilibrium relations. Sensors (electrodes, photodiodes, etc.) provide measurements on the progress of the titration. The state may refer to variables such as concentrations and to parameters such as sensitivities and equilibrium constants. Alternatively, a point of the titration curve and its derivatives can be regarded as a state.

The state-space approach is important, because it separates two sets of equations. The state equation is a dynamic model that describes the behaviour of the state in time (i.e., volume or wavelength). The measurement equation relates the observed output to the state of the system. Both equations may be subject to random disturbances. A discrete linear dynamic system is described by

$$\mathbf{x}(k) = \mathbf{F}(k,k-1)\mathbf{x}(k-1) + \mathbf{w}(k-1) \tag{1}$$

$$z(k) = \mathbf{h}^t(k)\mathbf{x}(k) + v(k) \tag{2}$$

Here, k is a discrete variable denoting a sequence number and $\mathbf{x}(k-1)$ is the n-dimensional state vector. The new state $\mathbf{x}(k)$ in the sequence is obtained by

the product of the $\mathbf{x}(k-1)$ and the $n \times n$ transition matrix $\mathbf{F}(k, k-1)$ with addition of system noise $\mathbf{w}(k-1)$. The state $\mathbf{x}(k)$ is weighted by the transposed measurement vector $\mathbf{h}^t(k)$ and the measurement noise $v(k)$ is added to yield the signal $z(k)$. The state-space model [1, 2] is often designed as a block diagram (Fig. 1). A state-space model is not unique. Given one state representation, any non-singular transformation of that state $\mathbf{x}(k) = \mathbf{T}(k)\mathbf{x}^*(k)$ is also an allowable description of the system. An alternative state-space model is generated by

$$\mathbf{x}^*(k) = \mathbf{T}(k)^{-1}\mathbf{x}(k)\ ;\ \mathbf{F}^*(k, k-1) = \mathbf{T}(k)^{-1}\mathbf{F}(k, k-1)\mathbf{T}(k-1) \tag{3}$$

$$\mathbf{w}^*(k-1) = \mathbf{T}(k)^{-1}\mathbf{w}(k-1)\ ;\ \mathbf{h}^{*t}(k) = \mathbf{h}^t(k)\mathbf{T}(k)$$

A system can be observed, when all the states can be evaluated, directly or indirectly, from the measurements. A sufficient number of linear independent equations is needed. Hence, when a certain system state or changes in that state cannot affect the output of the system, the system is said to be unobservable. The observability condition is that the matrix

$$\mathbf{M} = [\mathbf{h}, \mathbf{F}^t\mathbf{h}, \ldots, (\mathbf{F}^t)^{n-1}\mathbf{h}] \tag{4}$$

be of rank n, or the determinant $|\mathbf{M}| \neq 0$. Additional considerations (control, stability, etc.) of the state-space model are easily available [14].

State estimation

The state-space equations and available measurements can be used to estimate the state of the system. Given the measurements $\{z(1), z(2), \ldots, z(l)\}$, at index k, three kinds of estimation problems are of interest: (a) prediction, i.e., the estimate $\hat{\mathbf{x}}(k)$ occurs after the last available measurement ($k > l$); (b) filtering, i.e., the estimate $\hat{\mathbf{x}}(k)$ coincides with the last available measure-

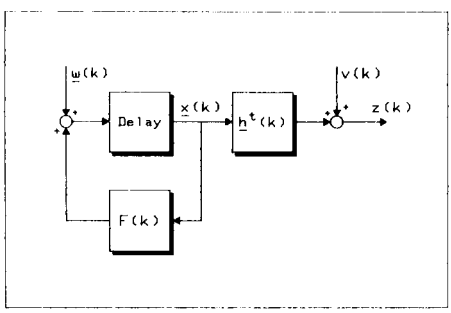

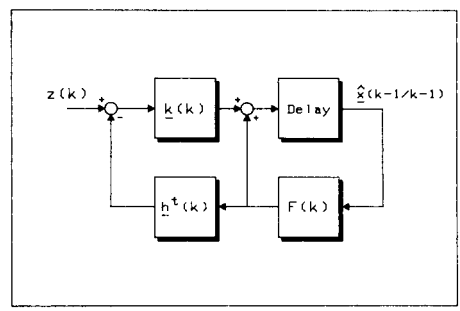

Fig. 1. A linear dynamic system. $\mathbf{x}(k)$ is the state vector, $\mathbf{F}(k, k-1)$ the transition matrix, $\mathbf{h}^t(k)$ the measurement vector and $z(k)$ the resulting signal. $\mathbf{w}(k)$ and $v(k)$ denote system noise and measurement noise, respectively. Delay is a forward time or sequence transition.

Fig. 2. The Kalman filter. $\hat{\mathbf{x}}(k-1/k-1)$ represents the last estimated state vector and $\mathbf{F}(k, k-1)$ the transition matrix used to predict the state vector $\hat{\mathbf{x}}(k/k-1)$. The measurement vector $\mathbf{h}^t(k)$, the gain vector $\mathbf{k}(k)$ and the signal $z(k)$ produce a new estimate $\hat{\mathbf{x}}(k/k)$. Delay is a forward sequence transition.

ment ($k = l$); and (c) smoothing, i.e., the estimate $\hat{\mathbf{x}}(k)$ falls within the span of available measurements ($k < l$). The estimate $\hat{\mathbf{x}}(k)$ is often described as $\hat{\mathbf{x}}(k/l)$, to show that measurements up to and including index l have been used. The commonly applied filtering technique for the state estimation with a linear dynamic system is the Kalman filter based on some prior knowledge [14]. The transition matrix $\mathbf{F}(k, k-1)$ and the measurement vector $\mathbf{h}^t(k)$ in the state-space model must be known in advance, as must the probability distributions of the state and noise terms. The system noise $\mathbf{w}(k-1)$ and the measurement noise $v(k)$ are defined as gaussian white-noise sequences with zero means and covariance matrices $\mathbf{Q}(k-1)$ and $\mathbf{R}(k)$, respectively. The state $\mathbf{x}(k)$ is normally distributed and independent of the noise, initialized by the estimate $\hat{\mathbf{x}}(0/0)$ and covariance matrix $\mathbf{P}(0/0)$.

The filtered estimate $\hat{\mathbf{x}}(k/k)$ may be determined by

$$\hat{\mathbf{x}}(k/k-1) = \mathbf{F}(k, k-1)\hat{\mathbf{x}}(k-1/k-1) \tag{5}$$

$$\mathbf{P}(k/k-1) = \mathbf{F}(k, k-1)\mathbf{P}(k-1/k-1)\mathbf{F}^t(k, k-1) + \mathbf{Q}(k-1) \tag{6}$$

$$\hat{\mathbf{x}}(k/k) = \hat{\mathbf{x}}(k/k-1) + \mathbf{k}(k)[z(k) - \mathbf{h}^t(k)\hat{\mathbf{x}}(k/k-1)] \tag{7}$$

$$\mathbf{P}(k/k) = \mathbf{P}(k/k-1) - \mathbf{k}(k)\mathbf{h}^t(k)\mathbf{P}(k/k-1) \tag{8}$$

$$\mathbf{k}(k) = \mathbf{P}(k/k-1)\mathbf{h}(k)[\mathbf{h}^t(k)\mathbf{P}(k/k-1)\mathbf{h}(k) + \mathbf{R}(k)]^{-1} \tag{9}$$

where $\mathbf{k}(k)$ is the $n \times 1$ filter gain vector. The $n \times n$ matrix $\mathbf{P}(k/k)$ can be interpreted as the covariance matrix of the estimation errors (i.e., the difference between $\mathbf{x}(k)$ and $\hat{\mathbf{x}}(k/k)$) and $\mathbf{P}(k/k-1)$ for the prediction errors between $\mathbf{x}(k)$ and $\hat{\mathbf{x}}(k/k-1)$.

The Kalman filter for the state equation is designed in Fig. 2. In Eqn. 7, new information is weighted on the basis of prior information. The weighting is a function of the uncertainty in the predicted state compared with the uncertainty in the measurement. After the effect of the initial phase has diminished, the covariance matrix $\mathbf{P}(k/k-1)$ in the filter is driven by the system-noise covariance matrix $\mathbf{Q}(k-1)$. When the elements of $\mathbf{Q}(k-1)$ are small compared with the measurement-noise covariance $\mathbf{R}(k)$, less weight is given to the new measurement. The filter disregards the predicted state when $\mathbf{Q}(k-1)$ is large with respect to $\mathbf{R}(k)$. The Kalman filter predicts the state one step ahead. To predict more steps ahead, Eqns. 5 and 6 are extended with $\hat{\mathbf{x}}(k/k) = \hat{\mathbf{x}}(k/k-1)$ and $\mathbf{P}(k/k) = \mathbf{P}(k/k-1)$ for each desired step. A multistep prediction may be used to skip missing measurements or for control of the sequence-dependent variable.

The Kalman filter combines prediction and filtering for the on-line improvement of the estimate from the current measurements based on past measurements. Smoothing can only be done off-line; obviously, all the measurements must be collected first. A smoother can be considered as a suitable combination of two filters. At each step in a forward sweep, the predicted and the estimated state with the associated covariance matrices are stored. Similarly, a second filter extrapolates backwards in the sequence. Subsequently,

the smoothed estimate and associated covariance matrix can be evaluated in terms of the stored quantities. The algorithm presented below is referred to as the fixed-interval smoother [14, 15]. Fixed-interval smoothing uses all measurements between 1 and N to estimate the state $\mathbf{x}(k)$ with $k \leqslant N$. The forward run is provided by a conventional Kalman filter. Hereafter, the backward filter and the smoother can be simplified for $k = N-1, N-2, \ldots, 1$ to

$$\hat{\mathbf{x}}(k/N) = \hat{\mathbf{x}}(k/k) + \mathbf{A}(k)[\hat{\mathbf{x}}(k+1/N) - \hat{\mathbf{x}}(k+1/k)] \tag{10}$$

$$\mathbf{P}(k/N) = \mathbf{P}(k/k) + \mathbf{A}(k)[\mathbf{P}(k+1/N) - \mathbf{P}(k+1/k)]\,\mathbf{A}^{t}(k) \tag{11}$$

$$\mathbf{A}(k) = \mathbf{P}(k/k)\mathbf{F}^{t}(k+1, k)\mathbf{P}(k+1/k)^{-1} \tag{12}$$

where $\hat{\mathbf{x}}(k/N) = \hat{\mathbf{x}}(k/k)$ for $k = N$, and $\mathbf{P}(k/N) = \mathbf{P}(k/k)$.

The state equation of the fixed-interval smoother is depicted in Fig. 3; it is a mirror image of the prediction part of the Kalman filter (Fig. 2). The stored estimates $\hat{\mathbf{x}}(k/k)$ and predictions $\hat{\mathbf{x}}(k+1/k)$ are processed by the smoother to obtain the smoothed estimate $\hat{\mathbf{x}}(k/N)$. The associated covariance matrices, $\mathbf{P}(k/k)$ and $\mathbf{P}(k+1/k)$, are incorporated in the gain matrix $\mathbf{A}(k)$ together with the transition matrix $\mathbf{F}(k+1, k)$. A state is said to be smoothable if the smoother provides a covariance matrix superior to that produced by a Kalman filter running backwards. Only states that are driven by system noise are smoothable. When $\mathbf{Q}(k-1)$ equals the zero matrix, the results of the smoother and the Kalman filter are equivalent. Other types of smoothers are available. The fixed-point smoother is concerned with achieving an estimate at a single fixed point in the sequence. In fixed-lag smoothing an estimate is produced for a fixed earlier period. From a computational viewpoint, these algorithms are quite similar to the fixed-interval smoother.

A discrete titration model

A potentiometric titration curve is obtained by plotting the measured potentials versus the volume of titrant added, and is more or less sigmoidal with one or more inflections. If the curve is divided into infinite small volume

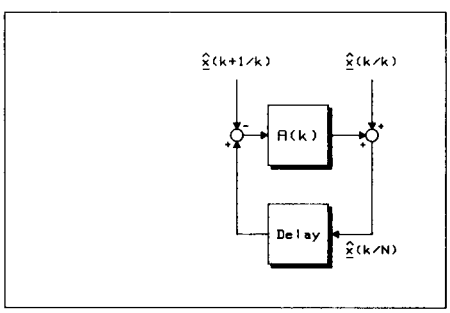

Fig. 3. The fixed-interval smoother. The stored estimate $\hat{\mathbf{x}}(k/k)$ and the prediction $\hat{\mathbf{x}}(k+1/k)$ of the Kalman filter are processed to produce the new smoothed state $\hat{\mathbf{x}}(k/N)$. $\mathbf{A}(k)$ is a gain matrix and Delay denote a backward sequence transition.

steps, ∂V, a Taylor approximation for the potential x is allowed at volume V

$$x(V + \partial V) = x(V) + \dot{x}(V)\partial V + \tfrac{1}{2}\ddot{x}(V)\partial V^2 + \ldots \tag{13}$$

After truncation, a discrete version of a second-order expansion can be obtained. With successive steps from volume $V(k-1)$ to $V(k)$ in the titration curve, and definition of the identities $\Delta V \equiv V(k) - V(k-1)$, $k-1 \equiv V(k-1)$ and $k \equiv V(k)$, gives the following set of difference equations

$$x(k) = x(k-1) + \dot{x}(k-1)\Delta V + \tfrac{1}{2}\ddot{x}(k-1)\Delta V^2 \tag{14}$$

$$\dot{x}(k) = \dot{x}(k-1) + \ddot{x}(k-1)\Delta V$$

$$\ddot{x}(k) = \ddot{x}(k-1)$$

The given set of difference equations is a bad approximation of the nonlinear titration curve. There is also noise involved on the measurements. Introduction of system noise and measurement noise with definition of $x_0 \equiv x$, $x_1 \equiv \dot{x}\Delta V$ and $x_2 \equiv \ddot{x}\Delta V^2$ gives the state-space model

$$\begin{pmatrix} x_0(k) \\ x_1(k) \\ x_2(k) \end{pmatrix} = \begin{pmatrix} 1 & 1 & \frac{1}{2} \\ 0 & 1 & 1 \\ 0 & 0 & 1 \end{pmatrix} \begin{pmatrix} x_0(k-1) \\ x_1(k-1) \\ x_2(k-1) \end{pmatrix} + \begin{pmatrix} w_0(k-1) \\ w_1(k-1) \\ w_2(k-1) \end{pmatrix} \tag{15}$$

$$z(k) = (1 \;\; 0 \;\; 0) \begin{pmatrix} x_0(k) \\ x_1(k) \\ x_2(k) \end{pmatrix} + v(k)$$

The volume step ΔV is incorporated in the state $\mathbf{x}(k)$. In order to obtain the desired derivatives, the similarity transformation (3) is valid

$$\mathbf{x}(k) = \begin{pmatrix} x_0(k) \\ x_1(k) \\ x_2(k) \end{pmatrix} ; \; \mathbf{x}^*(k) = \begin{pmatrix} x(k) \\ \dot{x}(k) \\ \ddot{x}(k) \end{pmatrix} \text{ and } \mathbf{T}(k) = \begin{pmatrix} 1 & 0 & 0 \\ 0 & \Delta V & 0 \\ 0 & 0 & \Delta V^2 \end{pmatrix} \tag{16}$$

In this way the state estimate given by model (15) can be transformed for plotting purposes. The observability criterion of the final state-space model is satisfied, i.e.,

$$\mathbf{M} = |\mathbf{h}, \mathbf{F}^t\mathbf{h}, \mathbf{F}^t\mathbf{F}^t\mathbf{h}| = \begin{vmatrix} 1 & 1 & 1 \\ 0 & 1 & 2 \\ 0 & \frac{1}{2} & 2 \end{vmatrix} \neq 0 \tag{17}$$

In the alternative state-space model, the volume step is involved in the transition matrix and will affect the observability condition for $\Delta V \to 0$.

By extending the state-space model to n terms, the transition matrix $\mathbf{F}(k, k-1)$ will expand with the element $1/(n-1)!$ and the similarity transformation matrix $\mathbf{T}(k)$ with ΔV^{n-1}. Upon increasing n, the observability criterion will converge to zero, which limits the number of derivatives in the state. As a result of the truncation of the discrete Taylor expansion, the last state variable exhibits a systematic delay of $1/(n-1)!\,\Delta V$ units.

It should be noted that the system noise exploits additional model errors to describe the nonlinearity of the titration curve caused by physical and chemical laws (i.e., the conservation law for mass and charge, equilibrium relations, Nernst equation, etc.). The input of the model is a certain addition of titrant (the sequence-dependent variable) and the output is measured as a potential.

In practice, the measurement noise variance $\mathbf{R}(k)$ in the model is known reasonably well. The system noise covariance $\mathbf{Q}(k-1)$, especially the element q_{33}, is used as a tuning parameter to describe the titration curve in a statistically correct way; q_{33} describes the overall effects of the physical and chemical relations and quantities involved on the steepness of a particular inflection, and is strongly dependent on the volume step, ΔV.

In the Kalman filter, the monitored innovations $\nu(k) = z(k) - \mathbf{h}^t(k)\hat{\mathbf{x}}(k/k-1)$ can be exploited for statistical testing of the model performance. The weighted sum of the squared normalized innovations or the quantity $\chi^2 = \Sigma_{k=1}^{N} \nu(k)^2/[\mathbf{h}^t(k)\mathbf{P}(k/k-1)\mathbf{h}(k) + \mathbf{R}(k)]$ is a chi-squared random variable with $N - n$ degrees of freedom. Similarly, the normalized residual in the fixed interval smoother can be used. For optimal tuning of q_{33}, a value of $\log[\chi^2/N] \approx 0$ (for $N \gg n$) must be found. At this point there is statistically no reason to reject the used state-space model, taking simultaneously the smallest system noise covariance into account. In addition, the autocorrelation function of the innovation sequence can be used for off-line checking of the model performance.

It is important to note that the transition matrix and the measurement vector in the state-space model contain only constants. Thus, the covariance matrices in the Kalman filter and fixed-interval smoother converge to a steady state. In practice, the steady-state covariance can be pre-computed with inclusion of the associated gains. The Kalman filter simplifies to Eqns. 5 and 7 only, and the fixed-interval smoother to Eqn. 10, with a considerable improvement of the computation time and memory requirements. At this point, the algorithms may be compared with the weighted digital filters based on polynomial least-squares regression [12, 13].

Proportional control of the titration to obtain equidistant measurements can be done by using a multistep prediction in the Kalman filter

$$x_0(k+i-1/k-1) - x_0(k-1/k-1) \geqslant \Delta x_0 \tag{18}$$

If the criterion Δx_0 is reached by predicting the titration curve $(i+1)$ steps ahead, i volume units are added to the solution. In practice, minimal and maximal steps ($\Delta V_{\min}$ and $\Delta V_{\max}$) are fixed in advance. The first titrant additions are done at steps ΔV_{init}, to provide an observable estimate. Similarly, algorithms for quality control or threshold control may be obtained. For variable increments of the volumes, the steady-state approach cannot be used.

Evaluation of the inflection point

The inflection points of a potentiometric titration curve can be found from the first or second derivative of the estimated curve. Simple arithmetic establishes the volume at which the second derivative is zero. The location of the inflection point V_{inf} is determined by linear interpolation

$$V_{inf} = V(i-1) + x_2(i-1)/[x_2(i-1) - x_2(i)]\,\Delta V \tag{19}$$

$$V_{set} = V(i-1) + [x_{set} - x_0(i-1)]/[x_0(i) - x_0(i-1)]\,\Delta V$$

with $\Delta V = V(i) - V(i-1)$. The setpoint volume V_{set} at x_{set} can be obtained similarly. A quadratic interpolation equation for the setpoint volume is also available, based on the second-order approach. The variance in the computed results may be obtained by using the first error propagation of $y = f(x_1, x_2, \ldots, x_n)$ with $\mathrm{var}(y) \cong \Sigma_{i=1}^{n}\Sigma_{j=1}^{n}(\partial f/\partial dx_i)^t \mathrm{cov}(x_i, x_j)(\partial f/\partial x_j)$. For the evaluated inflection point, this gives

$$\mathrm{var}\{V_{inf}\} \approx \{[x_2(i-1)^2 + x_2(i)^2]/[x_2(i-1) - x_2(i)]^4\}\, p_{33}\Delta V^2 \tag{20}$$

where p_{ij} denotes the i, jth element of the covariance matrix $\mathbf{P}(k/k)$ or $\mathbf{P}(k/N)$, respectively. This equation only holds for equal volume increments assuming a steady state p_{33}. The extension to the general case of variable volumes is trivial. The first term on the right-hand side in Eqn. 20 can be treated as a constant and will be further referred to as β. The corresponding information yield is $I_{inf} \propto -1/2\ 1d[\beta p_{33}\Delta V^2]$. This implies that the acquired information will increase if either ΔV or p_{33} decreases. The system noise covariance $\mathbf{Q}$ depends on ΔV, i.e., if ΔV decreases, the elements of $\mathbf{Q}$ will also decrease. In addition, the value of p_{33} is related to the noise covariances $\mathbf{Q}$ and $\mathbf{R}$, i.e., if either $\mathbf{Q}$ or $\mathbf{R}$ is decreased, p_{33} will decrease. To summarize, I_{inf} increases if the volume step ΔV, the system noise covariance $\mathbf{Q}$, or the measurement covariance $\mathbf{R}$ decreases. The information yield expresses the qualitative effects in the precision of the evaluated inflection point. The linearization of the difference equations is only approximately valid for an infinite small step ∂V. Consequently, increasing the discrete ΔV will produce less precise results. For the setpoint volume, the variance formula and conclusions are analogous.

The information formula reflects the well-established facts that maximal precision is found for the lowest possible ΔV and/or $\mathbf{R}$ values and that as many measurements as possible should be acquired around the inflection point(s). The constraints on precision are given by instrumental characteristics, i.e., the discrimination of the titrant addition and the noise covariance of the detector. Obviously, the estimation procedure can affect the accuracy of the result.

If the titration is controlled on-line in order to obtain equidistant measurements, very good precision within minimal analysis time may be approached.

EXPERIMENTAL

The simulation of a titration curve comprises two stages, computation of the signal from a chemical system and the introduction of noise. At equilibrium, a chemical system is described by the equilibrium relations and the conservation laws for mass and charge. The following equation can be derived for a multicomponent acid/base system [16]

$$\sum_{i=1}^{A} \{V_s C_a(i)/[1 + K_a(i)H]\} - \sum_{i=1}^{B} \{V_s C_b(i) . K_b(i)H/[1 + K_b(i)H]\}$$
$$+ (V_s + V_t)(K_w/H - H) - V_t C_t = 0 \qquad (21)$$

where V_s is the original volume of the sample, V_t the volume of titrant added, C_t the concentration of titrant, A and B the number of acids and bases with C_a and C_b their concentrations; K_w, K_a and K_b are equilibrium constants and H is the hydrogen ion concentration.

The titration is monitored potentiometrically, the relevant form of the Nernst equation being

$$\mathrm{pH} = -\log[\mathrm{H}^+] = (E^\circ - E)/(2.303\,S) \qquad (22)$$

where $S = RT/(nF)$ and all other symbols have their conventional meanings. After addition of a small amount of titrant, the hydrogen ion concentration H in the system is calculated with an iterative Newton–Raphson procedure with $f(H)$ based on Eqn. 21

$$H_{i+1} = H_i - f(H_i)/f'(H_i) \qquad (23)$$

until $|f(H_i)/H_{i+1} - f(H_i)/H_i| \leqslant \delta$ or $i \geqslant i_{max}$. The computed hydrogen ion concentration is fed to Eqn. 22 to obtain the required pH value.

There are two major sources of noise, from the measurements and from the imprecision of the volume additions. These are incorporated in the simulation by addition of gaussian white noise to the exact values. In order to produce the entire titration curve, this procedure is repeated for each volume addition.

As an example, the titration of phosphoric acid with sodium hydroxide solution was chosen. The data listed in Table 1 were used for the simulation. The theoretical equivalence points of phosphoric acid are at 1, 2 and 3 ml. Only the first two inflection points are visible. The setpoints are placed at the steep regions of the titration curve, i.e., the correct volumes at pH 5 and pH 9 are located at 0.994 ml and 1.996 ml, respectively.

The computer-controlled titration system with a combined glass pH electrode has been described [17]. Here, 50 ml of 0.0011 M phosphoric acid was titrated with 0.028 M sodium hydroxide. All solutions were kept at ionic strength 0.1 M potassium nitrate. In the real titration system, the measured potentials and volumes were used directly. The theoretical inflection points were located at 1.964 ml and 3.929 ml.

TABLE 1

The data used for the simulation of the titration system and the initial values of the Kalman filter

Titrant concentration	$C_t = 0.01$ M
Titrant volume	$V_t = 0$—6 ml in N steps of ΔV
Sample volume	$V_s = 10$ ml
Phosphoric acid $A = 3, B = 0$	$C_a(1) = 0.001$, $\log K_{a_1} = -2.12$
	$C_a(2) = 0.001$, $\log K_{a_2} = -7.21$
	$C_a(3) = 0.001$, $\log K_{a_3} = -12.67$
	$\log K_w = -14$
Noise standard deviation	$\sigma_{pH} = 0.01$ and $\sigma_{Vt} = 0$
Newton—Raphson stop criteria	$\delta = 10^{-10}$ and $i_{max} = 30$
Kalman filter start values	$\hat{\mathbf{x}}(0/0) = 0$ and $\mathbf{P}(0/0) = \mathbf{I}_n$ (identity matrix)
Noise covariances	$\mathbf{R}(k) = 10^{-4}$ and $\mathbf{Q}(k-1) = \begin{pmatrix} 0 & 0 & 0 \\ 0 & 0 & 0 \\ 0 & 0 & q_{33} \end{pmatrix}$

The graphic display of the estimated state was scaled according to the similarity back-transformation x_0, $x_1 \times \text{scale}/\Delta V$ and $x_2 \times (\text{scale}/\Delta V)^2$.

RESULTS

In order to demonstrate various effects in the behaviour of the estimation algorithms, the titration of phosphoric acid with sodium hydroxide was simulated as described above. A titration curve was generated with equidistant volume increments for $N = 200$ points ($\Delta V = 0.03$ ml). Figure 4(a) shows the results obtained with the weighted digital filter. The parameters to be adjusted for the weighted digital filter include type of function, width of measurement interval and number of repetitions [12, 13]. The correspondence with the tuning parameters q_{33} and R in the state estimation algorithms may be noted. For Fig. 4(a), a quadratic function, a window width of seven measurements and only one cycle were used. Figure 4(b) shows the performance of the Kalman filter for a system noise variance $q_{33} = 10^{-3}$ and measurement noise $\mathbf{R} = 10^{-4}$. It reveals a systematic delay in the evaluated inflection points obtained from the estimated second derivative. The state estimation of the fixed-interval smoother is shown in Fig. 4(c). The noise in the state estimates of the Kalman filter is reduced by this smoother. The location of the inflection point is estimated correctly apart from the truncation error $1/2\Delta V$. Figure 4(d) shows the diagonal elements of the corresponding covariance matrices as the titration proceeds. Because of the constant transition matrix and measurement vector, a steady state is reached.

The effect of the tuning parameter q_{33} in the model on various characteristics of practical interest is demonstrated in Fig. 5. Figure 5(a) shows the dependence of the steady-state covariance elements p_{ii} of the Kalman filter and fixed-interval smoother; if q_{33} decreases, the corresponding elements p_{ii}

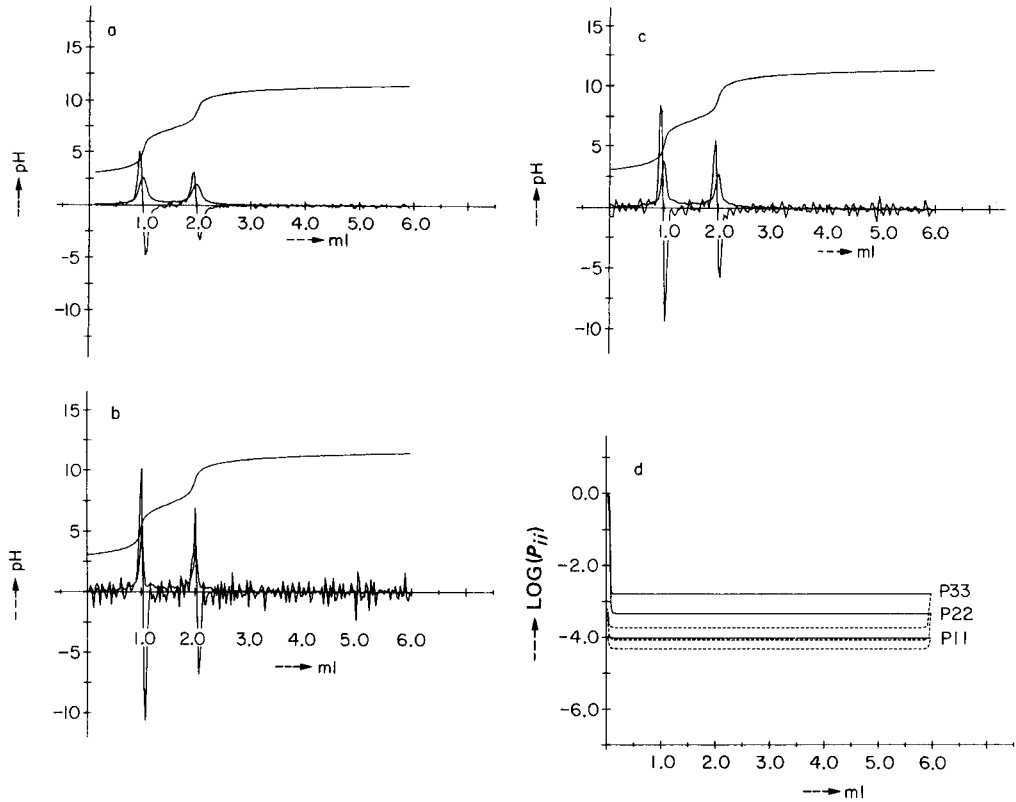

Fig. 4. The simulated titration curve (cf. Table 1) and differential plots. N = 200 and ΔV = 0.03 ml. For the graphics, a scaling factor 0.2 was used. (a) The weighted digital filter (quadratic, 7-points, one cycle); (b) the Kalman filter (q_{33} = 10^{-3} and R = 10^{-4}); (c) the fixed-interval smoother (same q_{33} and R). (d) Elements p_{ii} of covariance matrices P(k/k) and P(k/N): (—) Kalman filter; (---) fixed-interval smoother.

also decrease. The covariance elements of the smoother are always better than the Kalman filter because of the involved system noise. A similar observation was made for decreasing measurement noise covariance R(k). The convergence to the steady state depends on the magnitude of q_{33} with respect to R. When the ratio q_{33}/R is high, the steady state is reached very quickly (Fig. 4d). An increasing number of recursions are needed when this ratio tends to zero. The effect on the chi-squared value, $\log[\chi^2/N]$, for different N values and equal volume increments ΔV, is shown in Fig. 5(b). The performance was statistically tuned in order to obtain the element q_{33} for a given number of data. For the optimal q_{33}, $\log[\chi^2/N] \approx 0$ has to be found. Increasing N (i.e., decreasing the volume increment ΔV) produces a considerable decrease in the optimal value of q_{33}. As a consequence, the uncertainty in the predicted and estimated state also decreases, which is reflected in the steady-state co-

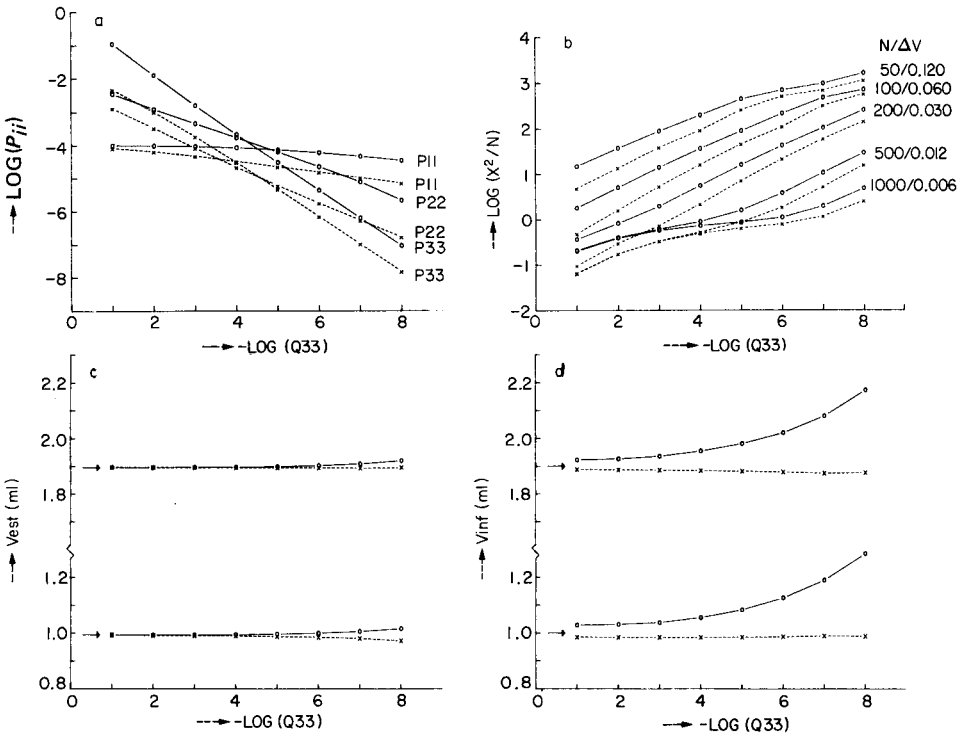

Fig. 5. The effect of the system noise covariance q_{33} on some characteristics (a—d). (Simulations based on the data in Table 1 with equal volume increments; measurement noise covariance at R = 10^{-4}.) (—) Kalman filter; (---) fixed-interval smoother. (a) Steady-state covariance matrices P(k/k) and P(k/N) (p_{ii} denotes a diagonal element); (b) χ^2 for different N values; (c) set points V_{set} at pH 5 and pH 9; (d) inflection points V_{inf}. The arrows in (c) and (d) indicate the theoretical values.

variance elements of Fig. 5(a) for decreasing values of q_{33}. For the smoother, the optimal values for q_{33} are always smaller than those for the Kalman filter, which is not surprising because the former provides a better covariance matrix when a non-zero system noise covariance is used. For N = 200, a q_{33} value of about 10^{-3} was found; this value was used in Fig. 4 to demonstrate the estimation algorithms. For N = 200 (i.e., ΔV = 0.03 ml), the evaluated results for the setpoints at pH 5 and pH 9 and the inflection points are shown in Fig. 5(c, d). The systematic deviation of the Kalman filter is clearly seen, though the effect is much less for the setpoints. The results obtained with the fixed-interval smoother are almost independent of the system noise covariance, except for the truncation error $1/2\Delta V$ in the last state variable. This observation is important in practical work, because the tuning parameter q_{33} may be chosen over a large range without affecting the precision of the final results.

Results obtained with the computer-controlled titrator are presented in

Fig. 6. The titration curve obtained with variable volume increments and equidistant potential measurements is shown in Fig. 6(a). The on-line state estimates obtained with the Kalman filter and with the smoother are depicted in Fig. 6(b, c). The corresponding covariance matrix elements are given in Fig. 6(d) which demonstrates that both estimation algorithms can be used with variable volume increments; the covariance elements are small around the inflection points. In the flat parts of the titration curve, these elements increase as a result of the control procedure applied. Some actual numbers related to Fig. 6 are listed in Table 2.

Conclusions

An on-line method for the evaluation of titration curves is presented. A Kalman filter predicts and filters the titration curve and its derivatives. The systematic deviation in the filtered state and the location of the evaluated

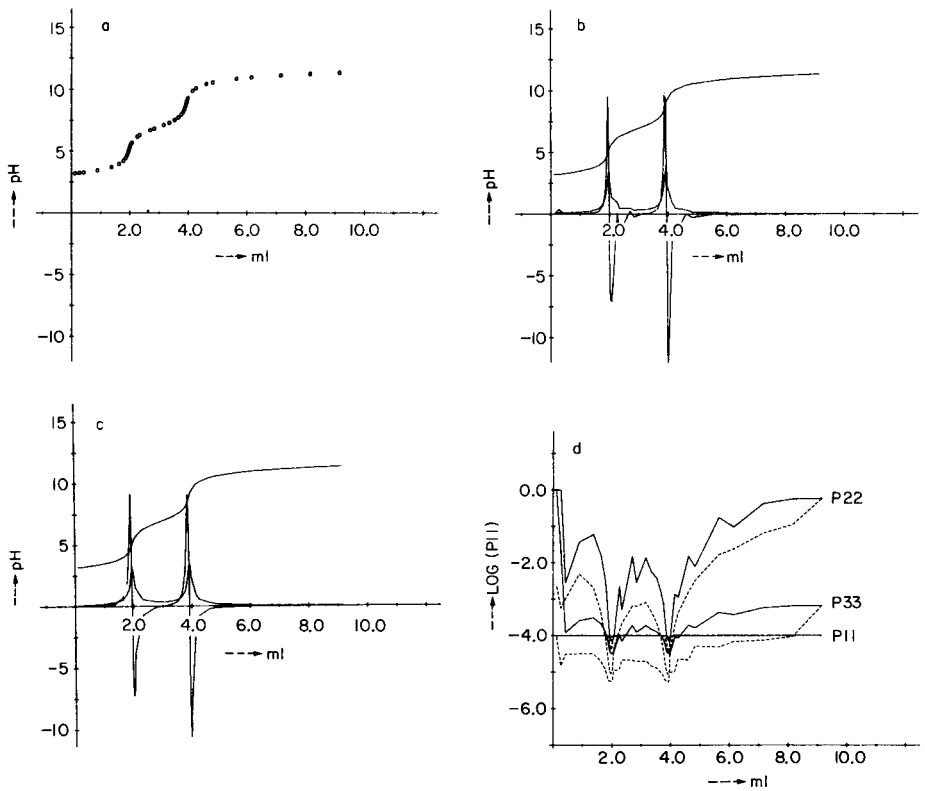

Fig. 6. Results of the control algorithm applied in a computer-controlled titrator for the titration of 50 ml of 0.0011 M phosphoric acid with 0.028 M sodium hydroxide. (A scaling factor 0.4 was used.) (a) Equidistant measurements (ΔV_{min} = 0.01 ml, ΔV_{max} = 1.00 ml, ΔV_{init} = 0.10 ml and Δx_0 = 0.2 pH units); (b) the Kalman filter ($q_{33} = 10^{-5}$ and $\mathbf{R} = 10^{-4}$); (c) the fixed-interval smoother (same q_{33} and $\mathbf{R}$ as for b). (d) elements p_{ii} of covariance matrices $\mathbf{P}(k/k)$ and $\mathbf{P}(k/N)$: (—) Kalman filter; (---) fixed-interval smoother.

TABLE 2

Results obtained with the Kalman filter and the fixed-interval smoother in the potentiometric titration of 50 ml of 0.0011 M phosphoric acid with 0.028 M sodium hydroxide[a]

Method	χ^2	V_{inf} (ml)	V_{set} (ml)
Kalman filter	18.4	1.988, 3.953	1.960, 3.941
Smoother	2.4	1.953, 3.918	1.960, 3.941

[a]The control algorithm for equidistant measurements was used with ΔV_{min} = 0.01 ml, ΔV_{max} = 1.00 ml, ΔV_{init} = 0.10 ml and Δx_0 = 0.2 pH units. The total number of points N = 41, and the smallest observed ΔV was 0.01 ml. Critical values $\chi^2(38, 0.025)$ = 22.9 and $\chi^2(38, 0.0975)$ = 56.9. Theoretical inflection points are 1.964 ml and 3.929 ml. The inflection points are not corrected for $1/2\Delta V$ = 0.005 ml.

inflection points is removed by the fixed-interval smoother. Implementation of the proposed algorithms allows variable volume increments, which is applied in a control procedure to obtain equidistant measurements. The precision of the final results is almost independent of the tuning parameters in the estimation algorithms. The precision-limiting factors are instrumental characteristics such as the minimal delivery of the buret and the noise variance of the detector. The best design to provide the highest precision within minimal analysis time in the evaluated results of a conventional titration operates on equidistant measurements. Extension to continuous titrations is possible and will be investigated in a later paper.

This work was supported by the Netherlands Research Organisation Z.W.O.

REFERENCES

1 A. H. B. Wu and H. V. Malmstadt, Anal. Chem., 50 (1978) 2090.
2 D. Betteridge and T. B. Goad, Analyst (London), 106 (1981) 257.
3 H. Bartels and P. Walsen, Z. Anal. Chem., 315 (1983) 109.
4 D. J. Legget, Anal. Chem., 50 (1978) 718.
5 T. F. Christiansen, J. E. Bush and S. C. Krogh, Anal. Chem., 48 (1976) 1051.
6 S. Ebel and B. Reyer, Z. Anal. Chem., 312 (1982) 346.
7 S. Wolf, Z. Anal. Chem., 250 (1970) 13.
8 H. J. Keller and W. Richter, Metrohm Bull., 2 (1971) 173.
9 W. Bartscher, Z. Anal. Chem., 297 (1979) 132.
10 T. W. Hunter, J. T. Sinnamon and G. M. Hieftje, Anal. Chem., 47 (1975) 497.
11 D. Betteridge, E. L. Dagless, P. David, D. R. Deans, G. E. Penketh and D. Shawcross, Analyst (London), 101 (1976) 409.
12 A. Savitsky and M. J. E. Golay, Anal. Chem., 36 (1964) 1627.
13 C. G. Enke and T. A. Niemann, Anal. Chem., 48 (1976) 705A.
14 A. Gelb (Ed.), Applied Optimal Estimation, MIT-Press, Cambridge, MA, 1974.
15 B. D. O. Anderson and J. B. Moore, Optimal Filtering, Prentice Hall, Englewood Cliffs, New York, 1979.
16 W. E. Gordon, J. Phys. Chem., 83 (1979) 1365.
17 A. M. van de Wijdeven, P. C. Thijssen and L. C. G. van Dongen, Laboratory Microcomputer, 3 (1984) 37.

Analytica Chimica Acta, 170 (1985) 279—285
Elsevier Science Publishers B.V., Amsterdam — Printed in The Netherlands

MATHEMATICAL TREATMENT OF CONCENTRATION PROFILES AND ANODIC CURRENT FOR AMPEROMETRIC ENZYME ELECTRODES

THOMAS SCHULMEISTER* and FRIEDER SCHELLER

Central Institute of Molecular Biology, Academy of Sciences, 1115 Berlin-Buch (German Democratic Republic)

(Received 9th January 1984)

SUMMARY

Formulae are presented for the exact solution of partial differential equations describing the transient behaviour of concentration profiles and the anodic current in amperometric enzyme electrodes. The mathematical treatment is based on a reaction/diffusion model in which the reaction rate depends linearly on the substrate concentrations. Numerical results are presented to demonstrate the feasibility of the given formulae.

Glucose in biological fluids is frequently determined by measuring the hydrogen peroxide produced in the presence of glucose oxidase [1—3], usually amperometrically at a platinum electrode [4—6]

$$\beta\text{-D-glucose} + O_2 + H_2O \rightarrow \text{D-gluconic acid} + H_2O_2 \quad (1)$$

$$H_2O_2 \rightarrow O_2 + 2H^+ + 2e^- \quad (2)$$

In order to optimize the operational parameters of the electrode (response time, precision, linear range), a mathematical model of this diffusion/reaction system may be useful. Theoretical study of the time-dependence of substrate and product profiles may help understanding of the general mechanisms of heterogeneous catalysis.

The present paper deals with a model of a commercial enzyme electrode for the determination of glucose in diluted whole blood samples [7, 8]. The first mathematical treatment of the transient behaviour of amperometric enzyme electrodes was published by Mell and Maloy [9, 10]. Other theoretical treatments of enzyme electrodes have appeared [11—21]. Explicit formulae have been given for the steady-state response of amperometric enzyme electrodes [9, 19, 22], and the prestationary kinetics of enzyme electrode models have been studied extensively [5, 9, 12, 14, 18, 19, 23—27]. The stationary operational mode of enzyme electrodes has been described [24] but most commercially available amperometric enzyme electrodes are based on kinetic principles and few formulae have been reported for the prestationary kinetics.

0003-2670/85/$03.30

The work reported here was stimulated by a study of spherical enzyme supports [25], in which the same equations were used but the boundary conditions allowed a simpler solution than is possible with a membrane arrangement.

THEORY

The catalytic mechanism of the glucose oxidase reaction is known to be of the "ping-pong" type [5, 28]. As suggested by Malpiece et al. [20], the diffusion/reaction system can be described by

$$\partial G/\partial t = D_G \, \partial^2 G/\partial r^2 - V$$

$$\partial O/\partial t = D_O \, \partial^2 O/\partial r^2 - V$$

$$\partial H/\partial t = D_H \, \partial^2 H/\partial r^2 + V$$

where $V = V_{max}/(1 + k_O/O + k_G/G)$ and G, O and H denote the concentrations of glucose, oxygen and hydrogen peroxide, respectively. The diffusion coefficients, D, and kinetic parameters, k, have the corresponding subscripts. The influence of the dialysis membrane inside the enzyme electrode and the concentration boundary-layer effect [17] are ignored, and it is assumed that hydrogen peroxide is not present in the well-stirred bulk solution. In the case of a product-sensitive two-substrate enzyme electrode, only the product is consumed at the electrode surface. At the start of the measurement, glucose and hydrogen peroxide are not present in the enzyme membrane which is equilibrated with oxygen. Therefore the boundary and initial conditions are [19, 24]

$$G(0, t) = G_B \, (\partial G/\partial r)(d, t) = 0 \text{ for } t > 0, \; G(r, 0) = 0 \text{ for } 0 < r < d \tag{3}$$

$$O(0, t) = O_B \, (\partial O/\partial r)(d, t) = -(D_H/D_O)(\partial H/\partial r)(d, t) \text{ for } t > 0,$$

$$O(r, 0) = \alpha O_B \text{ for } 0 < r < d \tag{4}$$

$$H(0, t) = 0 \quad H(d, t) = 0 \text{ for } t > 0, H(r, 0) = 0 \text{ for } 0 < r < d \tag{5}$$

where d and α denote the thickness of the enzyme membrane and the partition coefficient of oxygen [17], respectively; G_B means the bulk concentration of β-D-glucose. The oxygen consumed in glucose oxidation (reaction 1) is completely regenerated at the electrode surface (reaction 2). A loss of oxygen may be based on lateral diffusion. In hydrophilic gel membranes, oxygen diffuses between three and four times faster than glucose [17, 18]: $D_O \approx 3.4 D_G$. Its partition coefficient, α, is near unity [29]. Thus, the oxygen concentration in the membrane is always close to the saturation value, O_B, of the bulk solution with air bubbling [20]: $O_B = 0.265$ mmol l^{-1}. Consequently, for small and medium values of glucose concentration, the system is not limited by oxygen. This is clear from the coincidence of the linear parts of the experimental calibration curves in air-saturated and oxygen-bubbled background solutions.

The order of the kinetic parameters is known [5, 20, 30]: $k_O \approx 0.5$ mmol l^{-1} and $k_G \approx 100$ mmol l^{-1}. Thus, for the bulk concentration, $G_B \ll k_G$ and $O_B \approx k_O/2$. If it is assumed that $G(r, t) \leqslant G_B$ and $O(r, t) \leqslant \alpha O_B$, then oxygen can be eliminated as a variable substrate, and the model reduces to that of a one-substrate product-sensitive enzyme electrode, described by a first-order reaction rate.

By introducing $k = V_{max}/k_G$, V can be approximated quite accurately by $V = kG(r, t)$, and so

$$\partial G/\partial t = D_G \partial^2 G/\partial r^2 - kG(r, t) \tag{6}$$

$$\partial H/\partial t = D_H \partial^2 H/\partial r^2 + kG(r, t) \tag{7}$$

and the boundary and initial conditions (Eqns. 3 and 5) can be obtained. Equation 6 can be solved separately [31]

$$G(r, t) = G_B \left\{1 - \frac{4}{\pi} \sum_{n=0}^{\infty} \frac{(-1)^n}{2n+1} \cos\left[\frac{2n+1}{2} \frac{d-r}{d} \pi\right] \frac{k + u \exp[-(u+k)t]}{(u+k)}\right\} \tag{8}$$

with $u = D_G(2n+1)^2\pi^2/(2d)^2$. Inserting this expression into Eqn. 7, one can make use of a formula for linear parabolic differential equations [32]

$$H(r, t) = \int_0^t \int_0^d F(r, y, t-s) kG(y, s) \mathrm{d}y \, \mathrm{d}s \tag{9}$$

with the Green function

$$F(x, y, z) = (2/d) \sum_{m=1}^{\infty} \exp(-wz) \sin(m\pi x/d) \sin(m\pi y/d)$$

where $w = D_H(m\pi/d)^2$.

If u and w are used as defined above, Eqn. 9 can be written as follows

$$H(r, t) = \frac{2k}{\pi} G_B \sum_{m=1}^{\infty} \sin(m\pi r/d) \left\{\frac{1-(-1)^m}{mw}[1 - \exp(-wt)]\right.$$

$$+ \frac{4(-1)^m}{\pi} \sum_{n=0}^{\infty} \left[\frac{(-1)^n}{(2n+1)(k+u)}\left(\frac{k[1-\exp(-wt)]}{w}\right.\right.$$

$$\left.\left. + \frac{u[\exp(-(k+u)t) - \exp(-wt)]}{w-k-u}\right) \frac{4m}{4m^2 - (2n+1)^2}\right]\Bigg\} \tag{10}$$

The corresponding stationary solutions are [33]

$$G(r) = G_B \cosh[Q(r-d)]/\cosh(Qd) \tag{11}$$

$$H(r) = G_B\{[1/\cosh(Qd) - 1]r/d + 1 - \cosh[Q(r-d)]/\cosh(Qd)\}D_G/D_H \quad (12)$$

with $Q = (k/D_G)^{1/2}$.

The current $i(t)$ may be calculated from Faraday's law

$$i(t) = -2FAD_H(\partial H/\partial r)(d, t) \quad (13)$$

where F and A are the Faraday number and the electrode surface area, respectively. This and Eqn. 12 imply that the stationary current is [22]

$$i_{st} = -2FAD_G G_B[1/\cosh(Qd) - 1]/d \quad (14)$$

With the help of Eqns. 8 and 10, concentration profiles can be calculated for fixed values of time t, as well as time-dependent changes of the concentrations at fixed positions r within the enzyme layer. The calculated concentration profiles show the same qualitative behaviour as reported previously [9, 14, 19, 24].

The sensor considered uses the slope value $(di/dt)(t_m)$ at the moment t_m of the maximum time derivative of $i(t)$. This choice is not stringent because the dependence of the current, $i(t)$, and the time derivative of $i(t)$ on the glucose concentration, G_B, is linear for all fixed moments. The evaluation of $(di/dt)t_m$ is technically easy to achieve $(d^2i/dt^2 = 0)$. This principle has frequently been used [3, 34, 35] because the response time is considerably improved. The equation is

$$di/dt = -2FAD_H(d/dt)(\partial H/\partial r)(d, t) \quad (15)$$

The derived solutions may be used to calculate interesting quantities of the sensor in an explicit way. Differentiation of Eqns. 8 and 10 with respect to r (at the point $r = 0$), followed by integration with respect to time t, leads to formulae for the rates of transfer of glucose and hydrogen peroxide across the membrane/solution interface as well as to expressions of the total amounts of substance that have entered or left the enzyme membrane during time t [31]. Further, unknown kinetic parameters of the considered sensor can be estimated. With given current/time data and with knowledge of some of the electrode parameters, the remaining parameters can be calculated by a least-squares fit.

RESULTS AND DISCUSSION

This method was applied to data obtained from the sensor considered. The measured ratio of the diffusion coefficients of hydrogen peroxide and glucose was used: $D_H = 2.46D_G$. For the current/time data given in Table 1, the values obtained were as follows: $D_G = 1.53 \times 10^{-4}$ mm^2 s^{-1}, $D_H = 3.76 \times 10^{-4}$ mm^2 s^{-1}, $k = 0.95$ s^{-1} and $d = 0.094$ mm. Simulated current/time curves are shown in Fig. 1. The sum of least squares was less than 2.34 (nA)^2. The fit was very sensitive with respect to D_G and d. Because of the high enzyme

TABLE 1

Current/time relationship of the sensor[a]

Time (s)	Current (nA)			
	G_B = 0.043 mM	G_B = 0.085 mM	G_B = 0.171 mM	G_B = 0.341 mM
1.5	0.1	0.2	0.3	0.6
3.0	0.9	1.7	3.0	5.9
4.5	1.5	3.4	6.2	12.8
6.0	1.9	4.2	8.1	16.6
7.5	2.2	4.5	9.0	18.6
9.0	2.2	4.6	9.4	19.7
10.5	2.3	4.8	9.7	20.3
12.0	2.4	4.9	9.8	20.7
13.5	2.4	5.0	10.0	21.1
15.0	2.5	5.0	10.2	21.3

[a]Specific activity of glucose oxidase, 46 units/mg; gelatine, 2 mg cm^{-2}. Electrode surface A = 0.2 mm^2.

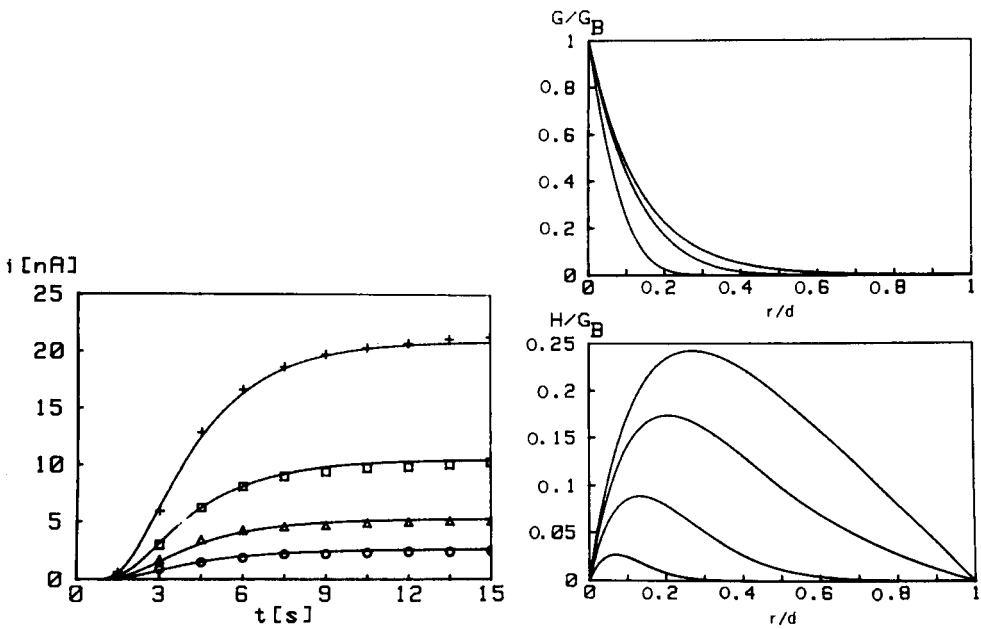

Fig. 1. Simulated current/time behaviour of the considered electrode as least-squares fits of the data in Table 1. (○) G_B = 0.043 mM, (△) G_B = 0.085 mM, (□) G_B = 0.171 mM, (+) G_B = 0.341 mM.

Fig. 2. Calculated concentration profiles for the sensor used. The profiles were obtained for t = 0.25, 1, 3, ∞ s (from below). The parameter values are given in the text. G and H are rendered dimensionless with the ratios involved. The substrate profile for t = 3 s and the stationary profile are nearly identical.

loading of the membrane of the sensor examined, this is not the case for the parameter k where the relative error is quite large. The other specific values of the sensor considered were t_m = 2.9 s and $(di/dt)(t_m) = G_B$ 13.6 nA s^{-1} mM^{-1}. Thus, the total concentration in the bulk solution (i.e., α- and β-glucose) can be obtained from the calibration equation of the sensor: G_{total} = 0.117 $(di/dt)(t_m)$ given as mM s nA^{-1}.

Several elegant theoretical studies of amperometric enzyme electrodes have been published [9, 10, 19, 24]. The present approach offers advantages. Usually, the transient behaviour of reaction/diffusion systems is investigated by numerical integration. This approach requires special numerical algorithms. For application in complex situations, explicit formulae may be preferable to approximations. The expressions presented are suitable for use on a simple programmable pocket calculator. Thus, extensive theoretical investigations as well as evaluation of the behaviour of commercially available enzyme electrodes become possible.

The formula for the anodic current described above makes it possible to fit unknown electrode parameters to current/time data measured by the sensor considered. It should be emphasized that a good fit demonstrates accordance with the chosen model, though this cannot be proved unequivocally.

All solutions derived are of theoretical value. The formulae are useful for describing qualitatively the process of glucose oxidation at membrane-covered electrodes. For more quantitative modelling, it becomes necessary to consider additional facts such as the nonlinearity of the glucose oxidation reaction rate [5, 9, 16], the oxygen dependence for high concentration values of glucose [5, 20, 28], the effect of stirring [9, 21, 26, 27] and the boundary layer effect [13, 15, 17]. Some of these features have been dealt with successfully by earlier workers but the models used involved special arrangements [5, 10, 14, 16, 17, 19], or were very complex [9, 14, 26, 27] or only the pseudo-steady-state behaviour was considered [11, 19, 21]. Modelling of all the effects simultaneously is extremely complicated. The advantage of explicit expressions is accompanied by relative simplification and the loss of exactness can be accepted in the system studied. The electrode considered works with diluted whole blood (glucose concentration below 0.5 mmol l^{-1}). Its kinetics can be approximated quite accurately by using linearization. This approach implies linear dependence of the measuring signal on the bulk concentration value of glucose; of course, for higher concentrations of glucose, nonlinear approaches are necessary.

As in most previous studies, the effects of stirring [26] and convection [15] were disregarded. At least, the signal has been shown to be independent of stirring [36]. The fact that the boundary layer effect is ignored in the proposed model is undoubtedly a flaw, but within the limits of a one-layer model a plausible description of this effect was impossible.

Some calculated concentration profiles for the sensor considered are shown in Fig. 2. Experimental data on concentration profiles for this sensor

are not available. Thus the applicability of the model has to be proved by direct measuring of concentration profiles.

REFERENCES

1 S. J. Updike and G. P. Hicks, Nature, 214 (1967) 986.
2 G. G. Guilbault and G. J. Lubrano, Anal. Chim. Acta, 60 (1972) 254.
3 D. R. Thevenot, R. Sternberg, P. R. Coulet, J. Laurent and D. C. Gautheron, Anal. Chem., 51 (1979) 96.
4 K. J. Vetter, Elektrochemische Kinetik, Springer, Berlin, 1961.
5 G. Bourdillon, J. P. Bourgeois and D. Thomas, J. Am. Chem. Soc., 102 (1980) 4231.
6 P. R. Coulet, R. Sternberg and D. R. Thevenot, Biochim. Biophys. Acta, 612 (1980) 317.
7 D. Pfeiffer, F. Scheller, M. Jänchen, K. Bertermann and H. Weise, Anal. Lett., 13 (1980) 1179.
8 M. Jänchen, F. Scheller, D. Pfeiffer, R. Pittelkow, P. Wiegand and J. Nentwig, Z. Med. Labortech. Diagn., 23 (1982) 39.
9 L. D. Mell and J. T. Maloy, Anal. Chem., 47 (1975) 299.
10 L. D. Mell and J. T. Maloy, Anal. Chem., 48 (1976) 1597.
11 W. J. Blaedel, T. R. Kissel and R. C. Boguslaski, Anal. Chem., 44 (1972) 2030.
12 G. G. Guilbault and G. Nagy, Anal. Chem., 45 (1973) 417.
13 D. F. Ollis and R. S. Carter, Jr., in E. K. Pye and L. B. Wingard, Jr. (Eds.), Enzyme Engineering, Vol. 2, Plenum Press, New York, 1974, p. 271.
14 F. R. Shu and G. S. Wilson, Anal. Chem., 48 (1976) 1679.
15 D. A. Gough and J. K. Leypoldt, Anal. Chem., 51 (1979) 439.
16 R. A. Kamin and G. S. Wilson, Anal. Chem., 52 (1980) 1198.
17 D. A. Gough and J. K. Leypoldt, AIChE J., 26 (1980) 1013.
18 D. A. Gough and J. K. Leypoldt, J. Electrochem. Soc., 127 (1980) 1278.
19 D. A. Gough and J. K. Leypoldt, in L. B. Wingard, E. Katchalski-Katzir and L. Goldstein (Eds.), Applied Biochemistry and Bioengineering, Vol. 3, Academic Press, New York, 1981, p. 175.
20 Y. Malpiece, M. Sharan, J.-N. Barbotin, P. Personne and D. Thomas, J. Biol. Chem., 255 (1980) 6883.
21 R. M. Ianniello and A. M. Yacynych, Anal. Chem., 53 (1981) 2090.
22 J. J. Kulys, M. V. Pesliakiene and A. S. Samalius, Bioelectrochem. Bioenerg., 8 (1981) 81.
23 P. W. Carr, Anal. Chem., 49 (1977) 799.
24 P. W. Carr and L. D. Bowers, Immobilized Enzymes in Analytical and Clinical Chemistry, Wiley, New York, 1980, p. 228.
25 R. Kühnau and J. Lasch, J. Theor. Biol., 84 (1980) 217.
26 P. Jochum and B. R. Kowalski, Anal. Chim. Acta, 144 (1982) 25.
27 H. F. Hameka and G. A. Rechnitz, J. Phys. Chem., 87 (1983) 1235.
28 M. K. Weibel and H. J. Bright, J. Biol. Chem., 246 (1971) 2734.
29 J. Romette, B. Froment and D. Thomas, Clin. Chim. Acta, 95 (1979) 249.
30 W. Kühn, D. Kirstein and P. Mohr, Acta Biol. Med. Ger., 39 (1980) 1121.
31 J. Crank, The Mathematics of Diffusion, 2nd edn., Clarendon Press, Oxford, 1956, Ch. 8.
32 M. N. Özisik, Heat Conduction, Wiley, New York, 1980.
33 R. Goldman, O. Kedem and E. Katchalski, Biochemistry, 7 (1968) 4518.
34 M. H. Keyes, F. E. Semersky and D. N. Gray, Enzyme Microb. Technol., 1 (1979) 91.
35 M. Koyama, J. Koezuka and Y. Sao, Toshiba Review No 132, 1981.
36 F. Scheller, D. Pfeiffer, I. Seyer, D. Kirstein, Th. Schulmeister and J. Nentwig, J. Bioenerg., 11 (1983) 155.

Analytica Chimica Acta, 170(1985) 287—293
Elsevier Science Publishers B.V., Amsterdam — Printed in The Netherlands

A RAPID AND PRECISE COMPUTER-AIDED METHOD FOR THE SPECTROPHOTOMETRIC DETERMINATION OF SUBSTANCES IN SOLUTION

ENRICO LEPORATI

Istituto di Chimica Generale ed Inorganica dell'Università degli Studi di Parma, Centro di Studio per la Strutturistica Diffrattometrica del C.N.R., Via M. D'Azeglio 85, 43100 Parma (Italy)

(Received 13th February 1984)

SUMMARY

The Newton—Raphson iteration method for the solution of mass-balance equations is used. Given accurate spectrophotometric data (absorbances, absorptivities) and equilibrium constants, this procedure permits rapid determination of substances in solution. The program is convenient to use and gives satisfactory results on a number of systems. The pyridoxal hydrochloride system was selected for evaluation of equilibrium constants and molar absorptivities from spectrophotometric and potentiometric data and was then used as the main test of the SPEDEAD program (SPEctrophotometric DEtermination by Absorbance Data).

Considerable progress has been made in both experimental design and numerical treatment of spectrophotometric (u.v.-visible) data in recent years. Some of the methods developed [1—3] have been designed primarily to resolve the problems of assessing the actual number of solute species and their concentrations, and of evaluating the equilibrium or rate constants for reactions taking place in solution. In this communication, some aspects of the procedure for the determination of substances are evaluated by various computer experiments and statistical results are discussed.

EXPERIMENTAL

Reagents. The chemicals used were of analytical-reagent grade. Pyridoxal hydrochloride (Merck) was dried before use. All the other reagents and standard solutions were prepared and purified as previously described [4—6].

Measurements. All the measurements (spectrophotometric and potentiometric) for the pyridoxal hydrochloride system were done at 25 ± 0.1°C and at an ionic strength of 1.0 mol dm^{-3} (KCl). Potentiometric measurements were made by using a Metrohm Titro-processor E636, equipped with a glass H268 electrode and a thalamide B343 reference electrode (both Schott-Jena Glass). For spectrophotometric measurements, a Jasco Uvidec-505 spectrophotometer was used with a DP-101 digital printer with steps of 5.0 nm in

0003-2670/85/$03.30

the range 230—470.0 nm. Different pH and ligand concentrations were selected as required. Spectra were measured for 23 different solutions of pyridoxal hydrochloride; for each solution, 49 absorbance data (to the third decimal place) were collected in the range 230—470 nm. In the potentiometric experiments, the standard potential of the system, E^0, and the concentration of the potassium hydroxide in solution were measured before and after each experiment by titration (density of the measuring points with a step of variable volume) of a known amount of hydrochloric acid in 1.0 M KCl with potassium hydroxide solution, according to Gran's method [7] using the NBAR computer program [8]. The ionic product K_w was obtained from the alkaline part of the same titration curve by using the NBAR program and varying its value until the average E^0 in alkaline media equalled that in acidic solution. The NBAR program was then used to calculate the concentration of the potassium hydroxide solution and the standard potential, E^0. The equivalence point, v_e, was evaluated, following the principles of Gran's procedure [8], by a least-squares method based on about 20 unequally spaced points in acidic and alkaline media. The differences between the intercepts in the acidic and alkaline ranges did not exceed the experimental error. The standard electrode potential, E^0, and the coefficients of the correction terms for the effect of liquid-junction potentials in acidic and basic solution were then obtained by the least-squares method from the Nernst equation, $E^0 = E - RTF^{-1} \ln [H^+]$, where

$$[H^+] = 0.5[(v_e - v)N/(v_0 + v)] + [0.25N^2(v_e - v)^2/(v_0 + v)^2 + K_w]^{1/2}$$

where v_0 is the initial volume, v the volume of potassium hydroxide added, v_e the volume of potassium hydroxide at the equivalence point, K_w the ionic product of water, and N the titre of the alkali solution. The functions reported in the Gran plot were: $(v_0 + v)10^{(E - E_j[H^+])/b}$ in the acidic range and $(v_0 + v)10^{(E_j[OH^-] - E)/b}$ in the alkaline range against v, where E are the e.m.f. values, $b = RTF^{-1}$ and E_j is the junction potential. The starting solutions for each potentiometric titration containing pyridoxal hydrochloride were prepared as previously described [9] and processed as monotonous curves (density of the measurements points with a step of constant volume) by Titroprocessor E636. The neutralization points in each potentiometric curve were evaluated by using different methods: the Metrohm interpolation (see Titroprocessor E636 manual), the Fortuin interpolation [10] and Gran's method. The mathematical methods of the Metrohm and Fortuin interpolations applied by the Titroprocessor E636, are not completely known. The agreement of the results obtained in order to determine the amount of pyridoxal hydrochloride present in solution was very good.

The protonation constants and the molar absorptivities were refined by handling the specific set of absorbance data (23 solutions, 49 wavelengths, 1127 points) by using the SQUAD program [1]. This program is based on the non-linear Gauss—Newton least-squares method [11], introduced by Tobias and Yasuda [12] and developed by later workers [13]. The conventional least-squares approach is used to calculate the shifts in the cumulative

formation constants, the partial derivatives being obtained numerically by incrementing the constants. The Newton-Raphson iteration method is also used in the COGSNR subroutine of the SQUAD program to solve the mass-balance equations. Unit weights were used in all calculations. If Beer's law is valid, then for each solution and wavelength, the absorbance A_c is defined by the equation

$$A_c = l \sum_{0}^{p} \sum_{0}^{q} \sum_{0}^{r} \beta_{pqr} [M]^p [H]^q [L]^r \epsilon_{pqr}$$

where ϵ_{pqr} and β_{pqr} are the molar absorptivity and the overall formation constant of the species $[M_pH_qL_r]$, respectively, and l is the pathlength of the cell used. The sum is extended over all the free and complexed species which are assumed to be present in the solution. The values of [H] are obtained from potentiometric measurements; all the other parameters are unknown. The sum of squares errors, used in the procedure of refinement, is defined by

$$U = \sum_{i=1}^{S} \sum_{k=1}^{T} |\Delta_{ik}|^2 = \sum_{i=1}^{S} \sum_{k=1}^{T} [A_{ik}^o - A_{ik}^c]^2 w_k$$

where A_{ik}^o and A_{ik}^c are the observed and calculated absorbance values, in which i refers to the ith solution and k to the kth wavelength, and S and T are the number of solutions and wavelengths, respectively.

The potentiometric data (8 solutions, 426 points) were treated by the BETAREF program [14], which computes the values of the cumulative formation constants that minimize the sum of the squared residual between the observed and calculated e.m.f. values:

$$U = \sum_{i=1}^{Z} w_i (E_i^{obs} - E_i^{calc})^2$$

TABLE 1

Stepwise and total protonation constants for pyridoxal hydrochloride system at 25°C and I = 1.0 mol dm^{-3} (KCl) using different refinement programs; estimated standard deviations are given in parentheses

	SQUAD	BETAREF		SQUAD	BETAREF
$\log \beta_{011}$ [a]	12.932 (5)	12.932 (1)	$\log K_w$	—	−13.205 (1)
$\log \beta_{021}$	21.214 (5)	21.210 (1)	U [c]	3.8034×10^{-2}	6.93109×10^3
$\log \beta_{031}$	25.112 (5)	25.149 (2)	SDA [d]	6.3951×10^{-3}	4.117
$\log K_2^H$ [b]	8.282 (5)	8.278 (1)	Z [e]	1127	426
$\log K_3^H$	3.898 (5)	3.939 (2)			

[a] $\beta_{pqr} = [M_pH_qL_r]/[M]^p[H]^q[L]^r$. [b] $\log K_n = \log \beta_{0n1} - \log \beta_{0n-11}$; $\sigma(\log K_n) = \{[\sigma^2(\log \beta_{0n1}) + \sigma^2(\log \beta_{0n-11})]/2\}^{1/2}$. [c] $U = \Sigma_{ik}(A_{ik}^o - A_{ik}^c)^2$ for SQUAD and $U = \Sigma_i w_i (E_i^{obs} - E_i^{calc})^2$ for BETAREF. [d] $SDA = (U/Ndf)^{1/2}$, where Ndf are the degrees of freedom of all data. [e] Z = number of data points.

TABLE 2

Calculated concentrations for solutions of the different systems by the SPEDEAD program[a]

Pyridoxal hydrochloride

Sol. 1 (C_L = 0.00009989 M, pH 3.091)

λ	A	C_c	RE
280	0.695	0.9859×10^{-4}	1.30
285	0.819	0.9961×10^{-4}	0.28
290	0.816	0.9979×10^{-4}	0.10
295	0.654	0.9981×10^{-4}	0.08
	Mean = 0.00009945		RSD = 0.58

Sol. 2 (C_L = 0.00009989 M, pH 2.768

A	C_c	RE
0.723	1.0022×10^{-4}	0.33
0.845	1.0072×10^{-4}	0.83
0.831	0.9978×10^{-4}	0.11
0.664	1.0013×10^{-4}	0.24
Mean = 0.00010021		RSD = 0.39

Sol. 3 (C_L = 0.00009989 M, pH 2.485)

A	C_c	RE
0.726	0.9965×10^{-4}	0.24
0.845	0.9968×10^{-4}	0.21
0.838	0.9976×10^{-4}	0.13
0.668	1.0012×10^{-4}	0.23
Mean = 0.00009980		RSD = 0.22

Sol. 4 (C_L = 0.00014983 M, pH 2.306)

λ	A	C_c	RE
280	1.093	1.4966×10^{-4}	0.11
285	1.272	1.4970×10^{-4}	0.09
290	1.261	1.4982×10^{-4}	0.01
295	1.012	1.5132×10^{-4}	0.99
	Mean = 0.00015012		RSD = 0.53

Sol. 5 (C_L = 0.00019978 M, pH 3.804)

A	C_c	RE
1.206	1.9932×10^{-4}	0.23
1.417	1.9940×10^{-4}	0.19
1.438	1.9926×10^{-4}	0.26
1.215	1.9992×10^{-4}	0.07
Mean = 0.00019947		RSD = 0.15

Sol. 6 (C_L = 0.00019978 M, pH 3.082)

A	C_c	RE
1.407	1.9932×10^{-4}	0.23
1.641	1.9957×10^{-4}	0.11
1.633	1.9958×10^{-4}	0.10
1.303	1.9846×10^{-4}	0.66
Mean = 0.00019923		RSD = 0.26

Sol. 7 (C_L = 0.00009989 M, pH 11.052)

λ	A	C_c	RE
235	0.817	0.9982×10^{-4}	0.07
240	0.849	0.9984×10^{-4}	0.05
245	0.790	0.9991×10^{-4}	0.02
250	0.614	0.9962×10^{-4}	0.27
255	0.385	0.9901×10^{-4}	0.88
	Mean = 0.0009964		RSD = 0.37

Sol. 8 (C_L = 0.00019978 M, pH 11.744)

A	C_c	RE
1.638	1.9976×10^{-4}	0.01
1.702	1.9980×10^{-4}	0.01
1.583	1.9995×10^{-4}	0.08
1.236	1.9969×10^{-4}	0.05
0.772	1.9845×10^{-4}	0.66
Mean = 0.00019953		RSD = 0.31

Sol. 9 (C_L = 0.00009989, pH 12.450)

A	C_c	RE
0.822	1.0000×10^{-4}	0.11
0.850	0.9994×10^{-4}	0.05
0.775	0.9982×10^{-4}	0.07
0.630	0.9984×10^{-4}	0.05
0.392	1.0085×10^{-4}	0.96
Mean = 0.000100091		RSD = 0.43

Neotorin	λ	500	510	520	530	540	Mean	SD	RSD
Sol. 1 (pH 8.350)	A	1.371	1.355	1.319	1.228	0.982	1.1047×10^{-4}	1.461×10^{-7}	0.13
Sol. 2 (pH 12.460)	A	1.368	1.510	1.592	1.601	1.495	1.0964×10^{-4}	8.460×10^{-8}	0.08
Sol. 3 (pH 10.420)	A	1.332	1.448	1.517	1.518	1.404	1.0992×10^{-4}	3.991×10^{-7}	0.36
Sol. 4 (pH 11.501)	A	1.357	1.496	1.578	1.587	1.482	1.0998×10^{-4}	3.693×10^{-7}	0.34

Neotorin	λ	480	490	500	510	520	Mean	SD	RSD
Sol. 5 (pH 5.381)	*A*	1.080	1.253	1.332	1.315	1.274	0.8801×10^{-4}	0.930×10^{-7}	0.11
Sol. 6 (pH 3.385)	*A*	1.345	1.551	1.642	1.618	1.558	1.0961×10^{-4}	2.088×10^{-7}	0.19
Sol. 7 (pH 2.367)	*A*	1.089	1.242	1.303	1.278	1.213	0.8762×10^{-4}	1.623×10^{-7}	0.19

Calcon	λ	550	560	570	580	590	600	610	620	630	Mean	SD	RSD
Sol. 1 (pH 10.064)	*A*	1.230	1.410	1.610	1.848	2.041	2.124	2.168	2.307	2.499	1.4119×10^{-4}	5.945×10^{-7}	0.42
Sol. 2 (pH 9.948)	*A*	0.999	1.139	1.293	1.479	1.638	1.698	1.735	1.862	2.023	1.1196×10^{-4}	6.963×10^{-7}	0.62
Sol. 3 (pH 9.608)	*A*	0.509	0.579	0.662	0.753	0.836	0.863	0.884	0.945	1.035	0.5668×10^{-4}	2.286×10^{-7}	0.40

Congo red	λ	320	330	340	350	360	460	470	480	490	500	510	Mean	SD	RSD
Sol. 1 (pH 10.460)	*A*	1.200	1.246	1.259	1.204	1.076	1.265	1.317	1.313	1.253	1.147	1.008	0.4773×10^{-4}	0.933×10^{-7}	0.20
Sol. 2 (pH 7.498)	*A*	1.193	1.240	1.254	1.201	1.074	1.277	1.329	1.325	1.266	1.160	1.020	0.4793×10^{-4}	2.95×10^{-7}	0.62
Sol. 3 (pH 6.298)	*A*	1.175	1.221	1.236	1.185	1.055	1.243	1.295	1.292	1.236	1.134	1.001	0.4748×10^{-4}	1.356×10^{-7}	0.29
Sol. 4 (pH 4.228)	*A*	0.787	0.802	0.802	0.764	0.689	0.644	0.665	0.692	0.712	0.722	0.726	0.4816×10^{-4}	2.798×10^{-7}	0.58

[a] A = absorbance; RE = relative error (%); C_L = concentration of substance calculated by potentiometric method; Mean = mean of the results; SD = standard deviation; RSD = relative standard deviation (%). [b] Equilibrium constants and absorptivities of neotorin are from [4] and those of calcon and congo red from [6].

where the sum is over all the potentiometric readings (Z) and w_i is the weighting factor assigned to the ith observation; w_i is calculated from $w_i = 1/\sigma_i^2$, where σ_i^2 is the estimated variance obtained from the equation $\sigma_i^2 = \sigma_E^2 + (\partial E_i/\partial v_i)^2 \sigma_v^2$. The partial differential $(\partial E_i/\partial v_i)$ is estimated from the slope of the potentiometric curve. Approximate values of the partial differential are calculated within the SPLINE subroutine, called from the WEIGHTS subroutine, using a cubic spline interpolation procedure, taken with modifications from Stanton and Hoskins [15]. At each experimental point, the concentration of all free reactants at equilibrium are calculated by means of the CCFR subroutine by solving simultaneous mass-balance equations using the Newton—Raphson iteration. At this point, control is passed back to the FUNV subroutine where the derivatives $(\partial E_i/\partial p_j)$ for each experimental point, with respect to the parameters (p_j) to be refined, are calculated. Approximate values of these quantities are obtained by a procedure which has greatly shortened the execution time.

BETAREF can be used to refine special parameters in addition to formation constants. These special parameters are quantities which are characteristic of each titration curve such as the initial amounts of reagents, their concentrations in the titration vessel, the standard cell potentials, the liquid-junction potentials and the initial volume of the solution. Other calculation procedures (input, output, shifts in the parameters to be refined, criteria of convergence, check and elimination of negative formation constants, statistical analysis of data) are not repeated here, because they have been widely used in previous programs such as MINIQUAD [16] and MIQUV [17] by many research groups.

A complete list of the experimental and theoretical absorbance data, as well as of the molar absorptivities, calculated by the SQUAD program, with the potentiometric data, is available from the author on request. All calculations were done on the CDC CYBER 70/76 computer of the "Consorzio per la Gestione del Centro di Calcolo Elettronico Interuniversitario" dell'Italia Nord Orientale, Casalecchio, Bologna, with financial support from the University of Parma.

The results of these refinements are summarized in Table 1 and show how the protonation constants obtained from the two sets of experimental data are almost indistinguishable.

RESULTS AND DISCUSSION

In routine analysis, especially when automated instrumental techniques are used, the rapid response possible offers some interesting advantages. Starting from experimental absorbances and pH values, calculated absorptivities and equilibrium constants, in the same experimental conditions, different systems were treated by the SPEDEAD program. The computations were done by taking a trial value of T_L (concentration of substance) for each solution and were iterated by successive approximations, at different

wavelengths, until the observed absorbance equalled that calculated through the equation

$$A_o \approx A_c = l \sum_{0}^{q} \sum_{0}^{r} \beta_{0qr}[H]_i^q [L]_i^r \epsilon(k)_{0qr}$$

within the discrimination limit of the instrument ($0.001 = |A_o - A_c|$).

The results, for four different samples, are presented in Table 2. The final results shown in the Table generally agree well with those obtained by the potentiometric method. It can be seen that the absorbance data can be measured in different conditions of both pH and wavelength (λ); further, the absorbance data, which need not correspond to the greatest absorption peak, must be neither too low nor too high. During the experiments, any substances interfering with the absorption phenomena must be absent. The detection limit of the method is nearly 0.05 mg l^{-1} for the compounds investigated here. This program has been also applied to the determination of metals in solution, but the results were not satisfactory owing to the low absorption of the free metal ion relative to the other species present at equilibrium. Statistical data for the determination of varying amount of substances are summarized in Table 2, from which it is clear that the reproducibility is good.

I am indebted to Ministero della Pubblica Istruzione, Rome, and Consiglio Nazionale delle Ricerche, Rome, for financial support. Particular thanks are extended to Professor A. Vacca for the use of his BETAREF program.

REFERENCES

1 D. J. Leggett and W. A. E. McBryde, Anal. Chem., 47 (1975) 1065.
2 H. Gampp, M. Maeder and A. D. Zuberbühler, Talanta, 27 (1980) 1037.
3 M. Maeder and H. Gampp, Anal. Chim. Acta, 122 (1975) 303.
4 M. Biagini Cingi, F. Bigoli, E. Leporati and M. A. Pellinghelli, J. Chem. Soc., Dalton Trans., (1982) 1411, 1965.
5 E. Leporati, Ann. Chim. (Rome), 73 (1983) 1.
6 F. Bigoli, E. Leporati and M. A. Pellinghelli, Ann. Chim. (Rome), 73 (1983) 481.
7 G. Gran, Analyst (London), 77 (1952) 661.
8 H. S. Harris and R. S. Tobias, Inorg. Chem., 8 (1969) 2259.
9 F. Bigoli, E. Leporati and M. A. Pellinghelli, J. Chem. Soc., Dalton Trans., Part 1, (1981) 1531, 1961.
10 J. M. H. Fortuin, Anal. Chim. Acta, 24 (1961) 175.
11 W. C. Hamilton, Statistics in Physical Sciences, The Roland Press Company, New York, 1964, p. 150.
12 R. S. Tobias and M. Yasuda, Inorg. Chem., 2 (1963) 1307.
13 See, e.g., I. G. Sayce, Talanta, 15 (1968) 1397.
14 A. Sabatini and A. Vacca, private communication.
15 R. G. Stanton and W. D. Hoskins, Numerical Analysis in Physical Chemistry, An Advanced Treatise, Academic Press, New York, 1975.
16 A. Sabatini, A. Vacca and P. Gans, Talanta, 21 (1974) 53.
17 A. Vacca and A. Sabatini, MINIQUAD and MIQUV, in D. J. Leggett (Ed.), Computational Methods for the Determination of Stability Constants, Plenum, New York, 1985.

Analytica Chimica Acta, 170 (1985) 295—300
Elsevier Science Publishers B.V., Amsterdam — Printed in The Netherlands

DETERMINATION OF FREE PHENYTOIN IN PLASMA BY ULTRAFILTRATION AND HIGH-PERFORMANCE LIQUID CHROMATOGRAPHY

TERRY D. MILLER and THOMAS C. PINKERTON*
Department of Chemistry, Purdue University, West Lafayette, IN 47907 (U.S.A.)
(Received 18th September 1984)

SUMMARY

A process for determining the free concentration of the highly protein-bound anticonvulsant drug phenytoin (5,5-diphenylhydantoin) is described. The procedure involves rapid isolation of the unbound drug from the drug/protein complex by ultrafiltration followed by high-performance liquid chromatography. Total time for a free phenytoin determination is about 15 min. The procedure is used to examine the protein-binding of phenytoin, as well as the effects of a displacer, salicylic acid. Commonly prescribed anticonvulsant drugs are resolved under the selected chromatographic conditions.

Therapeutic monitoring of the anticonvulsant drug phenytoin by high-performance liquid chromatography (h.p.l.c.) has been of interest in recent years [1—3]. Most of these studies seek to determine total phenytoin concentration. In vivo, however, the drug is highly protein-bound with only the small unbound fraction being therapeutically active [4]. Because binding depends on many factors, including the presence of displacers, other drugs or disease [5, 6], it would be advantageous to monitor the concentration of free phenytoin in blood plasma [7].

Procedures which determine total drug concentration do not detect shifts in binding equilibria. The narrow therapeutic range of phenytoin (1—2 μg ml^{-1} free drug) combined with the low toxic threshold (>2 μg ml^{-1}) allows a displacer, such as salicylic acid, to elevate the free drug concentration to a potentially dangerous level. Uremic patients also exhibit increased free phenytoin concentrations compared to normal controls [5—7].

In order to determine free drug concentration, the drug/protein complex must be separated from the unbound drug rapidly enough to avoid changing binding equilibria. Membrane ultrafiltration has been used successfully in protein-binding applications to determine free drug concentrations [8—10]. Its simplicity and low cost make it the method of choice.

Several anticonvulsant drugs are often prescribed simultaneously, prompting interest in multi-drug determinations [11—14]. The high efficiency of a 3-μm C18 column makes quantification of all common antiepileptic drugs possible within 7 min, nearly half the time required on a 25-cm column packed with 5-μm particulates.

0003-2670/85/$03.30

EXPERIMENTAL

Apparatus

An IBM LC9533 high-performance liquid chromatograph with a variable-wavelength ultraviolet detector was used. The separation was done at room temperature with a flow rate of 1 ml min^{-1} on a 3-μm C18 column (4.6 mm i.d. × 10 cm) with a 0.5-μm in-line protective filter. A 10-μl injection loop was used. The solutes were detected at 214 nm (0.025 absorbance full scale) and quantified by peak integration.

The ultrafiltration system consisted of an Amicon Model M-3 unit with 3-ml capacity and Amicon Diaflo-YM30 membranes (which restrict passage of species greater than 30 000 daltons) under 65 psi of nitrogen. Because the unit utilizes a magnetic stirring assembly during operation, heat transfer was prevented by placing a piece of foam rubber between the ultrafiltration unit and the stirrer.

Reagents and standards

The mobile phase consisted of methanol/acetonitrile/phosphate buffer (h.p.l.c.-grade solvents) in a ratio of 37:10:53 (v/v). The phosphate buffer was a 0.02 M KH_2PO_4 solution prepared with deionized/distilled water adjusted to pH 6.4 with sodium hydroxide and filtered through a 0.22-μm cellulose membrane.

Phenytoin (5,5-diphenylhydantoin) was obtained from Aldrich Chemical Company; other anticonvulsant drugs were obtained in kit form from Fisher Scientific. This "TheraChem Anticonvulsant/Theophylline Control" kit contained the following drugs in lyophilized serum: carbamazepine, ethosuximide, phenobarbital, phenytoin, primidone, theophylline and valproic acid. Stock solutions of phenytoin were prepared in methanol because of the low solubility of the drug in water.

To prevent any significant dilution of plasma proteins, the volume of stock solution added was kept small. The full range of drug concentrations could be achieved with addition of 100 μl or less of a concentrated stock solution (15 g l^{-1}). This small amount of methanol (<2%) did not cause any noticeable protein denaturation, although a significant effect was evident at a concentration of 6%.

Procedure

Ultrafiltration membranes were prepared for use by passing water through them under pressure to rinse off preservatives; the unit was then flushed with nitrogen to remove any excess of water. The cleaned unit was filled with 3 ml of plasma, and the desired amount of phenytoin stock solution was added. The system was allowed to equilibrate for 30 min with stirring before pressurization, after which the first 1—2 drops of ultrafiltrate were discarded. Subsequently, the ultrafiltrate was collected for a fixed period of time. Collection for 7 min yielded sufficient volume for 4—5 injections into the chromatograph.

RESULTS AND DISCUSSION

Calibration graphs and chromatographic resolution

Direct reverse-phase h.p.l.c. of plasma ultrafiltrate (Fig. 1A), to which various amounts of phenytoin had been added after filtration, yielded a linear calibration graph of integrated peak area (in arbitrary units) vs. free drug concentration over the range 4—48 mg l^{-1} (slope = 58 ± 1, intercept = —23 ± 41, std. error = 56, r = 0.999). Each point on the calibration graph represented the average of three trials. Phenytoin was found not to bind to the ultrafiltration membrane.

Several anticonvulsant drugs are often administered concomitantly. Under the recommended chromatographic conditions, phenytoin is easily resolved

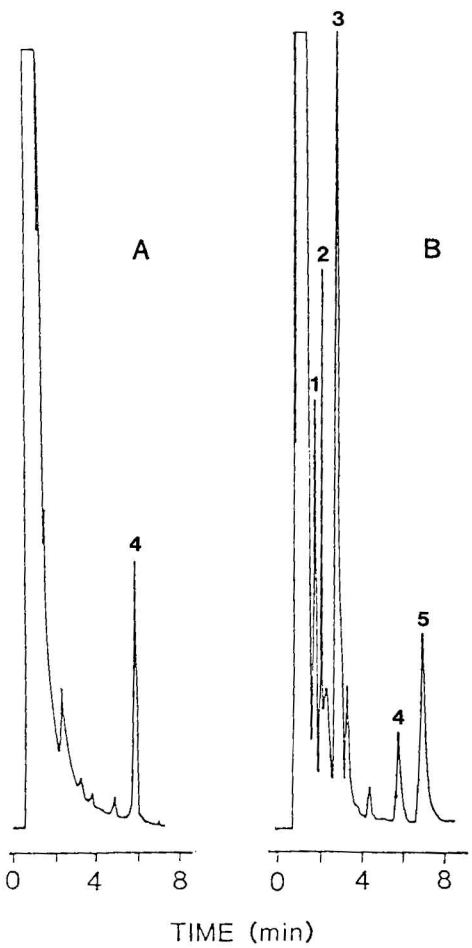

Fig. 1. Chromatograms: (A) phenytoin added to plasma ultrafiltrate (1.25 μg ml^{-1}); (B) Fisher anticonvulsant/theophylline control kit. Peaks: (1) ethosuximide; (2) primidone; (3) phenobarbital; (4) phenytoin; (5) carbamazepine.

(Fig. 1B) from the other drugs contained in the serum of the Fisher anticonvulsant kit. With the exception of theophylline, the anticonvulsant drugs can be quantified under the selected chromatographic conditions. Theophylline is eluted amid the endogenous plasma constituents.

Protein binding of phenytoin

The fundamental principles behind the protein binding of drugs are well established [4, 15]. Given mass-law considerations, the reversible binding of small molecular species with proteins can be expressed by

$$r = [n_1K_1D_f/(1 + K_1D_f)] + [n_2K_2D_f/(1 + K_2D_f)] + \ldots + [n_iK_iD_f/(1 + K_iD_f)] \quad (1)$$

where r is the ratio of moles of drug bound to total moles of protein in the system, n_i is the number of binding sites in the ith class of sites, K_i is the intrinsic affinity constant for the binding of the drug by the sites in the ith class, and D_f is the concentration of unbound drug (i.e., free drug concentration). If a single class of sites can be assumed, rearrangement of Eqn. 1 yields the familiar Scatchard plot (r/D_f vs. r) from the equation $r/D_f = nK - rK$. Further, the fundamental relationship between protein binding of a drug to a single class of sites and the fraction of drug bound (β) at equilibrium is expressed by

$$\beta = [1 + (D_f/nP_t) + (1/nKP_t)]^{-1} \quad (2)$$

where P_t is the total concentration of the specific protein involved in the binding.

A determination of the fraction of phenytoin bound to plasma proteins by the ultrafiltration/h.p.l.c. method described shows a significantly greater amount of drug bound than would be predicted by Eqn. 2, which assumes only a single class of sites is available (Fig. 2). This suggests that phenytoin is bound to more than one class of binding sites. The corresponding Scatchard plot, as expected, is also nonlinear (Fig. 3). Results shown here agree well with binding data obtained with radioactive labelling [4]. Previous investigators have ignored this nonlinearity and have calculated binding parameters based on a single class of sites by visually imposing a linear fit [5]. Nonlinear Scatchard data are much better represented by resolving the curve into two or three contributing components as described by Rosenthal [16]. Applying a two-binding-site model yields an estimate of binding parameters for the high-affinity ($K = 1.1 \times 10^5$ M^{-1}, $n = 0.23$) and the low-affinity ($K = 2.1 \times 10^3$ M^{-1}, $n = 3.98$) binding sites (Fig. 3), if it is assumed that phenytoin binds only to albumin at a plasma concentration of 3.8 g/100 ml. Odar-Cederlöf and Borgå [5] reported that 20% of the phenytoin is actually bound to plasma globulins. This probably explains the unreasonable value of 0.23 binding sites per macromolecule obtained for the high-affinity site. It is possible that the high-affinity sites are located on the globulins and not on albumin, as assumed in these calculations. Further speculation is inappropriate.

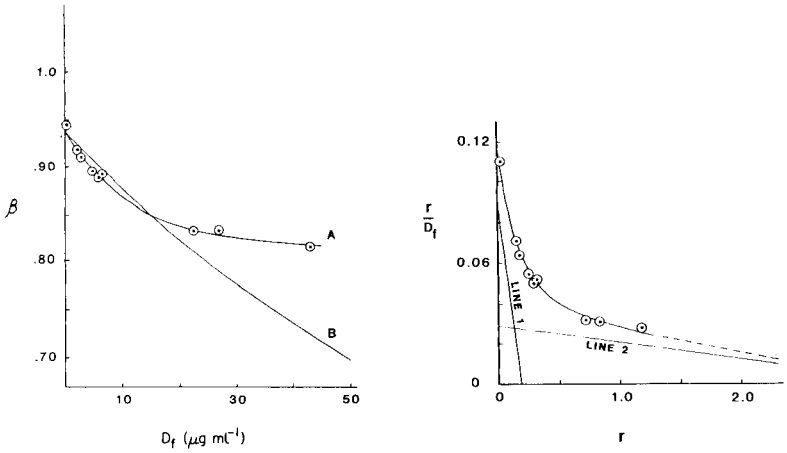

Fig. 2. Plots of fraction of drug bound (β) vs. free drug concentration (D_f): (A) Experimental binding data; (B) predicted curve based on Eqn. 2 and results from Lunde et al. [4] (β = 0.93 at D_f = 1 mg ml^{-1}).

Fig. 3. Scatchard plot (D_f is in μg ml^{-1}). (⊙) Experimental data; (1) high-affinity site (K = 1.1 × 10^5 M^{-1}, n = 0.23); (2) low-affinity site (K = 2.1 × 10^3 M^{-1}, n = 3.98).

Effects of a competitive displacer

A useful feature of being able to determine rapidly the free drug concentration in a plasma sample lies in the ability to monitor the fraction of the drug bound (β) in the presence of some protein-binding displacers. The fraction of drug bound as function of the competitive protein binding of a displacer is described [17] by

$$1 - \beta = (1 + KD_f + K'C_f)/(1 + KP_t + KD_f + K'C_f) \quad (3)$$

where K and K' are the affinity constants for the drug/protein complex and displacer/protein complex, respectively, and C_f is the concentration of free displacer. The fraction of phenytoin bound decreases linearly with increasing concentration of salicylic acid, a known drug displacer (Fig. 4).

Method evaluation

The proposed method offers a rapid determination of free phenytoin, with the use of the 3-μm column providing shorter analysis times and better efficiency compared to larger particulate packings. The dynamic range of the technique easily covers the commonly encountered therapeutic drug levels.

Centrifugal ultrafiltration techniques could also be used to isolate free phenytoin in place of the pressurized ultrafiltration described in this study, providing the added advantage that the user may prepare many samples simultaneously. Disposable centrifugal ultrafilters are available commercially.

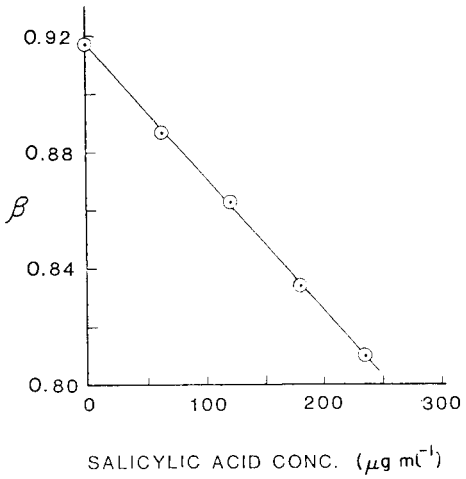

Fig. 4. Plot showing displacement of protein-bound phenytoin by salicylic acid. Total phenytoin concentration is 26 μg ml^{-1}. Regression equation: $y = -4.60 \times 10^{-4}x + 0.916$ ($r = 0.999$).

We gratefully acknowledge P. Low, D. Allen, M. Westfall, S. Waugh and L. Maneri for their generous assistance in obtaining plasma samples.

REFERENCES

1 B. Kinberger and A. Holmén, Clin. Chem., 28 (1982) 718.
2 R. J. Sawchuk and L. L. Cartier, Clin. Chem., 26 (1980) 835.
3 S. A. Chow, D. M. Charkowski and L. J. Fischer, Life Sci., 27 (1980) 2477.
4 P. K. M. Lunde, A. Rane, S. J. Yaffe, et al., Clin. Pharmacol. Ther., 11 (1970) 846.
5 I. Odar-Cederlöf and O. Borgå, Clin. Pharmacol. Ther., 20 (1976) 36.
6 D. W. Shoeman, D. M. Benjamin and D. L. Azarnoff, Ann. N.Y. Acad. Sci., 226 (1973) 127.
7 B. C. Thompson, Clin. Chem. News, 9 No.4 (1983) 12.
8 W. F. Blatt, S. M. Robinson and H. J. Bixler, Anal. Biochem., 26 (1968) 151.
9 R. L. Judd and A. J. Pesce, Clin. Chem., 28 (1982) 1726.
10 J. B. Witlam and K. F. Brown, J. Pharm. Sci., 70 (1981) 146.
11 S. J. Soldin and J. G. Hill, Clin. Chem., 22 (1976) 856.
12 P. M. Kabra, B. E. Stafford and L. J. Marton, Clin. Chem., 23 (1977) 1284.
13 G. K. Szabo and T. R. Browne, Clin. Chem., 28 (1982) 100.
14 P. M. Kabra, Altex Chromatogram., 2 No.3 (1979) 3.
15 A. Goldstein, Pharmocol. Rev., 1 (1949) 102.
16 H. E. Rosenthal, Anal. Biochem., 20 (1967) 525.
17 M. C. Meyer and D. E. Guttman, J. Pharm. Sci., 57 (1968) 895.

Analytica Chimica Acta, 170 (1985) 301—310
Elsevier Science Publishers B.V., Amsterdam — Printed in The Netherlands

DETERMINATION OF METHYLMALONIC ACID AFTER DIAZONIUM DERIVATIZATION BY HIGH-PERFORMANCE LIQUID CHROMATOGRAPHY

DANA K. MORGAN and NEIL D. DANIELSON*
Department of Chemistry, Miami University, Oxford, OH 45056 (U.S.A.)
(Received 24th February 1984)

SUMMARY

The use of a single prederivatization step in conjunction with high-performance liquid chromatography (h.p.l.c.) is described for the determination of methylmalonic acid (MMA). The method is based on the reaction of MMA and 4-diazobenzenesulfonic acid, which produces a derivative that has a molar absorptivity of about 9×10^3 l mol^{-1} cm^{-1} at 353 nm. The derivatization reaction is optimized for various parameters. A reagent concentration of 3.3 mM at a reaction pH of 4.6 and a temperature of 100° C are optimal. The reaction product is separated from the excess of reagent and other interfering components by using a polystyrene-divinylbenzene column and a highly aqueous mobile phase. After a simple clean-up step, it is possible to quantify MMA in urine at about 0.8 mg l^{-1} with linear response up to 32 mg l^{-1}.

Methylmalonic acid (MMA) is an important compound to monitor for certain studies of living systems. Patients suffering from a vitamin B_{12} deficiency have shown evidence of an elevated urinary excretion of MMA because this vitamin is required for the conversion of MMA to succinic acid [1]. Several studies have suggested that this increase has clinical value as a test for vitamin B_{12} deficiency [2—4]. An increase in urinary MMA can also be due to an inherited metabolic disorder caused by a deficiency of methylmalonyl CoA mutase activity caused either by a defect of the apoenzyme or by a defect in the metabolism of its B_{12} coenzyme. This metabolic disorder is especially common in newborns; thus, routine screening of newborns [5] and pregnant women [4] can lead to early detection and treatment. Methyl malonate has also been found to be incorporated from the growth medium of various micro-organisms to accelerate the biosynthesis of antibiotics, such as erythromycin [6] and candicidin [7].

Methylmalonic acid has been quantified previously by two main techniques, gas chromatography (g.c.) and spectrophotometry. Many attempts have been made to convert MMA into an appropriate ester which can then be separated by g.c. with normal detection techniques and/or with mass spectrometry [4, 5, 8—10]. The major problem with the g.c.-based methods is that it is necessary, by a complex, time-consuming extraction, to remove the MMA

0003-2670/85/$03.30

from an aqueous medium into an organic solvent for esterification. The spectrophotometric method based on the reaction between MMA and the *p*-nitrobenzenediazonium (NBD) ion has received some attention, but the reaction product or products have not been characterized. This assay is susceptible to many interferences; thus, ion-exchange or extraction is needed to clean up the sample [2, 3, 11]. In addition, the sample solution must be degassed because carbon dioxide interferes with the color development.

Thin-layer chromatography has been applied for the determination of MMA in various physiological fluids and was suitable for the screening of patients [12, 13]. The direct determination of urinary MMA has recently been reported by high-performance liquid chromatography (h.p.l.c.) with detection at 200 nm [14, 15]. This technique suffers from two major limitations. Because so many compounds absorb at 200 nm, the chromatography of urinary samples requires several hours. The second problem is the poor molar absorptivity of MMA even at 200 nm. Other techniques like isotachophoresis [16] and an enzymatic reaction system [17] have also been reported.

The possibility of using h.p.l.c. after a single derivatization step to form a colored derivative of MMA would appear to be a viable alternative. The NBD color reaction was found not to be well suited to h.p.l.c. because the reaction product had to be maintained at pH > 12.5. Another drawback was that both the reagent and the product have poor solubility in aqueous solutions. However, the coupling of various aromatic diazo reagents with compounds containing an active methylene group is well known [18]. To permit detection in the high u.v. region but retain a product that is compatible with reverse-phase h.p.l.c., 4-diazobenzenesulfonic acid (DBS) was studied as a derivatizing agent for MMA. This reaction was optimized as a function of absorbance with reagent concentration, reaction pH, and reaction temperature. In addition, the two products of the reaction were separated by h.p.l.c. and tentatively identified. Effects of interfering compounds and adaptation of the method for urinary MMA were investigated.

EXPERIMENTAL

Apparatus

The h.p.l.c. system was assembled with various components as follows. The Altex Model 110A pump (Altex, Berkeley, CA) was modified with a tee-configuration pulse dampener consisting of a 52 cm × 4.6 mm stainless-steel tube. The injector, equipped with a 130-μl sample loop, was a Rheodyne Model 7010 with a loop filter port (Rheodyne Model 7011). A 5 cm × 4.6 mm i.d. precolumn and a 15 cm × 4.6 mm i.d. working column were used. The pre-column was packed with 8-μm macroporous polystyrene/divinylbenzene resin (Interaction Chemicals, Mountain View, CA) using a Model 10-600-30 pneumatic amplifier pump (SC Hydraulic Engineering, Los Angeles, CA) and a high-pressure slurry packer (Alltech, Deerfield, IL). The working column

was a Hamilton PRP-1 column (Hamilton, Reno, NV). An Altex Model 153 constant-wavelength (340 nm) detector was used to monitor the column effluent. Peaks were recorded with a Fisher Recordal Model 5000 (Houston Instruments).

All spectrophotometric work was done with a Hewlett-Packard Model 8450 spectrophotometer equipped with a Model 9872B x-y plotter (Hewlett-Packard).

Chemicals

All water used was deionized and doubly distilled. Methylmalonic acid (MMA) was supplied by Aldrich, and *p*-nitrobenzenediazonium tetrafluoroborate (NBD) and 4-diazobenzenesulfonic (DBS) acid by Fluka. The 4-diazobenzenesulfonic acid was washed with cold methanol and dried before use. An AG3-X4A resin (20—50 mesh; Bio-Rad Laboratories) was used for sample pretreatment. All chemicals were of reagent grade or the highest purity available and were stored as recommended.

Procedures

Optimization of 4-diazobenzenesulfonic acid concentration. Aliquots (5 ml) of 26.0 mg l^{-1} MMA were treated with 5 ml of 1 M acetate buffer, pH 4.30, which varied in concentration of DBS. The solution was then heated for 5 min in a boiling water bath and, after cooling, made alkaline by addition of 0.5 ml of 50% (w/v) sodium hydroxide solution. The spectrum of this solution was immediately measured.

Optimization of reaction pH. A 5-ml aliquot of 26.0 mg l^{-1} MMA solution was added to 1 ml of 31.2 mM DBS and 4 ml of 2 M acetate buffer at various pH values. The mixture was heated and made alkaline as above and the spectrum was recorded.

Absorption dependence on pH. A 20-ml aliquot of a 245 mg l^{-1} MMA solution was added to a flask that contained 60 ml of 30 mM DBS and 60 ml of 1 M acetate buffer, pH 4.30. The flask was placed in a boiling water bath for 5 min. Then 3 M sodium hydroxide was added while the pH was measured. At intervals of 0.5 pH units, an aliquot was removed and the u.v.-visible spectrum was recorded. The aliquot was returned to the flask and the process was continued. All data obtained were corrected for dilution.

Optimization of reaction temperature. A 5-ml aliquot of 48.5 mg l^{-1} MMA solution was mixed with 1 ml of 31 mM DBS and 4 ml of 2 M acetate buffer, pH 4.60. The flask was placed in a constant-temperature bath of ethylene glycol for 5 min. After cooling, the samples were injected into the h.p.l.c. system.

Calibration graph. A 0.75-ml aliquot of a 2 M acetate (pH 4.60) solution which was 8.70×10^{-3} M in DBS and 15.4×10^{-3} M in sodium nitrite was added to a 2-ml volumetric flask. The flask was diluted to the mark with the appropriate standard solution. After mixing by inversion, the flask was placed in a boiling water bath for 5 min. After cooling, the samples were injected into the h.p.l.c. system.

Recommended procedure for urine samples. A cleanup column was made by packing a Pasteur pipet with the AG3-X4A weak anion-exchange resin to make a 5.5 cm × 0.6 cm column. This column was conditioned by passing 10 ml of 2.0 M acetate buffer, pH 4.60, at a vacuum-assisted flow rate of about 3 ml min^{-1}. The urine was stored at 0° C and then, upon warming to room temperature, filtered to remove any precipitates. The urine sample was diluted with water (3 + 2, v/v) before assay.

A 3-ml aliquot, which had been adjusted to pH 4.60 with hydrochloric acid or sodium hydroxide, was loaded on the clean-up column at a gravity-controlled flow rate of about 1.0 ml min^{-1}; then 0.72 M hydrochloric acid was passed through at about the same flow rate. The first 5-ml fraction was discarded. The second 5-ml fraction, which contained all the MMA, was collected and then assayed by the calibration procedure described above.

RESULTS AND DISCUSSION

Optimization of reaction conditions

Initially, a reaction procedure similar to that reported by Giorgio and Plaut [2] was followed. The spectra of both the reagent blank and the MMA/DBS product (Fig. 1) showed a band at 353 nm that was due to the complex. When the blank spectrum was subtracted, a band appeared at 526 nm. However, its molar absorptivity was about one third of the 353-nm value.

The optimum reaction conditions for formation of the MMA/DBS complex were then examined. The first parameter investigated was the DBS concentration. The results (Fig. 2) indicated a constant increase in net absorbance with DBS concentration up to 3.1 × 10^{-3} M. Between 3.1 and 3.4 × 10^{-3} M, the net absorbance was almost constant but it decreased at higher

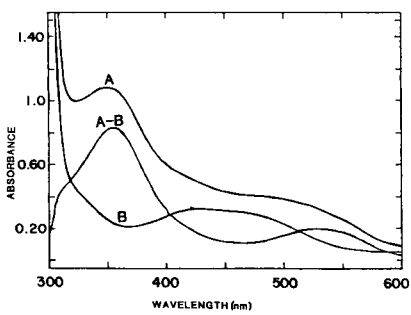

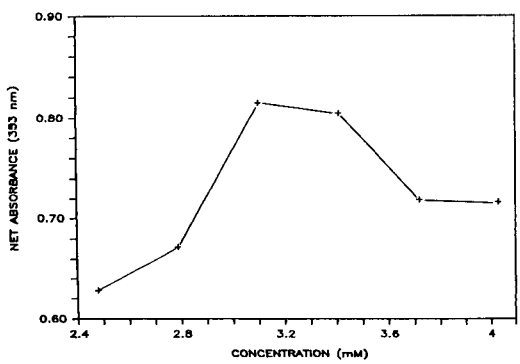

Fig. 1. Ultraviolet-visible spectrum of the MMA complex (A), the blank (B), and the difference (A—B). Concentration of MMA was 24.6 mg l^{-1}.

Fig. 2. Net absorbance of the MMA/DBS complex, at 353 nm, as a function of DBS concentration. The MMA concentration was kept constant at 26.0 mg l^{-1}.

concentrations because of the large increase in the reagent blank. These results were reproduced by a similar h.p.l.c. study of the separated reaction product. A DBS concentration of 3.25×10^{-3} M was used for all subsequent studies.

As was found by Giorgio and Plaut [2], the reaction pH was very critical. The optimum pH was shown to be 4.5—4.6 (Fig. 3), which is similar to that reported for the NBD reagent [2]. The absorbance of the MMA/DBS reaction product with change in pH was studied and was found to read a maximum at pH >11.5 (Fig. 4). At pH 10.5, the MMA/NBD product would suffer a 55% loss in absorbance; however, only a 17% loss was found for the MMA/DBS derivative. The molar absorptivity of the product at 353 nm under these conditions was about 9×10^3 l mol^{-1} cm^{-1}, which was about twice that obtained for the MMA/NBD derivative at 620 nm.

From 60 to 100° C, the peak area of the product increased linearly with temperature, but at higher temperatures, no significant change was observed. Thus, to simplify experimental conditions, a boiling water bath was used. Previous workers [11] using the NBD spectrophotometric method found that the color development was incomplete at reaction temperatures below 94°C whereas precipitation occurred above 96°C. No precipitation of the MMA/DBS complex occurred at 100° C.

Chromatography of diazotized MMA

Figure 5 shows typical chromatograms of both a blank and a 106 mg l^{-1} MMA standard, with the mobile phase adjusted to pH 11.00. To simplify the experimental procedure, decrease dilution effects, and reduce the possible carbon dioxide interference on the color development, solutions at pH 4.60 were injected into the chromatograph. There are three major differences between the standard chromatogram and the blank. The first is the off-scale peak at 4.4 min (peak 1) which is caused by overlap of peaks from the excess

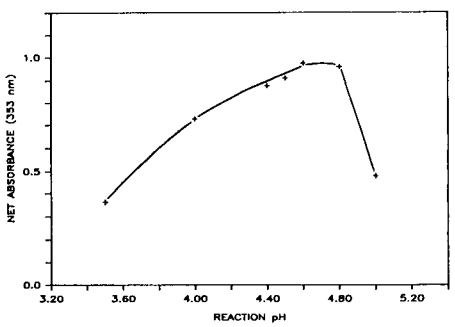

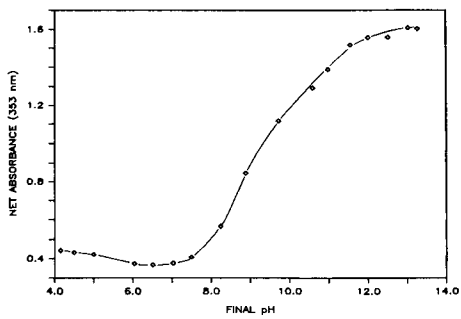

Fig. 3. Net absorbance of the MMA/DBS complex, at 353 nm, as a function of reaction pH. The MMA was kept constant at 26.0 mg l^{-1} and all buffers were 1 M acetate.

Fig. 4. The absorbance of the complex as a function of final reaction pH. The MMA concentration was kept constant at 35.0 mg l^{-1}.

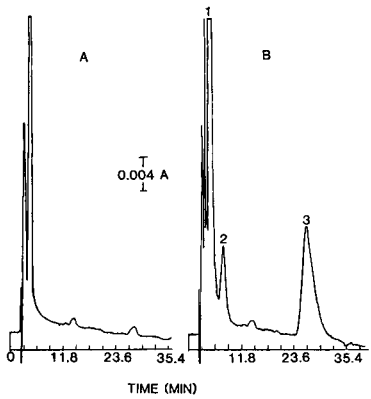

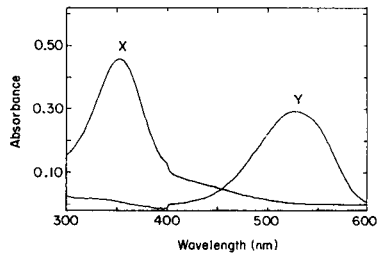

Fig. 5. (A) Chromatogram of the reagent blank; (B) chromatogram of a 106 mg l^{-1} MMA standard. Absorbance full scale, 0.04. Mobile phase was 90%, 0.03 M Na_3PO_4 (pH 11.00)/ 10% methanol; flow rate, 0.8 ml min^{-1}; 36.4° C.

Fig. 6. Ultraviolet-visible spectra of the 4.6-min fraction (X) and of the 27.0-min fraction (Y). Reference cell contained the mobile phase used in Fig. 5.

reagent and a product. Two other peaks appear at about 8 min (peak 2) and about 27 min (peak 3). The second peak is thought to be due to some impurity because it was not concentration-dependent. Decreasing the detector sensitivity confirmed that peak 1 was actually two components and that the second peak of the pair (peak 1B) and peak 3 both depended on the MMA concentration. Peaks 1B and 3 were tentatively identified by fraction collection and subsequent u.v.-visible spectroscopy as shown in Fig. 6. Based on the respective wavelength maxima of 353 and 530 nm, the products of the MMA/DBS reaction were tentatively assigned structures X and Y (R = CH_3) as follows:

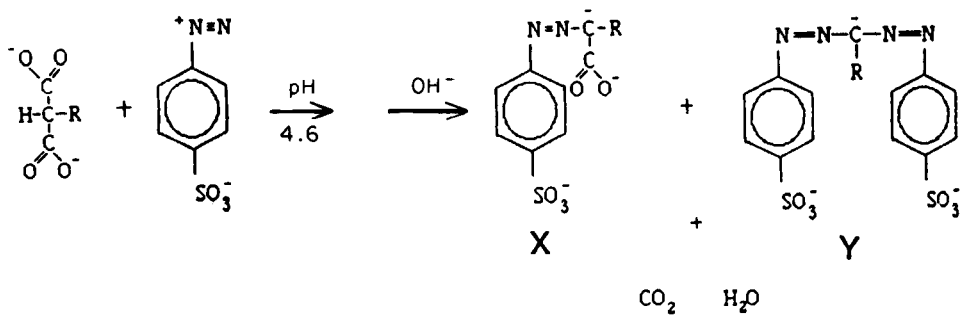

This would be consistent with the structures that have been previously suggested [18—21] for related malonic acid derivatives. In addition, the observed retention order of the excess of DBS, compound X, and compound Y can be easily explained by the hydrophobic reversed-phase mechanism.

The formation of peak 1B could be markedly increased by the presence of sodium nitrite in the DBS reagent stock solution, whereas addition of nitrite after the heating step had no effect. For a change in nitrite concentration from 2 to 12 mM, an increase in the area of peak 1B by a factor of 5 was observed. Peak 3 was less affected by nitrite, but was reduced at nitrite levels above 10 mM and had an optimum concentration range between 1 and 2 mM. Peak 1B was not enhanced when either hydrazine or periodate was present at the 10 mM level, indicating that the effect was specific to nitrite. The reason for this product yield enhancement by nitrite is unclear; it has been suggested [19] that nitrite would cause nitrosation to the corresponding oxime, HO_3S—Ar—N=N—CH=N—OH.

Figure 7 shows chromatograms of a blank and a 106 mg l^{-1} MMA standard, for which the mobile phase pH has been lowered to 9.00. Peak 1B was eluted at 13 min and was well separated from the excess of reagent. The peak at 21 min was due to the impurity. Peak 3 did not elute from the column when this mobile phase was used although reaction conditions were identical to those in Fig. 6. The mobile phase conditions in Fig. 7 were used in construction of a calibration graph based on the area of peak 1B. A slope of 0.234 ± 0.003 cm^2 mg l^{-1} and an intercept of 0.286 ± 0.157 cm^2 with a correlation coefficient of 0.996 were calculated for this plot. The linear range extended to at least 35 mg l^{-1} with a detection limit (signal/noise ratio of 2) of about 0.5 mg l^{-1}. Despite the low mobile phase pH, this detection limit was more than adequate. The reproducibility for a 0.96 mg l^{-1} sample was 1.33% for 5 trials.

Application to urine samples

The initial goal was to determine urinary MMA without any sample clean-up. When spiked urine was used, there was a marked reduction in the peak

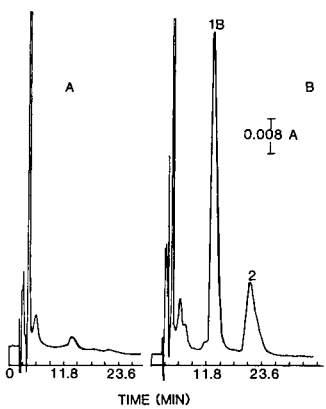

Fig. 7. (A) Chromatogram of the reagent blank; (B) chromatogram of a 106 mg l^{-1} MMA standard. Absorbance full scale, 0.04. Mobile phase was 90% 0.03 M borate (pH 9.00)/ 10% methanol; flow rate, 0.8 ml min^{-1}; 36.4°C.

area of the MMA/DBS product. Because there was some interference from likely components in urine such as tyrosine, tryptophan, ascorbic acid, and uric acid, a slight sample clean-up was deemed necessary to achieve reliable determination of urinary MMA. Several clean-up systems (extraction with ether or ether/alcohol mixtures, and preconcentration of MMA on a cartridge packed with a strong anion-exchange resin) were tried. These methods suffered from either the difficulty in extracting the MMA quantitatively from the matrix with the solvents tested, or the inability to remove the MMA from the resin. The best method developed involved passing the sample through a Bio-Rad AG3-X4A weak anion-exchange column. It was necessary to adjust the sample pH above the pK_a of MMA, 3.07, to permit quantitative retention of the MMA. An acetate buffer, pH 4.60, was found to be suitable for trapping MMA on the resin; no MMA appeared in the eluent. The Bio-Rad resin was better suited than another weak anion-exchange resin, poly(2-vinylpyridine), because loading and elution of the MMA were both quantitative. A calibration graph for standard MMA samples after the weak anion-exchange pretreatment was linear up to 32.0 mg l^{-1} MMA. The loading capacity of the resin was the limiting factor; the response decreased at 38 and 43 mg l^{-1}. The linear region had a slope of 0.137 ± 0.009 cm^2 mg l^{-1} and an intercept of 0.332 ± 0.162 cm^2 with a correlation coefficient of 0.991. Despite the necessity of diluting the urine, the detection limit was very respectable at 0.8 mg l^{-1}. This value is competitive with the 0.1 mg l^{-1} reported for a g.c./m.s. method [10].

A comparison of Figs. 8 and 9 shows the need for, and the efficiency of, the clean-up procedure. Figure 8 shows three chromatograms of urine samples without the clean-up procedure. Chromatogram A, for an unreacted urine sample, shows no co-eluting peak at 13 min, corresponding to the retention time of peak 1B. Derivatization of the urine sample produced a poorly resolved peak for the MMA product (chromatogram B). Another urine aliquot spiked with 16.0 mg l^{-1} MMA (chromatogram C) produced only a small change in peak area; the recovery of MMA was estimated to be about 40%. After aliquots of these same samples underwent the simple column clean-up, the chromatograms of derivatized MMA were much clearer (Fig. 9). An unspiked urine sample (chromatogram A) gave a well resolved peak which correlated with a urinary MMA concentration of 14 mg l^{-1}. Two other unspiked urine samples were found to contain 7 and 13 mg l^{-1} MMA, respectively, consistent with the accepted normal range (less than 20 mg l^{-1}) [10]. When the sample was spiked with 16.0 mg l^{-1} MMA (chromatogram B) and compared to a corresponding standard (chromatogram C), the experimental concentration of MMA was 28 mg l^{-1}, corresponding to a recovery of 91%. The average recovery of spikes for two different samples was 98%. These chromatograms definitely show that this method can be used for routine quantitation of normal urinary MMA. Elevated urinary MMA samples could be assayed accurately after dilution. Simultaneous pretreatment of many samples by means of a Vac-elute apparatus and use of a liquid chromato-

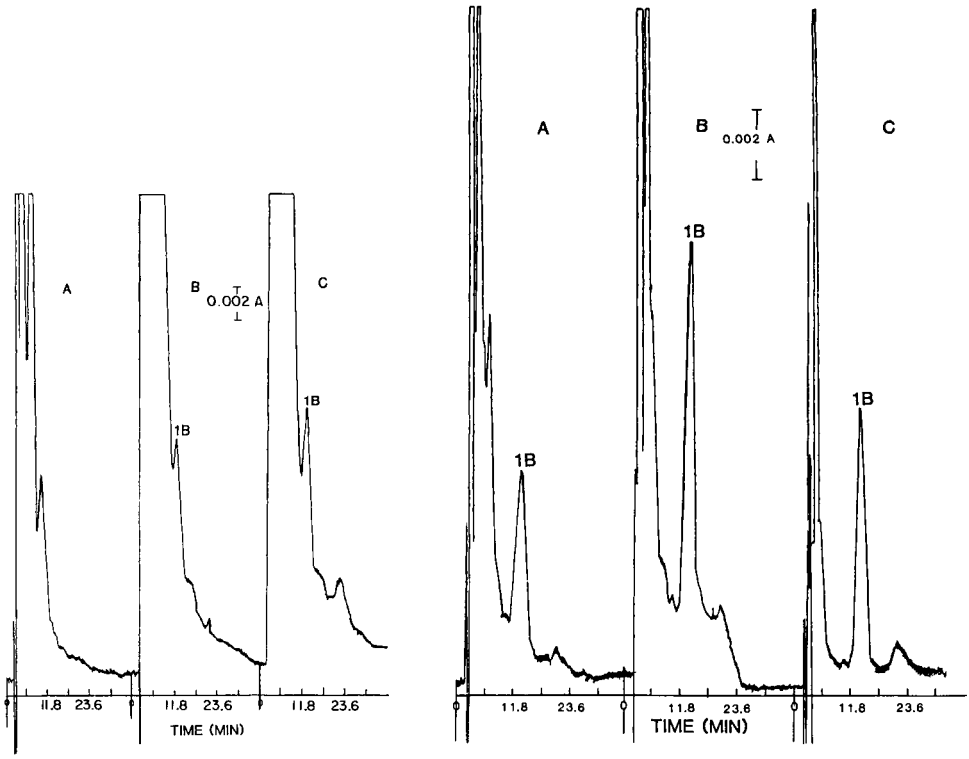

Fig. 8. Chromatograms of urine samples without clean-up: (A) unreacted urine; (B) reacted urine; (C) urine spiked with 16.0 mg l^{-1} MMA. Chromatographic conditions are the same as in Fig. 7.

Fig. 9. Chromatograms of cleaned-up urine samples and a standard: (A) cleaned-up urine; (B) cleaned-up urine spiked with 16.0 mg l^{-1} MMA; (C) a 16.0 mg l^{-1} MMA standard that has been cleaned up. Chromatographic conditions are the same as in Fig. 7.

graph with an automatic injector would help improve sample throughput.

The use of DBS for the determination of MMA has several advantages over the conventional NBD method. The first advantage is a higher molar absorptivity and a lesser dependence on pH for color development. The sulfonic acid derivative has a greater water solubility and thus is better suited for h.p.l.c. Finally, adaptation of this derivatization procedure has offered particular promise for the determination of other malonic acid derivatives such as carboxyglutamic acid [22].

We thank Miami University Faculty Research Committee and Sigma Xi for support of this project. We also thank Interaction Chemicals for their gift of resin. D. K. Morgan gratefully acknowledges support provided by a Dissertation Fellowship from Miami University.

REFERENCES

1 A. L. Lenninger, Principles of Biochemistry, North Publishers, New York, 1982, p. 522.
2 A. J. Giorgio and G. W. E. Plaut, J. Lab. Clin. Med., 66 (1965) 667.
3 A. Green, Clin. Pathol., 21 (1968) 221.
4 H. D. Bakker, A. H. Van Gennip, M. Duran and S. K. Wadman, Clin. Chim. Acta, 86 (1978) 349.
5 M. Maties, V. E. Shih, J. Evans and H. L. Levy, Clin. Chim. Acta, 114 (1981) 303.
6 S. M. Friedman, T. Kaveda and J. W. Corcoran, J. Biol. Chem., 239 (1964) 2386.
7 E. F. Martin and L. E. McDaniel, Eur. J. Appl. Microbiol., 3 (1976) 135.
8 R. F. Gibbs, K. Itiaba, O. A. Mamer, J. C. Crawhall and B. A. Cooper, Clin. Chim. Acta, 38 (1972) 447.
9 E. J. Norman, H. K. Berry and M. D. Denton, Biomed. Mass Spectrom., 6 (1979) 546.
10 E. J. Norman, O. J. Martelo and M. D. Denton, Blood, 59 (1978) 1128.
11 J. M. Gawthorne, J. Watson and E. L. R. Stokstad, Anal. Biochem., 42 (1971) 555.
12 H. R. Bhatt, A. Green and J. C. Linnell, Clin. Chem., 30 (1982) 311.
13 D. B. Hyman, A. M. Saunders and K. Tanaka, Clin. Chem. Acta, 132 (1983) 219.
14 D. N. Buchanan and J. G. Thoene, Anal. Biochem., 124 (1982) 108.
15 M. J. Bennett and C. E. Bradey, Clin. Chem., 30 (1984) 542.
16 M. Hiroaki, K. Sasaki and H. Kodama, J. Chromatogr., 190 (1980) 501.
17 E. P. Frenkel and R. L. Kitchens, Blood, 49 (1977) 1396.
18 P. G. Walker, Biochem. J., 58 (1954) 699.
19 S. M. Parmerter, Organic Reactions, Vol. 10, Wiley, New York, 1959, p. 13.
20 H. C. Yao and P. Resnick, J. Am. Chem. Soc., 84 (1962) 3514.
21 R. O. C. Norman, Principles of Organic Synthesis, 2nd edn., Wiley, New York, 1978, p. 447.
22 N. D. Danielson, Y. P. Wu, D. K. Morgan and J. L. Glajch, Anal. Chem., 57 (1985) 185.

Analytica Chimica Acta, 170 (1985) 311—317
Elsevier Science Publishers B.V., Amsterdam — Printed in The Netherlands

DETERMINATION OF THE TWO-PHASE EQUILIBRIUM CONSTANTS OF COPPER(II)-MODIFIED SILICA GELS USED IN LIQUID CHROMATOGRAPHY

F. GUYON, J. DESBARRES and R. ROSSET*

Laboratoire de Chimie Analytique, Ecole Supérieure de Physique et Chimie de Paris, 10 Rue Vauquelin, 75005 Paris (France)

(Received 27th July 1984)

SUMMARY

Silica gels modified with copper(II) are currently used in ligand-exchange liquid chromatography. The main species present at the surface of the stationary phase is shown to be $(\equiv SiO)_2Cu(NH_3)_2(H_2O)_x$. Measurements of the ammonia concentration in the mobile and stationary phases are combined with computer-assisted calculations to determine the following apparent equilibrium constants: for $\equiv SiOH + NH_3 \rightleftharpoons \equiv SiO^-NH_4^+$, $\log K = -0.2$; for $(\equiv SiO)_2Cu + NH_3 \rightleftharpoons (\equiv SiO)_2Cu(NH_3)$, $\log \beta_1 = 2.8$; and for $(\equiv SiO)_2Cu + 2NH_3 \rightleftharpoons (\equiv SiO)_2Cu(NH_3)_2$, $\log \beta_2 = 4.0$. A distribution diagram of the different species present at the surface of copper-modified silica gel is given. Under the usual operating conditions for ligand-exchange chromatography ($pNH_3 < 1$), more than 60% of the silanol groups which fix copper(II) have a silicate structure with two moles of ammonia per mole of copper(II).

Silica gels modified with metal ions and especially those modified with copper(II) are used in ligand-exchange chromatography to achieve many separations [1—6]. However, as in other fields, applications have preceded studies of the mechanisms involved and, above all, studies of the species that react at the surface of the so-called copper silicate gel for chromatography.

That silica gels fix metal cations has been known for a long time. In 1930, Smith and Reyerson [7] reported the fixation of Cu^{2+} and Ni^{2+} ions; Kolthoff and Stenger [8] showed that Ca^{2+} was fixed but it was not until 1964 that Vydra and Markova [9] presented a mechanism which provided a convincing explanation for these fixations: silanol groups present at the surface of silica react, by an acid/base reaction, with the metal/ammine complexes in solution. This reaction may be formulated as follows:

$$n{\equiv}SiOH + M(NH_3)_p^+ \rightarrow (\equiv SiO)_n M(NH_3)_q + nNH_4^+$$

with $n + q = p$. Unger and Vydra [10] confirmed this hypothesis and showed that the metal is fixed proportionally to the specific surface area of the silica and, thus, to the number of silanol groups.

It appears useful to continue this study in focussing on the case of copper

0003-2670/85/$03.30

silicate, for which the applications in chromatography are by far the most numerous. To understand the overall chemical process, it is instructive to break it into its constituent reactions and to provide a value for the mass-action constant for each reaction.

The following equilibria must be considered. The silanol groups are acids in the Brønsted sense and they are neutralized by ammonia

$$\equiv SiOH + NH_3 \rightleftharpoons \equiv SiO^-NH_4^+ \quad (1)$$

The pK_a of the surface silanol groups was determined by Schindler and Kamber [11] at 25°C in 0.1 mol l^{-1} sodium perchlorate medium. They proposed a pK_a value of 6.8 ± 0.2.

The exchange reaction between the ammonium ions and the ammine copper(II) ions in solution, e.g., the tetramminecopper(II) ion which is predominant, is

$$2(\equiv SiO^-NH_4^+) + Cu(NH_3)_4^{2+} \rightleftharpoons (\equiv SiO^-)_2Cu(NH_3)_x^{2+} + 2NH_4^+ + (4-x)NH_3 \quad (2)$$

This reaction proceeds strongly to the right. If an aqueous solution or aqueous organic solution of ammonia is allowed to percolate through a column of copper silicate gel, the concentration of copper(II) in the effluent is found to be less than 6 μmol l^{-1}; this shows that dissociation of $(\equiv SiO^-)_2Cu(NH_3)_x^{2+}$ is not important. Equilibrium 2 can be described from reaction 1 and from formation of the amminecopper(II) complexes at the surface of the copper silicate gel

$$(\equiv SiO)_2Cu + NH_3 \rightleftharpoons (\equiv SiO)_2CuNH_3 \quad (3)$$

$$(\equiv SiO)_2CuNH_3 + NH_3 \rightleftharpoons (\equiv SiO)_2Cu(NH_3)_2 \quad (4)$$

etc. It does not seem necessary to take into account weak interactions such as the hydrogen bonds. There is always plenty of water in the liquid phase and the silanol groups are likely to be solvated only by water. Then, if it can be proved that x cannot be greater than 2, the problem is reduced to that of determining the constants of reactions 1, 3 and 4.

EXPERIMENTAL

Copper(II) silicate gel was obtained by successive equilibration of a chromatographic silica gel with an ammoniacal solution of copper(II) sulphate. This is best achieved by percolating the latter through a column of silica gel and rinsing afterwards with an aqueous solution of ammonia.

The following experimental observations must be taken into account by a theoretical model. First, the copper silicate gel obtained does not contain sulphur. Therefore, the sulphate anion of the copper salt is not involved in the fixation reaction. The same applies to other anions (nitrate, etc.). Secondly, the quantity of fixed metal increases with the specific surface area: silica gels with specific surface areas of 450—500 m^2 g^{-1} (Kieselgel 60,

Merck) and 600 m^2 g^{-1} (Spherosil XOA600, Prolabo) fix, respectively, 0.65 and 0.85 mmol of copper(II) under the above operating conditions, i.e., there is a quasi-proportionality between the specific surface area and the quantity of fixed copper(II). Thirdly, only a certain fraction of the silanol groups present at the surface of the silica gel participates in the formation of the copper(II) complex. A batch of Kieselgel 60 with a measured specific surface area of 420 m^2 g^{-1} fixes 0.61 mmol of copper(II) per gram of silica. The surface of the silica contains on average 5 silanol groups per nm^2 [12], thus the number of silanol groups per gram of silica is 2.1×10^{21}; if a copper ion is fixed by two silanol groups, then the maximum quantity of fixed copper should be $2.1 \times 10^{21}/(2 \times 6.02 \times 10^{23}) = 1.75$ mmol g^{-1} and only 35% of the silanol groups have reacted with the copper(II). Finally, when the copper silicate gel, obtained as described above, is dehydrated by heating at 120°C for 8 h under atmospheric pressure, the gel retains the blue coloration that characterizes the complexation of copper(II) by ammonia. In order to remove the ammonia from the gel, it is necessary to heat at 180°C under reduced pressure for 12 h. It is only after such treatment that the gel acquires the green coloration characteristic of copper(II) solvated by $\equiv SiO^-$.

Determination of the number of ammonia molecules

Experimental observations show that copper silicate gel has the form of macromolecule containing 65% of $\equiv SiOH$ groups neutralized as $\equiv SiO^-NH_4^+$ and 35% of $(\equiv SiO)_2Cu(NH_3)_x$. The formula should approximate $[\equiv SiO^-NH_4^+]_{0,65} \cdots [(SiO)_2Cu(NH_3)_x]_{0,35}$. However, such formulation unnecessarily complicates the writing of mass-action laws and it is much simpler to consider a model in which the $\equiv SiOH$ and $(\equiv SiO)_2Cu$ sites react independently. Therefore, in a copper silicate gel, the total quantity of ammonia is taken as the sum of the ammonia-complexing copper(II) and the ammonia fixed on the residual silanol groups. To make allowance for the two phenomena, these residual silanol groups are considered to have a reactivity which is very similar to that of the silanol groups on the untreated silica. Thus, in order to obtain the quantity of ammonia fixed by copper(II) on a certain mass of copper(II) silicate gel, 65% of the quantity of ammonia fixed by the same mass of untreated silica is subtracted from the total quantity that has been fixed by the copper(II) silicate gel. In the same way as Bjerrum [13], the molar ratio $[NH_3]/[Cu]$ at the surface of the silica gel is chosen in order to follow the fixation of ammonia.

Procedures. Two procedures were used: a static method by simple equilibration and a dynamic method by percolation through a column. All measurements were made at 20 ± 1°C. These two methods produced concordant results.

For the static method, a sample of silica (2.5 g) was agitated for 15 min with 20 ml of an aqueous solution of ammonia, the initial concentration of which was known; once equilibrium had been attained, the ammonia concentration was determined in the supernatant liquid by acidimetry. For the

dynamic method, a stainless steel column (15 × 0.48 cm) was filled with dry silica (about 1.5 g); then an aqueous solution containing a known concentration of ammonia was percolated through the column. The quantity of fixed ammonia was measured by analyzing the saturation front at the column outlet by a continuous measurement of the pH of the mobile phase. The two procedures were used with both untreated silica and silica treated with amminecopper(II) ions and from which the ammonia had been removed as indicated above.

RESULTS

Figure 1 shows a plot of the molar ratio $[NH_3]/[Cu(II)]$ vs. pNH_3 after subtracting 65% of the values obtained for the same pNH_3 on untreated silica (following the above hypothesis concerning the similar reactivity of silanol groups). The molar ratio is observed to tend towards a value near 2 as the ammonia concentration in the liquid phase increases (several molar). Therefore, two copper coordination sites must form complexes with ammonia and the silica surface may be formulated as

$$\equiv Si-O \diagdown \quad Cu(NH_3)_2(H_2O)_x \quad \diagup O-Si \equiv$$

Similar results were obtained by Ichikawa and Yoshida [14] who used a spin-echo method which demonstrated that copper(II) fixed on silica gel is coordinated only with two moles of ammonia. The similarity of the conclu-

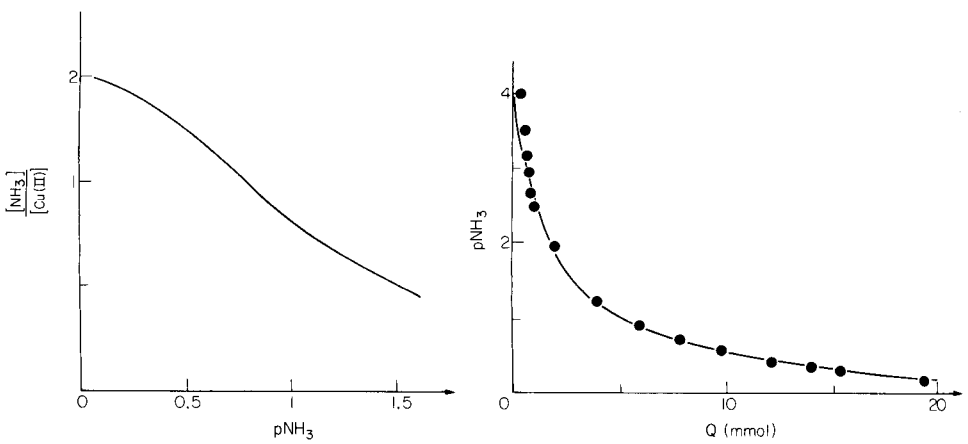

Fig. 1. Variation of the molar ratio $[NH_3]/[Cu(II)]$ in the copper silicate gel as a function of pNH_3 in the solution.

Fig. 2. Simulation of the fixation of ammonia on the copper silicate gel. Curves showing the variation of pNH_3 in solution as a function of the quantity Q of added ammonia. Definitive choice of constants: $\log K = -0.2$, $\log \beta_1 = 2.8$, $\log \beta_2 = 4.0$.

sions drawn from the present chemical measurements and from a physical method accessing the molecular nature of the interactions seems to validate the hypothesis made on the identical reactivity of the silanol groups. It must be noted that Ichikada and Yoshida were not interested in determining equilibrium constants.

Determination of equilibrium constants

The three fundamental equilibria which can be used to describe the complete set of reactions are given by Eqns. 1, 3 and 5

$$(\equiv SiO)_2Cu + 2NH_3 \rightleftharpoons (\equiv SiO)_2Cu(NH_3)_2 \qquad (5)$$

The corresponding mass-action constants are

$$K = [\equiv SiOH]\,[NH_3]\,/[\equiv SiO^-NH_4^+]$$

$$\beta_1 = [(\equiv SiO)_2CuNH_3]\,/[(\equiv SiO)_2Cu]\,[NH_3]$$

$$\beta_2 = [(\equiv SiO)_2Cu(NH_3)_2]\,/[(\equiv SiO)_2Cu]\,[NH_3]^2$$

In these expressions the bracketed quantities refer to concentrations and thus the equilibrium constants are apparent, valid only for the given experimental conditions. In addition, they are two-phase constants: they involve both concentrations in the silica gel [$\equiv$SiOH, $(\equiv SiO)_2Cu$ and $(\equiv SiO)_2Cu(NH_3)_p$] and ammonia concentrations in the liquid phase. However, there is no need to distinguish between the two types of concentration because each of them is involved in only one phase; it is assumed here that the classical laws of chemical equilibria can be applied. To evaluate K, β_1 and β_2, the TOT computer program [15] was applied. Using the classical model employed in solution chemistry and given the concentrations introduced as well as the reaction constants, this program calculates the concentrations of all existing species. Conversely, if one knows the introduced quantities and the experimentally measured concentrations, it allows one to change the reaction constants until satisfactory agreement is gained between calculated and measured concentrations. In this way, one can rapidly determine mass-action constants without the need to use a more complicated regression program which would have to be adapted for each problem.

The first step was to determine the constant K of equilibrium 1 between ammonia and the silanol groups. This value is necessary in order to determine the constants β_1, β_2 of the equilibria 4 and 5. The results obtained for untreated silica were used; the value found was $\log K = -0.2$. The fixation of ammonia on the copper silicate gel was then examined. By the successive approach, the values obtained (at 20°C) were $\log K = -0.2$, $\log \beta_1 = 2.8$ and $\log \beta_2 = 4.0$.

Figure 2, which compares experimental and calculated values for the variation of pNH_3 as a function of the quantity Q of added ammonia, shows good agreement for the chosen equilibrium constants. It is interesting to compare these values with those characterizing the formation of amminecopper(II)

complexes in aqueous solution [13]. At 18°C and in 2 mol l^{-1} ammonium nitrate, $pK_1 = 3.99$, $pK_2 = 3.34$, $pK_3 = 2.73$ and $pK_4 = 1.97$. These values mean that the predominating species are $Cu(NH_3)_4^{2+}$ up to $pNH_3 = 1.97$, $Cu(NH_3)_3^{2+}$ in the pNH_3 range 1.97—2.73, $Cu(NH_3)_2^{2+}$ in the pNH_3 range 2.73—3.34, $Cu(NH_3)^{2+}$ in the pNH_3 range 3.34—3.99, and Cu^{2+} at lower concentrations of ammonia. It may be noted that in the case of copper silicate two coordination sites of copper are saturated by fixation to the silica and the values for the two successive complexes with ammonia must be compared with pK_3 and pK_4. Accordingly, for copper silicate, $\log K_1 = -2.8$ and $\log K_2 = -1.2$ ($\log K_2 = -(\log \beta_2 - \log \beta_1)$) can be compared with $\log K_3 = -2.73$ and $\log K_4 = -1.97$ for the amminecopper(II) complexes. The orders of magnitude are the same.

Distribution diagram

Figure 3 shows the distribution diagram for species present at the surface of copper silicate as a function of pNH_3 in the liquid phase, as given by the TOT program. It can be seen that for the ammonia concentrations classically used in ligand-exchange chromatography, i.e., $pNH_3 < 1$, more than 60% of the copper silicate groups fix two ammonia molecules. Besides the simply neutralized silanol, which is in the ammonium form $\equiv SiO^-NH_4^+$, the preponderant species at the surface is therefore

$$\equiv SiO \diagdown \quad Cu(NH_3)_2(H_2O)_x \quad \diagup OSi\equiv$$

Conclusion

At the surface of a silica gel which has been treated with an ammoniacal solution of copper(II), there exist various species, the most important of which are neutralized silanol groups $\equiv SiO^-NH_4^+$ (about 65%) and for $pNH_3 < 1$

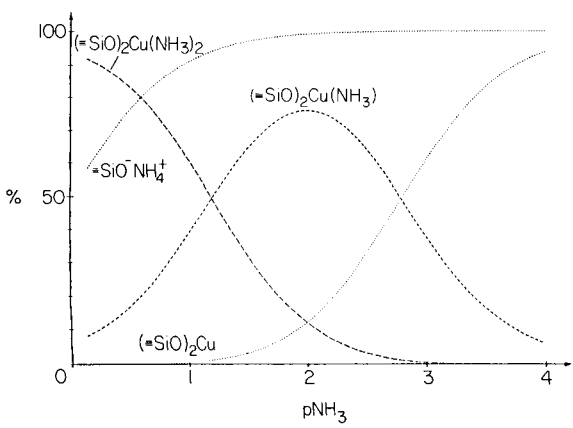

Fig. 3. Distribution diagram for the species present in the silica as a function of pNH_3.

a diamminecopper(II) silicate solvated by some water molecules, $(\equiv SiO)_2Cu(NH_3)_2(H_2O)_x$. This structure provides a good explanation for the various separations that can be achieved with this stationary phase. The separations involve not only ligand exchange but also partition between the mobile phase and the water molecules solvating the silanol groups and the diamminecopper(II) silicate.

REFERENCES

1 M. Caude and A. Foucault, Anal. Chem., 51 (1979) 459.
2 F. Guyon, A. Foucault and M. Caude, J. Chromatogr., 186 (1979) 677.
3 A. Foucault, M. Caude and L. Oliveros, J. Chromatogr., 185 (1979) 345.
4 E. Schmidt, A. Foucault, M. Caude and R. Rosset, Analusis, 7 (1979) 366.
5 F. Guyon, A. Tambute, M. Caude and R. Rosset, J. Chromatogr., 229 (1982) 475.
6 F. Guyon, M. Caude and R. Rosset, Analusis, 12 (1984) 321.
7 G. W. Smith and L. H. Reyerson, J. Am. Chem. Soc., 52 (1930) 2584.
8 I. M. Kolthoff and V. A. Stenger, J. Phys. Chem., 38 (1934) 475.
9 F. Vydra and V. Markova, J. Inorg. Nucl. Chem., 26 (1964) 1319.
10 K. K. Unger and F. Vydra, J. Inorg. Nucl. Chem., 30 (1968) 1075.
11 P. Schindler and H. R. Kamber, Helv. Chim. Acta, 51 (1968) 1781.
12 R. K. Iler, The Chemistry of Silica, Wiley, New York, 1979.
13 J. Bjerrum, Metal Ammine Formation in Aqueous Solution, P. Haase, Copenhagen, 1957.
14 T. Ichikawa and H. Yoshida, J. Chem. Phys., 75 (1981) 2485.
15 R. Rosset, D. Bauer and J. Desbarres, Chimie Analytique des Solutions et Microinformatique, Masson, Paris, 1979.

Analytica Chimica Acta, 170 (1985) 319—324
Elsevier Science Publishers B.V., Amsterdam — Printed in The Netherlands

KOMPLEXBILDUNG UND EXTRAKTION VON ZINN MIT POTENTIELL DREIZÄHNIGEN DIANIONISCHEN LIGANDEN

E. UHLEMANN* und H. REICHMANN

Pädagogische Hochschule "Karl Liebknecht", DDR-1500 Potsdam (Deutsche Demokratische Republik)

H. MEHNER

Akademie der Wissenschaften der DDR, Zentralinstitut für Physikalische Chemie, DDR-1199 Berlin-Adlershof (Deutsche Demokratische Republik)

(Eingegangen den 20. August 1984)

SUMMARY

(Complex formation and liquid-liquid extraction of tin with potentially tridentate dianionic ligands.)

Pulse polarography was used to study the extraction of tin(IV) from chloride solution with potentially tridentate dianionic ligands under unbuffered conditions. The ligands usually contained enolizable groups or were produced by splitting heterocyclic rings. The most favourable extractant was 2-(2'-hydroxyphenyl)-quinolin-8-ol, which extracted tin in the pH region 2—8; all other ligands gave good extraction only at pH 6—8. In the organic phase, 1:1 chelates are formed in all cases. The composition of the complexes was also proved by the isolation of the solid compounds. These complexes were characterized by their Mössbauer parameters.

ZUSAMMENFASSUNG

Mit Hilfe der Rechteckwellenpolarographie wurde die Extraktion von Zinn(IV) aus Chloridlösung mit potentiell dreizähnigen dianionischen Liganden im ungepufferten Milieu untersucht. Die Liganden enthielten meist enolisierbare Gruppen oder wurden durch Spaltung heterocyclischer Ringe gebildet. Als günstigstes Extraktionsmittel erwies sich 2-(2'-Hydroxyphenyl)-chinolin-8-ol, welches Zinn im pH-Bereich von 2—8 extrahiert, während alle anderen Liganden gute Ergebnisse nur bei pH 6—8 zeigten. In der organischen Phase liegen in allen Fällen 1:1-Chelate vor. Die Komplexzusammensetzung wurde auch durch Isolierung von Verbindungen im festen Zustand überprüft. Die Charakterisierung der Komplexe erfolgte durch die Mössbauer-Parameter.

Als günstiges Extraktionsmittel und photometrisches Reagens für Zinn hat sich Salicyliden-*o*-aminothiophenol erwiesen [1—3]. Die relativ gute Beständigkeit dieser Verbindung erklärt sich aus der Tatsache, daß im Ausgangszustand *o*-Hydroxyphenylbenzthiazolin (1) vorliegt [4], welches erst mit anwesenden Metallionen oder durch Spaltung mit Alkali zu Verbindungen der dreizähnigen Schiffschen Base reagiert [4, 5]. Mit Zinn bildet sich in jedem Falle ein Zinn(IV)-Neutral chelat [2, 6]; eingesetztes Zinn(II) unterliegt

0003-2670/85/$03.30

einer spontanen Oxydation. Nach diesen Befunden erschien es zweckmäßig, weitere potentiell dreizähnige dianionische Liganden auf ihr Komplexbildungs-und Extraktionsvermögen gegenüber Zinn zu untersuchen. Dafür wurden die folgenden Liganden ausgewählt: 2′-Hydroxyphenylpicolin-2-ylketon 2 [7], 2-(2′-Hydroxyphenyl)-chinolin-8-ol 3 [8], *N*-(Pyrid-2-yl)-2-

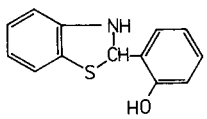

1

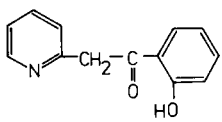

2

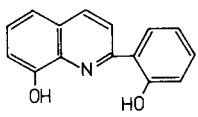

3

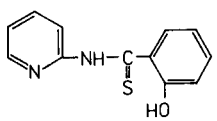

4

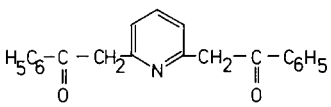

5

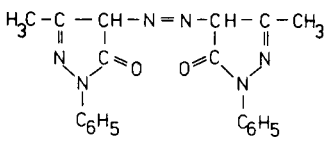

6

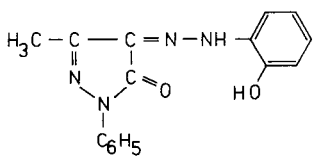

7

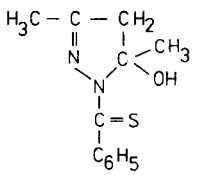

8

hydroxythiobenzamid 4, 2,6-Diphenacylpyridin 5 [9], 3,3′-Dimethyl-1,1′-diphenyl-4,4′-azopyrazol-5-on 6 [10], 1-Phenyl-3-methyl-4-[2′-hydroxyphenyl]hydrazonopyrazol-5-on 7 und 1-Thiobenzoyl-3,5-dimethyl-5-hydroxypyrazol 8. Alle Liganden enthalten enolisierungsfähige Gruppen oder leicht spaltbare Ringsysteme (1, 8).

EXPERIMENTELLES

Extraktionsmittel und Extraktionsuntersuchungen

Die benötigten Liganden wurden nach Literaturangaben dargestellt und kamen als chloroformische $2{,}5 \cdot 10^{-3}$ M Lösung zum Einsatz. Als Zinn(IV)-Standardlösung diente $5 \cdot 10^{-5}$ M $(NH_4)_2SnCl_6$-Lösung, die 5 M an Salzsäure war. Als wäßrige Phase wurden 10 ml Zinn(IV)-Standardlösung vorgelegt, mit 10 ml 5 M KOH neutralisiert und der pH-Wert durch Zugabe kleiner Portionen 0,01 M, 0,1 M oder 1 M KOH bzw. 0,1 M oder 1 M HCl variiert. Die Extraktionsuntersuchungen erfolgten mit jeweils 15 ml dieser Lösung. Das Volumen der organischen Phase betrug ebenfalls 15 ml, so daß ein hundertfacher Überschuß an Extraktionsmittel gegeben war. Nach der

Phasentrennung wurde der pH-Wert unter Verwendung des pH-Meßgerätes MV 84 (VEB Präcitronic Dresden) mit dem Elektrodensystem GA 50 N und SE 20 vermessen.

Die Bestimmung des Zinngehaltes erfolgte in 10 ml der wäßrigen Phase mit Hilfe der Rechteckwellenpolarographie am Polarographen OH-104 (Radelkis, Budapest). Als Meßzelle diente die polarographische Zelle nach Berg (VEB Jenaer Glaswerk Schott und Gen.) mit Quecksilbertropfelektrode (Durchmesser 0,05 nm, Tropfzeit 2,1 s pro Tropfen). Die gewählte Empfindlichkeit betrug $30 \cdot 10^{-9}$ A T s^{-1}, die Rechteckwellenamplitude 20 mV und der Ohmsche Widerstand der Apparatur $\gtrdot 100\Omega$. Der Grundelektrolyt war 5 M an KCl. Die Meßproben wurden zur Entfernung von Sauerstoff 5 min mit Reinststickstoff gespült und bei 25° C untersucht.

Darstellung von Zinnchelaten

Methode A. $SnCl_2 \cdot H_2O$ (1,04 g; 0,005 mol) werden in 50 ml konzentrierter Essigsäure gelöst und langsam zu einer siedenden Lösung von 0,01 mol des jeweiligen Liganden in 100 ml Methanol gegeben. Die Lösung läßt man bis zur Kristallisation am Sieden, saugt dann noch heiß ab und wäscht mit warmem Methanol. Ölig anfallende Verbindungen werden nach Verreiben mit Ether kristallin.

Methode B. Natriumisopropanolat (1,31 g; 0,016 mol) werden in 100 ml wasserfreiem Benzen gelöst und mit 0,08 mol des jeweiligen Liganden 2 h am Rückfluß erhitzt. Dann tropft man 1,04 g (0,004 mol) $SnCl_4$ zu und läßt weitere 2 h sieden. Das gebildete NaCl wird abgesaugt, das Lösungsmittel im Vakuum entfernt und der zurückbleibende Zinnkomplex mit heißem Wasser gewaschen.

Mössbauer-Spektren. Die Mössbauer-Spektren wurden bei der Temperatur von flüssigem Stickstoff aufgenommen. Als Strahlungsquelle diente $^{119}CaSnO_3$, die Isomerieverschiebung wurde gegen SnO_2 vermessen. Die Spektren wurden mit Hilfe eines Computers simuliert.

ERGEBNISSE UND DISKUSSION

Extraktionsuntersuchungen

Zur Untersuchung von Extraktionsgleichgewichten des Zinns erwies sich die Rechteckwellenpolarographie als gut geeignet. Jedoch mußte auf Zusatz von Puffersubstanzen verzichtet und die Anwesenheit einer genügend hohen Chloridkonzentration gewährleistet werden.

Die Zeitabhängigkeit der Extraktion wurde im Bereich des pH-Wertes hälftiger Extraktion bestimmt. Für ausgewählte Liganden sind die Verhältnisse in Abb. 1. dargestellt. In den meisten Fällen sind zur Einstellung des Extraktionsgleichgewichtes 20 min ausreichend, lediglich bei *N*-(Pyrid-2-yl)-2′-hydroxythiobenzamid und 2-(2′-Hydroxyphenyl)-chinolin-8-ol werden Schüttelzeiten von 90 bzw. 120 min benötigt. Die Untersuchung der pH-Abhängigkeit der Extraktion ergab nur geringfügige Unterschiede zwischen

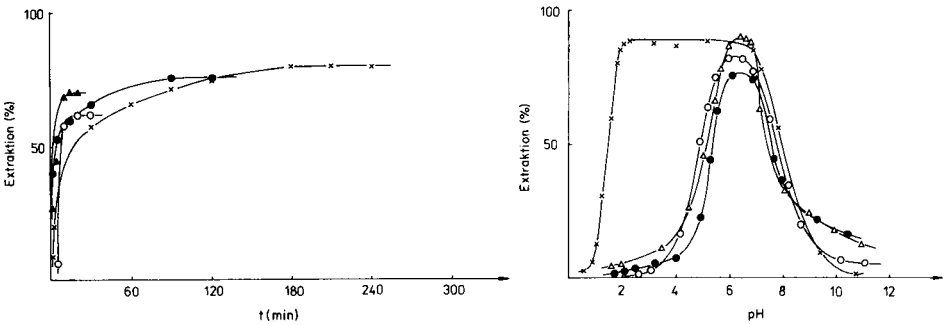

Abb. 1. Zeitabhängigkeit der Extraktion von Zinn(IV): (•) *N*-(Pyrid-2-yl)-2′-hydroxythiobenzamid; (×) 2-(2′-Hydroxyphenyl)-chinolin-8-ol; (○) 2′-Hydroxyphenylpicolin-2-yl-keton; (▲) 2,6-Diphenacylpyridin.

Abb. 2. pH-Abhängigkeit der Extraktion von Zinn(IV): (×) 2-(2′-Hydroxyphenyl)-chinolin-8-ol; (○) 2′-Hydroxyphenylpicolin-2-yl-keton; (△) 2-(2′-Hydroxyphenyl)-benzthiazolin; (•) *N*-(Pyrid-2-yl)-2′-hydroxythiobenzamid.

den untersuchten Extraktionsmitteln. Einige charakteristischen Angaben enthält Tabelle 1. Maximale Extraktion des Zinns erfolgte im pH-Bereich von 5,5 bis 7,5. Eine Ausnahme bildet lediglich 2-(2′-Hydroxyphenyl)-chinolin-8-ol, das bereits bei pH 2 maximale Extraktionsausbeuten erreicht und wie die anderen Liganden erst oberhalb pH 8 einen Rückgang der Extraktion zeigt. Einige typische Extraktionskurven sind in Abb. 2 wiedergegeben.

Zur Ermittlung der Komplexzusammensetzung wurde die Abhängigkeit der log *D*-Werte von pH-Wert und Logarithmus der Ligandkonzentration bestimmt. Die Ergebnisse enthalten die Abb. 3 und 4. Aus der Abhängigkeit der Verteilung von der Ligandkonzentration folgt in allen Fällen das Vorliegen von 1:1-Komplexen in der organischen Phase. Ein ähnliches Bild liefert die pH-Abhängigkeit von log *D*. In fast allen Fällen ist auf die Freisetzung eines Protons bei der Komplexbildung zu schließen. Demnach betätigen sich diese Liganden bei der Extraktion von Zinn(IV) als zweizähnig. Eine Ausnahme bildet auch hier wieder 2-(2′-Hydroxyphenyl)-chinolin-8-ol, welches bei der Komplexbildung zwei Protonen abgibt und somit dreizähnig reagiert. Jedoch vermag auch dieser Ligand nicht alle am Zinn gebundenen Chloridionen zu substituieren, so daß im Extrakt immer Gemischtligandkomplexe vorliegen.

Darstellung von Zinn(IV)-Komplexen

Die durch Extraktion erhaltenen Ergebnisse wurden durch Darstellung einiger Zinn(IV)-Komplexe in Substanz überprüft (vgl. Tab. 1). Die Synthese erfolgte auf zwei unterschiedlichen Wegen, einmal durch Umsetzung der Liganden mit Zinn(II)-chlorid in essigsaurer Lösung [5], zum anderen durch Reaktion mit Zinn(IV)-chlorid in Gegenwart von Natriumisopropanolat [11]. Identische Ergebnisse wurden nur mit 2-Hydroxyphenyl-chinolin-8-ol erhalten. Auch bei Einsatz von Zinn(II)-chlorid wurde hier stets das chloridfreie

TABELLE 1

Kenngrößen der Zinnextraktion ($c_M = 2{,}5 \cdot 10^{-5}$ mol l^{-1}, $c_{Ligand} = 2{,}5 \cdot 10^{-3}$ mol l^{-1})

Ligand	$pH_{0,5}$	R_{max} (%)	pH (R_{max})
1	5,2	91	6,5
2	4,9	82	6,0
3	1,5	89	2,3
4	5,3	77	6,2
5	5,1	89	6,6
6	4,6	93	6,2
7	5,2	79	6,9
8	4,7	85	6,3

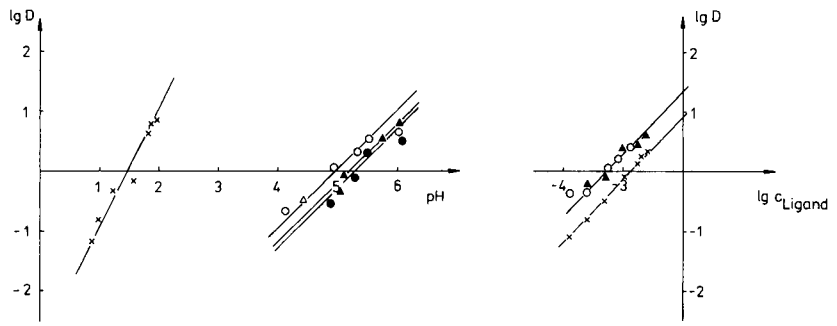

Abb. 3. Log D/pH-Darstellung der Extraktion von Zinn(IV): (×) 2-(2'-Hydroxyphenyl)-chinolin-8-ol; (○) 2'-Hydroxyphenylpicolin-2-yl-keton; (▲) 2-(2'-Hydroxyphenyl)-benzthiazolin; (●) *N*-(Pyrid-2-yl)-2'-hydroxythiobenzamid.

Abb. 4. Abhängigkeit der Zinnextraktion von der Ligandkonzentration: (×) 2-(2'-Hydroxyphenyl)-chinolin-8-ol; (○) 2'-Hydroxyphenylpicolin-2-yl-keton; (▲) 2,6-Diphenacylpyridin.

Zinn(IV)-chelat mit oktaedrischer Struktur isoliert. Bei den anderen Liganden verlief die Oxydation des Zinn(II) nicht quantitativ, und die von Methode A gewonnenen Produkte enthielten nach Auswertung ihrer Mössbauer-Spektren noch ca. ein Drittel der Zinn(II)-Verbindung. Ein typisches Mössbauerspektrum ist in Abb. 5 dargestellt, für alle untersuchten Verbindungen sind die Mössbauerparameter in Tabelle 2 zusammengefaßt. Eindeutige Zinn(IV)-Verbindungen sind nach Methode B darstellbar. Dabei vermögen die Liganden aber nicht alle Koordinationsstellen des Zinns zu besetzen, es bilden sich Dichloro-bis(ligand)-Zinn(IV)-Verbindungen mit oktaedrischer Struktur, in denen koordiniertes Chlorid relativ fest gebunden ist. Die Liganden betätigen sich dabei lediglich als zweizähnig. Im Falle des Komplexes mit 2,6-Diphenacylpyridin wird dies zusätzlich am Auftreten der ungestörten ν(CO)-Bande bei 1680 cm^{-1} sichtbar.

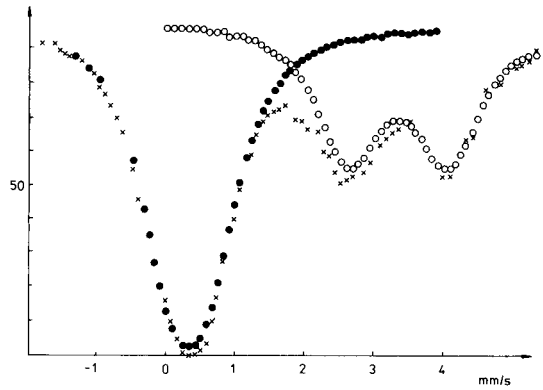

Abb. 5. Mössbauerspektren der Sn(II)- und Sn(IV)-Chelate mit 2'-Hydroxyphenyl-picolin-2-yl-keton: (○) berechnete Punkte für Sn(II); (●) berechnete Punkte für Sn(IV); (×) Meßpunkte.

TABELLE 2

Eigenschaften synthetisierter Zinn(IV)-Chelate

Ligand	Komplex	Schmelztemperatur (°C)	Analyse [% ber. (gef.)]			Mössbauer-Daten		
			N	Sn	Cl	δ (mm s^{-1})	Δ_Q (mm s^{-1})	Γ (mm s^{-1})
2	SnL_2Cl_2	259—60	4,56 (3,81)	19,32 (17,80)	11,54 (10,52)	0,27	0,51	1,19
3	SnL_2	>360	4,75 (4,50)	20,14 (19,03)	—[a]	0,32	0,33	1,08
5	SnL_2Cl_2	130	3,42 (3,10)	14,50 (14,00)	8,66 (8,50)	0,32	0,36	1,09

[a]61,15(60,00) %C; 3,08(3,08) %H.

LITERATUR

1 G. R. E.C. Gregory und P. G. Jeffery, Analyst (London), 92 (1967) 293.
2 E. Uhlemann und V. Pohl, Anal. Chim. Acta, 65 (1973) 319.
3 H. Imuro und M. Suzuki, Anal. Chim. Acta, 118 (1980) 129; Talanta, 28 (1981) 73.
4 F. J. Goetz, J. Heterocycl. Chem., 4 (1967) 80; 5 (1968) 509.
5 E. Uhlemann und V. Pohl, Z. Chem., 9 (1969) 385; Z. Anorg. Allg. Chem., 397 (1973) 162.
6 H. Schnorr, V. Pohl, E. Uhlemann und Ph. Thomas, Z. Chem., 13 (1973) 143.
7 E. Uhlemann, H. Reichmann, R. Stößer und H. Köppel, Z. Chem., 24 (1984) 140.
8 A. Corsini und R. M. Cassidy, Talanta, 21 (1974) 273.
9 G. Scheuing und L. Winterhalder, Liebigs Ann. Chem., 473 (1929) 123.
10 W. Pelz, D.B.P. (patent of BRD) 1 090 354 (1961).
11 B. P. Bachlas, H. Sharma, J. C. Maire und J. J. Zuckermann, Inorg. Chim. Acta, 71 (1983) 227.

Analytica Chimica Acta, 170 (1985) 325—329
Elsevier Science Publishers B.V., Amsterdam — Printed in The Netherlands

Short Communication

THE DETERMINATION OF GOLD IN VEGETATION BY ELECTROTHERMAL ATOMIC ABSORPTION SPECTROMETRY

ROBERT R. BROOKS* and SHAMILA D. NAIDU

Department of Chemistry, Biochemistry and Biophysics, Massey University, Palmerston North (New Zealand)

(Received 6th August 1984)

Summary. A method is described for determining nanogram quantities of gold in vegetation. The sample is digested with fuming nitric acid. After addition of hydrochloric acid, the gold is extracted into 1 ml of 4-methylpentan-2-one; the organic layer is back-extracted with distilled water to remove iron interference, and gold in the organic layer is determined by electrothermal (graphite furnace) atomic absorption spectrometry. Limits of detection depend on the volume of organic phase used but can be as low as 0.2 ng g^{-1} for an original sample weight of 1 g.

Determination of gold in vegetation has been receiving increasing attention in recent years because of heightened interest in biogeochemical prospecting for this element [1, 2]. Since Lungwitz [3] first reported in 1900 that the gold content of vegetation might indicate mineralization in the substrate, many attempts have been made to quantify gold in vegetation. One of the earlier attempts was a wet chemical technique [4] in which sulphides were precipitated from a solution of the plant material (*Equisetum* sp., horsetails), were weighed and were assumed to be all gold sulphides. These workers reported a staggering 610 $\mu g\ g^{-1}$ in the ash of *Equisetum palustre* and gave to horsetails a totally undeserved reputation of being "gold accumulators". A later paper [5] pointed out that horsetails do not accumulate gold and that the sulphides previously precipitated were in fact mainly arsenic.

Another technique which has been used for quantifying gold in vegetation involves fire-assay procedures [3, 6] in which at least 10 g of plant ash was used as the starting material. The large sample size, slowness and poor sensitivity of this method have been a disadvantage.

By far the commonest technique used for determining gold is neutron activation analysis [7]. The vegetation is powdered, pelleted, irradiated with neutrons and counted after an appropriate cooling period. Apart from the cost, another problem is interference from arsenic which usually has a concentration in plant material at least 1000 times higher than gold; the energy peak at 559.1 keV for arsenic-76 is close to that of gold-198 at 411.8 keV.

Because of the renewed interest in gold determinations in vegetation, there is clearly a need for a rapid, inexpensive and simple technique for

0003-2670/85/$03.30

determining gold at the ng g^{-1} range in vegetation. For this purpose, the potential of extraction coupled with electrothermal atomic absorption spectrometry is of obvious application. Virtually no work has been done on vegetation, however, although rocks [8] and waters [9] have been analysed for gold by various modifications of this procedure. As far as is known, the only analogous procedure is by Baker [10] in which gold is extracted from hydrochloric acid solutions of vegetation into 4-methylpentan-2-one (MIBK); a limit of detection of 5 ng g^{-1} was reported.

The paucity of methods for quantifying gold by electrothermal atomic absorption spectrometry is due, at least partly, to the very real problems involved in the dissolution of the sample with mineral acids and the concomitant problem of interference from co-extracted iron. A recently developed method for determining gold at levels down to 0.2 ng g^{-1} is reported here. The method involves dissolution of gold from vegetation by attack with an oxidizing acid mixture, extraction of gold as the tetrachloro complex, $HAuCl_4$, into MIBK and quantification of gold in the organic phase by electrothermal atomic absorption spectrometry. By extracting the gold from about 20 ml of aqueous phase into as little as 0.2 ml of MIBK, an initial enrichment by a factor of about 100 is achieved.

Experimental

Apparatus. Electrothermal atomization was done with a Varian-Techtron Model 63 carbon rod atomizer in the graphite tube option (graphite furnace). The spectrometer was a Varian-Techtron AA5 model with automatic background correction provided by a deuterium lamp.

Recommended procedure. Digest a 1-g sample of finely ground plant material (leaves, stalks, twigs, bark or wood) with 10 ml of fuming nitric acid in a 50-ml borosilicate squat beaker warmed gently over a water bath. After dissolution is virtually complete (ca. 5 min), add 8 ml of concentrated hydrochloric acid and a little bromine vapour. Reduce the volume to about 3 ml over the water bath, transfer to a 20-ml glass centrifuge tube and adjust the volume to 5 ml with 6 M hydrochloric acid. Dilute to 15 ml with distilled water to give an acid strength of about 2 M. Add 1 ml of MIBK, stopper, and shake for 2 min. Allow to settle and remove most of the aqueous layer with a bulb pipette leaving about 4 ml behind. Dilute again to 15 ml with distilled water, stopper and shake for a second time for about 2 min. The MIBK layer is often cloudy after the second shaking and the sample is then centrifuged for about 1 min. After both equilibrations, the organic layer is reduced in volume from 1.0 to 0.55 ml.

Appropriate aliquots (10 μl here) are then introduced to the graphite furnace. The instrumental settings used for the Model 63 carbon rod atomizer were: drying cycle, 3.5 V for 30 s (ca. 120° C); ashing cycle, 6.0 V for 15 s (ca. 400° C); atomizing cycle: 8.0 V for 2 s (2000° C).

Standards and blanks are treated throughout in the same manner as the samples.

Development of the method

In selecting the appropriate volume of MIBK to use to extract gold from solution, consideration must be given to the solubility of the organic solvent at different acidities. The volume of MIBK selected must be sufficient to allow for its dissolution into the aqueous phase while still leaving sufficient for the extraction process to occur. Figure 1 shows the solubility of MIBK in various concentrations of hydrochloric acid. The values were obtained by shaking equal volumes of organic and aqueous phases together in a burette sealed at both ends and measuring the final volumes at equilibrium.

Reducing the volume of MIBK added to 20 ml of hydrochloric acid (2 M) containing nanogram quantities of gold has the effect of increasing the sensitivity of the method. This is illustrated in Fig. 2. It has been shown [9] that gold has a distribution ratio of about 2000 between 2 M hydrochloric acid and MIBK. If this value is used, 98% of the gold is extracted when 1.0 ml of MIBK is added to 20 ml of aqueous phase and the final volume of the organic phase reduces to 0.7 ml. Though sensitivity is increased by a factor of 20 when 0.4 ml of MIBK is used (0.1 ml remains as organic phase),

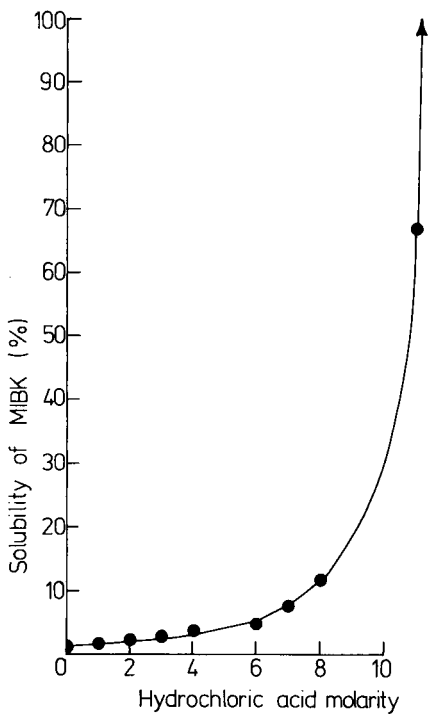

Fig. 1. Solubility of MIBK in hydrochloric acid solutions.

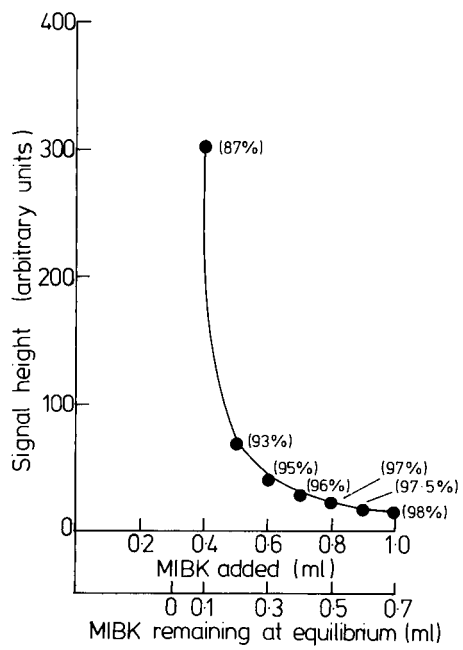

Fig. 2. Gold signal as a function of volume of MIBK added to 20 ml of 2 M hydrochloric acid. Values in parentheses refer to total extraction of gold from the aqueous phase.

the resultant volume (extracting 87% of the gold) is so small that there are problems of its removal for introduction into the graphite furnace. Even if this can be achieved in a reproducible manner, results can still be somewhat erratic because of the irreproducibility of final volumes as small as 0.1 ml. In practice, it was found that addition of 1 ml of MIBK gave satisfactory results and a limit of detection of 1 ng g^{-1} gold for an original sample mass of 1 g. The detection limit was reduced to 0.2 ng g^{-1} when 0.5 ml of MIBK was used.

The stability of the tetraaurate complex in MIBK was tested by extracting 1 μg of gold from 150 ml of 2 M hydrochloric acid into 10 ml of MIBK. The absorption signal was measured at 5 intervals over a period of 17 days; there was no detectable loss of gold during this period.

The volatility of gold(III) chloride. Gold (5 ng) as gold(III) chloride was absorbed on each of six 0.5-g samples of silica. The samples were dried, and heated for 1 h at a different temperature (100, 200, 300, 400, 500 and 600° C) for each sample. The gold was then leached from the silica with aqua regia. The solutions were taken almost to dryness and were diluted with 20 ml of 2 M hydrochloric acid. The gold was extracted into 1.0 ml of MIBK and quantified as above. The results are shown in Fig. 3 from which it will be noted that appreciable loss of gold occurred above 300° C.

Dissolution of gold from vegetation samples. By far the greatest problem in the determination of nanogram quantities of gold in vegetation lies in destruction of the organic matter and subsequent dissolution of the gold without loss by volatilization. A further problem is the concomitant extraction of iron into the organic layer which causes major interference with the

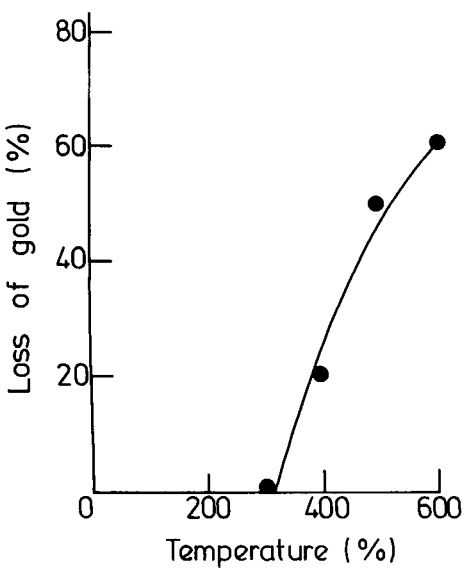

Fig. 3. Loss of gold trichloride on heating.

gold signal. This latter problem was overcome by back-extracting the iron(III) into ca. 0.5 M hydrochloric acid as described in the recommended procedure.

With most oxidizing acid mixtures commonly employed for destroying organic matter, gold is readily lost by volatilization at temperatures exceeding 100°C, particularly with the 1:4 perchloric/nitric acid mixtures commonly used. Experiments showed that virtually all the gold was removed by this procedure. Similarly, concentrated nitric, fuming nitric, and nitric/sulphuric acid mixtures gave incomplete recoveries at temperatures above 100°C. A mixture of fuming nitric acid and aqua regia (the latter formed by adding hydrochloric to the nitric acid after oxidation is nearly complete) was found to give full recovery of gold if the operations were conducted in glassware heated over a water bath. It is noteworthy that polypropylene beakers gave a significant gold blank when used for these digestions.

Limit of detection, precision and accuracy

The limits of detection were about 1 ng for 1.0 ml of MIBK and about 0.2 ng for 0.5 ml of organic phase. The relative standard deviation for ten replicate extractions of gold from a sample of powdered wood containing about 170 ng g^{-1} gold was 10.1%. For lower concentrations, the precision would probably be about 25% at the 5 ng g^{-1} level.

It was difficult to establish the accuracy of the technique because of the virtual complete absence of vegetation standards in which gold has been determined. However, a value of 1.8 ± 1 ng g^{-1} gold was obtained by Gladney [11] for the NBS standard Orchard Leaves. These values were obtained by neutron activation analysis and were for six replicate analyses of the material. Values of 4.0 and 4.5 ± 1 ng g^{-1} gold were obtained here for two samples of this material when the proposed method was used. This is in reasonable agreement with the data of Gladney if consideration is taken of the extremely low concentrations involved.

REFERENCES

1 R. R. Brooks, Biological Methods of Prospecting for Minerals, Wiley, New York, 1983.
2 R. R. Brooks, J. Geochem. Explor., 17 (1982) 109.
3 E. E. Lungwitz, Eng. Min. J., 69 (1900) 500.
4 B. Nemec, J. Babička and A. Oborsky, Bull. Int. Acad. Sci. Bohême, 1 (1936) 1.
5 R. R. Brooks, J. Holzbecher and D. E. Ryan, J. Geochem. Explor., 16 (1981) 24.
6 H. V. Warren and R. E. Delavault, Bull. Geol. Soc. Am., 61 (1950) 123.
7 C. A. Girling, P. J. Peterson and M. J. Minski, Sci. Total Environ., 10 (1978) 79.
8 R. R. Brooks, A. K. Chatterjee, P. K. Smith, D. E. Ryan and H. F. Zhang, Chem. Geol., 35 (1982) 87.
9 R. R. Brooks, A. K. Chatterjee and D. E. Ryan, Chem. Geol., 33 (1981) 163.
10 W. E. Baker, Coll. Org. Matter Biol. Syst. Min. Explor., UCLA, Feb. 1983, Abs. p. 8.
11 E. S. Gladney, Anal. Chim. Acta, 118 (1980) 385.

Analytica Chimica Acta, 170 (1985) 331—336
Elsevier Science Publishers B.V., Amsterdam — Printed in The Netherlands

Short Communication

DETERMINATION OF SOME PHOSPHORUS-CONTAINING COMPOUNDS BY FLOW INJECTION WITH A MOLECULAR EMISSION CAVITY DETECTOR

J. L. BURGUERA and M. BURGUERA*

Departamento de Química, Facultad de Ciencias, Universidad de Los Andes, Apartado Postal 542, Mérida 5101-A (Venezuela)

DANIEL FLORES

Instituto de Zoología Tropical, Facultad de Ciencias, Universidad Central de Venezuela, Caracas (Venezuela)

(Received 20th August 1984)

Summary. The use of molecular emission cavity analysis combined with a flow-injection system for the determination of nanogram amounts of some organophosphorus compounds and phosphorus oxo-anions is described. Sensitivity, calibration linearity, precision and detection limits were measured for each compound. Simultaneous determinations of some ternary mixtures of these compounds are also described. Sample throughput is 20 h^{-1}.

Several workers have described the determination of phosphorus by flow injection analysis (f.i.a.) based on spectrophotometric detection [1—5]. Their approaches differ slightly but all are based on the formation of coloured species such as yellow 12-molybdophosphate or molybdenum blue. The lowest limit of detection reported is 50 ng P ml^{-1} as phosphate [4]. Total recoveries of 99.1% P have readily been achieved [3], and the sample rate is always ca. 120 samples h^{-1} [1—5]. The different systems have been employed to assay plant digests [1, 2], serum [6], fertilizers [7] and soil extracts [3, 5].

Recent flame photometric methods for the determination of phosphorus rely on the measurement of a band emission at 528 nm derived from HPO molecules which form in a cool, hydrogen-rich flame. In this manner, sub-nanogram amounts of inorganic and organic phosphorus-containing compounds have been determined by aspiration of their liquid samples into the flame [8—12]. The HPO emission has also been detected by molecular emission cavity analysis (m.e.c.a.) [13] in a hydrogen/nitrogen/air flame, the detection limit for phosphoric acid being 10 μg P ml^{-1}. Belcher et al. [15] determined simultaneously some binary mixtures of organophosphorus compounds (e.g., trimethyl phosphate and triphenyl phosphate) by the resolution of their m.e.c.a. peaks. Their mixture was resolved on the basis of their t_m values (the time elapsed from flame ignition to maximal emission).

0003-2670/85/$03.30

Flow injection analysis (f.i.a.) has recently been used in conjunction with m.e.c.a. for the determination of sulphur anions such as sulphide, sulphite and sulphate [16]. The main advantages of the method are considered to be good sensitivity, high sampling rate (100 h^{-1}), good reproducibility (3% relative standard deviation), discrimination between different sulphur anions, and continuous monitoring the chemiluminescence emission without the need to cool the cavity between sample injections.

This communication deals with the advantages of a m.e.c.a./f.i.a. system for determining nanogram amounts of some organophosphorus and inorganic phosphorus compounds. In addition, mixtures of these compounds may be determined based on the temporal resolution of their emission peaks.

Experimental

The instrumental assembly used has been described [16]. The cavities were made from brass, and are described below.

All reagents used were of analytical grade. Deionized, double-distilled water was used throughout. Preliminary tests and optimization of the experimental parameters were done with 50 ng P as orthophosphoric acid. Solutions of organophosphorus compounds were prepared in ethanol/water (1:20 v/v).

General procedure. The sample was injected into a carrier stream of water via a rotary valve (Rheodyne, model 7125) to which a loop of suitable volume was attached. The cavity was permanently situated within the flame, and the sample was introduced into it with the carrier stream. After sample introduction, the chemiluminescence emission of HPO was measured at 528 nm against time. All emission values were based on peak-height measurements.

Results and discussion

Optimization of analytical parameters. The effects of flow rate, sample volume, length and diameter of the tubing, flame composition, etc. were investigated. The highest emission peaks with least tailing were obtained under the conditions listed in Table 1. Typical calibration peaks are shown in Fig. 1.

The effect of sample volume on the signal is shown in Fig. 2A. The sensitivity increased with increasing sample volume. The injection of volumes smaller than 4 μl into the carrier stream gave lower and irreproducible results, but the injection of volumes larger than 7 μl led to less intense, multi-peaked signals. Greatest sensitivity and reproducibility were achieved by injecting 5 μl of sample. When the length of tubing was changed within the range 10—15 cm, it was found that a similar signal was obtained with 10- and 15-cm lengths when 5-μl samples were injected (Fig. 2B). When the tubing length was decreased to 8 or 7 cm, the reproducibility and sensitivity deteriorated slightly. Lengths >20 cm gave lower, irreproducible, multi-peaked signals.

When the carrier solution flow rate was decreased from 0.16 to 0.12 ml min^{-1}, the signal decreased (by 15%) and broadened (Fig. 3A) and the

TABLE 1

Optimal parameters used in the m.e.c.a./f.i.a. system for the determination of phosphorus-containing compounds

M.e.c.a.		F.i.a.	
Wavelength (nm)	528	Sample volume (μl)	5
Slit width (nm)	1.0	Carrier flow rate (ml min^{-1})	0.16
Cavity at flame center		Tubing: length[a] (cm)	15
Burner diam. (cm)	1.5	i.d. (mm)	0.75
Cavity angle below horizontal	2.5°		
Flame: H_2 (l min^{-1})	1.6		
N_2 (l min^{-1})	5.5		
Water-cooling flow rate (ml min^{-1})	350		

[a]Distance between sample injection point and the m.e.c.a. cavity.

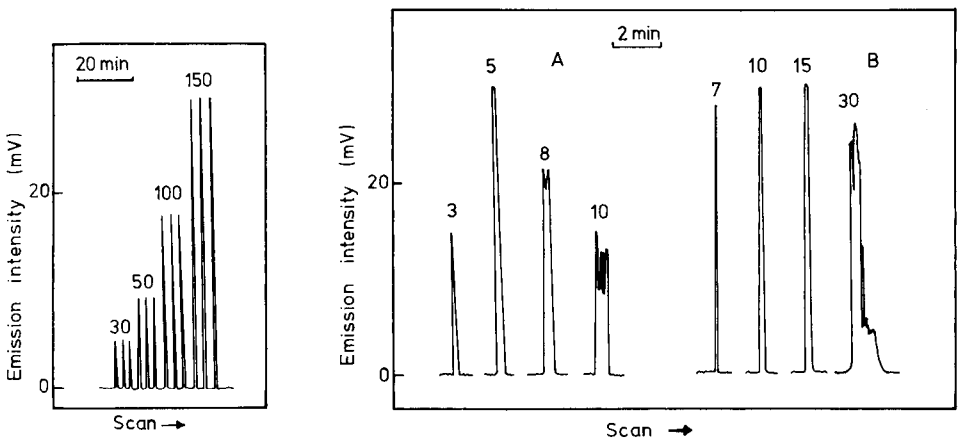

Fig. 1. Continuous recording of signals obtained by injecting triplicate phosphate standards under the optimal conditions. (Numbers represent ng of P.)

Fig. 2. Effects of sample volume (A) and length of tubing (B) on responses for 50 ng P as phosphate. Numbers on the peaks represent: (A) sample volume injected in μl; (B) tubing length in cm. Conditions otherwise as in Table 1.

maximum sampling rate decreased from 20 to 15 h^{-1}. When the flow rate was >0.18 ml min^{-1}, lower irreproducible multi-peaked responses were obtained, as were obtained previously [16]. At low flow rates, the sample zone became less diluted but stayed in the analytical line for a longer period; at $\geqslant$0.20 ml min^{-1}, the cavity flooded, the unvaporized liquid sputtered and no emission was obtained. A flow rate of 0.16 ml min^{-1} was a good compromise between the rate at which the carrier stream reaches the cavity and the rate of solvent evaporation from it, minimizing solvent effects on generation of emission within the cavity.

The effect of using tubing of different internal diameters was investigated; each tube was connected to a different cavity with a hole drilled on its wall of the same diameter as the tubing [16]. When the internal diameter was increased from 0.5 to 0.75 mm, the peak height increased (Fig. 3B). However, broadening and tailing of peaks were found when wider-bore tubing was used, because of excessive dispersion of the sample zone. Relatively low dispersion should therefore be maintained. This is easily achieved because the length of tubing and the pumping rate are small.

Analytical characteristics. Under the optimum conditions (Table 1), a linear calibration graph was obtained for peak heights vs. amount of phosphorus as phosphate in the range 10—220 ng P. The relative standard deviation was 3.2% (10 results at 50 ng P). The signal is available within 150 s after sample injection, and about 20 measurements can be made per hour.

Phosphite, hypophosphite and some organophosphorus compounds, namely, trimethylphosphite ($TMPO_3$), triethylphosphite ($TEPO_3$) and tributylphosphine (TBP), can be determined similarly. The time between sample injection and appearance of the peaks (t) and some analytical characteristics for the above species are summarized in Table 2. Calibration graphs were prepared for all the compounds investigated, under the optimal conditions for phosphate. Table 2 shows that the m.e.c.a./f.i.a. response depends on the nature of each compound, and that different phosphorus-containing compounds give an emission response of different relative magnitude. The sensitivity for the inorganic anions is in the order $PO_2^{3-} > PO_3^{3-} > PO_4^{3-}$, while for the organophosphorus compounds the order is generally TBP > $TMPO_3$ > $TEPO_3$. The sensitivity always increases with decreasing oxygen content of the compounds, as observed by Belcher et al. [15].

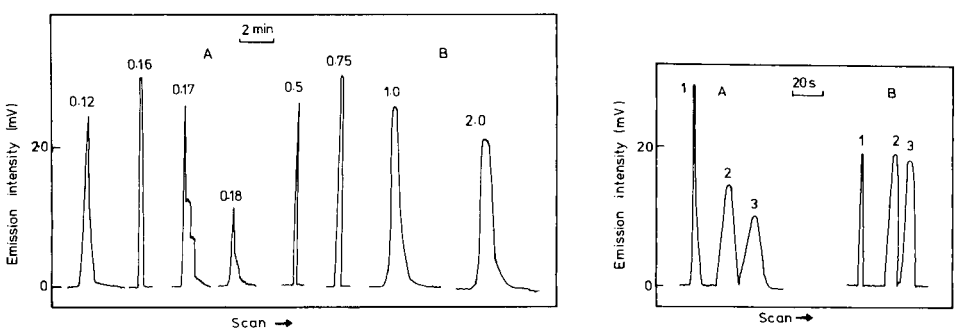

Fig. 3. Effects of flow rate (A) and tubing internal diameter (B) on responses for 50 ng P as phosphate. Numbers on the peaks represent: (A) flow rate in ml min^{-1}; (B) tubing i.d. in mm. Conditions otherwise as in Table 1.

Fig. 4. Responses from ternary mixtures. Peaks in A: (1) H_3PO_2; (2) H_3PO_3; (3) H_3PO_4. Peaks in (B): (1) TBP; (2) $TMPO_3$; (3) $TEPO_3$. (50 ng P for each compound; conditions as in Table 1.)

TABLE 2

Characteristics for various phosphorus compounds

Compound	t^a (s)	Linear calibration range (ng P)	Sensitivity (mV/ng P)[b]	Detection limit (ng P)[c]	R.s.d.[d] (%)
H_3PO_4	150	10—220	0.96	5.0	3.2
H_3PO_3	135	10—180	1.38	3.0	2.3
H_3PO_2	114	5—60	2.90	0.4	2.0
$TMPO_3$	78	10—200	1.68	2.5	4.2
$TEPO_3$	90	10—250	1.65	1.5	5.0
TBP	59	2.5—110	1.76	0.5	1.9

[a]Time from injection to maximum peak response. [b]Slope of calibration graph. [c]2σ value. [d]10 determinations of 50 ng P.

Because t is different for each compound investigated (Table 2), it should be possible to determine simultaneously mixtures of inorganic or organic phosphorus compounds. Figure 4A shows the resolved peaks from a ternary mixture of hypophosphite, phosphite and phosphate. Tributylphosphine can also be resolved (Fig. 4B) from trimethylphosphite and triethylphosphite. As the peaks of all the compounds studied are resolved, there is no effect of one component on the peak height of the others, and the calibration graphs coincide with those obtained for single substances.

The application of this method may be advantageous for determination of different mixtures, with a single injection, of organic and inorganic phosphorus compounds, where the need for selectivity is greater than that for sensitivity, e.g., detergents, geothermal fluids and fertilizers. Also, with this method it is not necessary to cool the cavity between injections as in conventional m.e.c.a. Applications of the method reported here are currently being studied and will be reported later.

This work was supported by the C.D.C.H. of the Andes University, Mérida, Venezuela. (Proyect TC-05-84).

REFERENCES

1 J. Růžička and J. W. B. Stewart, Anal. Chim. Acta, 79 (1975) 79.
2 J. W. B. Stewart and J. Růžička, Anal. Chim. Acta, 82 (1976) 137.
3 B. F. Reis, E. A. G. Zagatto, A. O. Jacintho, F. J. Krug and H. Bergamin F°., Anal. Chim. Acta, 119 (1980) 305.
4 Y. Hirai, N. Yoza and S. Ohashi, Anal. Chim. Acta, 115 (1980) 269.
5 L. Sung, Z. Gao, L. Li, X. Ya and Z. Fang, Fenxi Xuaxue Anal. Chem., 9 (1981) 586.
6 E. H. Hansen and J. Růžička, Anal. Chim. Acta, 81 (1976) 371.
7 E. H. Hansen, F. J. Krug, A. K. Ghose and J. Růžička, Analyst (London), 102 (1977) 705.
8 H. Dräger and B. Dräger, German Pat. 1,133,918, July, 1962.
9 R. M. Dagnall, K. C. Thompson and T. S. West, Analyst (London), 93 (1968) 72.

10 A. Syty and J. A. Dean, Appl. Opt., 7 (1969) 1331.
11 W. N. Elliott, C. Heathcate and R. A. Mostyn, Talanta, 19 (1972) 359.
12 G. L. Everett, T. S. West and R. W. Williams, Anal. Chim. Acta, 68 (1974) 387.
13 R. Belcher, S. L. Bogdanski and A. Townshend, Anal. Chim. Acta, 67 (1973) 1.
14 S. L. Bogdanski, Ph.D. Thesis, Birmingham University, 1973.
15 R. Belcher, S. L. Bogdanski, O. Osibanjo and A. Townshend, Anal. Chim. Acta, 84 (1976) 1.
16 J. L. Burguera and M. Burguera, Anal. Chim. Acta, 157 (1984) 177.

Analytica Chimica Acta, 170 (1985) 337—340
Elsevier Science Publishers B.V., Amsterdam — Printed in The Netherlands

Short Communication

THE ACCURACY OF THE VAPOUR-INJECTION CALIBRATION METHOD FOR THE DETERMINATION OF MERCURY BY AMALGAMATION/COLD-VAPOUR ATOMIC ABSORPTION SPECTROMETRY

R. DUMAREY*, E. TEMMERMAN, R. DAMS and J. HOSTE

Institute for Nuclear Sciences, Rijksuniversiteit Gent, Proeftuinstraat 86, B-9000 Gent (Belgium)

(Received 26th September 1984)

Summary. A vapour-injection method is described for the calibration of mercury determinations. Its accuracy depends mainly on the temperature of the mercury-saturated air, which must be lower than the ambient temperature. By preconditioning the syringe, initial irreproducible measurements caused by sorption are avoided. Under optimal conditions, the precision of the injection in the range 1—100 ng of mercury is generally better than 1%.

Cold-vapour atomic absorption spectrometry has become the most popular technique for determining mercury, mainly because of its simplicity, sensitivity and low cost. Generally, two different methods of calibration are applied, either reduction/aeration of mercury standard solutions or the injection of known amounts of mercury vapour.

The use of standard solutions shows some important limitations. At low concentrations ($<\mu g\ l^{-1}$), the solutions become unstable. This is caused partly by sorption of the mercury on the vessel walls and partly by volatilization [1]. Therefore, diluted solutions must be prepared freshly which means a considerable loss of time. Some authors have reported an improved stability on addition of strongly oxidizing agents (e.g., nitric acid, potassium dichromate or potassium permanganate) or complexing agents (e.g., cysteine) [2, 3]. However, this implies a high blank contribution and the possible introduction of systematic errors arising from the numerous dilutions needed.

The injection method is not subject to these limitations. The calibration is fast, precise and accurate if some precautions are taken. The method is also free of contamination and matrix effects. This communication describes the application of the injection method for the standardization of amalgamation/cold-vapour atomic absorption spectrometry. Special attention is given to factors influencing the accuracy of this calibration technique.

0003-2670/85/$03.30

Experimental

Spectrometric apparatus. The apparatus used was a modified Coleman MAS-50 [4]. The mercury from the sample is preconcentrated by amalgamation on gold-coated sand, the permanent absorber, which is connected directly to the optical cell of the spectrometer. The collector is heated at 800°C while purified nitrogen carrier gas flows at a rate of 460 ml min^{-1}. The mercury released is measured at the 253.7-nm line. The output signal is fed to an integrator for area calculation. A more detailed description of the analytical set-up is available [5].

Calibration equipment. The set-up is shown in Fig. 1. The mercury-saturated air is supplied from a closed 350-ml flask, containing 30—40 ml of mercury. The inner pressure is kept at atmospheric pressure by means of a side-arm which is open to the air via a capillary. The connection is below the mercury level to prevent dilution. The flask is placed in a thermostat (±0.1°C). The saturated air is removed via a three-layer septum by using a calibrated gas-tight syringe (Hamilton 1000 series).

The mercury vapour is injected through an injection port with septum while the carrier gas is flowing and is collected on the permanent gold-coated silica sand from which it is later desorbed thermally. By injecting several different volumes of air, a complete calibration line can be recorded at the beginning of each series of measurements. Standards are run intermittently to verify the stability of the system.

Results and discussion

The injection method calls for preconcentration of the mercury, preferably on gold [5]. In the case of reduction/aeration, this technique offers several advantages compared to the direct measurement. As shown in Fig. 2, the

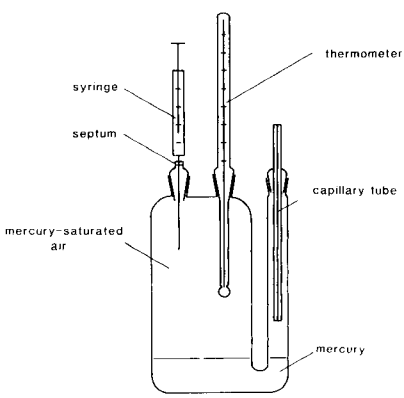

Fig. 1. Calibration equipment.

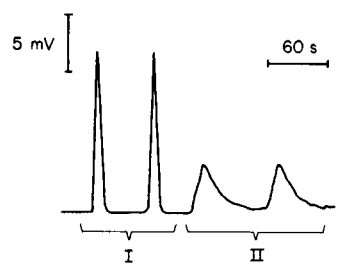

Fig. 2. Influence of thermal desorption vs. aeration on the peak shape: (I) preconcentration on gold; (II) direct injection. (5 ng Hg; 90-s aeration; 460 ml min^{-1} nitrogen.)

sensitivity is improved by the much faster release of mercury on heating compared to aeration. Also, matrix effects and interferences are eliminated, at least if the sample solution is aerated long enough, typically for 90 s. However, for best accuracy, it is recommended to determine the minimum aeration time required for each type of sample independently.

The amount of mercury vapour per volume of air at the saturation point is calculated from the ideal gas law. For example, 1 ml of air at 20° C and 101.325 Pa contains 65.66 × 10^{-12} mol of mercury, corresponding to 13.17 ng. The validity of the calculation was checked by processing standard solutions. The difference between the two methods was less than 3% in the range 1—50 ng of mercury. The reproducibility of five replicate injections was better than 1% above 1 ng. Volumes at the limit of the syringe range gave poor precision.

At an ambient temperature of 19° C, the temperature of the water bath was varied from 15° C to 25° C. The effect is shown in Fig. 3. The dashed line represents the theoretical peak areas, calculated from tabulated vapour pressures. Below ambient temperature, the theoretical and the measured values are identical. Above it, an increasing deviation is found, the measured areas giving the lower values. This is explained by condensation of the mercury on the inner walls of the syringe. Therefore, the temperature of the water bath must always be kept below ambient temperature.

Figure 4 illustrates the effect of syringe preconditioning on the reproducibility of the signal. Syringes were preconditioned by pulling in the maximum volume of saturated air and leaving for 10 min, with the needle inside the flask. Without such pretreatment, the signals become constant only after 3 injections. The initial loss is caused by a partial sorption of the mercury on the syringe walls. With a preconditioned syringe, both the peak height and peak area are reproducible from the first injection. Accordingly, a pretreated

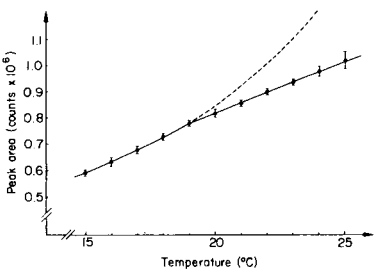

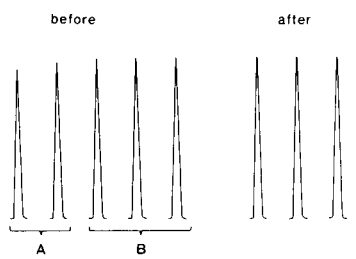

Fig. 3. Influence of the water bath temperature on the accuracy of the injection calibration method: (– – –) calculated; (——) measured.

Fig. 4. Influence of syringe preconditioning on reproducibility (12 ng Hg; Recorder at 20 mm min^{-1}/0.1 V full scale). Before conditioning, mean peak heights (absorbance) were 0.238 ± 0.001 (0.2%) for B and 0.232 ± 0.009 (3.7%) for A + B, the corresponding areas being 648695 ± 3332 (0.5%) and 638248 ± 17622 (2.8%). After conditioning, the mean peak height and area were 0.241 ± 0.001 (0.2%) and 61743 ± 4469 (0.7%).

syringe is needed for recording the calibration line and injections should be made from the highest volume to the lowest, successively.

The re-establishment of the equilibrium between liquid and gaseous mercury depends on the cleanness of the pool surface. After some time, the mercury at the surface becomes oxidized by atmospheric oxygen. The upper layer must then be removed and purified by distillation.

Care must be taken when large volumes are withdrawn. Above 5 ml, a few minutes must elapse before saturation is regained. After several injections, the flask must be opened to relieve the partial vacuum. The air from the flask should be withdrawn slowly. Afterwards, the transfer to the absorber should be as fast as possible to avoid losses by diffusion of mercury through the needle tip.

One of the authors (R. Dumarey) is indebted to the Interuniversitair Instituut voor Kernwetenschappen (IIKW) for financial support.

REFERENCES

1 G. E. Batley and D. Gardner, Water Res., 11 (1977) 745.
2 C. Feldman, Anal. Chem., 46 (1974) 99.
3 H. V. Weiss, W. H. Shipman and M. A. Guttman, Anal. Chim. Acta, 81 (1976) 211.
4 R. Dumarey, R. Heindryckx and R. Dams, At. Spectrosc., 2 (1981) 51.
5 R. Dumarey, R. Heindryckx, R. Dams and J. Hoste, Anal. Chim. Acta, 107 (1979) 159.

Analytica Chimica Acta, 170 (1985) 341—346
Elsevier Science Publishers B.V., Amsterdam — Printed in The Netherlands

Short Communication

FLUORIMETRIC ASSAY OF REDOX ACTIVITY IN CELLS[a]

ERHARD SEVERIN*, JOACHIM STELLMACH and HANS-MARTIN NACHTIGAL

Institut für Strahlenbiologie der Universität Münster, Hittorfstrasse 17, D-4400 Münster (Federal Republic of Germany)

(Received 5th September 1984)

Summary. A simple, sensitive procedure is described for measurement of the redox activity of single cells based on cyanotolyltetrazolium chloride which is reduced to a fluorescent monoformazan. Its efficiency is studied by incubating vital ascites tumor cells or cells treated with different fixatives, under different oxygen concentrations. Redox activity (fluorescence of the formazan) and DNA content (fluorescence of Hoechst dye 33378) of ascites tumor cells are measured simultaneously for the first time, by flow cytometry.

Although reduction/oxidation (redox) couples and systems are of great importance in biochemistry and biological chemistry, many questions regarding them remain to be answered. When biological oxidations are studied at the cellular and sub-cellular level, tetrazolium salts have proved to be suitable as electron acceptors [1]. These redox dyes have been used in many bio-, cyto-, and histo-chemical studies since 1941, when Kuhn and Jerchel [2] drew attention to their possible value in biochemical research. When a recently developed fluorescent tetrazolium salt, cyanotolyltetrazolium chloride (CTC) [3] was used, its reduction was found to occur mainly on the cell surface of Ehrlich ascites tumor cells (EATC), phagocytes and mouse liver cells [3, 4], though the tetrazolium salt formazan reaction has often been used for the intracellular determination of oxidative enzymes. The following experiments are thought to provide further support for these earlier results. They may also help in the development of an automated method for clinical application.

Experimental

The incubation and elution techniques were done as described by Stellmach [3]. The EATC were sucked off from the peritoneal cavity of NMRI mice 6—9 days after implantation. Following withdrawal, vital cells were incubated for no more than 15 min.

Fixation of cells. Two different fixatives were tested. With aqueous 0.3% (w/v) glutaraldehyde solution (pH 7.25), freshly harvested cells were suspended in the fixative and centrifuged immediately for 5 min. The sediment

[a]Presented at the International Symposium on Quantitative Luminescence Spectrometry in Biomedical Sciences, Gent, Belgium, September 3—6, 1984.

0003-2670/85/$03.30

was suspended in Puck medium (15 mM NaCl, 5 mM KCl, 4 mM $NaHCO_3$; pH 7.45). With ethanol as fixative, the ascites were centrifuged and the sediment was mixed with ethanol (25, 70 or 90% v/v), centrifuged again and suspended in Puck medium or in phosphate-buffered saline (pH 7.40; PBS). Some cells were fixed with ethanol for 24 h and also for 3 weeks and stored during this time at 4°C.

Incubation. All incubations were done in a shaking water bath at 37°C. Usually 2×10^6 cells per ml of Puck medium or PBS buffer were incubated. In some experiments, nitrogen or oxygen was passed vigorously through the medium for at least 15 min before and then during incubation.

The following concentrations were used: 1 mM CTC (for preparation, see [3]), 1 mM nitroblue tetrazolium salt (NBT; Serva, Mannheim), 0.5 mM Meldola blue (MB; Boehringer), 50 mM sodium succinate or sodium lactate (Serva), 5 mM sodium cyanide (Merck).

The CTC formazan was eluted with ethanol as described by Stellmach [3], and the NBT-formazan was eluted with alkaline dimethylformamide [5]. The absorbance of the CTC formazan was measured at 450 nm and that of NBT formazan at 715 nm, respectively, with a Zeiss RPQ-20A spectrophotometer. The fluorescence spectra were obtained with a Perkin-Elmer fluorimeter 650-10S at a bandwidth of 2 nm. All spectra are uncorrected.

Flow cytometry. A home-made flow cytometer similar to the ICP-22 (formerly Phywe, Göttingen, now Ortho-Physics, Westwood, MA) was used to measure simultaneously the formazan fluorescence of each cell and the DNA content after the DNA had been stained with Hoechst 33378.

Results

The CTC formazan only fluoresces in the solid state, not in solution. It is readily soluble in many polar organic solvents. For possible applications of CTC in biochemistry and medicine, it is important that CTC formazan is readily soluble in pure ethanol but not in dilute aqueous ethanol (<50% ethanol). The fact that unreduced CTC is not fluorescent in the visible range of the spectrum is another advantage (see Fig. 1). The dependence of formazan production on CTC concentration was tested for vital and for prefixed cells. If vital cells are incubated for more than 20 min, the cells aggregate and the subsequent elution will be very irreproducible. Therefore, vital cells were incubated for ⩽20 min, whereas prefixed cells even after an incubation time of more than 30 min showed an increase of formazan production. The amount of formazan produced by prefixed cells was only about 50% of that produced by vital cells (Fig. 2). For prefixed cells, the amount of formazan increased linearly with the CTC concentration, above 0.1 mM CTC. With vital cells, the plot is linear up to 0.25 mM of CTC and then levels off.

To establish whether there is a correlation between the redox activity and the viability of the cells, both vital cells and cells prefixed for different times (see Fig. 3) were incubated. With the exception of a 25% (v/v) ethanolic solution, all fixatives equally diminished formazan production. This effect

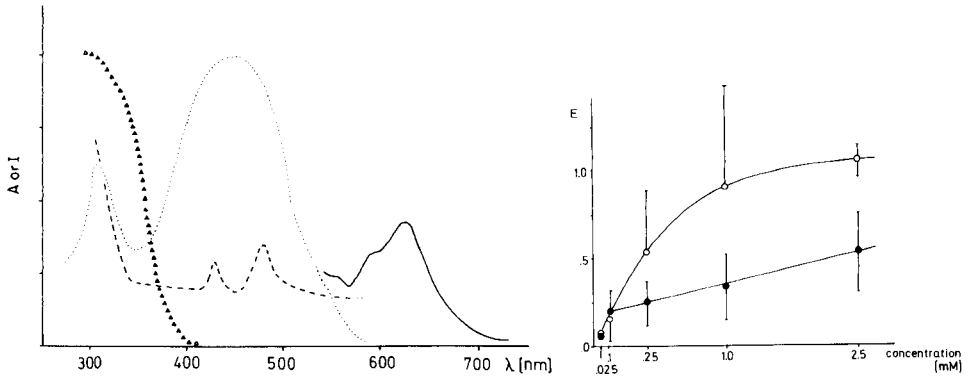

Fig. 1. Absorption spectra: (△) CTC in phosphate-buffered saline; (···) CTC formazan in ethanol. (---) Excitation spectrum of solid CTC formazan at an emission wavelength of 630 nm: (—) emission spectrum of solid CTC formazan at an excitation wavelength of 450 nm.

Fig. 2. Relation between the amount of cellular formazan measured as absorbance (A) and the tetrazolium salt concentration: (•) fixed cells incubated for 30 min; (○) vital cells incubated for 20 min.

was independent of fixation time. When cells were incubated after a 3-week fixation with different fixatives, the absorbance after formazan elution was ca. 0.1. Fluorescence microscopy revealed a striking difference compared to vital cells. Whereas the formazan crystals of vital or briefly (5 min) prefixed cells were predominantly on the cell surface, after long fixation periods most of the formazan precipitate could be detected within the cells, though the amount of formazan, of course, was much smaller compared to vital or briefly prefixed cells.

To compare the commonly used tetrazolium salt NBT to the new CTC salt, the same number of vital cells was incubated with equimolar solutions of NBT or CTC (Fig. 4). When cyanide was present, the absorbance of the NBT formazan after elution was about 4 times higher than that of the CTC formazan (incubation time 10—20 min). Without cyanide, very similar absorbances were obtained after elution of the formazan with the appropriate solvent.

An attempt was made to assess the oxygen sensitivity of CTC by measuring the formazan production from cells incubated in reaction mixtures equilibrated with either nitrogen or oxygen and comparing it with the yield from cells incubated in air. The highest formazan yield was obtained in the ungassed sample (Fig. 5). Formazan production increased similarly in all samples when cyanide was added (cf. Fig. 4).

This study was a preliminary to developing an automated procedure for correlating the redox activity of single cells with other independent cell parameters. By this means, a better understanding of the redox metabolism of single cells might be provided. A two-parameter distribution of redox

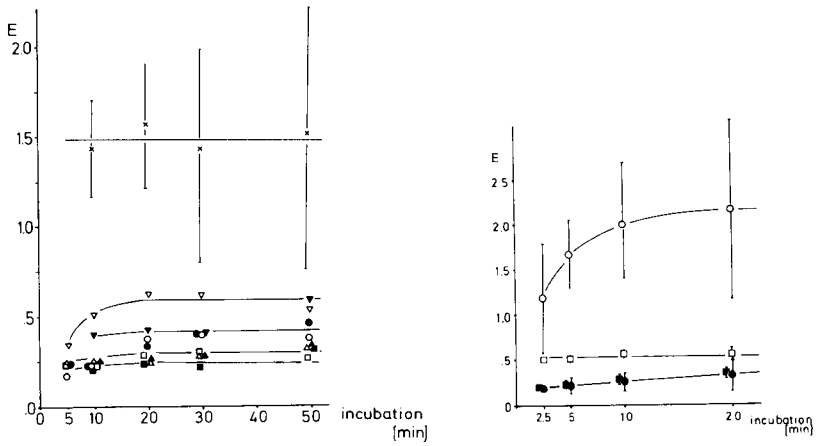

Fig. 3. Formazan production from vital cells (×) and after fixation with: (○) glutaraldehyde; (▽) 25% ethanol; (△) 70% ethanol; (□) 90% ethanol. Open symbols indicate fixation time of 5 min; filled symbols indicate fixation for 24 h. Incubation with succinate, Meldola blue and cyanide; mean values of results of 3 experiments; error bars indicate 1 standard deviation.

Fig. 4. Formazan production form vital cells incubated with: (○) NBT; (□) CTC. Open symbols indicate addition of cyanide; filled symbols indicate the absence of cyanide. Error bars as in Fig. 3.

activity and DNA content of vital ascites tumor cells is shown in Fig. 6. Each point in this figure represents a single cell indicating the two fluorescence intensities (DNA dye and formazan content) by its position. Thus, a detailed distribution of redox activity in the ascites cell population is obtained. Considering the rise of the abscissa, which is recognizable by the vanishing line

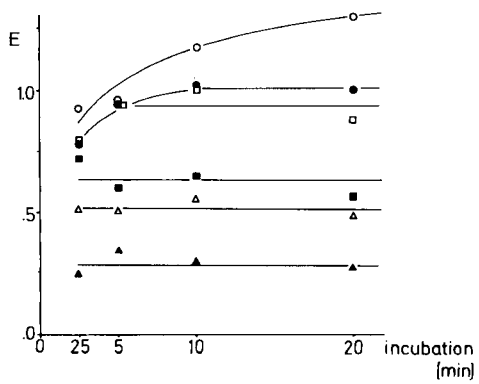

Fig. 5. CTC formazan production from vital cells incubated with cyanide (open symbols) and without cyanide (filled symbols). Incubation was done: (○) in air; (□) after outgassing with nitrogen; (△) after outgassing with oxygen. Mean values of four experiments with relative standard deviations of 42—75%.

Fig. 6. Distribution of DNA content and redox activity in mouse ascites tumor cells measured by flow cytometry (photographed from a storage oscillograph). Abscissa: DNA fluorescence after staining with Hoechst dye. Ordinate: formazan fluorescence after incubation of vital cells with succinate and Meldola blue for 20 min. The big cluster on the left represents G_1 cells; the big cluster on the right represents cells in the G_2 and M phases. The points in between correspond to cells in the DNA-synthesis phase. The points accumulated beneath, especially on the left, represent cells that do not produce formazan.

of the lowest points, cells in the G_2 and M phases of the intermitotic cycle appear to produce no more formazan than G_1-phase cells.

Discussion

Robertson et al. [6] observed that reduction of the tetrazolium salt, NBT, was increased by cyanide. Hassan and Fridovich [7] tried to explain the effect by suggesting that cyanide inhibits the electron flow from cytochrome oxidase and so causes the preceding electron carriers of the electron transport chain to pile up in the reduced state. The increased electron shunting action of the electron carrier would produce increased reduction of the tetrazolium salt.

In oxygen-equilibrated solutions, oxygen competes with the tetrazolium salt for the reducing species. Therefore, the formazan yield is very low in oxygenated samples. Cells incubated under nitrogen surprisingly produced less formazan than cells incubated aerobically by gently shaking the suspension under atmospheric oxygen pressure. However, the low oxygen concentration appeared to provide so little oxygen for respiration to the dense tumor cell suspension that the cells were virtually anoxic. The lesser formazan production of the cells gassed with nitrogen may be an artefact caused

by detachment of formazan crystals from the mechanically stressed cells (caused by gas bubbles) and loss to the medium.

Unexpectedly, the tetrazolium salt was reduced almost exclusively on the cell surface. The detection of this formazan localization by light microscopy may be due to the unusual fluorescence property of the reduced form of CTC, compared to commonly used tetrazolium salts which are reduced to non-fluorescent formazans [8]. In this respect, the present data are consistent with the results of De Bari and Needle [9] who found that the membrane of vital cells was quite impermeable to the free NBT cation. Therefore, viable cells should generate less formazan than fixed cells which enable extracellular reagents to penetrate the membrane and react with intracellular redox enzymes. In this study, however, more formazan was obtained from the eluate of vital cells than from fixed cells. This apparent contradiction was solved by microscopic observation of the incubated Ehrlich ascites tumor cells. In vital cell preparations, many free formazan crystals were seen in the incubation medium. These crystals were eluted in the same way as the crystals generated on the cell membrane resulting in high formazan yield from the vital cell extract. Gently fixed cells carried more formazan crystals on their cell surface than vital cells. Therefore, it is concluded that tetrazolium salt reduction takes place mostly under the influence of membrane-bound redox enzymes that are known to exist on the surface of many cells. Of course, partial intracellular tetrazolium salt reduction by other reducing species (e.g., dehydrogenases or thiol-containing biomolecules or α-hydroxycarbonyls or related compounds [6]) cannot be ruled out.

REFERENCES

1 A. G. E. Pearse, Histochemistry, Theoretical and Applied, Vol. 2, 3rd edn. Churchill, Livingstone, London, 1972.
2 R. Kuhn and D. Jerchel, Ber. Dtsch. Chem. Ges., 74 (1941) 941, 949.
3 J. Stellmach, Histochemistry, 80 (1984) 137.
4 E. Severin and J. Stellmach, Acta Histochem., 75 (1984) 101.
5 F. P. Altman, Histochemie, 22 (1970) 256.
6 P. Robertson Jr., S. E. Fridovich, H. P. Misra and I. Fridovich, Arch. Biochem. Biophys., 207 (1981) 282.
7 H. M. Hassan and I. Fridovich, in T. E. King, H. S. Mason and M. Morrison (Eds.), Oxidases and Related Redox Systems, Pergamon Press, Oxford, 1984, p. 151.
8 F. Wohlrab, E. Seidler and K. D. Kunze, Histo- und Zytochemie dehydrierender Enzyme, J. A. Barth, Leipzig, 1979.
9 V. A. De Bari and M. A. Needle, Histochemistry, 56 (1978) 155.

Analytica Chimica Acta, 170 (1985) 347—352
Elsevier Science Publishers B.V., Amsterdam — Printed in The Netherlands

Short Communication

FLUORIMETRIC DETERMINATION OF TRACE HYDROGEN PEROXIDE IN WATER WITH A FLOW INJECTION SYSTEM

HOON HWANG and PURNENDU K. DASGUPTA*
Department of Chemistry, Texas Tech University, Lubbock, TX 79409-4260 (U.S.A.)
(Received 5th November 1984)

Summary. A fluorimetric flow-injection procedure with a single reagent solution containing *p*-hydroxyphenylacetic acid, peroxidase and ammonia permits the determination of aqueous hydrogen peroxide in the range 10^{-8}—10^{-4} M; 30—60 samples can be processed per hour. The method exhibits a wide linear range and is insensitive to sample pH within the range 2—6.

The determination of trace levels of hydrogen peroxide has become important because H_2O_2 is currently believed to play a key role in the atmospheric transformation of sulfur dioxide to sulfuric acid via aqueous phase reactions in hydrometeors [1—3]. Although many selective spectrophotometric and electrochemical methods have been described, the requisite sensitivity for applications to precipitation and cloudwater limits the approaches to the more sensitive luminescence methods. The oxidation of luminol by H_2O_2 is catalyzed by transition metal ions, enzymes and certain other biomolecules; chemiluminescence is produced. A Cu^{2+}-catalyzed luminol method has been reported for quantifying H_2O_2 in environmental samples [4], but there is some doubt about the selectivity of the luminol method; other oxidants (e.g., nitrogen dioxide) may produce chemiluminescence under similar conditions [5].

Fluorescence procedures are capable of yielding detection limits similar to those of chemiluminescence methods under optimum conditions. The oxidation of fluorescent 6-methoxy-1,2-benzopyrone by H_2O_2, catalyzed by peroxidase, quenches the fluorescence; this has been used to quantify H_2O_2 [6, 7]. However, if possible, it is preferable to form a fluorescent product from a nonfluorescent substrate. Keston and Brandt [8] reported the use of leucodiacetyldichlorofluorescein as a substrate for the peroxidase/peroxide system; a detection limit (S/N = 3) of 2×10^{-8} M H_2O_2 can be estimated from their data. The utility of the procedure is hindered by the need to synthesize the substrate.

As a result of a systematic study of a number of structurally related substrates for the peroxidase-mediated determination of peroxide, Guilbault et al. [9] found *p*-hydroxyphenylacetic acid (PHPA) to be particularly attrac-

0003-2670/85/$03.30

tive. This substrate is oxidized by H_2O_2 to form a fluorescent dimer

$$2O^-C_6H_4COO^- + H_2O_2 \xrightarrow{\text{Peroxidase}} (O^-C_6H_3COO^-)_2 + 2H_2O$$

Lazrus et al. [10] found that the dimer fluoresces optimally at pH $\geqslant$ 10 and devised an air-segmented continuous flow procedure in which the pH of the flow stream is increased to $\geqslant$10 with sodium hydroxide after the reaction has proceeded at a lower pH. In parallel studies conducted in this laboratory, an unsegmented continuous flow (flow injection) system was preferred for automation. The procedure reported below does not require a separate addition of alkali and enables sub-μg l^{-1} levels of H_2O_2 to be determined routinely.

Experimental

Equipment. A ratio-recording spectrofluorimeter (NOVA; Baird Instrument Corp, Bedford, MA) equipped with a 30-μl flow-through cell was used. The optimum excitation and emission wavelengths were 329 and 412 nm, respectively; 10-nm slit widths and 1-s integration were used.

Reagents. p-Hydroxyphenylacetic acid (Eastman Kodak) was recrystallized twice from hot water with small amounts of activated charcoal added for decolorization.

Distilled-deionized water was freed from peroxide by adding (per liter) 10 ml of a solution of catalase (from bovine liver; Sigma Chemical Co.); the solution contained 0.5 mg of catalase in 100 ml of 0.5 M phosphate buffer, pH 7. After 1 h, the water was boiled for 2 h to denature the protein shortly before use. All reagents and standards were prepared in this water and stored away from direct exposure to bright light.

The buffered PHPA/peroxidase reagent was prepared by dissolving 3 g of purified PHPA and 0.156 g of disodium ethylenediaminetetraacetate in 500 ml of 0.1 M ammonia. The pH of this solution was about 9.5. Peroxidase (type II, typically 75—150 units/mg; Sigma) was added (450 units/100 ml) shortly before use. This solution was usable for 24—48 h when stored at ambient temperature; the enzymatic activity decreased slowly, presumably due to degradation of the protein.

Hydrogen peroxide standards were prepared from a stock solution, standardized by classical iodimetric methods. Standards containing less than 10^{-6} M H_2O_2 were prepared immediately before injection.

Flow system. A two-channel Gilson Minipuls-2 peristaltic pump (slow speed drive module) was used for pumping the peroxidase/PHPA/ammonia reagent (1.23 mm i.d. PVC tubing, flow rate 0.28 ml min^{-1}) and the carrier water stream (3.16 mm i.d. PVC tubing, flow rate 1.33 ml min^{-1}). Sample was injected into the carrier stream from a manually actuated fluorocarbon rotary valve (Rheodyne Type 50). The carrier and reagent streams were mixed at a low-volume T-joint and then directed to the detector via a mixing/delay line. Several methods to ensure good radial mixing have been reported [11, 12]. Several mixing geometries were investigated, including the single bead string reactor [12]; it was found that a simple knotted delay line pro-

vided the best results. The delay line was made of teflon tubing (115 cm long, 0.8 mm i.d.) containing a total of 33 knots placed at reasonably regular intervals. The flow scheme is shown in Fig. 1.

Results and discussion

Quantitation of traces of H_2O_2 is important not only to improve the current understanding of several atmospheric processes, including acidity of precipitation, but it is also a key step in the clinical determination of glucose via glucose oxidase.

The main difficulty with a single-step procedure for the dimerization reaction is that the maximal activity of the enzyme, in the absence of any activator, is reached at pH 5.5. At pH 7.5, the enzymatic activity decreases to $\leqslant 10\%$ of its maximum value, and at pH $\geqslant 9.0$ the enzyme is virtually inactive in the absence of an activator [13]. In contrast, the dimer fluoresces optimally only at high pH. The pure dimer was prepared by allowing a solution of PHPA at pH 5.5 containing a little peroxidase to react with a slight stoichiometric excess of H_2O_2 for 4 days and isolating it by thin-layer chromatography. The fluorescence of the resulting dimer solution was measured as a function of pH, as shown in Fig. 2. The intersection point of the extrapolated linear segments gives the pK_a value of the nonfluorescent/fluorescent transition [14]; the value found was 7.85. Maximal fluorescence will be attained by pH 9.5 (computed fraction of dimer in fluorescent form at pH 9.5 is 0.98). Although successful determinations were done with the enzyme reaction at pH 5.5 and then addition of sodium hydroxide to raise the pH to $\geqslant 9.5$, the accompanying dilution was deemed undesirable.

The problem then was to achieve a fast reaction rate at pH 9.5. Although the overall rate can be increased to a degree by increasing the concentrations of the enzyme and PHPA, both have limited solubilities. Further, the enzyme preparation of requisite purity is expensive. The presence of nitrogenous ligands are known to activate peroxidase [13], the enzyme remaining active at pH levels significantly above its optimum pH. The rate of fluorescence development as an aliquot of H_2O_2 was added to a PHPA/peroxidase reagent buffered at pH 9.5, with various nitrogenous buffer systems, was measured at a total buffer concentration of 0.1 M. Virtually no reaction was observed with a nonnitrogenous buffer such as phosphate. When the buffer was based on EDTA, a very weak nitrogen base, the rate was only marginally faster than with phosphate. The rates of fluorescence development with Tris,

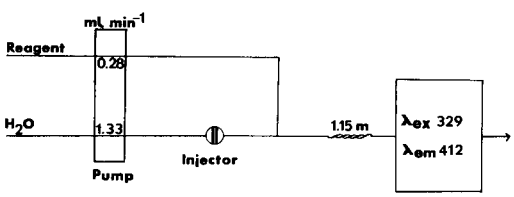

Fig. 1. Schematic diagram of the flow system.

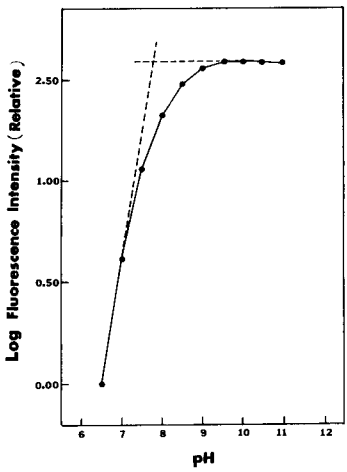

Fig. 2. Relative fluorescence intensity of PHPA dimer as a function of pH.

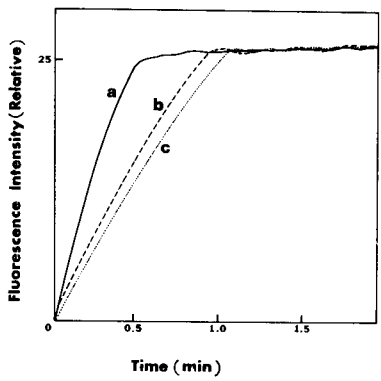

Fig. 3. Kinetic response curves for the oxidation of PHPA by H_2O_2 catalyzed by peroxidase at pH 9.5 in three buffer systems: (a) ammonia; (b) ethylenediamine; (d) tris(hydroxymethyl)aminomethane.

ethylenediamine and ammonia-based buffers are shown in Fig. 3; the reaction rate increases in the stated order. The maximum fluorescence intensity attained was essentially identical to that obtained by a two-step reaction.

Clearly, an ammonia-based buffer at pH 9.5 sufficiently activates the enzyme to enable the kinetics of the desired reaction to be compatible with the flow system. Some aspects of this activation of peroxidase are noteworthy. At pH 9.5, virtually all the Tris (pK_a = 8.08) is in the free base form (96%), while a significant fraction (36%) of the ammonia (pK_a = 9.75) and a small fraction (7%) of the ethylenediamine (pK_a = 10.63) are in the free base form. Activation of the enzyme depends on the K_b of the ligand and the free ligand concentration in such a manner that ammonia with an intermediate K_b and free base concentration produces the best results. Fridovich [13] suggested that the ligand (L) binds to the enzyme (E) to form the activated enzyme (EL) with an association constant ($E + L \rightleftharpoons EL$) of ca. 10^4 when L is ammonia. The association constant is much greater (10^7) when L is hydroxide, but the resulting adduct is inactive. Consequently, regardless of the nature of the nitrogen base, because of the greater competitive inhibitory binding of hydroxide, it is not possible to increase the overall rate by attempting to raise the pH beyond 9.5 and thereby increase the concentration of the free nitrogen base, e.g., for ethylenediamine.

System performance. The reproducibility (relative standard deviation, n = 7) of the system at low concentrations is 7.1% at 1 $\mu g\,l^{-1}$, 5.7% at 2 $\mu g\,l^{-1}$, 2.7% at 4 $\mu g\ l^{-1}$, 0.3% at 8 $\mu g\ l^{-1}$, and 0.2% at 16 $\mu g\ l^{-1}$. The relatively poor

reproducibility at the lowest levels can be ascribed not to the limitations of the system but to the difficulty of reproducibly preparing and injecting such low levels of hydrogen peroxide. According to the guidelines established by the American Chemical Society [15], the limit of detection (S/N = 3) is $\leqslant 0.3\ \mu g\ l^{-1}$ or 10^{-8} M H_2O_2, based on the standard deviation of the $1\ \mu g\ l^{-1}$ H_2O_2 signal. The sample volume for low-level determinations is 500 μl. System dispersion is such that at the peak, the dispersion factor is unity. System dispersion could be reduced by using narrower tubes and lower flow rates, resulting in a lower sample requirement. However, with a relatively large flow cell volume (30 μl), attainable improvements were judged marginal and sample availability (cloud water, precipitation) was not a limiting factor. The sample throughput rate of 30 h^{-1} was considered acceptable. A smaller sample size (50 μl) permits a higher throughput rate (60 h^{-1}) for the higher concentrations (1 mg l^{-1}) found in rainwater [16, 17].

Calibration plots were linear from 10^{-8} to 10^{-4} M H_2O_2. A 500-μl sample loop was used for concentrations up to 3×10^{-5} M; a 50-μl sample loop was used for higher concentrations. It should be noted that although smaller amounts of the enzyme or PHPA than the amounts recommended here cause only a marginal loss in sensitivity for low-level samples, the principal undesirable effect of using less reagent is a smaller linear range.

The results reported here pertain to a reagent used within 2—8 h of final preparation (peroxidase addition). The typical background and analyte signals, in arbitrary fluorescence units, were: 40 for pure water flowing through the detector, 53 for the system blank and 16.4 units net signal for a 500-μl, 9-$\mu g\ l^{-1}$ sample. After 24 h and 48 h of storage at room temperature, the system blanks increased to 82 and 127 units, respectively. Interestingly, the corresponding analyte responses increased also, to 18.0 and 19.7 units net signal, respectively, for a 9-$\mu g\ l^{-1}$ sample. These increases were very reproducible. After 48 h, however, the determination of very low concentrations was obviously impaired.

Because atmospheric precipitation samples are frequently acidic, effects of the sample pH were studied by adjusting the pH of the peroxide standards with sulfuric acid. Less than 5% decrease in the signal level was observed in reducing the pH from 6 to 2 with the large sample loop. No discernible change in signal level was observed with the smaller loop.

This work was supported by the U.S. Environmental Agency through grant no. R810894-010. This report has not been subjected for review by Environmental Protection Agency and therefore does not necessarily reflect the views of the Agency and no official endorsement should be inferred.

REFERENCES

1 D. Moller, Atmos. Environ., 14 (1980) 1067.
2 J. G. Calvert, B. G. Heikes, W. R. Stockwell, V. A. Mohnen and J. A. Kerr, in W. Jaeschke (Ed.), Chemistry of Multiphase Atmospheric Systems, Springer, Heidelberg, 1984.

3 H. Hwang and P. K. Dasgupta, Environ. Sci. Technol., 19 (1985) 255.
4 G. L. Kok, T. P. Holler, M. B. Lopez, H. A. Nachtrieb and M. Yuan, Environ. Sci. Technol., 12 (1978) 1072.
5 G. J. Wendel, D. H. Stedman, C. A. Cantrell and L. Damrauer, Anal. Chem., 55 (1983) 937.
6 W. A. Andreae, Nature, 175 (1955) 859.
7 H. Perschke and E. Broda, Nature, 190 (1961) 257.
8 A. S. Keston and R. Brandt, Anal. Biochem., 11 (1965) 1.
9 G. G. Guilbault, P. Bragnac and M. Juneau, Anal. Chem., 40 (1968) 1256.
10 A. L. Lazrus, G. L. Kok, J. A. Lind, S. N. Giltin and S. McLaren, Anal. Chem. 57 (1985), in press.
11 J. Růžička and E. H. Hansen, Flow Injection Analysis, Wiley, New York, 1981.
12 J. M. Reijn, W. E. Van der Linden and H. Poppe, Anal. Chim. Acta, 123 (1981) 229.
13 I. Fridovich, J. Biol. Chem., 238 (1963) 3921.
14 P. K. Dasgupta, Anal. Chem., 53 (1981) 2084.
15 American Chemical Society Committee on Environmental Improvement, Anal. Chem., 52 (1980) 2242.
16 G. L. Kok, Atmos. Environ., 14 (1980) 653.
17 K. Yoshizumi, K. Aoki, I. Nouchi, T. Okita, T. Kobayashi, S. Kamakura and M. Tajima, Atmos. Environ., 18 (1984) 395.

Analytica Chimica Acta, 170 (1985) 353—357
Elsevier Science Publishers B.V., Amsterdam — Printed in The Netherlands

Short Communication

A FAST PREPARATIVE METHOD FOR THE GAS CHROMATOGRAPHY OF POLYCARBOXYLIC ACIDS IN AQUEOUS AND SALT SOLUTIONS

I. MOLNÁR-PERL* and M. PINTÉR-SZAKÁCS

Institute of Inorganic and Analytical Chemistry, L. Eötvös University, Budapest (Hungary)

(Received 7 March 1984)

Summary. In aqueous solutions (with or without salts) containing carboxylic acids, water can be bound with anhydrous sodium sulphate at a molar ratio of $[Na_2SO_4]/[H_2O] \geqslant 0.9$. This is used prior to gas chromatography of aliphatic and aromatic di- and poly-carboxylic acids (oxalic to mellitic acid) in aqueous matrices (solutions, suspensions). Such acids are extracted quantitatively into diethyl ether within 8—10 min, which is much faster than conventional methods. Esterification is done with diazomethane.

Esterification under anhydrous conditions is a classical and general requirement [1] but most practical problems involve the analysis of aqueous and salt-containing aqueous solutions. Thus, the gas chromatographic determination of carboxylic acids measurable only as esters is slowed down significantly by the time-consuming separations (distillation, extraction) that precede fast esterification. Much work has been done to decrease the time and labour needed for the preparation of samples for gas chromatography (g.c.). The direct preparation of derivatives without separation, and/or the possibility of fast dehydration are equally important for routine qualitative and quantitative evaluation of carboxylic acids in foods, fruits and juices, as well as in industrial and geochemical matrices.

In the case of carboxylic acids easily esterifiable with alcohols in the presence of mineral acids, direct esterification of the aqueous solutions is rapid [2—9]. For other carboxylic acids, that are not easily esterified because of steric hindrance, the dehydration process must be accelerated; such acids can be esterified only under anhydrous conditions, preferably with diazomethane in ether solutions.

For the discrete extraction of carboxylic acids with low carbon number from biological liquors, ferments, etc., methanol/chloroform mixtures [10, 11] or ether [12] have been used. There is, however, no analogous information on the distribution properties of aliphatic and aromatic di- and poly-carboxylic acids such as appear in the organic content of soils and rocks [13—15] and in industrial alumina processes [16, 17]; these acids are usually difficult to esterify. Existing methods use continuous liquid-liquid extraction for 16 h [16], 24 h [14, 15], 48 h [13] or even longer [17].

0003-2670/85/$03.30

In an earlier paper [8], a new method was suggested for the direct esterification of C_1—C_{20} fatty acids in aqueous solutions in the presence of anhydrous sodium sulphate in an homogeneous butanol/water/sulphuric acid solution [9]. In the present communication, anhydrous sodium sulphate is used to allow fast esterification of other carboxylic acids, but especially highly carboxylated acids which normally require lengthy continuous extraction.

Experimental

Reagents. All reagents and model acids were of analytical purity (Reanal, Hungary, Budapest). Ether was purified by distillation first from phosphorus pentoxide and then from sodium hydroxide.

Procedure. An accurately weighed portion of the solution or suspension from industrial or geochemical samples (e.g., soil extracts) containing 0.01—20 mg of the individual carboxylic acids and 1 or 2 ml of water are introduced into a 100-ml thick-walled beaker (4—5 cm diameter, 8—10 cm tall). Then 10 or 20 g of anhydrous sodium sulphate is added and the mixture is homogenized quickly. If the sample contains volatile fatty acids, the beaker is placed in an ice-bath after the addition of 10 ml of diethyl ether. Thereafter 1 ml of concentrated sulphuric acid is added dropwise, the mixture is homogenized again and 40 ml of diethyl ether is added. The mixture is stirred several times, and then the ether phase is filtered into a vacuum distillation flask through a funnel wadded with cotton wool with sodium sulphate on it to retain the solid phase quantitatively. Dissolution is repeated with four further 50-ml portions of ether. The combined ether extracts containing the carboxylic acids are evaporated on a water-bath at ambient temperature to 30—40 ml, and mixed with an ether solution of diazomethane for the esterification of poly-carboxylic acids. After 30 min, the excess of ether and diazomethane is removed by vacuum distillation. From the residue, solutions from 5 μl to 2 ml can be prepared depending on the amount of the carboxylic acids present.

If the C_1—C_5 fatty acids in the ether extract are also to be measured (the $>C_6$ fatty acids are determined as methyl esters prepared with diazomethane), an aliquot or all of the ether extract is converted to the butyl esters and subjected to gas chromatography [8].

Gas chromatography. A Chromatron G.C. H.F.18.3 gas chromatograph (Berlin, D.D.R.) was used with a flame ionization detector (FID) and a stainless-steel column (2 m × 3 mm i.d.). The carrier gas was nitrogen at 60 ml min^{-1}. The column packing was 80—100 mesh Chromasorb W-AW-DMCS wetted with 15% (w/w) Dexsil-300. The column was programmed from 60 to 340°C at a rate of 16°C min^{-1}, and kept at 340°C for 25 min. The evaporator and FID were held at 340°C.

The C_1—C_{20} fatty acids were measured as described earlier [8].

Results and discussion

Results obtained by the commonly used techniques of extraction with discrete fractions or continuous liquid-liquid extraction for some C_1—C_{20} fatty acids, C_2—C_{16} aliphatic dicarboxylic acids and aromatic polycarboxylic acids with 2—6 carboxy groups are summarized in Fig. 1. As can be seen, fatty acids with $>C_3$ were present quantitatively in the first fractions in both the discrete and continuous extractions. Oxalic and mellitic acids, which are most difficult to extract, cannot be isolated by the discrete method within a reasonable number of fractions. Their isolation by the present continuous technique required 96 h.

Optimal conditions for preparative procedure suggested here were established by considering the amount of anhydrous sodium sulphate in relation to the water to be bound, the molar ratio of sodium sulphate and sulphuric acid, and the amount of ether needed for quantitative dissolution. In earlier work [8], it was shown that anhydrous sodium sulphate binds 5 mol of water per mole at the boiling temperature of the butanol/water/sulphuric acid system, i.e., esterifications were quantitative in solutions with a molar ratio of $[Na_2SO_4]_{anh.}/[H_2O] \geqslant 0.2$. The present experiments, made at room temperature and/or with ice-cooling, showed that for quantitative dehydration, a molar ratio of anhydrous sodium sulphate to water $\geqslant 0.9$ was needed, i.e., to bind 1 ml of water, at least 7.5 g of anhydrous sodium sulphate is necessary. The use of more anhydrous sodium sulphate provided the same results if the appropriate amount of sulphuric acid was added (Table 1).

The optimum molar ratio of sulphuric acid to sodium sulphate was $\geqslant 0.19$ for the extraction of every carboxylic acid studied. Similar results were obtained when 2—3 times more sulphuric acid was used (Table 1, columns 1, 2, 3). When the amount of sulphuric acid was less than the optimum, more ether was needed for quantitative extraction of the carboxylic acids. The

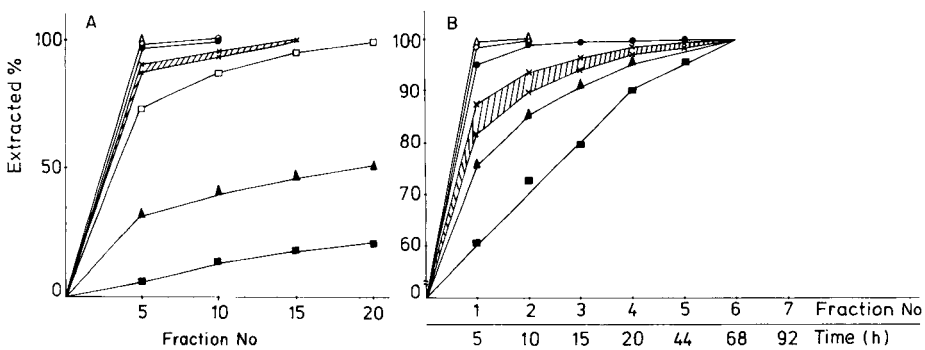

Fig. 1. Extraction yield of aliphatic and aromatic di- and poly-carboxylic acids: (A) discrete extractions; (B) continuous liquid-liquid extraction. Acids: (○) formic; (●) acetic; (△) propionic; (×, shaded area) succinic (in B only), glutaric, adipic, pimelic, *o*-phthalic, trimellitic, trimesic, pyromellitic; (▲) oxalic; (□) succinic; (■) mellitic. Conditions: 2 ml of aqueous solution containing 10 or 20 mg of the organic acid was extracted; 1 M H_2SO_4 was used; for (A), the volume of each extraction fraction was 2 ml; for (B), 100 ml of diethyl ether was circulated.

TABLE 1

The gas-chromatographic determination of di- and poly-carboxylic acids as methyl esters[a]

Carboxylic acid	Peak area[b]						SD	RSD (%)
	a	b	1	2	3	Mean		
Oxalic	1355	1295	1293	1300	1332	1315	27.4	2.1
Succinic	2559	2690	2586	2600	2552	2597	55.3	2.1
Glutaric	2593	2885	2895	2859	2954	2837	140.9	5.0
Adipic	2641	2731	2864	2867	2643	2749	112.0	4.1
Benzoic	3184	3141	3178	3060	3293	3171	66.2	2.1
o-Phthalic	3557	3386	3548	3344	3724	3514	155.5	4.4
Trimellitic	1839	1918	2030	2011	2055	1971	135.7	6.7
Trimesic	2893	2884	2772	3072	3051	2934	125.7	4.3
Pyromellitic	2273	2379	2311	2356	2427	2349	51.2	2.2
Benzenepentacarboxylic	2193	2145	2154	2260	2099	2170	67.8	3.1
Mellitic	2365	2043	2084	2184	2319	2199	141.2	6.4

[a]Columns a and b relate to direct esterification of the acids, done in parallel. Columns 1—3 relate to extraction from 2 ml of aqueous solution by the proposed method. The amount of each carboxylic acid used was 10—12 mg. For columns 1—3, the $[H_2SO_4]/[Na_2SO_4]_{anh.}$ and $[Na_2SO_4]_{anh.}/[H_2O]$ ratios used were, respectively, 0.19 and 1.27; 0.255 and 1.27; and 0.38 and 1.27, 0.90 or 1.90. In the final case, the means of the five sets (a, b, 1—3) of data are presented. [b]Peak area in arbitrary units, equivalent to 1 μg of the acid.

sulphuric acid and sodium sulphate form a "buffer"; a larger amount of sodium sulphate and/or a smaller amount of the acid than the optimum increases the amount of ether needed.

The optimum conditions described under Experimental gave the results shown in Fig. 2A for the dissolution of all the carboxylic acids tested. The five successive extractions with 40-ml portions of diethyl ether for 30—60 s each, take 8—10 min altogether. The tendencies of distribution when extrac-

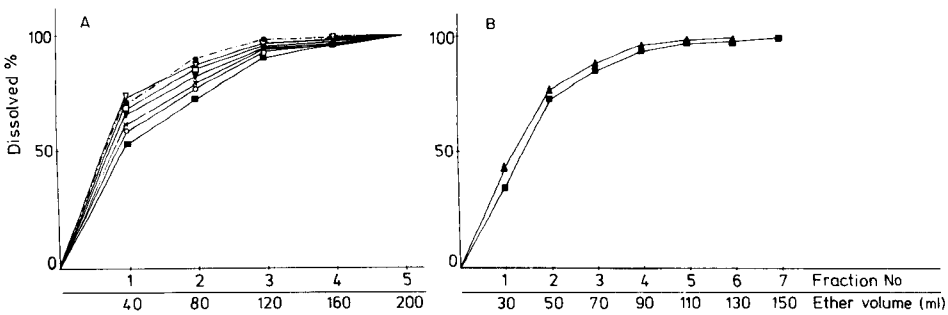

Fig. 2. Dissolution yield of aliphatic and aromatic di- and poly-carboxylic acids: (A) proposed optimal conditions (see Experimental); (B) 20-ml ether portions stirred for 1 min each. Acids: (▽) oxalic, succinic, glutaric, adipic; (▲) oxalic (in B only); (□) benzoic; (●) *o*-phthalic; (▼) trimellitic, trimesic; (×) pyromellitic; (○) benzenepentacarboxylic; (■) mellitic. Conditions: 2 ml of aqueous solution containing 10 or 20 mg of the organic acid was extracted.

tions are done with 20-ml portions of ether stirred magnetically for 1 min are shown in Fig. 2B; the distribution curves of the other carboxylic acids tested fell between the curves for oxalic and mellitic acids. Comparison of Fig. 2A and B indicates that the extraction with smaller ether fractions saves ether but takes longer (15—20 min) than the recommended procedure. The amount of diethyl ether needed can be reduced to a quarter of the optimum if the extraction is done in a glass funnel with a G_3 sintered filter and each ether fraction is removed by a suction pump. This technique, however, must be avoided if the solutions contain volatile carboxylic acids.

Table 1 provides information on the variability under different conditions. The amounts of carboxylic acids measured directly and after extraction from aqueous solutions under different conditions agree satisfactorily within the error limits of the measurements.

REFERENCES

1 A. Darbre, in K. Blau and G. S. King (Eds.), Handbook of Derivatives for Chromatography, Heyden, London, 1978, p. 39.
2 P. J. Mavrikos and G. Eliopoulos, J. Am. Oil Chem. Soc., 50 (1973) 174.
3 K. S. Bricknell, P. T. Sugihara and I. Brook, Abstr. Annu. Meet. Am. Soc. Microbiol., 44 (1976).
4 I. Brook, K. S. Bricknell, G. D. Overturf and S. M. Finegold, J. Infect. Dis., 137 (1978) 348.
5 K. S. Bricknell, I. Brook and S. M. Finegold, Chromatographia, 12 (1979) 22.
6 G. N. Jham, F. F. F. Teles and L. G. Campos, J. Am. Oil Chem. Soc., 59 (1982) 132.
7 A. J. Appleby and I. E. O. Mayne, J. Gas Chromatogr., 5 (1967) 266.
8 I. M. Perl and M. P. Szakács, Chromatographia, 17 (1983) 328, 493.
9 I. M. Perl, A. Kisfaludi and M. P. Szakács, J. Chem. Eng. Data, 29 (1984) 66.
10 K. Tanaka, M. A. Budd, M. L. Efron and K. J. Isselbacher, Proc. Natl. Acad. Sci. (U.S.A.), 56 (1966) 236.
11 V. Mahadevan and L. Zieve, J. Lipid Res., 10 (1969) 338.
12 D. B. Drucker, J. Chromatogr. Sci., 8 (1970) 489.
13 S. N. Khan and M. Schnitzer, Can. J. Chem., 49 (1971) 2302.
14 I. A. Neuroud and M. Schnitzer, Agrochimica, XIX (1975) 116.
15 S. M. Skinner and M. Schnitzer, Anal. Chim. Acta, 75 (1975) 207.
16 G. Lever, Light Metals, Proc. AIME 107th Annu. Meet. Vol. II. (1978) 71.
17 P. Roumeliotis, K. K. Unger, G. Kudermann and G. Winkhaus, Chromatographia, 15 (1982) 107.

Analytica Chimica Acta, 170 (1985) 359—363
Elsevier Science Publishers B.V., Amsterdam — Printed in The Netherlands

Short Communication

NEUTRAL CARRIER POTASSIUM-SELECTIVE ELECTRODES WITH LOW RESISTANCES

TIMOTHY A. NIEMAN* and GEORGE HORVAI[a]

Department of Chemistry, University of Illinois, 1209 W. California St., Urbana, IL 61801 (U.S.A.)

(Received 18th October 1984)

Summary. Valinomycin-based electrodes for potassium are described which have resistances as low as 5 kΩ. Addition of a mixture of tetraphenylborate and a quaternary ammonium salt lowers the resistance to 1—3% of that without the additive. The electrode retains high selectivity for K^+ over Na^+ even in the presence of a large excess of the tetraphenylborate additive over the carrier.

Ion-selective electrodes based on neutral carriers were first used by Stefanac and Simon [1, 2]. Electrodes based on neutral carriers for K^+, Ca^{2+}, NH_4^+, and other species are widely used in chemical and clinical analysis. Early electrode constructions consisted of a solution of the neutral carrier in an involatile organic solvent absorbed by a porous membrane. Recent macroscopic electrodes are, almost invariably, made with plasticized poly(vinyl chloride) (PVC) membranes. The neutral carrier is dissolved in the plasticizer. The plasticizer/PVC ratio is typically 2:1 by weight, and the neutral carrier is a few percent by weight. Microelectrodes have been fabricated from glass capillaries with tip diameters around 1 μm. The state of the art of neutral carrier electrodes is excellently covered in a recent review [3].

Commercially available neutral carrier electrodes (e.g., the K^+-selective electrodes of Philips and Orion) have resistances in the range of 5 to 30 MΩ. This range is reasonable for work with the usual laboratory pH/mV meters. Nevertheless, electrodes with lower resistances would be welcome for several practical reasons. They would be less prone to noise pickup; bulky shielded cables would be less essential; and ordinary digital voltmeters could be used for potential measurement. Our interest in electrodes with low resistances developed from work with bipolar pulse conductometric monitoring of ion-selective electrodes, in which measurement quality depends on electrode resistance. However, for all the reasons cited above, the availability of characterized low-resistance ion-selective electrodes might influence the design of clinical and industrial potentiometric systems.

[a] On leave from: Institute for Analytical Chemistry, Technical University, H-1111 Budapest, Gellert-ter 4, Hungary.

0003-2670/85/$03.30

The electrical conduction mechanism of these membranes is an intriguing problem and is part of the more general problem of describing why and how these electrodes exhibit selective and Nernstian behavior. These questions have been reviewed by many authors [4—7] and are the sole subject of a recent monograph [8].

In this communication, the construction of neutral carrier electrodes with resistances as low as 5 kΩ is described. Different membrane compositions are compared and conclusions are drawn on the working mechanism of these electrodes. Most notably, it is shown that neutral-carrier ion-selective electrodes can be prepared which function well, yet contain an excess of "background electrolyte" compared to the neutral carrier.

Experimental

Instrumentation and measurements. Potentials were measured with a Corning model 130 pH/mV meter. Resistances were measured with a specially constructed bipolar pulse conductance instrument [9] by establishing the slope of the current/voltage curve [10]; bipolar pulses of 0.2 or 2 ms total duration were used. Resistances measured were similar to those obtained with a 1-kHz impedance bridge (General Radio 1650A).

Reference electrodes were either Corning Ag/AgCl electrodes filled with 0.1 M sodium chloride or Ag/AgCl electrodes made here by electrolytic deposition of silver chloride on 22-gauge silver wire.

Stirring of the sample solution had virtually no influence on the potential values measured. All potential measurements were made with an unshielded wire of about 50-cm length connecting the inner reference electrode to the ISE input of the meter. This caused no noise in the readings.

Reagents. Valinomycin was from Sigma and Aliquat-336 (tricaprylylmethylammonium chloride) and high-molecular-weight PVC from Aldrich. Bis(2-ethylhexyl)sebacate (DOS), 2-nitrophenyl octyl ether (NPOE), potassium tetrakis(4-chlorophenyl)borate (KTCPB), dibutyl sebacate (DBS), and 1,2-dimethyl-3-nitrobenzene (DMNB) were purchased from Fluka as reagent grades specified for use in ion-selective electrodes. Reagent-grade NaCl, KCl, tetradodecylammonium bromide (TDAB; Fluka), sodium tetraphenylborate (NaTPB; Mallinckrodt), and tetrahydrofuran (THF; Baker) were used; the THF contained butylated hydroxytoluene (BHT) as a stabilizer. All chemicals were used as obtained. Water was purified in a Continental/Millipore Milli-Q reagent-grade water system.

Preparation of membranes and electrodes. Electrodes were made either as described by Craggs et al. [11] or in a Philips type IS-561 electrode body. Membranes were prepared in the same way for both. The necessary amount of plasticizer was first weighed into a glass vial. Then a solution of valinomycin and PVC in THF was added. Additional additives (NaTPB, Aliquat, KTCPB and TDAB) were also added as solutions or suspensions in THF. The total volume was typically between 2 and 3 ml. The solution was then transferred into a 22-mm i.d. teflon ring fixed on a teflon plate. After evaporation of the THF, the disk obtained weighed 32—36 mg. If the density of the

membranes is taken as approximately 1.0 g cm^{-3}, then the average membrane thickness is 0.1 mm.

If the Philips electrode was used, 7-mm diameter disks were cut from the membrane and set into the electrode body. Otherwise, the whole membrane was glued to the end of a 16-mm i.d., 22-mm o.d. vinyl tube with VLP clear vinyl repair fluid (P.D.I. Inc., St. Paul, MN). Neither the tube nor the glue contributed significantly to the membrane conductivity or selectivity. Some of the membranes turned cloudy in contact with water, but this did not apparently influence their potentiometric behavior.

The inner reference electrode was always a Ag/AgCl wire, and the inner filling solution was 10^{-3} M KCl in 10^{-1} M NaCl.

Results and discussion

Table 1 shows the compositions and resistances of several membranes. Electrodes 2—9 were calibrated in potassium chloride solutions with the ionic strength adjusted to 0.1 M with sodium chloride. This made it possible, in one calibration run, to obtain information about K^+/Na^+ selectivity and about the K^+ response above ca. 10^{-4} M. The reference electrode was usually the Corning Ag/AgCl electrode, but resistances were measured against a Ag/AgCl wire electrode.

Electrodes 1 and 10 were inert (i.e., valinomycin-free) to evaluate the contributions of the valinomycin and the various additives to the resistance. Electrode 9 did not show any reasonably stable potassium-selective behavior. The other electrodes gave calibration curves (log C vs. E) that were linear over at least 10^{-2} to 10^{-4} M K^+, with slight negative deviation at 10^{-1} M and 10—20 mV positive deviation at 10^{-5} M caused by the sodium interference. The negative deviation at 10^{-1} M K^+ was more pronounced with electrodes 5 and 6

TABLE 1

Properties of representative membranes (22-mm diameter, 0.1-mm thick)
(The mass of PVC used was 16.5 mg in each case; except for electrodes 1 and 10, which contained no valinomycin, 0.35 μmol of valinomycin was added)

No.	Resistance (kΩ)	Plasticizers added (mg)				Other additives (μmol)			
		DOS	NPOE	DBS	DMNB	NaTPB	KTCPB	Aliquat	TDAB
1	4900	34	—	—	—	—	—	—	—
2	250	27	7	—	—	—	—	—	—
3	48	27	7	—	—	0.15	—	—	—
4	35	27	8	—	—	—	0.15	—	—
5	10	27	7	—	—	0.75	—	0.59	—
6	8	27	7	—	—	—	0.75	0.59	—
7	7	28	7	—	—	0.75	—	—	0.59
8	5	—	—	29	9	—	0.75	0.59	—
9	21	26	7	—	—	0.75	—	—	—
10	10	26	7	—	—	0.75	—	0.59	—

than with the other useful electrodes. The slopes of the calibration lines were 57—59 mV/decade for electrodes 2—4 and 56—57 mV/decade for electrodes 5—8. Potential drift after a concentration change was small for electrodes 2—4. Electrodes 5—8 would typically drift 1—3 mV in the first 3 min after a decade concentration change, but remained stable after this time. Long-term stability was not investigated systematically, but none of the useful electrodes showed significant change in calibration lines one month after the first calibration run. Membranes 5—8 were therefore somewhat inferior to electrodes 2—4 with respect to stability and slope, equivalent in K^+/Na^+ selectivity, and superior in specific resistance.

There are basically three ways to achieve low electrode resistance: increasing the membrane surface area, decreasing the membrane thickness, and decreasing the specific resistance. Here, the membrane area was increased and its thickness was decreased to the limits of practical utility. Larger electrodes would be inconvenient and thinner membranes would be too fragile. Further decrease in resistance was achieved by lowering the specific resistance through certain additives.

Membranes 2 and 3 were prepared according to accepted recipes; the only difference between the membranes is that 3 contains NaTPB which reduces the specific resistance considerably. It has been stated that NaTPB cannot be present in a molar excess over valinomycin [12]. This is confirmed by comparing the present results with membranes 3 and 9. Membrane 3 contained less NaTPB than valinomycin and functioned very well; membrane 9 contained more NaTPB than valinomycin and was not useful. The problems observed with an excess of NaTPB over valinomycin have been attributed to interaction between the K^+—valinomycin complex and the tetraphenylborate anion; in the presence of an excess of tetraphenylborate, all valinomycin would be bound and thus electrode behavior would be determined by the excess of tetraphenylborate which behaves as an ion exchanger [13].

Because the maximum concentration of valinomycin is limited by solubility, NaTPB would seem to be limited in use for lowering membrane resistance. An important finding from this work was that an excess of tetraphenylborate can be tolerated without any loss of the high K^+/Na^+ selectivity typical for valinomycin when the tetraphenylborate was present together with a sufficient amount of a hydrophobic quaternary ammonium ion (membranes 5—8). The exact nature of the quaternary ammonium compound is apparently not critical because Aliquat-336 (mainly trioctylmethylammonium chloride) and tetradodecylammonium bromide worked just as well (compare membranes 5 and 7). NaTPB could also be replaced by the chloroderivative, KTCPB, without losing the high K^+/Na^+ selectivity. The K^+/Ca^{2+} selectivity was also retained by these compositions with low resistance. It is possible that selectivity against other ions may be altered; further work is needed to evaluate these membrane compositions completely. Plasticizers other than the DOS-NPOE mixture could also be used without degrading performance (membrane 8). Neutral carriers other than valinomycin may behave in similar fashion, as

indicated by preliminary experiments with the ammonium-selective carrier nonactin.

By comparing the resistance of membrane 10 with that of the other membranes, it is seen that the low specific resistances of the new membranes are due to the additives and independent of the neutral carrier. This appears to be an important observation with respect to the working mechanism of these membranes. It indicates that valinomycin can behave as a potentiometrically selective ligand even in the presence of a "background electrolyte". Preliminary experiments showed that transport selectivity was also preserved.

It is hoped that neutral carrier electrodes with low resistance, such as those reported here, will prove useful in the electrochemical study of the mechanism of ion-selective electrodes. Such studies have always been rendered difficult by the high specific resistances of the membranes. Further electrochemical characterization of membranes of the type described here is in progress.

We are grateful to Travenol Laboratories (Morton Grove, IL) for supporting this research.

REFERENCES

1 Z. Stefanac and W. Simon, Chimia, 20 (1966) 436.
2 Z. Stafanac and W. Simon, Microchem. J., 12 (1967) 125.
3 D. Ammann, W. E. Morf, P. Anker, P. C. Meier, E. Pretsch and W. Simon, Ion-Selective Electrode Rev., 5 (1983) 3.
4 R. P. Buck, Anal. Chem., 44 (1972) 270R; 46 (1974) 28R; 48 (1976) 23R; 50 (1978) 17R.
5 G. H. Fricke, Anal. Chem., 52 (1980) 259R.
6 M. E. Meyerhoff and Y. M. Fraticelli, Anal. Chem., 54 (1982) 27R.
7 M. A. Arnold and M. E. Mayerhoff, Anal. Chem., 56 (1984) 20R.
8 W. E. Morf, The Principles of Ion-Selective Electrodes and of Membrane Transport, Elsevier, Amsterdam, The Netherlands, and Akademiai Kiado, Budapest, Hungary, 1981.
9 R. F. Geiger, Ph.D. Thesis, University of Illinois, Urbana, IL, 1983.
10 C. R. Powley and T. A. Nieman, Anal. Chim. Acta, 139 (1982) 61.
11 A. Craggs, G. J. Moody and J. D. R. Thomas, J. Chem. Educ., 51 (1974) 541.
12 W. E. Morf and W. Simon, in H. Freiser (Ed.), Ion Selective Electrodes in Analytical Chemistry, Vol. 1, Ch. 3, Plenum Press, New York, 1978.
13 P. C. Meier, W. E. Morf, M. Laubli and W. Simon, Anal. Chim. Acta, 156 (1984) 1.

ANALYTICA CHIMICA ACTA, VOL. 170 (1985)

AUTHOR INDEX

AUTHOR INDEX

VOLUMES 161—170

SUBJECT INDEX

VOLUMES 161–170

B

C

D

E

F

G

H

I

K

L

M

N

O

P

Q

R

S

T

U

V

W

Y

Z

TECHNIQUE INDEX

VOLUMES 161—170

Atomic absorption spectrometry

Mass spectrometry; Conducting electrodes; Biological materials; Trace metals; Spark-source 164(1984)83

Rubidium; Blood; Flame 165(1984)257

Plasmas; Calcium; Waters; Brines; Sulphate; Inductively-coupled; Internal reference 166(1984)51

Mineral suspensions; Plasmas; Direct current 166(1984)61

Biological materials; Plasmas; Sulphur; Vacuum-ultraviolet; Inductively-coupled 166(1984)283

Activ. analysis; At. abs. spectrometry; Particle discrimination effects; Trace metals; Waters 167(1985)161

Spectrophotometry; Phosphorimetry; Fluorimetry; Chromatography; At. abs. spectrometry; Organized molecular assemblies; Micelles; Review 169(1985)1

Hydrothermal extraction; Potassium; Sodium; Rubidium; Caesium; Rocks; With lithium hydroxide 169(1985)179

Boron; Fluoride interference; Molecular emission 169(1985)377

Flow system; Molecular emission cavity analysis; Organophosphorus compounds; Phosphorus oxo-anions 170(1985)331

Flow system

Spectrophotometry; Potentiometry; Flow injection analysis; Integrated microconduits; Gas-diffusion; Ion-exchange 161(1984)1

Spectrophotometry; Amperometry; Flow injection analysis; Strongly reducing agents; Vanadium(II) 161(1984)27

Spectrophotometry; Molybdenum; Steels 161(1984)245

Fluorimetry; Cyanide 161(1984)257

Emission spectrometry; Hydride generation; Arsenic; Plasmas; Inductively-coupled 161(1984)275

Voltammetry; Dopamine; Stopped-flow linear sweep; Reticulated vitreous carbon electrode 161(1984)325

Spectrophotometry; At. abs. spectrometry; Iron; Speciation 161(1984)375

Data-processing with microcomputers; On-line 161(1984)393

Spectrophotometry; Flow injection analysis; Nitrate; Nitrite; Strongly reducing agents; Uranium(III) 162(1984)1

Spectrophotometry; Water; Flow injection analysis; Karl Fischer reagent 162(1984)9

H.p.l.c.; Amperometry; Phenolic ethers; Opiates; Bromine generation 162(1984)19

Voltammetry; Computer-controlled potentiostat 162(1984)175

Anod. stripping voltammetry; Flow injection analysis; Cadmium 162(1984)189

Spectrophotometry; Lithium; Serum; Chromogenic crown ether 162(1984)285

Fluorimetry; Terbium; Ternary complex 162(1984)305

Spectrophotometry; Extracellular enzymes; Fermentation; Membrane separations 163(1984)3

Kinetic analysis; Fluorimetry; Enzyme reactor 163(1984)67

Spectrophotometry; Cephalosporins; Enzyme reactor 163(1984)73

Mass spectrometry; Spectrophotometry; Potentiometry; Fermentation 163(1984)101

H.p.l.c.; Thermom. analysis; Dialysis probe; Fermentation 163(1984)135

Potentiometry; Urea; Semiconductor gas sensor; Serum; Urease 163(1984)143

Gas chromatography; Microbial epoxidation; Propene; Butene 163(1984)207

Mass spectrometry; Fermentation 163(1984)219

Kinetic analysis; Spectrophotometry; Fermentation; Clinical analyser in biotechnology 163(1984)257

Potentiometry; Waters; Sulphide; Gas diffusion 163(1984)293

Amperometry; Substrates of dehydrogenases; Biological materials; Electrocatalytic NADH oxidation 163(1984)299

Ion exchange; At. abs. spectrometry; Trace metals; Sea water 164(1984)23

Ion exchange; At. abs. spectrometry; Trace metals; Waters 164(1984)41

Spectrophotometry; Thermal lens effect; Iron 164(1984)91

Spectrophotometry; Fluorimetry; Chemiluminescence; Glucose; Plasma; Enzyme reactor 164(1984)103

Photoacoustic spectroscopy; Mercury; Differential detector 164(1984)119

Voltammetry; Ammonia; Air; Waters; Semiconductor gas sensor 164(1984)127

Potentiometry; Flow injection analysis; Nitrate-selective electrode; Flow-through tubular; PVC matrix 164(1984)147

Spectrophotometry; Extraction; Flow injection analysis; Film formation; Dispersion 164(1984)233

Kinetic analysis; Fluorimetry; Copper; Foods; Serum; Stopped-flow; Catalytic 165(1984)177

Fluorimetry

Gas chromatography

Immunoassay

Infrared spectrometry

Ion exchange

Kinetic analysis

Pulse polarography

Thermometric analysis

Thin-layer chromatography

Titrimetry

Turbidimetry

Voltammetry

X-ray fluorescence spectrometry

ANALYTICA CHIMICA ACTA

INFORMATION FOR AUTHORS

Analytica Chimica Acta publishes original papers, short communications, preliminary communications, and reviews dealing with every aspect of modern chemical analysis, both fundamental and applied.

Reviews are written by invitation of the editors, who welcome suggestions for subjects. Short communications are usually complete descriptions of limited investigations, and should generally not exceed six printed pages. Preliminary communications of important urgent work can be printed within four months of submission, if the authors are prepared to forego proofs.

Submission of papers

Authors should submit three copies of the manuscript in double-spaced typing on one side of the paper only, with a margin of 4 cm, on pages of uniform size. If any variety of machine copying is used (e.g., xerox), authors should ensure that all copies are easily legible and that the paper used can be written on with both ink and pencil. Authors are advised to retain at least one copy of the manuscript. Manuscripts should be preceded by a sheet of paper carrying (a) the title of the paper, (b) the name and full postal address of the person to whom proofs are to be sent, (c) the number of pages, tables and figures.

Manuscripts should be sent to the editorial addresses given on the covers of current issues; submission to the publisher leads to delays. Submission of a manuscript implies that the work described has not been, and will not be, published elsewhere (except as an abstract, or as part of a lecture, review or academic thesis). Upon acceptance of the manuscript, the author(s) will be asked to transfer the copyright of the article to the publisher. This transfer will ensure the widest possible dissemination of information.

The preferred language of the journal is English, but French and German manuscripts are also acceptable. For authors whose first language is not English, French or German, linguistic improvement is provided as part of the normal editorial processing.

Notes on the preparation of manuscripts

Authors are given every latitude, consistent with clarity and brevity, in the style and form of their papers. Very useful advice is provided in the Handbook for Authors issued by the Royal Society of Chemistry and the American Chemical Society.

Title and initial layout. All manuscripts should be headed by a concise but informative title. This is followed by the names of the authors, and the address of the laboratory where the work was carried out. The author to whom correspondence should be addressed must be indicated by an asterisk (without a footnote). If the present address of an author is different from that mentioned, it should be given in a footnote. Acknowledgements of financial support should not be made in footnotes, but at the end of the paper.

Summary. Research papers and reviews begin with a Summary (50–250 words) which should comprise a brief factual account of the contents of the paper, with emphasis on new information. Short communications and preliminary communications require summaries, which should not exceed 50 words. Uncommon abbreviations, jargon and reference numbers must not be used. The Summary should be suitable for use by abstracting services without rewriting. Papers in French or German require a Résumé or Zusammenfassung preceded by a Title and Summary in English; authors are encouraged to provide translations where necessary.

Introduction. The first paragraphs of the paper should contain an account of the reasons for the work, any essential historical background (as briefly as possible and with key references only) and preliminary experimental work.

Experimental. The experimental methods may be described after the introductory material, or after the discussion of results, depending on the nature of the paper. Detailed experimental descriptions should, however, be restricted to one section of the paper, and not scattered throughout the text. Working procedures should be given in the imperative mood; sufficient detail should be given to allow any reasonably experienced worker to carry out the procedure. Detailed descriptions of well known techniques and equipment are unnecessary, as are simple preparations of reagents or solutions, and lists of common chemicals. Manufacturers should be named only if the product differs essentially from that of other manufacturers. Local suppliers for multinational concerns should not be named. In writing, complete sentences should be used, and procedural steps should not be numbered.

Results and discussion. These may be treated together or separately. In discussing results, unnecessary repetition of experimental detail, unsupported elaboration of hypotheses, and verbose exposition of ideas should be avoided. Chemical formulae should not be used in the text unless confusion is likely to arise from the use of names. Formulae should, however, be used for brevity in tables and figures. Calculations well known to specialists are unnecessary. Conclusions should be added only if needed for interpretation; they should not be used as extended summaries nor should they duplicate the summary.

Acknowledgements. These should be kept as short as possible, and placed, without a heading, at the conclusion of the text.

References

The references should be collected at the end of the paper, numbered in the order of their appearance in the text (*not* arranged alphabetically), and typed on a separate sheet. If the paper forms part of a series, the reference to the previous part should appear as the first reference, the number being cited at the title of the paper. References given in tables should be numbered according to the position of the table in the text. Every reference listed must be cited in the text. Reference numbers in the text are set in square brackets on the line.

In the list of references, the following forms should be adopted.

Journals

1 W. Lund and M. Salberg, Anal. Chim. Acta, 76 (1975) 131.

2 M. McDaniel, A. D. Shendrikar, K. D. Reizneir and P. W. West, Anal. Chem., 48 (1976) 2240.

The title of the journal must be abbreviated as in the Bibliographic Guide for Editors and Authors.

Books

1 D. D. Perrin, Masking and Demasking of Chemical Reactions, Interscience–Wiley, New York, 1970, p. 188.

2 S. Hofmann, in G. Svehla (Ed.), Wilson and Wilson's Comprehensive Analytical Chemistry, Vol. 9, Elsevier, Amsterdam, 1979, p. 89.

Titles of papers are unnecessary. Citations of reports which are not widely available (e.g., reports from government research centres) should be avoided if possible. Authors' initials should not be used in the text, unless real confusion could be caused by their omission. If the reference cited contains three or more names, only the first author's name followed by et al. (e.g., McDaniel et al.) should be used in the text; but the reference list must contain the initials and names of *all* authors.

Tables, computer programs, and figures

Tables and figures must be essential for the clear and concise presentation of the material. The same information should not be given in tables and figures, and material from the published literature should not be reproduced.

Tables. All tables should be numbered with Arabic numerals, and have brief descriptive headings; they should be typed on separate pages. The layout should be given serious thought, so that the significance of the results can be grasped quickly. Column headings should be brief.

Tables with only two or three headings are best printed horizontally, e.g.,

Hg^{2+} added (μg)	1.0	2.0	3.0	5.0
Extraction (%)	95.0	99.8	99.5	89.0

Experimental information which is relevant to all the results in the table is best given in parentheses immediately after the heading. No column should contain the same number or unit throughout its length. Footnotes to tables are denoted by superscript a, b, c... The units used should be clearly stated. Confusion can arise from the use of powers in column headings. The following usage is recommended: e.g., if molar absorptivities are listed, the heading should be ε (10^4 l mol^{-1} cm^{-1}) so that a number 2.32 in the column signifies 23 200.

Alphanumeric computer output is usually unsuitable for reproduction and should therefore be retyped and presented as tables; capitals can be used to simulate computer output if such simulation is essential for illustration.

Computer programs. Algorithms should be described clearly and concisely by means of a suitable algorithmic notation, although a standard high-level programming language may also be used. Complete program listings are not normally admissible. Flow charts should be avoided in favour of a textual or tabulated description of the program or data flow. Statements on the portability of the software described to other computer systems, as well as on its availability to interested readers, should be given.

Figures. Figures should be prepared in black waterproof drawing ink on drawing or tracing paper of the same size as that on which the manuscript is typed. One original (or sharp glossy print) and two photostat (or other) copies are required. Attention should be given to line thickness, lettering (which should be kept to a minimum) and spacing on axes of graphs, to ensure suitability for reduction during printing. Axes of a graph should be clearly labelled, along the axes, and outside the graph itself.

The following standard symbols should be used in graphs:

▼ ▽ ■ □ + × ● ○ ▲ △

All figures should be numbered with Arabic numerals, and require descriptive legends. Explanatory information should be placed not in the figure, but in the legend, which should be typed on a separate sheet of paper. Simple straight-line graphs are not acceptable, because they can readily be described in the text by means of an equation or a sentence. Claims of linearity should be supported by regression data that include slope, intercept, standard deviations of the slope and intercept, standard error, and the number of data points; correlation coefficients are optional.

Photographs should be glossy prints and be as rich in contrast as possible; colour photographs cannot be accepted. In general, line diagrams are more informative and less liable to dating than photographs of equipment, which are therefore not usually acceptable.

Computer outputs for reproduction as figures must be good quality on blank paper, and should preferably be submitted as glossy prints.

Nomenclature, abbreviations and symbols

In general, the recommendations of the International Union of Pure and Applied Chemistry (IUPAC) should be followed, and attention should be given to the recommendations of the Analytical Chemistry Division in the journal *Pure and Applied Chemistry* (see also *IUPAC Compendium of Analytical Nomenclature*, 1978).

Basic SI and other accepted metric nomenclature are given in the Appendix. In accordance with IUPAC rules, the mass number, atomic number, number of atoms and ionic charge should be designated by a left upper index, a left lower index, a right lower index and a right upper index, respectively, placed round the atomic symbol. For example, the phosphate ion should be designated as PO_4^{3-} (*not* PO_4^{-3} or PO_4^{---}), and phosphorus-32 as ^{32}P (*not* P^{32} or P-32).

The Stock notation for the indication of stoichiometric valency states (and indirectly the proportion of the constituents) should be used. Examples are iron(III) chloride rather than ferric chloride, and potassium hexacyanoferrate(II) rather than potassium ferrocyanide. These rules are valid for French and German as well as English usage.

The use of nanometre (nm) and micrometre (μm) for the expression of analytical wavelengths has long superseded mμ or Å or μ, all of which should be avoided, although Å is sensibly retained in crystallographic work.

Natural or Naperian logarithms should be denoted by ln and decadic logarithms by log.

Molarity (mol l^{-1} or M) is the preferred concentration unit, but normality (N) can be used for convenience if it does not introduce ambiguity.

Unusual abbreviations require definition when first used. Abbreviations for long chemical names (e.g., EDTA, HEDTA, TBAH, en, pn, Tris) are useful, especially in equations, tables or figures. For ease of distinction, well known techniques may be abbreviated by using lower-case letters and full stops, such as, g.c.-m.s., u.v., i.r., a.a.s., ^{13}C-n.m.r., a.s.v., d.p.p., etc. In the interests of clarity, however, excessive use of abbreviations is not encouraged.

Ambiguity in expressing dilution can be avoided by the use of, e.g., (1 + 2) rather than 1:2 which could mean either one part diluted with two parts or one part diluted to twice its volume.

Symbols, formulae and equations should be written with great care, capitals and lower-case letters being distinguished where necessary. Greek letters and unusual symbols should be defined by name in the left-hand margin beside their first appearance in the paper. Wherever possible, mathematical expressions should be typed on one line, by using brackets, e.g., {[()]}, and the solidus, e.g., $A/b = x^{1/2}/(u+v)^{5/6}$; this is valuable in conserving vertical space. Particular attention should be given to the correct sequence of brackets and to the correct placing of superscripts and subscripts in complicated equations; careful proof-reading of such equations is essential. Short equations should not be numbered unless required for subsequent reference.

Decimal points should be indicated by full stops in papers written in English and by commas in French and German papers. All decimal numbers smaller than unity should include a leading zero (e.g., 0.11).

Appendix

Basic SI units

metre	m	candela	cd
kilogram	kg	mole	mol
second	s	(an Avogadro number of	
ampere	A	particles such as atoms,	
degree Kelvin	K	molecules, ions, electrons.)	

Derived SI units

joule	J	kg m^2 s^{-2}	farad	F	A s V^{-1}
newton	N	J m^{-1}	weber	Wb	V s
watt	W	J s^{-1}	henry	H	V s A^{-1}
coulomb	C	A s	tesla	T	V s m^{-2}
volt	V	J A^{-1} s^{-1}	hertz	Hz	s^{-1}
ohm	Ω	V A^{-1}	degree Celsius	°C	K − 273.15

Other units

litre	l	10^{-3} m^3	hour	h	3.6×10^3 s
gram	g	10^{-3} kg	dyne	dyn	10^{-5} N
poise	P	10^{-3} m^{-1} s^{-1}	atmosphere	atm	101.325 kN m^{-2}
electron volt	eV	1.6021×10^{-19} J	molar	M	mol l^{-1}
calorie	cal	4.184 J	molal	*m*	mol kg^{-1}
minute	min	60 s	curie	Ci	3.7×10^{10} s^{-1}

Prefixes to abbreviations for the names of units indicating

Multiples		Sub-multiples			
tera ($\times 10^{12}$)	T	milli ($\times 10^{-3}$)	m	pico ($\times 10^{-12}$)	p
giga ($\times 10^9$)	G	micro ($\times 10^{-6}$)	μ	femto ($\times 10^{-15}$)	f
mega ($\times 10^6$)	M	nano ($\times 10^{-9}$)	n	atto ($\times 10^{-18}$)	a
kilo ($\times 10^3$)	k				

(Continued from outside back cover)

 0003-2670/85/$03.30

Printed in The Netherlands

VOL. 170 No. 2 ANALYTICA CHIMICA ACTA APRIL 15, 1985

CONTENTS

(Abstracted, Indexed in: Anal. Abstr.; Biol. Abstr.; Chem. Abstr.; Curr. Contents Phys. Chem. Earth Sci.; Life Sci.; Index Med.; Mass Spectrom. Bull.; Sci. Citation Index; Excerpta Med.)

(Continued on inside back cover)